

**Western Australian School of Mines: Minerals, Energy and Chemical  
Engineering**

**Pyrolysis and Combustion of Phosphorus-containing Solid Fuels:  
Char Structure, Char Reactivity and Particulate Matter Emission**

**Xujun Chen**

**This thesis is presented for the Degree of**

**Doctor of Philosophy**

**of**

**Curtin University**

**May 2019**

**Declaration**

To the best of my knowledge and belief this thesis contains no material previously published by any other person except where due acknowledgment has been made.

This thesis contains no material which has been accepted for the award of any other degree or diploma in any university.

---

**To my beloved family**

**ABSTRACT**

Phosphorus (P)-containing biomass and wastes as fuels have ample supply and the combustion of these fuels is of significant importance for reducing fossil fuel consumption and greenhouse gas (GHG) emission. The abundance of P in these P-containing solid fuels may play an important consideration during the combustion of these fuels, from char formation/structure, char reactivity, to particulate matter emission. During solid fuel combustion, pyrolysis is the first step and generates char and volatiles. Volatiles combustion is fast so that char combustion is the key step that dictates the design and operation of the reactor. The char reactivity is strongly dependent on char structure, which is strongly influenced by the properties of the parent fuels and pyrolysis conditions. Pyrolysis of P-containing solid fuels results in chars with the presence of P, which can be an important factor in affecting char structure and reactivity. The occurrence forms of P in the parent fuels (hence in char) are also expected to be important. During the combustion of volatiles and char generated from P-containing solid fuels, the presence of P may also play an important role in particulate matter (PM) emission. Therefore, understanding char structure, char reactivity and PM emission is fundamentally important to efficient and clean combustion of these P-containing solid fuels. Unfortunately, there are still considerable research gaps on these topics, in despite of the previous research efforts made.

Consequently, this PhD study reports a systematic study on the structure and reactivity of char samples as well as the PM emission during combustion of P-containing solid fuels. Via the research program in this PhD thesis, seven key objectives have been achieved, including (1) having established a new method for quantifying various occurrence forms of P in solid fuels; (2) having investigated the

effect of reactor configurations on the release and transformation of P during the pyrolysis of P-containing biomass, taking advantage of the new P characterisation method; (3) having examined the effect of different forms of phosphorus in P-containing biomass on char structure and char reactivity; (4) having obtained new understanding on the role of *in situ* volatiles with distinctly-different chemistry during volatile–char interactions (the interactions between *in situ* volatiles and char during pyrolysis) in char structure and char reactivity; (5) having revealed new insights into the effect of water vapour on PM emission during the respective oxyfuel combustion of volatiles and char generated from pyrolysis of P-containing contaminated biomass samples; (6) having reported the critical role of volatile–char interactions in PM emission during combustion of *in situ* volatiles generated from P-containing biosolid; and (7) having revealed the effect of volatile–char interactions on PM emission during combustion of char samples under air and oxyfuel conditions. The main conclusions are summarized as follows.

First, a new 3-step method has been developed for separating and quantifying the total P in a solid fuel into five major P-containing fractions, which consists of three organic P-containing fractions (i.e. acid-soluble organic P, two acid-insoluble organic P including P in lipids and P in other acid-insoluble organic structures such as nucleic acids) and two inorganic P-containing fractions (i.e. acid-soluble inorganic P and acid-insoluble inorganic P). The results from validation using different standards and application of the new method to seven different solid fuels demonstrate that this new method is suitable for accurately quantifying various forms of P in solid fuels.

Second, it has been found that pyrolysis reactor configurations exert substantial effect on transformation and release of P during pyrolysis of P-rich rice bran at 400–900 °C. Higher heating rate during fast pyrolysis above 400 °C in fixed-bed/drop tube reactor could increase P release, in comparison with slow heating pyrolysis in fixed-bed

reactor. Volatile–char interactions significantly enhance P release during pyrolysis in fixed-bed/drop tube reactor with continuous feeding. Notably, more than 95% of the released P in volatiles are presented in tar as organically-bound P that can be completely converted into water-soluble P or phosphorus oxides during *in situ* combustion at 950 °C. Organic potassium phytate is the dominate P in rice bran while it is thermally unstable even at 400 °C. Above 800 °C, acid-soluble inorganic P can be transformed into acid-insoluble inorganic P species during pyrolysis.

Third, both organic and inorganic P substantially increase char yields during biomass pyrolysis at 1000 °C due to the enhanced crosslinking by P-containing structures in the char. The presence of P in biochars from the fast pyrolysis of various P-loaded biomass samples plays an important role in the evolution of char structure and intrinsic reactivity measured during low-temperature oxidation at 500 °C in air under chemical-reaction-controlled regime. After pyrolysis and subsequent char oxidation, all P in biomass either as organic or inorganic P are found to be present in the form of acid-insoluble organic structures. For char prepared from acid-washed wood, char reactivity increases with char conversion due to the increasing pore surface area at higher conversion. Comparatively, for char prepared from acid-washed wood loaded with various P at char conversion below 60%, the presence of P increases char intrinsic reactivity due to the enhanced crosslinking and reduced condensation of char structures. However, at conversions above 60%, the P-containing species in char leads to a significant decrease in char reactivity, due to the formation of abundant C-O-P bonds, that is highly resistant to the oxidation in air, in the reacting chars. The presence of P associated with oxygen and carbon also significantly affect char chemistry during char conversion.

Fourth, under non-catalytic conditions, volatiles with distinctly-different chemistry have different impacts on char reactivity and char structure during volatile–char

interactions. The reactivity of char after *in situ* volatile–char interactions increases with increasing O/H molar ratio of volatiles due to different roles played by H-containing and O-containing reactive species in the volatiles. Specifically, H-containing reactive species substantially enhance the condensation of the aromatic ring systems within the char, thus slightly decreasing the H content in char and making char structure more inert, while O-containing reactive species in volatiles can react with char to form C-O complex oxides that mitigate the carbon structure from condensing, thus increasing O and H content in char and enhancing char reactivity.

Fifth, water vapour can substantially alter PM emission during the respective combustion of *in situ* volatiles and char generated from fast pyrolysis of a P-containing contaminated wood at 1300 °C. During *in situ* volatile combustion, water vapour significantly increases the emission of PM with aerodynamic diameter <0.1 µm (i.e. PM<sub>0.1</sub>) due to enhanced nucleation, coagulation and condensation of fine particles. During char combustion, water vapour might enhance char fragmentation, thus increasing the emission of PM with aerodynamic between 1 and 10 µm (i.e. PM<sub>1-10</sub>). For trace elements, during *in situ* volatile combustion, water vapour alters the PSDs but has little effect on the yields of volatile elements (As, Cr, Ni, Cu and Pb) in PM<sub>1</sub>. During char combustion, the presence of water vapour also increases the yields of As and Cr while decrease the yield of Ni in PM<sub>0.1</sub>.

Sixth, volatile–char interactions play an important role in enhancing PM<sub>1</sub> emission during combustion of volatiles from P-rich biosolid. Specifically, volatile–char interactions lead to significant changes in the particle size distributions (PSDs) of PM and substantial increase in the yield of PM<sub>1</sub>, dominantly PM<sub>0.1</sub>. Small non-oxygenated reactive species in the fresh volatiles can react with char to enhance the release of alkalis (Na and K) as well as P and S in the biosolid chars. The released Na, K, P and S can then react to form alkali metaphosphate and sulphate which subsequently form

PM<sub>1</sub> during volatiles combustion. Evidently, volatile–char interactions also enhance the release of Pb and Cr from biosolid chars and then contribute to PM<sub>1</sub> emission.

Seventh and last, volatile–char interactions also exert significant effect on PM<sub>10</sub> emission during combustion of P-containing biosolid chars at 1300 °C. The interactions between chars and small non-oxygenated reactive species in volatiles substantially decrease the yield PM<sub>1</sub>, dominantly PM<sub>0.1</sub> during char combustion. The interactions between oxygen-free volatiles and char also reduce char macroporosity, leading to a reduction in the yield of PM<sub>1-10</sub>, while the interactions between O-containing reactive species and char play opposite roles. Higher heating rate with shorter aging process during pyrolysis significantly weakens the effect of volatile–char interaction on PM<sub>1</sub> emission but intensifies its effect on PM<sub>1-10</sub> emission. The combustion atmospheres have little effect on the net yield of PM contributed by volatile–char interactions. Notably, volatile–char interactions have little influence on the forms of alkali and alkaline earth metallic (AAEM) species and P in PM<sub>10</sub>, i.e. as (Na, K)PO<sub>3</sub> in PM<sub>1</sub> and (Mg,Ca)<sub>3</sub>(PO<sub>4</sub>)<sub>2</sub> in PM<sub>1-10</sub>.



### ACKNOWLEDGEMENTS

I gratefully acknowledge the Curtin International Postgraduate Research Scholarship (CIPRS) provided by Curtin University for my PhD study and Australian Research Council via its Discovery Projects Scheme to partially support my PhD research project.

Especially, I would like to express my warmest and deepest gratitude to my supervisor, Professor Hongwei Wu, for his guidance, teaching, training, inspiration, patience as well as constant support during my whole PhD research project. He is an excellent advisor and creative researcher from whom I have learnt so much and I am so lucky to have him as my supervisor.

In addition, I'm very grateful for the chance of accessing several innovative reactor systems available in the research team, including the quartz volatile-char interaction reactor and the multi-stage pyrolysis/combustion reactor system. These key reactor systems were designed by Prof. Wu and other team members. Particularly, I'm grateful to Dr. Sui Boon Liaw for his contribution to various aspects of the research work carried out in my PhD study.

Great thanks also go to other staff from Western Australian School of Mines: Minerals, Energy and Chemical Engineering for their assistance. I also deeply acknowledge our other group members: Mingming Zhang, Yun Yu, Matthew Witham, Chao Feng, Bing Song, Wenran Gao, Changya Deng, Jinxiu Liu, Zhiliang Wu, Fanhui Guo, and Sigit Abdurrakhman in our research group for their helps in many aspects. I will always value and cherish the friendship we established during my study in Australia. I would also like to express my deep appreciation to Melina Miralles, Ann Carroll, Roshanak Doroushi, Jason Wright, and especially, Andrew

## **ACKNOWLEDGEMENTS**

---

Chan for their technical support and laboratory assistance. Special thanks also go to Greg Lott in Craig Mostyn Group and Dave Beresford in Eastern Metropolitan Regional Council for supplying the waste samples used in my research project.

Most importantly, I would like to thank all my families for their unyielding and unconditional love, care, encouragement, company and support.

**LIST OF PUBLICATIONS****Papers Published in Refereed International Journals**

[1] **Xujun Chen**, Hongwei Wu. Transformation and release of phosphorus during rice bran pyrolysis: Effect of reactor configuration under various conditions, *Fuel* **2019**, 255, 115755.

[2] **Xujun Chen**, Sui Boon Liaw, Hongwei Wu. A new method for quantifying phosphorus of various occurrence forms in solid fuels, *Energy & Fuels* **2019**, 33, 3311–3321.

[3] **Xujun Chen**, Hongwei Wu. Volatile–char interactions: Roles of *in situ* volatiles with distinctly-different chemistry in determining char structure and reactivity, *Proceedings of the Combustion Institute* **2019**, 37, 2749-2755.

[4] **Xujun Chen**, Sui Boon Liaw, Hongwei Wu. Effect of water vapour on particulate matter emission during oxyfuel combustion of char and *in situ* volatiles generated from rapid pyrolysis of chromated-copper-arsenate-treated wood, *Proceedings of the Combustion Institute* **2019**, 37, 4319-4327.

[5] **Xujun Chen**, Sui Boon Liaw, Hongwei Wu. Effect of volatile–char interactions on PM<sub>10</sub> emission during the combustion of biosolid chars under air and oxyfuel conditions, *Combustion and Flame* **2018**, 197, 290–303.

[6] Sui Boon Liaw, **Xujun Chen**, Yun Yu, Mário Costa and Hongwei Wu. Effect of particle size on particulate matter emissions during biosolid char combustion under air and oxyfuel conditions, *Fuel*, 2018, 232, 251-256.

[7] **Xujun Chen**, Sui Boon Liaw, Hongwei Wu. Important role of volatile–char interactions in enhancing PM1 emission during the combustion of volatiles from biosolid, *Combustion and Flame* 2017, 182, 90–101.

### **Paper(s) to Be Submitted to Refereed International Journals**

[8] **Xujun Chen**, Hongwei Wu. Effect of different forms of phosphorus in biomass on the evolution of char structure and char reactivity, manuscript completed and to be submitted to *Proceedings of the Combustion Institute, Volume 38*.

**TABLE OF CONTENTS**

ABSTRACT.....	III
ACKNOWLEDGEMENTS.....	VIII
LIST OF PUBLICATIONS.....	X
TABLE OF CONTENTS.....	XII
LIST OF FIGURES.....	XVIII
LIST OF TABLES.....	XXV
CHAPTER 1 INTRODUCTION.....	1
1.1 Background and motive.....	1
1.2 Scope and objectives.....	3
1.3 Thesis Outline.....	4
CHAPTER 2 LITERATURE REVIEW.....	7
2.1 Introduction.....	7
2.2 Sources and issues of P-containing solid fuels.....	8
2.2.1 Sources of P-containing solid fuels.....	8
2.2.2 Operational challenges.....	10
2.2.3 Environmental concerns.....	12
2.3 Occurrence of phosphorus in solid fuels.....	13
2.3.1 Inorganic phosphorus.....	13
2.3.2 Organic phosphorus.....	14
2.4 Methods for quantifying phosphorus of various occurrence forms in solid fuels.....	14
2.4.1 Conventional methods for quantifying P with different forms in solid fuels.....	15
2.4.2 Summary.....	20
2.5 Pyrolysis characteristics of P-containing solid fuels: volatile–char interactions, char structure and char reactivity.....	20
2.5.1 The significance of volatile–char interactions during solid fuels pyrolysis.....	20
2.5.2 Factors influencing char structure and reactivity.....	22

## TABLE OF CONTENTS

---

2.5.3 Role of phosphorus in solid fuels pyrolysis .....	26
2.5.4 Summary .....	27
2.6 Transformation and release of phosphorus during P-containing solid fuels pyrolysis and combustion.....	27
2.6.1 Phosphorus transformation mechanism during pyrolysis and combustion .....	28
2.6.2 Factors influencing P release during pyrolysis and combustion .....	29
2.6.3 Summary .....	32
2.7 PM <sub>10</sub> emission during combustion of P-containing solid fuels.....	32
2.7.1 The mechanisms of PM <sub>10</sub> emission during combustion of P-containing solid fuels .....	33
2.7.2 PM <sub>10</sub> emission under oxyfuel combustion conditions.....	35
2.7.3 Distribution and occurrence of phosphorus in PM <sub>10</sub> during combustion of P-containing solid fuels.....	38
2.7.4 Indirect evidence on roles of volatile–char interactions in PM <sub>10</sub> emission.....	39
2.7.5 Summary .....	41
2.8 Conclusions and research gaps .....	42
2.9 Research objectives of current study .....	43
CHAPTER 3 RESEARCH METHODOLOGY AND ANALYTICAL TECHNIQUES .....	45
3.1 Introduction.....	45
3.2 Methodology .....	45
3.2.1 A New method for quantifying phosphorus of various occurrence forms in solid fuels.....	47
3.2.2 Transformation and release of phosphorus during pyrolysis of P-containing biomass in reactors with different configurations under various conditions .....	47
3.2.3 Roles of phosphorus in evolution of char structure and char reactivity .....	48
3.2.4 Volatile–char interactions: roles of <i>in situ</i> volatiles with distinctly-different chemistry in determining structure and reactivity of char from P-containing biosolid..	48
3.2.5 Effect of water vapour on PM <sub>10</sub> emission during combustion of <i>in situ</i> volatiles and char from fast pyrolysis of P-containing contaminated wood.....	49

---

## TABLE OF CONTENTS

---

3.2.6 Effect of <i>in situ</i> volatile–char interactions on PM emission during the combustion of volatiles from P-containing biosolid.....	49
3.2.7 Effect of volatile–char interactions on PM <sub>10</sub> emission during combustion of P-containing biosolid chars under air and oxyfuel conditions .....	50
3.3 Experimental .....	50
3.3.1 Sample preparation .....	50
3.3.2 Reactor systems for pyrolysis experiments.....	53
3.3.3 Reactor system for <i>in situ</i> volatile–char interactions.....	56
3.3.4 Combustion reactor and PM collection system.....	57
3.4 Instruments and analytical techniques .....	63
3.4.1 Proximate and ultimate analysis .....	63
3.4.2 Quantification of inorganic species in solid fuels and PM .....	63
3.4.3 Char structure.....	65
3.4.4 Char reactivity.....	66
3.4.5 X-ray photoelectron spectroscopy measurement .....	66
3.4.6 Surface area of char samples.....	67
3.4.7 Particle size distributions and macroporosity of char samples .....	67
3.4.8 Conclusions.....	68
CHAPTER 4 A NEW METHOD FOR QUANTIFYING PHOSPHORUS OF VARIOUS OCCURANCE FORMS IN P-CONTAINING SOLID FUELS.....	69
4.1 Introduction.....	69
4.2 Evaluation of the SMT method for quantifying different forms of phosphorus in solid fuels.....	71
4.3 A new method for quantifying P of various forms in solid fuels.....	72
4.3.1 Overview of the new method.....	72
4.3.2 Key steps of the new method .....	73
4.4 Validation and application of the new method .....	76
4.4.1 Standard samples for validation.....	76
4.4.2 Validation of the new method.....	79

---

## TABLE OF CONTENTS

---

4.4.3 Application of the new method.....	84
4.5 Conclusions.....	86
CHAPTER 5 EFFECT OF REACTOR CONFIGURATIONS ON TRANSFORMATION AND RELEASE OF PHOSPHORUS DURING P-RICH BIOMASS PYROLYSIS UNDER VARIOUS CONDITIONS .....	88
5.1 Introduction.....	88
5.2 Changes in char chemistry during pyrolysis under various conditions.....	90
5.3 Release and distributions of P during rice bran pyrolysis.....	92
5.4 Transformation of phosphorus in char during pyrolysis in different reactor systems..	96
5.5 Conclusions.....	99
CHAPTER 6 EFFECTS OF PHOSPHORUS ON CHAR STRUCTURE AND REACTIVITY OF BIOCHARS PREPARED FROM ACID-WASHED BIOMASS LOADED WITH P OF VARIOUS FORMS .....	101
6.1 Introduction.....	101
6.2 Char yield during biomass pyrolysis and phosphorus retention in char .....	102
6.3 Effect of phosphorus on chemistry of char sample prepared from biomass pyrolysis	105
6.4 Effect of phosphorus with different occurrence forms on char reactivity.....	106
6.5 Effect of phosphorus with different occurrence forms on char carbon structure .....	109
6.6 Conclusions.....	114
CHAPTER 7 VOLATILE-CHAR INTERACTIONS: ROLES OF <i>IN SITU</i> VOLATILES WITH DISTINCTLY-DIFFERENT CHEMISTRY IN DETERMINING STRUCTURE AND REACTIVITY OF CHAR PREPARED FROM P-CONTAINING BIOSOLID.....	115
7.1 Introduction.....	115
7.2 Distinct differences in chemistry of volatiles produced for <i>in situ</i> volatile-char interactions.....	116
7.3 Variations in char chemistry during <i>in situ</i> volatile-char interactions.....	119
7.4 Effect of volatiles chemistry on char reactivity after <i>in situ</i> volatile-char interactions .....	121
7.5 Effect of volatiles chemistry on char carbon structure after <i>in situ</i> volatile-char interactions.....	123



## TABLE OF CONTENTS

---

7.6 Conclusions.....	125
CHAPTER 8 EFFECT OF WATER VAPOUR ON PM EMISSION DURING COMBUSTION OF <i>IN SITU</i> VOLATILES AND CHAR FORM FAST PYROLYSIS OF P-CONTAINING CONTAMINATED WOOD .....	127
8.1 Introduction.....	127
8.2 Effect of water vapour on the properties of PM <sub>10</sub> during the combustion of <i>in situ</i> volatiles and char .....	129
8.3 Effect of water vapour on the emission of major elements in PM <sub>10</sub> during the combustion of <i>in situ</i> volatiles and char.....	131
8.4 Effect of water vapour on the emission of trace elements during the combustion of <i>in</i> <i>situ</i> volatiles and char.....	137
8.5 Conclusions.....	139
CHAPTER 9 IMPORTANT ROLE OF VOLATILE–CHAR INTERACTIONS IN ENHANCING PM <sub>1</sub> EMISSION DURING COMBUSTION OF VOLATILES FROM P-CONTAINING BIOSOLID .....	141
9.1 Introduction.....	141
9.2 Properties of char and samples used for generating volatiles with <i>in situ</i> volatile–char interactions.....	142
9.3 Direct Evidence on the importance of Volatile–char Interactions in PM Emission ..	147
9.4 Changes in major and trace elements distributions in PM due to volatile–char interactions.....	151
9.5 Further discussion .....	155
9.6 Conclusions.....	162
CHAPTER 10 EFFECT OF VOLATILE–CHAR INTERACTIONS ON PM <sub>10</sub> EMISSION DURING THE COMBUSTION OF P-CONTAINING BIOSOLID CHARS UNDER AIR AND OXYFUEL CONDITIONS.....	164
10.1 Introduction.....	164
10.2 The properties of char samples used for volatile–char interactions.....	164
10.3 Effect of <i>in situ</i> volatile–char interactions on PM <sub>10</sub> emission during char combustion in air .....	169

## TABLE OF CONTENTS

---

10.4 Effect of <i>in situ</i> volatile–char interactions on the emission of trace elements in PM <sub>10</sub> during char combustion in air .....	180
10.5 Effect of pyrolysis conditions on PM <sub>10</sub> emission during the combustion of char that experienced interactions with volatiles .....	184
10.6 Differences in PM <sub>10</sub> emission during the combustion of volatile–interacted chars under air and oxyfuel conditions.....	187
10.7 Conclusions.....	189
CHAPTER 11 CONCLUSIONS AND RECOMMENDATIONS .....	191
11.1 Introduction.....	191
11.2 Conclusions.....	192
11.2.1 A new method for quantifying phosphorus of various occurrence forms in solid fuels.....	192
11.2.2 Effect of reactor configurations on the transformation and release of phosphorus during pyrolysis under various conditions .....	193
11.2.3 Effect of phosphorus in biomass on char structure and reactivity .....	193
11.2.4 Volatile–char interactions: Roles of <i>in situ</i> volatiles with distinctly-different chemistry in determining structure and reactivity of char prepared from P-containing biosolid.....	194
11.2.5 Effect of water vapour on PM <sub>10</sub> emission during oxyfuel combustion of char and <i>in situ</i> volatiles generated from rapid pyrolysis of P-containing contaminated wood .....	194
11.2.6 Important role of volatile–char interactions in PM <sub>10</sub> emission during the combustion of volatiles from P-containing biosolid .....	195
11.2.7 Effect of volatile–char interactions on PM <sub>10</sub> emission during the combustion of P-containing biosolid chars under air and oxyfuel conditions .....	196
11.3 Recommendations.....	197
REFERENCES .....	199
APPENDIX I: COPYRIGHT PERMISSION STATEMENTS .....	215
APPENDIX II: ATTRIBUTION TABLES .....	221

**LIST OF FIGURES**

Figure 1-1 Thesis map..... 6

Figure 2-1 The SMT method protocol for quantifying organic and inorganic phosphorus in solid fuels<sup>89</sup> ..... 17

Figure 2-2 A schematic diagram of volatile–char interactions during solid fuels pyrolysis or combustion ..... 21

Figure 2-3 Possible mechanisms of P transformation and release during pyrolysis and combustion of P-containing solid fuels, summarized based on literature review findings<sup>4,8,13,21,29,66,127-130</sup> ..... 28

Figure 2-4 Reaction pathways of the P-containing species during rice bran combustion, based on equilibrium calculations<sup>4</sup> ..... 29

Figure 2-5 Possible controlling mechanisms for PM emission in a combustion system<sup>138</sup> ..... 33

Figure 2-6 Flowsheet of oxyfuel combustion for power generation with CO<sub>2</sub> capture and storage<sup>25</sup> ..... 36

Figure 2-7 Schematic diagram of the two-stage pyrolysis/combustion reactor system used for combustion of *in situ* biomass volatiles<sup>19</sup> ..... 40

Figure 3-1 Research methodology linked with the research objectives in this thesis 46

Figure 3-2 Pyrolysis reactor systems used in this thesis<sup>104</sup> ..... 53

Figure 3-3 Two-stage reactor systems for *in situ* volatile-char interactions ..... 56

Figure 3-4 Schematic diagram of the two-stage pyrolysis/combustion reactor system<sup>12</sup> ..... 59

Figure 3-5 Schematic diagram of the three-stage pyrolysis/combustion reactor system ..... 61

Figure 3-6 Schematic diagram of Raman peak deconvolution for a low-rank solid fuel

char samples <sup>142</sup> .....	65
Figure 4-1 Recovery of P in organic phosphate after sequential extraction according to the SMT method. A: D-fructose 6-phosphate disodium salt hydrate; B: Phytic acid sodium salt hydrate; C: Adenosine 5'-monophosphate monohydrate; D: 1,2-Dioleoyl-SN-glycero-3-phosphoric acid sodium salt; E: Deoxyribonucleic acid sodium salt .....	72
Figure 4-2 A schematic diagram of the new method for fractionation and quantification of P with various occurrence forms in solid fuels. $P_t$ and $P_{as}$ represent total phosphorus and acid-soluble phosphorus in solid fuel, respectively. $P_{as-in}$ and $P_{ai-in}$ represent acid-soluble inorganic P and acid-insoluble inorganic P, respectively. $P_{as-or}$ , $P_{li}$ and $P_{na}$ represent acid-soluble organic P, P in phospholipids and P in other acid-insoluble organic structures such as nucleic acids, respectively .....	73
Figure 4-3 Conversion of organic phosphorus to $PO_4^{3-}$ , $P_2O_7^{4-}$ and $P_3O_{10}^{5-}$ by UV irradiation for 8 h. A: adenosine 5'-monophosphate monohydrate; B: Cytidine 5'-triphosphate disodium salt; C: phytic acid sodium salt hydrate; D: D-fructose 6-phosphate disodium salt hydrate; E: sodium hexametaphosphate; F: sodium pyrophosphate tetrabasic .....	80
Figure 4-4 Contents of phosphorus in P-loaded AWMW samples, quantified using the new method (open circle) and existing SMT method (open square); (a) $P_{as-in}$ in Standards SA1-SA5; (b) $P_{ai-in}$ in Standards SB1-SB5; (c) $P_{as-or}$ in Standards SC1-SC5; (d) $P_{li}$ in Standards SD1-SD5; (e) $P_{na}$ in Standards SE1-SE5 .....	82
Figure 4-5 Comparison of P with various forms in seven different solid fuel samples, quantified using the SMT method and the new method proposed in this study, including (a) distribution of P in these solid fuels determined by the new method; the percentages of (b) inorganic and (c) organic P in these solid fuels quantified using the new method and SMT method .....	84
Figure 5-1 Char yields at different pyrolysis temperatures during pyrolysis in (a) Type	

## LIST OF FIGURES

---

A, fixed-bed reactor; (b) Type B, drop-tube/fixed-bed reactor with continuous feeding; (c) Type C, drop-tube/fixed-bed reactor with pulsed feeding .....	91
Figure 5-2 The release of P during pyrolysis of rice bran at different temperatures in a fixed-bed reactor (Type A) and in drop-tube/fixed-bed reactor with continuous feeding (Type B) and pulse feeding (Type C) .....	93
Figure 5-3 The mass balance of P during pyrolysis of rice bran in a fixed-bed reactor (Type A) and in drop-tube/fixed-bed reactor with continuous feeding (Type B) and pulse feeding (Type C). The P in volatiles includes P in gas and P in tar. The P in tar is calculated by P contents in char and in gas .....	94
Figure 5-4 Recovery of P via combustion of volatiles produced in situ from rice bran pyrolysis in Type D reactor system with either continuous feeding and pulse feeding at 500–900 °C .....	95
Figure 5-5 Mass percentage of water-soluble inorganic species leached from rice bran via water leaching .....	96
Figure 5-6 Qualitative analysis of water-soluble P in leachate from rice bran using IC .....	97
Figure 5-7 Distributions of P in char samples produced from pyrolysis in (a) fixed-bed reactor (Type A) and in drop-tube/fixed-bed reactors with (b) continuous feeding (Type B) and (c) pulse feeding (Type C) under different temperatures. RT represents rice bran sample prepared at room temperature .....	97
Figure 6-1 Char yields during pyrolysis of wood samples (left Y axis) and phosphorus retention (right Y axis) in char samples prepared from fast pyrolysis at 1000 °C .....	102
Figure 6-2 (a) Specific reactivities of char samples measured at 500 °C in air by TGA. The relative experimental error for char reactivity measurement is 3%; (b) BET pore surface area of char samples; (c) Reactivity per unit pore surface area of char samples .....	107

## LIST OF FIGURES

---

Figure 6-3 Peak fractions of (a) D band and (b) ( $G_r + V_l + V_r$ ) band out of the total peak area, and (c) peak area ratio of $S_{(G_r + V_l + V_r)}/S_D$ (c) in chars with different char conversions.....	111
Figure 6-4 (a) Phosphorus retention and (b) O/C and P/C molar ratios in chars with different char conversions .....	112
Figure 7-1 Chemistry of volatiles generated <i>in situ</i> from PE, DAWB, PEG and cellulose for <i>in situ</i> volatile–char interactions at 1000 °C, including (a) weight percentage and (b) mole percentage of elemental compositions and (c) O/H and H/C molar ratios.....	119
Figure 7-2 Char yields after holding or <i>in situ</i> volatile–char interactions at 1000 °C in Stage II reactor .....	120
Figure 7-3 Specific reactivities of Char-holding and chars after interactions with different <i>in situ</i> volatiles at 410 °C in air determined by TGA .....	121
Figure 7-4 Peak fractions of (a) D band and (b) ( $G_r + V_l + V_r$ ) band out of the total peak area, and (c) peak area ratio of $S_{(G_r + V_l + V_r)}/S_D$ (c) in chars in the absence or presence of <i>in situ</i> volatile–char interactions .....	123
Figure 8-1 PSDs of PM collected during the combustion of (a) <i>in situ</i> volatiles and (b) char under oxyfuel conditions at 1300 °C and different water vapour contents .....	129
Figure 8-2 Yields of PM collected during combustion of (a) <i>in situ</i> volatiles and (b) char under oxyfuel conditions at 1300 °C and different water vapour contents .....	130
Figure 8-3 PSDs of major elements in the PM collected during combustion of (a–j) <i>in situ</i> volatiles and (k–t) char under oxyfuel conditions with different water vapour contents .....	131
Figure 8-4 Yields of major elements in PM collected during combustion of (a–j) <i>in situ</i> volatiles and (k–t) under oxyfuel conditions with different water vapour contents	133
Figure 8-5 PSDs of trace elements in PM collected during the combustion of (a–g) <i>in situ</i> volatiles and (h–n) char under oxyfuel conditions with different water vapour	

contents .....	137
Figure 8-6 Yields of trace elements in PM collected during the combustion of (a–g) in situ volatiles and (h–n) char under oxyfuel conditions with different water vapour contents .....	138
Figure 9-1 Retention of (a) major and (b) trace elements in acid-washed biosolid after acid-washing of the biosolid sample, expressed as % of those in biosolid.....	142
Figure 9-2 Release of (a) major and (b) trace elements in the volatiles generated <i>in situ</i> from the fast heating pyrolysis of acid-washed biosolid. The AW BFH800 volatiles and AW BFH1000 volatiles are generated <i>in situ</i> from fast heating pyrolysis of acid-washed biosolid at 800 and 1000 °C, respectively, for volatile–char interactions experiment.....	145
Figure 9-3 Retention of (a) major and (b) trace elements in chars produced from slow heating pyrolysis of biosolid at 800 (BSH800 Char) and 1000 °C (BSH1000 Char) .....	146
Figure 9-4 The PSDs of PM collected from the combustion of fresh volatiles generated from cellulose, polyethylene and AW biosolid without or with interactions with slow heating biosolid char at (a) 800 °C and (b) 1000 °C, respectively.....	147
Figure 9-5 Net yield of PM during volatiles combustion, contributed by the interactions between volatiles generated from (a) cellulose, (b) polyethylene, (c) AW biosolid and chars at 800 °C and 1000 °C, respectively .....	148
Figure 9-6 PSDs of major elements in PM collected from the combustion of fresh volatiles generated from cellulose, polyethylene, AW biosolid and the respective volatiles after interactions with slow heating biosolid char at (a–j) 800 °C and (k–t) 1000 °C, respectively .....	151
Figure 9-7 PSDs of trace elements in PM collected from the combustion of fresh volatiles generated from cellulose, polyethylene and AW biosolid and the respective volatiles after interactions with slow heating biosolid char at (a–g) 800 °C and (h–n)	

## LIST OF FIGURES

---

1000 °C, respectively .....	152
Figure 9-8 Net yields of (a-d and g-j) major and (e-f and k-l) trace elements in PM from the combustion of volatiles from cellulose, polyethylene and AW biosolid, contributed by the volatile-char interactions at (a-f) 800 °C and (g-l) 1000 °C, respectively .....	154
Figure 9-9 Molar ratios of (Na+K)/(P+2S) in the net PM <sub>0.1</sub> released due to volatile-char interactions. Stages A-D represent PM <sub>0.1</sub> collected from the backup filter and stage 1-3 of the DLPI, respectively .....	156
Figure 9-10 (a) Yields of biosolid slow heating chars after volatile-char interactions; and the net release of (b) major and (c) trace elements from the biosolid slow heating chars as a result of volatile-char interactions .....	157
Figure 9-11 (a) Molar ratios of (Na+K)/(P+2S) for the net elements released from the chars as a result of volatile-char interactions; (b) collection efficiency for the net elements released from chars as a result of volatile-char interactions as PM <sub>0.1</sub> .....	160
Figure 10-1 Yields of chars after volatile-char interactions or holding at 1000°C in the Stage II of the two-stage quartz reactor .....	167
Figure 10-2 Release of (a) major and (b) trace elements during slow and fast heating pyrolysis for the preparation of chars at 1000°C .....	168
Figure 10-3 PSDs of PM <sub>10</sub> from the combustion of (a and b) slow heating char and (c and d) fast heating char and its volatile-interacted char under (a and c) air and (b and d) oxyfuel conditions.....	169
Figure 10-4 PSDs of PM <sub>10</sub> from the combustion of (a and b) slow heating char and (c and d) fast heating char and its volatile-interacted char under (a and c) air and (b and d) oxyfuel conditions.....	170
Figure 10-5 The net yields of PM contributed by the interactions (a) between slow heating char (SHC) and polyethylene volatiles; (b) between SHC and double acid-washed biosolid volatiles; (c) between fast heating char (FHC) and polyethylene	



## LIST OF FIGURES

---

volatiles; and (d) between FHC and double acid-washed biosolid volatiles .....	171
Figure 10-6 PSDs of major elements in PM <sub>10</sub> during char combustion. The left two columns represent results from the combustion of SHCs under air and oxyfuel conditions while the right two columns represent the results from the combustion of FHCs under air and oxyfuel conditions, respectively .....	173
Figure 10-7 Yields of major elements during char combustion under air (left column) and oxyfuel (right column) conditions .....	174
Figure 10-8 Net yields of major elements in PM contributed by volatile–char interactions .....	175
Figure 10-9 Release of key inorganic species during volatile–char interactions at 1000 °C. Release of other major elements (i.e., Ca, Mg, Fe, Al and Si) and trace elements (i.e., As, Cd, Co, Mn, V, Cu, Ni and Zn) during volatile–char interactions are negligible.....	177
Figure 10-10 Particles size distributions (by volume) of char particles. (a) Cumulative, (b) Distribution.....	178
Figure 10-11 Macroporosity of char particles produced from slow heating char and fast heating char with or without volatile–char interactions.....	178
Figure 10-12 PSDs of of trace elements in PM <sub>10</sub> during char combustion. The left two columns represent results from the combustion of SHCs under air and oxyfuel conditions while the right two columns represent the results from the combustion of FHCs under air and oxyfuel conditions, respectively .....	182
Figure 10-13 Yields of trace elements in PM during char combustion under air (left column) and oxyfuel (right column) conditions .....	183
Figure 10-14 Net yields of trace elements in PM contributed by volatile–char interactions .....	184
Figure 10-15 The molar ratios of (Na + K)/P in PM <sub>0.1</sub> and (Ca + Mg)/P in PM <sub>1-10</sub> generated during char combustion under air and oxyfuel conditions .....	189

## LIST OF TABLES

Table 2-1 A summary of some published methods used for determining phosphorus in solid fuels <sup>1,9,40,42,49,53,69,74,75,77-99</sup> .....	19
Table 2-2 A summary of some investigations into P release during pyrolysis and combustion of P-containing solid fuels <sup>4,13,20,56,66,129,135,136</sup> .....	30
Table 3-1 A summary of heating rate and residence time in the isothermal zone of the reactors shown in Figure 3-2.....	53
Table 4-1 Proximate and ultimate analyses of solid fuels used in this study.....	70
Table 4-2 Contents (mg/kg_solid fuels, db) of inorganic species in solid fuels .....	70
Table 4-3 Contents (mg/kg_solid fuels, db) of inorganic species in acid-washed samples.....	76
Table 4-4 Contents and recovery of P with different forms in standards SF, SG and SH samples determined by SMT and the proposed new method.....	78
Table 4-5 Contents and recovery of P with different forms in standards SF, SG and SH samples determined by SMT and the proposed new method.....	83
Table 5-1 The properties of rice bran used in Chapter 5 .....	89
Table 5-2. Ultimate analyses of char samples prepared from rice bran pyrolysis in reactors with different configurations .....	92
Table 6-1 The properties of acid-washed mallee wood used in Chapter 6 .....	102
Table 6-2 Distributions of different forms of P in char samples and ultimate analysis of char after pyrolysis and partially-converted char samples after oxidation .....	104
Table 6-3 Contents (mg/kg, dry basis) of inorganic species in char samples prepared from fast pyrolysis of wood samples at 1000 °C .....	105
Table 6-4 Distributions of P groups associated with carbon structure in char samples with different char conversions .....	113
Table 7-1 The properties of samples used in Chapter 7 .....	117

## LIST OF TABLES

---

Table 7-2 The concentrations (mg/kg, dry basis) of inorganic species in DAWB and DAWB char.....	117
Table 7-3 The char yields of PE, DAWB, PEG and cellulose after <i>in situ</i> volatiles generation.....	118
Table 7-4 The content (mg/kg, dry basis) of inorganic species in char in the absence or presence of <i>in situ</i> volatile–char interactions.....	120
Table 7-5 Ultimate analysis of DAWB char, Char-holding and chars after <i>in situ</i> volatile–char interactions.....	121
Table 8-1 Properties of the P-containing contaminated wood used in Chapter 8....	128
Table 8-2 Yields of Na and K in PM <sub>1</sub> and the alumina reactor tube during volatiles combustion and Al in the solutions from water washing of the alumina reactor tube of the DTF.....	135
Table 9-1 Properties of biosolid, acid-washed biosolid, cellulose, polyethylene and slow heating biosolid chars prepared at 800°C and 1000°C, respectively.....	143
Table 10-1 Properties of biosolid, polyethylene (PE), double acid-washed biosolid (DAWB) and char samples.....	165

## CHAPTER 1 INTRODUCTION

### 1.1 Background and motive

Phosphorus (P) plays important roles in almost all life forms<sup>1</sup> and thus a key element in the solid fuels.<sup>2,3</sup> The abundant supply of P-containing solid fuels guarantees the long-term thermochemical utilization of these fuels as an effective way to combat climate change.<sup>4</sup> Among various thermochemical technologies, combustion is considered as a practical and economic one for utilizing P-containing solid fuels.<sup>5,6</sup> However, because of the presence of P, the utilisation of these solid fuels may face significant operating challenges and lead to undesired environmental concerns.<sup>4</sup> Therefore, fundamental research into the behaviour of these P-containing solid fuels during combustion is of great importance and in great need.

Phosphorus may be present in solid fuels in various occurrence forms.<sup>7</sup> The content and occurrence form of P can be important factors governing the transformation of P during thermal utilization of P-containing solid fuels. Emission of P may also pose a potential threat to the environment.<sup>8</sup> Therefore, accurate quantification of phosphorus with various occurrence forms is critical to thermochemical utilization of P-containing solid fuels. Several conventional methods have been developed to separate and analyse single or multiple phosphorus in various solid fuels over the last several decades.<sup>9</sup> However, each of those methods has its own shortcoming and major limitations.<sup>9</sup> Therefore, a new method is urgently needed for quantifying P of various occurrence forms in P-containing solid fuels.

As solid fuel particles are injected into the reactor, pyrolysis of these fuel particles is the first step reaction of the combustion process, generating volatiles and char. The properties of volatiles and char can substantially affect the characteristics of subsequent combustion.<sup>10-12</sup> For example, the transformation of phosphorus during

pyrolysis of P-containing solid fuels plays important roles in the release of phosphorus or further transformation during subsequent combustion<sup>13</sup> as well as the bio-availabilities of phosphorus in the resultant char samples.<sup>4,8,14</sup> Furthermore, the reactivity of char generated from solid fuel pyrolysis is a key factor governing the overall efficiency of a combustion system. It is known that char reactivity can be significantly affected by char structure and catalytic species in char, which are in turn influenced by many factors such as the *in situ* interactions between volatiles and char (the so-called *in situ* volatile–char interactions) during pyrolysis.<sup>15-18</sup> Therefore, understanding the transformation of P during the pyrolysis of P-containing solid fuels as well as the structure and reactivity of the resultant char samples are of critically importance to the combustion applications of P-containing solid fuels, such as optimizing combustion conditions for enhancing combustion efficiency and mitigating environmental concerns.

It has been demonstrated that the separate combustion of *in situ* volatiles and char could lead to significantly different pathways for particulate matter (PM) emission,<sup>19-21</sup> which is a notoriously environmental issue.<sup>22</sup> For example, combustion of volatiles mainly produces submicron PM with easily vaporizable elements, while char combustion dominantly generates supermicron PM with refractory elements.<sup>12,19,20,23,24</sup> However, although it was speculated,<sup>19,23</sup> the roles of volatile–char interactions played in PM emission is still unknown during the combustion of volatiles and char from P-containing solid fuels. This also applies to oxyfuel combustion, which is a promising technology to achieve near-zero carbon emission when applied to fossil fuels,<sup>25</sup> in addition to the conventional air combustion. Under oxyfuel combustion conditions, the effect of water vapours in the recycled flue gas on PM emission also becomes very important so that it is of great need to investigate the effect water vapours on PM emission during separate combustion of volatiles and char under oxyfuel conditions.

## 1.2 Scope and objectives

In light of these critical research gaps, this thesis has completed a systematic research program to investigate the pyrolysis and combustion of P-containing solid fuels with seven specific objectives:

- (1) To develop a new method for quantifying phosphorus of various occurrence forms in solid fuels;
- (2) To investigate the effect of reactor configurations on the transformation and release of phosphorus during pyrolysis of P-containing biomass under various conditions;
- (3) To study the effect of different forms of phosphorus in P-containing solid fuels on char structure and reactivity;
- (4) To investigate the roles of *in situ* volatiles with distinctly-different chemistry in determining char structure and char reactivity during volatile–char interactions;
- (5) To examine the effect of water vapours on PM emission during oxyfuel combustion of *in situ* volatiles and char from fast pyrolysis of P-containing contaminated biomass;
- (6) To provide direct evidence on the effect of *in situ* volatile–char interactions on PM emission during combustion of *in situ* volatiles from P-containing biosolid;
- (7) To investigate the effect of volatile–char interactions on PM emission during combustion of P-containing biosolid char samples under air and oxyfuel combustion conditions.

### 1.3 Thesis Outline

To elaborate the research gaps and fully achieve those objectives, 11 chapters are included in this thesis (including this chapter) as listed below with the diagrammatic structure of this thesis shown in Figure 1-1.

- Chapter 1 introduces the background and objectives of this thesis;
- Chapter 2 reviews the up-to-date literature on the sources and issues of P-containing solid fuels, phosphorus occurrence and its quantification methods, transformation of phosphorus during pyrolysis and combustion of P-containing solid fuels, structure and reactivity of char samples and PM emission produced from combustion of P-containing solid fuels, finally leading to the identification of key research gaps and outlining of specific objectives of the present study;
- Chapter 3 summarizes the research methodology and techniques used in this study, along with detailed descriptions of the experimental equipment, analytical instruments and sample preparation;
- Chapter 4 develops a new method for quantifying phosphorus with various occurrence forms in solid fuels;
- Chapter 5 investigates the transformation and release of P during pyrolysis of a P-rich biomass under different conditions;
- Chapter 6 reports the effect of phosphorus with different occurrence forms on char structure and char reactivity;
- Chapter 7 investigates the roles of *in situ* volatiles with distinctly-different chemistry in char structure and char reactivity during volatile–char interactions;
- Chapter 8 demonstrates the influence of water vapours on PM emission during oxyfuel combustion of char and *in situ* volatiles from fast pyrolysis of a contaminated wood;
- Chapter 9 reveals the roles of *in situ* volatile–char interactions on PM emission

during combustion of *in situ* volatiles;

- Chapter 10 investigates the effect of volatile–char interactions on PM emission during combustion of different biosolid char samples under air and oxyfuel conditions;
- Chapter 11 draws the major conclusions in the present study and points out the recommended work for future research.



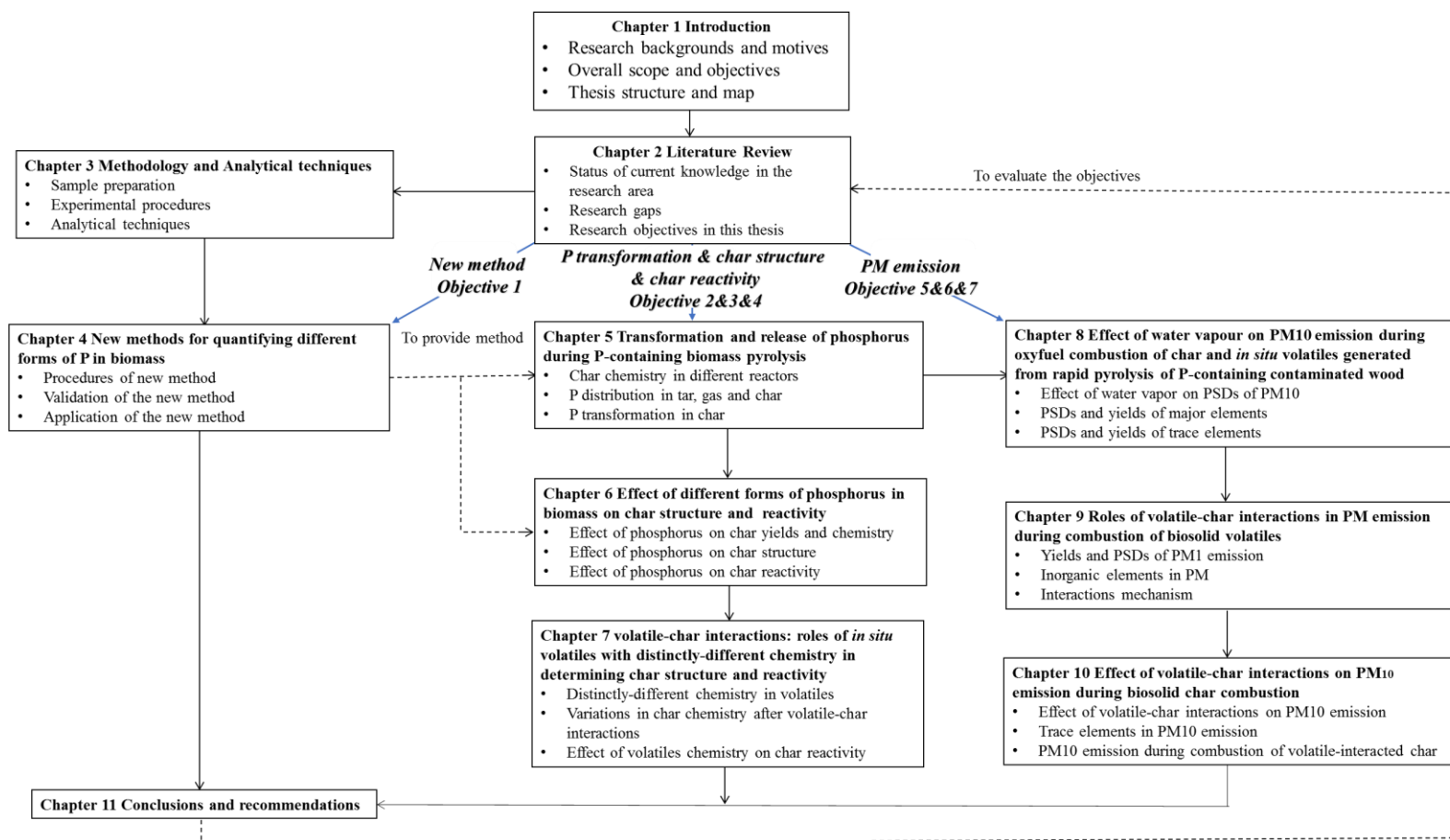


Figure 1-1 Thesis map

## CHAPTER 2 LITERATURE REVIEW

### 2.1 Introduction

Phosphorus is one of the key elements in solid fuels and the proper utilization of those P-containing solid fuels for heat and power production is of great significance for combating climate change.<sup>4,21</sup> The abundant supply of P-containing solid fuels and its significant economic values guarantee their long-term utilization.<sup>26,27</sup> Various technologies have been developed to utilise P-containing solid fuels, among which combustion is still considered as the most practical and economical.<sup>4,27,28</sup> However, combustion of P-containing solid fuels still has several operating challenges as well as environmental concerns.<sup>6,21,29-32</sup> One of the major concerns is related to the substantial emission of particulate matter (PM),<sup>12,20,21,23</sup> which is notoriously harmful to the health of human being. In addition, pyrolysis is not only a promising technology for processing P-containing solid fuels, but also the first step during combustion.<sup>33,34</sup> On the one hand, the structure and reactivity of the char produced from pyrolysis can significantly influence the efficiency and stable operation of the combustion system.<sup>35-38</sup> Furthermore, the transformation of phosphorus during pyrolysis can directly affect the issues generated during subsequent combustion.<sup>13,39</sup> Therefore, understanding char structure and reactivity, P transformation, and PM emission is fundamentally significant for the sake of environment and economic benefit.

Accordingly, the objective of this chapter is to review the factors governing char structure, char reactivity and PM emission with the focus adjusted on the roles of phosphorus in pyrolysis and combustion of P-containing solid fuels. It starts with a brief description of the sources and issues of P-containing solid fuels, then move to the occurrence of phosphorus in solid fuels, the existing methods for the

quantification of different forms of phosphorus, char structure and reactivity, followed by the transformation and release of phosphorus as well as PM emission during P-containing solid fuel combustion. This chapter concludes with the specific research gaps identified by the literature review and the objectives of this PhD project.

## **2.2 Sources and issues of P-containing solid fuels**

### **2.2.1 Sources of P-containing solid fuels**

Phosphorus plays key roles in growth or energy storage in all life forms.<sup>1</sup> Therefore, phosphorus is widely present in both plant and animal cells at variable concentrations.<sup>7</sup> Those P-containing solid fuels are widely available to energy industry and are considered as an important source for thermochemical applications as a strategy to reduce fossil fuel consumption and thereby CO<sub>2</sub> level in atmospheres.<sup>4</sup> According to its origin, P-containing solid fuels could be categorized into plant tissues, municipal solid wastes, animal wastes, and coal samples. Notably, compared with other solid fuels, coal samples usually have significantly low contents of phosphorus,<sup>21</sup> thus it is not considered in this study.

- **Plant tissues**

Plant including land and aquatic plant is the primary P-containing solid fuels.<sup>40</sup> Phosphorus plays important roles in biological activities, such as photosynthesis, phosphorylation and metabolism.<sup>1</sup> It is also a requisite component of nucleic acid structure and therefore is important in cell division and development of new tissues.<sup>7</sup> In addition, phosphorus is associated with energy transformations in plants. A plant first absorbs bioavailable phosphorus in ionic forms from soil or water by root systems and then transfers between different plant tissues. Almost all plant tissues contain phosphorus at various contents.<sup>7</sup> Particularly, seed-originated biomass such as grain,

bran or rapeseed meal/cake (a by-product from biodiesel production) is characterized by its significantly high P content compared to other plant tissues.<sup>4</sup>

- **Municipal solid waste**

Municipal solid waste includes biosolid and contaminated solid waste. Biosolid is by far the most abundant by-product of wastewater treatments and is undergoing a rapid growth.<sup>5,41</sup> However, biosolid may contain some undesirable components, e.g. organic and inorganic toxic substances, and pathogenic or disease-causing micro-organisms.<sup>32</sup> The abundant toxic compounds in biosolid, especially heavy metals, could be dangerous to both plants and animals.<sup>23</sup> Particularly, biosolid has a high phosphorus content and is a potential source of P nutrient.<sup>39</sup> However, the significant presence of phosphorus and nitrogen in biosolid may lead to uncontrollable growth of aquatic plants.<sup>4,42,43</sup> Therefore, its processing and disposal is a complex environmental problem in this field.<sup>44</sup>

Contaminated solid waste is generated from various applications of biomass materials, including demolition wood, packing wood, phytoremediation scavengers, chromated copper arsenate treated wood and paper recycling wastes etc.<sup>45,46</sup> During these applications, concentrations of some harmful inorganic species (such as As, Cd, Cr, Cu, Hg, Mn, Ni, Pb, Se, Tl and V) might be elevated in the resultant contaminated biomass waste.<sup>43,47</sup>

The abundant heavy metals render the disposal or process of biosolid and contaminated solid waste extremely cautious.<sup>5</sup> Currently, the main outlets for disposal of biosolid and contaminated solid waste are recycling as fertilizer, land filling, dumping in the sea and thermochemical utilization.<sup>5,41,44,48</sup> However, thermochemical utilization is still considered as a promising and practical approach,<sup>5</sup> other pathways are increasingly limited due to the potential soil and water pollution caused by heavy metals and phosphorus in these solid wastes.<sup>48</sup>

- **Animal wastes**

Animal wastes mainly come from livestock, poultry, dairy production and aquaculture.<sup>49</sup> It can be manure from animals or by-products of meat or fish processing.<sup>50</sup> The animal waste production was estimated to be 369 million tons in US alone in 2012.<sup>51</sup> However, animal waste is a critical concern to the public and environment because it has the potential to spread pathogens and contaminate both water and atmospheres.<sup>50,52</sup> Therefore, a proper disposal of animal wastes is a major sanitation problem in the world. Animal wastes have been applied as organic manure in traditional farming and remain an important source of nitrogen and phosphorus in modern agriculture.<sup>8,53</sup> Part of animal wastes could also be fermented to produce combustible gases such as methane.<sup>54</sup> However, those method are not effective in killing the pathogens in animal wastes.<sup>55</sup> Alternatively, some animal wastes, such as chicken litter and meat and bone meal (MBM) have been used as a secondary fuel for co-combustion with coal.<sup>56,57</sup>

### **2.2.2 Operational challenges**

Practically, combustion is the most important method for processing P-containing solid fuels. It uses over a range of outputs to convert the chemical energy stored in solid fuels into heat, mechanical power, or electricity using various facilities such as stoves, furnaces, boilers, steam turbines.<sup>5,58,59</sup> Stationary combustion of these P-containing solid fuels or co-combustion with coal is especially attractive because of its high conversion efficiency ranging from 20% to 40%.<sup>60</sup> However, the combustion of P-containing solid fuels is regarded as a complex process with technical challenges as well as environmental concerns associated with the typical fuel characteristics, i.e. high P contents.

- **Slagging**

During combustion at high temperatures, P-containing solid fuels have a high tendency to form slag where the behaviour of phosphorus seems to play a critical role.<sup>4,29</sup> For example, recent researches on combustion of different cereal grains have concluded that phosphorus could combine with alkali and alkaline earth metallic species (AAEMs) and silicon to form low-temperature melting crystalline phases, thus aggravating slagging during P-containing solid fuels combustion.<sup>2,3,29</sup>

- **Corrosion**

It is known that acidic gases (such as HCl and SO<sub>2</sub> or/and SO<sub>3</sub>) in flue gas will cause corrosion issues during solid fuel combustion.<sup>30,61</sup> High P content in P-containing solid fuels can accelerate corrosion for the following reason.<sup>27</sup> Generally, the acidic gas can condensate in presence of alkali metals as a result of chemical reaction to form alkali salts (such as sulfates, chlorides, carbonates, and phosphates). Among these salts, phosphates are the most thermally stable species.<sup>27</sup> Therefore, in high P-containing flue gas, the available alkali metals will first react with P to form phosphates, and result in other acidic gases remaining in flue gas and aggravating corrosion.

- **Bed agglomeration**

Bed agglomeration is known to occur during P-containing solid fuel combustion or co-combustion with coal.<sup>26,31,62</sup> A recent study further revealed that potassium–phosphate chemistry is the key factor dominating bed agglomeration.<sup>3,31</sup> Specifically, potassium phosphate first attacks silica sand surface and form a continuous and uniform K-rich layer, followed by formation of potassium silicates with a low melting point.<sup>31</sup> Then calcium in a form of calcium chloride could be transported to the sand surface to generate sticky layers of K-Ca-silicates. These sticky layers might further attract more phosphorus-rich particles, thus accelerating bed

agglomeration.<sup>31</sup>

- **Deactivation of catalyst**

Phosphorus species in P-containing solid fuels have been reported to increase deactivation rates of selective catalytic reduction (SCR) catalysts in coal fired power plants.<sup>56</sup> An investigation into co-combustion of MBM and biosolid with coal found that P-containing acid could cause deactivation of active vanadia ( $V_2O_5$ ) sites of SCR catalyst.<sup>63</sup> The deactivation of SCR catalysts also depends on combustion temperature and phosphorus/vanadia ratio.<sup>64</sup> Beck et al. revealed out that pore condensation caused by deposition of P-containing flue gas is a major deactivation mechanism.<sup>56</sup>

### 2.2.3 Environmental concerns

The major environmental concerns associated with utilization of P-containing solid fuels are eutrophication in water system and particulate matter (PM) emission in atmospheres.

- **Eutrophication**

Eutrophication characterized by excessively rapid growth of plant and algae is caused by the enrichment of mineral nutrients (especially P and N) in water system,<sup>65</sup> which has long been regarded as a major cause of aquatic ecosystem impairment. One prime source of P is from thermochemical processing of P-containing solid fuels,<sup>66</sup> where P can be released in gas form or remained in the by-products (i.e. char, ash and fly ash) thus potentially reinforcing the eutrophication.<sup>53</sup>

- **PM emission**

P-containing solid fuel combustion would generate large quantity of PM including fly ash particles and unburned soot.<sup>21</sup> The size of those PM can range from nanometre to

millimetre.<sup>67,68</sup> While large PM particles could be collected by gas cleaning devices, PM with size smaller than 10  $\mu\text{m}$  ( $\text{PM}_{10}$ ) could be potentially emitted with exhaust gas and contribute to air pollution.<sup>19</sup> Therefore,  $\text{PM}_{10}$  is an important indicator of air pollution since it can result in several diseases threatening human health.<sup>22</sup> In addition, fine PM particles can also induce ash-related issues (such as slagging, fouling, corrosion), lowering the running efficiency and shortening the life of combustion facilities.<sup>68</sup> Therefore, a thorough understanding of  $\text{PM}_{10}$  emission during combustion of P-containing solid fuels is critical for air pollution control and developing solutions for those operational issues, and thus an important aspect of this PhD project.

In summary, P-containing solid fuels have ample supply and their disposal demands careful regulation due to the potential environmental concerns. Thermochemical utilization of P-containing solid fuels can provide valuable energy resource at a competitive cost; however, the operating challenges warrants further research and development.

### 2.3 Occurrence of phosphorus in solid fuels

Phosphorus can present in solid fuels in various occurrence forms that are categorized into inorganic phosphorus and organic phosphorus.

#### 2.3.1 Inorganic phosphorus

Inorganic phosphorus mainly exists in form of orthophosphate ( $\text{PO}_4^{3-}$ ) in most solid fuels.<sup>69</sup> However, orthophosphate has a strong tendency to form condensed phosphate via P–O–P bonds.<sup>70</sup> Typical condensed phosphates include metaphosphate [ $\text{P}_n\text{O}_{3n}^{-n}$  ( $n \geq 1$ )] and polyphosphate [ $\text{P}_n\text{O}_{3n+1}^{-(n+2)}$  ( $n > 1$ )], which are reported to widely present in P-containing solid fuels (e.g. plant, biosolid and poultry waste as well as their char product). These inorganic phosphorus generally combine with metallic elements (e.g. Na, K, Ca, Mg, Fe, Al) to form phosphate salts or minerals such as variscite,<sup>71</sup> apatite



---

and calcium phosphate silicate.<sup>72</sup>

### 2.3.2 Organic phosphorus

In general, organic phosphorus is more likely bonded to organic structure via phosphate ester bonds (P–O–C) rather than P–C bonds.<sup>73</sup> The phosphate group linked to organic molecules is mainly orthophosphate groups ( $-\text{PO}_4$ ) while pyrophosphate ( $-\text{P}_2\text{O}_7$ ) and tripolyphosphate groups ( $-\text{P}_3\text{O}_{10}$ ) may also present in some P-containing organic species, such as adenosine diphosphate (ADP) and adenosine triphosphate (ATP).<sup>7</sup> Depending on the chemical structure of the linked organic molecules, organic P-containing species in solid fuels can be categorized into sugar phosphate, inositol phosphate, nucleotides, phospholipid and other organic structures such as nucleic acids.<sup>7,74</sup>

Overall, different solid fuels contain various forms of phosphorus. For example, phosphorus in seed and algae-originated biomass is dominantly organic P,<sup>75</sup> while that in animal bone waste and plant biomass is mainly inorganic P.<sup>76</sup> The occurrence form of P and its combinations with other inorganic species determines the mobility and bioavailability of phosphorus in solid fuels. More importantly, it could potentially result in different transformation and release behaviours during thermochemical utilization of those P-containing solid fuels.

## 2.4 Methods for quantifying phosphorus of various occurrence forms in solid fuels

As described in Section 2.3, phosphorus is present in P-containing solid fuels in various occurrence forms. It is prerequisite to quantify these phosphorus species for the proper handling and utilization of P-containing solid fuels. This section reviews the existing methods for quantification of phosphorus species in solid fuels, with detailed elaboration on the disadvantages of each method.

### 2.4.1 Conventional methods for quantifying P with different forms in solid fuels

Several methods have been developed to separate or analyse the form of phosphorus in various solid fuels over the last several decades, including methods based on colorimetry,<sup>9,69,77-83</sup> physicochemical fractionation method,<sup>40,53,74,82,84-86</sup> Enzyme hydrolysis,<sup>42,87,88</sup> and sequential extraction method.<sup>1,49,75,89-99</sup> Table 2-2 presents some reported methods for separating and analysing various forms of P in solid fuels with the brief description summarized below.

- Colorimetry

The colorimetry method was first proposed by Bell and Doisy in 1920 and it is still the fundamental method for quantification of inorganic P.<sup>80</sup> P-containing solid fuel such as plant tissues is first extracted using acid solutions, and then the acid extracts react with vanadate and molybdate under acid conditions to form a blue phosphomolybdate complex, which can then be quantified by spectrometer. However, only orthophosphate could form the blue complex and be quantified, the non-orthophosphate such as condensed phosphate and organic phosphorus cannot generate coloured complex,<sup>9,82,83</sup> thus resulting in underestimation of both inorganic and organic P in solid fuels.

- Physicochemical fractionation

The physicochemical fractionation method is developed in recent decades via combination with sophisticated detection technologies such as X-ray absorption near edge structure (XANES)<sup>53,74,82</sup> and <sup>31</sup>P nuclear magnetic resonance spectroscopy (NMR).<sup>40,84,85</sup> Compared with the colorimetry method, physicochemical fractionation is more powerful and can *in situ* detect different forms of P in P-containing biomass without destroying P-containing biomass.<sup>9</sup> Nevertheless, it demands advanced detection technologies which are not only uneconomical and inaccessible but also

time-consuming in terms of sample preparation.<sup>9</sup> In addition, the quantification of P using these techniques is known to have high detection limits and requires experienced spectroscopists.<sup>9,82</sup>

- Enzyme hydrolysis

Enzyme hydrolysis is mainly used in detecting organic phosphorus in animal waste and plant tissues.<sup>42,87,88</sup> This method is based on the hydrolysis of organic phosphate into inorganic phosphate in the presence of specific enzymes, such as alkaline phosphatase and phytase as catalyst in different buffer solutions.<sup>88</sup> However, it can only target specific organic phosphorus in plant tissues or animal waste due to the unicity of those enzymes.<sup>97</sup> In addition, the quantification of inorganic P after enzyme hydrolysis is also based on colorimetry method, thus also incompetent for other inorganic phosphorus such as pyrophosphates and metaphosphates.

- Sequential extraction

Sequential extraction methods are practical and commonly employed in phosphorus fractionation due to the low cost and relatively simple procedure. Several sequential extraction methods have been developed to separate and quantify different forms of phosphorus in plant and animal waste using different solutions, as shown in Table 2-2. Among those sequential extraction methods, the standards, measurements and testing (SMT) method<sup>89,91,92</sup> is most commonly used to quantify organic and inorganic P in P-containing biomass with the protocol shown in Figure 2-1. This method is initially designed for quantification of bioavailable P in sediment and was later adopted to indirectly quantify organic P in solid fuels. It bases on the assumption that inorganic P is soluble in the acid solution (1M HCl) while the acid-insoluble organic P-containing specie can be converted into acid-soluble orthophosphate after thermal treatment (at 450 °C for 3 h in air).

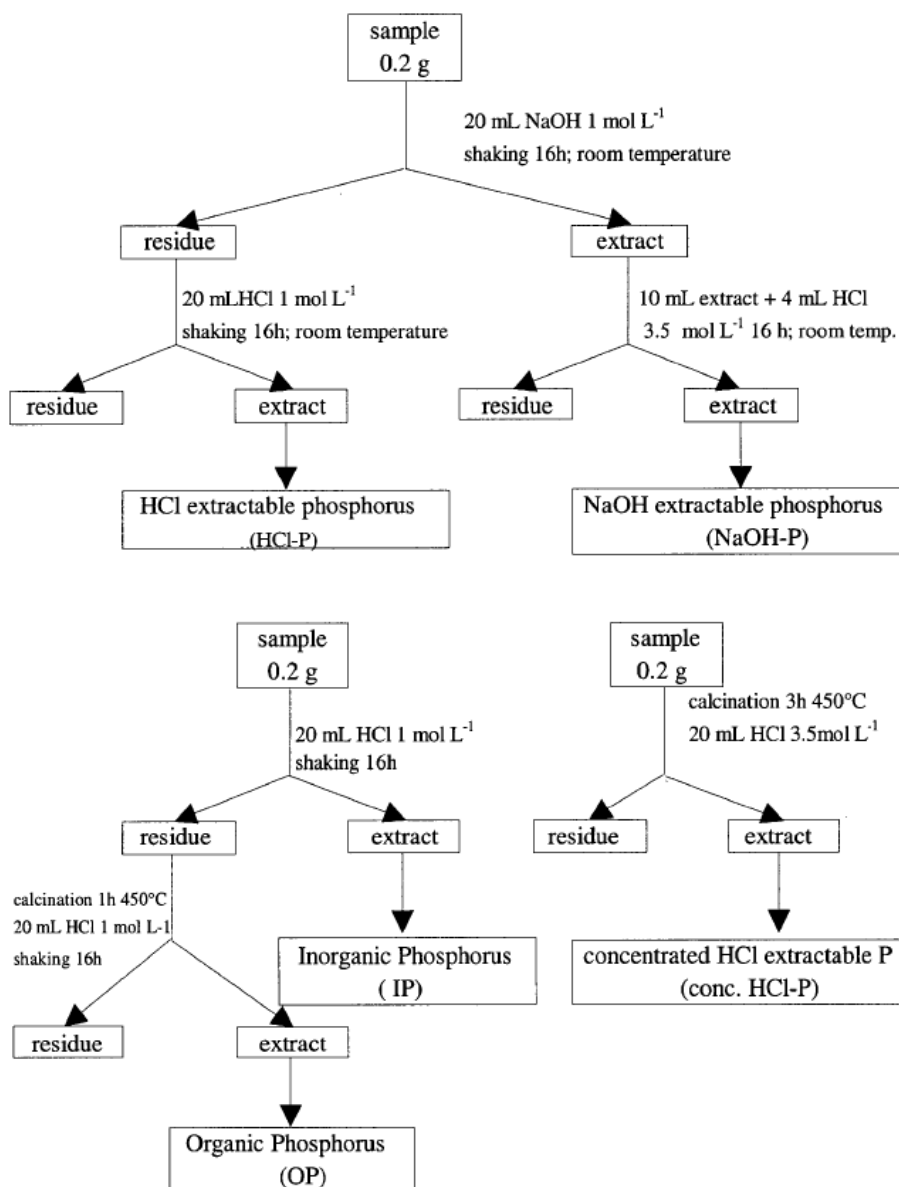


Figure 2-1 The SMT method protocol for quantifying organic and inorganic phosphorus in solid fuels<sup>89</sup>

However, these existing sequential extraction methods can potentially lead to low mass balance of phosphorus for some solid fuels due to at least the following five major shortcomings:

- First, these sequential extraction methods use acids for extraction then quantify

acid-soluble inorganic P using the aforementioned colorimetry method. However, other abundant inorganic species such as Si, Fe, Cu, etc. in solid fuels may also be extract and interfering P quantification using spectrophotometer.<sup>9,81</sup>

- Second, the inorganic condensed phosphates in the acid extract can be misclassified as organic P as they are not detectable using the subsequent colorimetry method.<sup>9,82,83</sup>
- Third, the SMT method<sup>89,91,92</sup> assumes that all the inorganic P are in the acid solution (1M HCl) while all the organic P-containing species are in the residue and can be converted into acid-soluble orthophosphate after thermal treatment. Such assumptions may be invalid as some organic P are soluble in the acid solution and some of the organic P in the residue may be lost during thermal treatment, which will be evaluated in Chapter 4.
- Fourth, existing sequential extraction methods assume that all inorganic P are soluble in acids, while acid-insoluble P compounds, such as  $\text{AlPO}_4$ , long-chain condensed phosphate<sup>100</sup> and phosphorus combined with silicate which may present in some solid fuels<sup>101</sup> are not taken into consideration.
- Fifth and last, the existing sequential extraction methods need at least 0.6 g of solid fuel samples. However, in lab-scale experiments, producing such a required quantity for some samples (such as char) might be very time-consuming.

Table 2-1 A summary of some published methods used for determining phosphorus in solid fuels<sup>1,9,40,42,49,53,69,74,75,77-99</sup>

Method	Literature	Sample	P forms	Sample size (g)	Chemicals	Instruments	Advantages	Disadvantages
<b>Colorimetry method</b>	Refs <sup>69,77-80</sup>	Biomass, biosolid and animal tissue	Acid-soluble orthophosphate	1.0	Acids, Vanadate and molybdate	Spectrophotometer	1. Moderate conditions. 2. accurate in determining orthophosphate.	1. interference from Si, Fe, Cu, etc. <sup>81</sup> 2. cannot quantify non-orthophosphate. <sup>9,82,83</sup>
<b>Physico-chemical fractionation method</b>	Refs <sup>53,74,82</sup>	Solid samples	Organic and inorganic P	1.0		XANES	can analyse samples <i>in situ</i> .	1. not easily accessible and require experienced spectroscopists. <sup>82</sup> 2. high detection limits
	Refs <sup>40,84,85</sup>	Solid samples	Organic and inorganic P	1.0	NaOH and EDTA	<sup>31</sup> P NMR	1. Common chemicals. 2. can <i>in situ</i> detect the exact forms of some P.	1. Cannot detect all organic and inorganic P. <sup>86</sup> 2. <sup>31</sup> P NMR is not easily accessible. 3. high detection limits and have interference from paramagnetic cations. <sup>82</sup>
<b>Enzyme hydrolysis method</b>	Refs <sup>42,87,88</sup>	Animal tissue, algae, biomass	Organic P	1.0	Phosphatase	Spectrophotometer	1. simple procedure. 2. moderate conditions.	1. cannot detect non- hydrolysable organic P. 2. cannot detect inorganic P and exact forms of organic P.
<b>Sequential extraction</b>	Refs <sup>89,91,92</sup> for SMT method	Sludge, biosolid and coal	organic P and acid-soluble inorganic P	0.6	HCl, NaOH solutions	Spectrophotometer	1. accessible chemicals. 2. can detect different inorganic P.	1. Poor accuracy and P recovery. <sup>90</sup> 2. limited information on organic P occurrence forms. 3. high temperature conditions. 4. cannot detect acid-insoluble inorganic P.
	Refs <sup>1,93-96</sup>	Biomass	acid-soluble organic and inorganic P	1.0-5.0	Acids, organic solvents, MgCl <sub>2</sub> and NH <sub>4</sub> Cl.	Spectrophotometer	1. accessible chemicals. 2. moderate conditions. 3. can detect some organic P.	1. limited information on inorganic P species. 2. cannot achieve complete P recovery. <sup>97</sup> 3. cannot detect acid-insoluble inorganic P.
	Refs <sup>49,75,98,99</sup>	Animal tissue	organic P	1.0-5.0	Acids, organic solvents and KOH	Spectrophotometer	1. accessible chemicals. 2. Simple procedure.	limited information on inorganic P species.

### 2.4.2 Summary

Through several methods have been developed over the last several decades to separate and quantify different forms of phosphorus, none of the existing methods can be applicable to accurately quantify both organic and inorganic phosphorus in P-containing solid fuels in lab-scale. Therefore, a new method is necessarily developed to achieve this purpose, which is one of the objectives of this study.

### 2.5 Pyrolysis characteristics of P-containing solid fuels: volatile–char interactions, char structure and char reactivity

Pyrolysis is a relatively low-cost technology for converting biomass into high-value biofuels including bio-oil, char and gas.<sup>34</sup> More importantly, it is also the first step of combustion and gasification.<sup>15</sup> After pyrolysis, the conversion of char is the decisive step for subsequent combustion and gasification reactions. The overall efficiency of char conversion highly depends on char reactivity which is governed by char structure. In addition, the *in situ* generated volatiles during pyrolysis can also influence the subsequent combustion and gasification reactions via the so-called volatile–char interactions.<sup>15</sup> Therefore, this section first introduces the volatile–char interactions during solid fuels pyrolysis and then summarizes the factors governing char structure and char reactivity, followed by a review on the role of phosphorus in solid fuel pyrolysis. Finally, the research gaps in the area of char structure and char reactivity are summarized.

#### 2.5.1 The significance of volatile–char interactions during solid fuels pyrolysis

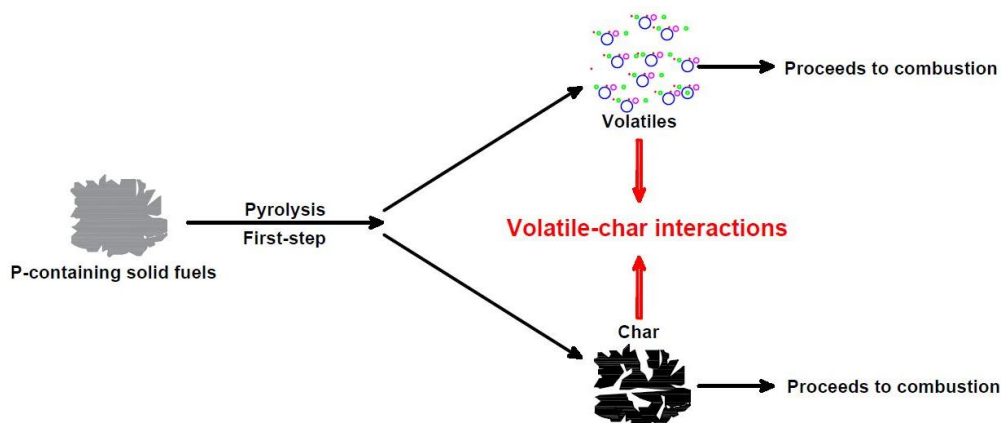


Figure 2-2 A schematic diagram of volatile–char interactions during solid fuels pyrolysis or combustion

Once solid biomass particles are subjected into a reactor for combustion, they will first experience rapid devolatilization and generate volatiles and char particles. Conventional approaches generally assume that the volatiles and char proceed independently to combustion process. However, as shown in Figure 2-2, volatiles and char could strongly interact with each other during the ongoing pyrolysis and this volatile–char interactions may potentially take place under various conditions.<sup>102</sup> For example, in a fluidised-bed reactor, solid fuel particles are continuously fed into the reactor and continuously generate fresh volatiles, the pyrolyzing char particles will be constantly surrounded by the volatiles cloud. The *in situ* volatiles contain abundant reactive species including radicals (such as H radicals) as reactive intermediates<sup>103</sup> and those reactive species could strongly react with char particles for an extensive period in the bed, leading to significant changes in char and volatiles properties.<sup>16,17</sup> Actually, the *in situ* volatiles also inevitably interact with char particles in many other commonly used reactors such as fixed-bed and entrained-flow reactors although could be less significant.<sup>17,102</sup> In other words, different reactor configurations could result in different extents of volatile–char interactions and thus vary char and volatiles properties to different extents.<sup>104</sup>



### 2.5.2 Factors influencing char structure and reactivity

Char conversion is the rate-controlling step of the combustion processes. The char combustion rate can significantly affect heat release, char burnout as well as temperature profile, and thus is of great significance to energy efficiency and stable operation of combustion systems.<sup>105</sup> Generally, according to solid/gas reaction kinetics,<sup>106,107</sup> char combustion can occur in three different kinetic regimes including chemical reaction, bulk diffusion, gas-phase diffusion. The exact kinetic regime depends on combustion temperature, char particle size, reactor type, and reaction atmospheres.<sup>105</sup> In the case of pulverized solid fuel combustion, the small sizes of fuel particles promotes rapid boundary layer diffusion, so the heterogeneous char combustion is governed by the intrinsic reactivity of char.<sup>105</sup> Therefore, intrinsic char reactivity is a critical factor to consider in reactor design and system operation for thermochemical processes.<sup>108</sup> Extensive studies<sup>10,16,18,105,109</sup> have been conducted to investigate the intrinsic char reactivity. It was found that intrinsic char reactivity is directly affected by inherent catalysts in char and char structure. Furthermore, the char structure actually determines the physico-chemical forms of catalytic inorganic matter bonded to the carbon skeleton at the molecular level.<sup>17,35</sup> Therefore, it is essential to understand the structural characteristics of char prepared under specific conditions and its effect on intrinsic reactivity of char samples. The factors influencing char structure and char reactivity are summarized below.

- Operating parameters

Operation parameters influencing char structure and reactivity mainly includes pyrolysis temperature, pressure and heating rate. Particularly, pyrolysis temperature is the dominating factor governing char structure and reactivity.<sup>110</sup> Specifically, char structure becomes less amorphous with increasing pyrolysis temperature,<sup>105</sup> thus resulting in the reduction in intrinsic char reactivity.<sup>111</sup> Lu et al.<sup>105</sup> found that char

structure becomes more ordered with decreasing heating rate and char reactivity increases with increasing heating rate.<sup>36,112</sup> During biomass pyrolysis, increasing pyrolysis pressure is found to decrease intrinsic reactivity.<sup>113</sup>

- Thermal annealing

Hurt et al.<sup>110</sup> investigated the effect of short thermal annealing (0–3 s) at 700–2400 °C on char reactivity using biomass (i.e., pinus radiata) and concluded that thermal annealing between 10 ms and 2 s has no significant effect on char reactivity. Wu et al.<sup>114</sup> conducted thermal annealing processes at mild temperatures (750–900 °C) using mallee wood and found that thermal annealing plays an important role in char reactivity, especially during the initial 60 min. During thermal annealing, at least part of the reactive and amorphous carbon structures of char are converted into larger and more inert ring systems, although little graphitization of carbon structure with three dimensional development is evidenced.

- Inherent catalysts

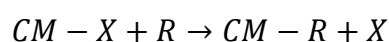
The roles of inherent catalysts in char reactivity have been extensively investigated in recent decades. Alkali and alkaline earth metallic species (AAEMs) are the most common and pronounced catalytic species in char,<sup>35</sup> while other inorganic species such as Fe and Ni may also have non-negligible catalytic effect on char reactivity.<sup>115</sup> Generally, more concentrated inherent catalysts in char lead to higher char reactivity.<sup>10,116</sup> However, the physico-chemical forms<sup>10,117,118</sup> and distribution<sup>111</sup> of inherent catalysts could also play significant role in char reactivity. For example, Na in form of NaCl and sodium carboxylates (–COONa) has very different catalytic effects on char reactivity.<sup>118</sup> Alkali metals may react with silica to form silicates during pyrolysis, thus reducing char reactivity.<sup>115</sup> Initially, char reactivity can be enhanced by highly dispersed CaO on char surface however it could be weakened by the growth of CaO crystallite with the progress of char being consumed.<sup>111</sup> In

addition, char structure can considerably affect the catalytic activity of some inherent inorganic species.<sup>10,116</sup> For instance, the catalytic activity of Na is reduced with the increase in aromaticity of char structure that takes place with increasing char conversion level. It is also reported that the presence of AAEMs could facilitate the formation of amorphous carbon structure in char, which in turn affects the dispersion of Na and thus its catalytic performance.<sup>16,37,116</sup>

- Volatile–char interactions

As described in Section 2.5.1, volatiles could inevitably interact with char particles during pyrolysis and combustion of solid fuels, which significantly influences the properties of both volatiles and char. Wu et al.<sup>16</sup> first investigated the effects of volatile–char interactions on the reactivity of chars from a Victorian brown coal using a novel reactor configuration at 900 °C. It was found that volatile–char interactions can result in drastic decrease in char reactivity due to the volatilization of Na and the condensation of ring structures in char.<sup>16</sup> A further study using biomass at 800–1000 °C demonstrated that volatile–char interactions could also lead to additional volatilisation of other AAEMs with the monovalent and divalent species behaving differently.<sup>103</sup>

The essence of volatile–char interactions is considered as the reactions between radicals in volatile and the active sites on char,<sup>103</sup> as illustrated by the following equation:<sup>102</sup>



where CM represents char matrix, X represents active AAEMs on char matrix, and R represents radicals in volatile. The radicals displace the AAEMs on char matrix and thus lead to volatilization of AAEMs. The volatilization of AAEMs caused by volatile–char interactions is different in biomass and brown coal due to their compositional and structural differences.<sup>103</sup>

In addition, H radicals in volatiles are known to play a vital role in volatile–char interactions due to their mobility and small size. Specifically, H radicals could deeply penetrate into the char matrix and adsorb onto aromatic ring systems, and then break cross-linking structures and activate aromatic rings.<sup>102</sup> The activated aromatic rings favour the condensation of small aromatic rings (less than 6 fused rings) to form large ones, making char structure more inert. Moreover, volatile–char interaction is also reported to greatly influence the amounts of O-containing functional groups in char during brown coal gasification.<sup>17</sup>

Those previous studies are based on single volatiles, while during co-gasification or combustion, different solid fuels samples with distinctly-different fuel chemistry might be simultaneously fed into the reactors, and thus generate volatiles with distinctly-different chemistry. For example, waste plastic such as polyethylene (PE) contains carbon and hydrogen only, hence its pyrolysis produces volatiles free of oxygen while pyrolysis of fuels rich in oxygen produces volatiles containing abundant oxygenated species. Therefore, *in situ* volatiles with distinctly-different chemistry could be generated during pyrolysis due to the differences in the chemistry of raw fuel. S. Krerkkaiwan et al.<sup>119</sup> investigated the interactions between different coal char samples and volatiles generated from xylene, cellulose and rice straw in a rapid-heating thermobalance reactor. The results show that the volatiles from rice straw exert the greatest influence on reducing char gasification reactivity. This was attributed to the high aromatic compounds in rice straw volatiles, which trends to form inert coke/soot over char surfaces. However, it is still unclear about the specific role of *in situ* volatiles with distinctly-different chemistry in determining carbon skeleton structure and the resultant effects on char reactivity. This will be studied in this PhD project.

- Reaction atmospheres

The effects of various reaction atmospheres on char structure and reactivity have been studied, including steam and O<sub>2</sub>. Keown et al.<sup>109</sup> reported that char reactivity could be significantly reduced even within 20s during gasification of char with steam due to the enhanced release of AAEMs and condensation of carbon structure caused by the generation of abundant H radicals. Another study<sup>105</sup> shows that the gradual consumption of carbon in air decreases the amorphous fraction of char and increases the aromaticity and average crystallite size of char, thus decreasing char reactivity.

### 2.5.3 Role of phosphorus in solid fuels pyrolysis

As one of the most significant inorganic elements, phosphorus plays an important role in pyrolysis of solid fuels. Investigations on fast pyrolysis of P-impregnated beech wood showed that P could catalyse the pyrolytic decomposition of biomass and modify the yields of pyrolysis products.<sup>33,120</sup> Specifically, when P concentration is below 0.5 wt %, increasing P in biomass decreased the bio-oil yield and increased yields of char and pyrolytic water.<sup>33</sup> The impregnation of (NH<sub>4</sub>)<sub>2</sub>HPO<sub>4</sub> onto pine wood with zeolite as a catalyst could improve the yields of high-value petrochemicals (olefins and aromatic hydrocarbons) while decrease the yields of low-value alkanes during catalytic fast pyrolysis of pine wood and low-density polyethylene mixtures.<sup>121</sup> Further increase (above 0.5 wt %) in P concentration has minimal effect on fast pyrolysis products distributions while may cause serious processing problems such as agglomeration and corrosion, as elaborated in Section 2.2.2. Jones et al.<sup>122,123</sup> found that P shifts cellulose decomposition to lower temperature during pyrolysis via catalysing dehydration and subsequent depolymerization reactions. The addition of P is also reported to enhance the formation of light aliphatic hydrocarbons during catalytic pyrolysis of biomass.<sup>33</sup>

Recent studies<sup>124-126</sup> on the activation of carbon materials using highly concentrated

(85%, w/w) phosphoric acid show that P could form thermally stable phosphate-like complex that remain on the carbon surface and act as a physical barrier for the reaction with oxygen, thus resulting in the high oxidation resistance during non-isothermal oxidation of activated carbon from 300–900 °C. However, the contents of phosphorus in P-containing solid fuels is much lower (< 5 wt%) and whether the mechanism on the highly ordered carbonaceous materials could be extrapolated to the P-containing solid fuels is unknown. More importantly, the effect of different forms of phosphorus on the evolution of structure and intrinsic reactivity of char samples still needs to be investigated.

#### **2.5.4 Summary**

Volatile–char interactions can significantly influence char structure and char reactivity. However, the roles of *in situ* volatiles with distinctly-different chemistry are still unclear and thus need further investigation. Additionally, inorganic species especially AAEMs play important roles in enhancing char reactivity and the evolution of char structure during pyrolysis of solid fuels. However, as an indispensable inorganic specie in P-containing biomass, the effects of P with different forms of occurrence on the evolution of char structure and char reactivity are largely unknown. This PhD project will investigate into the roles of both the *in situ* volatiles and P in determining char structure and reactivity.

#### **2.6 Transformation and release of phosphorus during P-containing solid fuels pyrolysis and combustion**

Fundamental understanding on transformation and release of P during pyrolysis is of great importance for thermochemical utilizations of P-containing solid fuels. This section first describes currently reported mechanisms of phosphorus transformation, followed by factors influencing P release during pyrolysis and combustion of solid fuels. Finally, the research gaps in this field are proposed.

### 2.6.1 Phosphorus transformation mechanism during pyrolysis and combustion

The transformation and release of P during pyrolysis and combustion of P-containing solid fuels is relatively less understood compared to other inorganic species such as Na, K, Cl and S in solid fuels. Possible pathways and mechanisms of P transformation are summarized and presented in Figure 2-3.

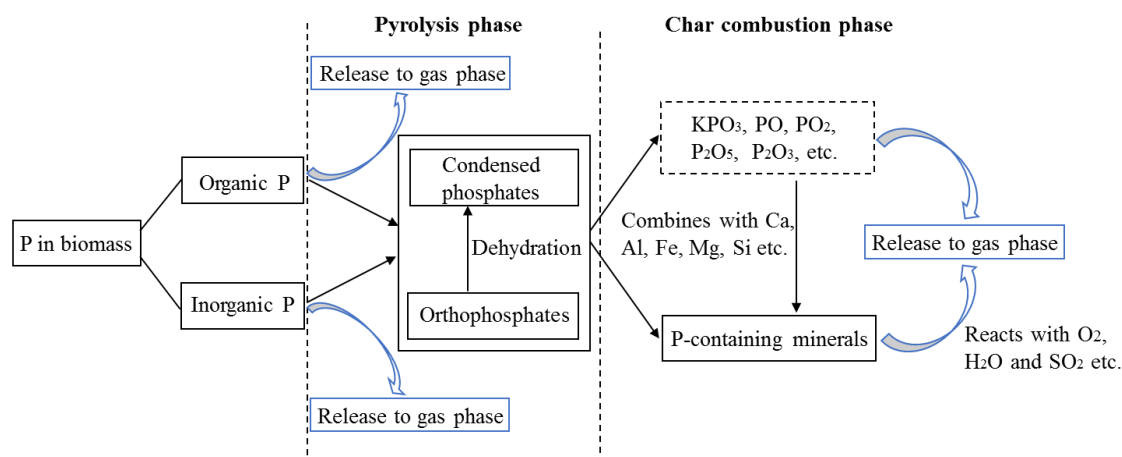


Figure 2-3 Possible mechanisms of P transformation and release during pyrolysis and combustion of P-containing solid fuels, summarized based on literature review findings<sup>4,8,13,21,29,66,127-130</sup>

During pyrolysis phase, organic P is considered thermally unstable and would be rapidly released or/ and mineralised to inorganic P.<sup>128,131</sup> Part of the inorganic P is also reported to be released during this process.<sup>13</sup> Meanwhile, the majority of inorganic P would react with other inorganic species (e.g. Ca, K, Al, Fe) in P-containing solid fuels and be transformed into orthophosphates and condensed phosphates especially pyrophosphates in char.<sup>8,132,133</sup> During pyrolysis, some orthophosphates in char could also be transformed into condensed phosphates via dehydration. For example, dicalcium phosphate (CaHPO<sub>4</sub>) could be decomposed into dicalcium diphosphate (Ca<sub>2</sub>P<sub>2</sub>O<sub>7</sub>) at temperatures lower than 400 °C.<sup>4</sup>

During char combustion phase, some inorganic P in char would be directly released in forms of condensed phosphates and various phosphorus oxides.<sup>134</sup> For example,  $\text{KH}_2\text{PO}_4$  might be transformed into  $\text{KPO}_3$ , which would be vaporized at  $\sim 900^\circ\text{C}$  during solid fuel combustion.<sup>4</sup> While the remaining inorganic P species in char would be further transformed into more stable P-containing minerals via combination with other inorganic species.<sup>4,33</sup> Notably, the released P in gas phase could also react with various inorganic species such as Ca, Mg, Al, Si in solid char samples, thereby returning to solid phase by generating thermally stable P-containing minerals.<sup>4,62</sup> On the other hand, the solid P-containing species could also react with  $\text{H}_2\text{O}$ ,  $\text{SO}_2$  and  $\text{O}_2$ , etc to form gaseous P-containing species such as  $\text{P}_2\text{O}_5$  and  $\text{KPO}_3$ .<sup>4,66</sup> A classic study<sup>4</sup> on rice bran combustion proposed the possible reaction pathways of the P- and K-containing species with K/P molar ratio  $<1$  in gas phase, as summarized in Figure 2-4.

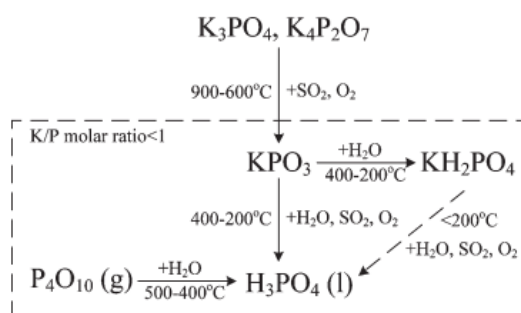


Figure 2-4 Reaction pathways of the P-containing species during rice bran combustion, based on equilibrium calculations<sup>4</sup>

### 2.6.2 Factors influencing P release during pyrolysis and combustion

As stated in Section 2.2, the release of P could directly lead to some operating and environmental issues. Therefore, several studies have been conducted to investigate the factors governing P release during pyrolysis and combustion of P-containing solid fuels. The experimental conditions and main conclusions are summarized in Table 2-2.



The main influence factors include temperatures, atmosphere, occurrence of phosphorus and other inorganic species in solid fuels, which are detailed subsequently.

Table 2-2 A summary of some investigations into P release during pyrolysis and combustion of P-containing solid fuels<sup>4,13,20,56,66,129,135,136</sup>

Study	Sample	Reactor	Temperature	Main conclusions
<b>Pyrolysis</b>				
Liu <sup>66</sup>	Biosolid	Tube reactor	900–1300 °C	Organic P is released at T < 1100 °C while inorganic P is released at T > 1200 °C.
Elias <sup>13</sup>	Biosolid	Tube reactor	25–1300 °C	P is released at T > 800 °C in forms of PO, PO <sub>2</sub> , P <sub>2</sub> and P <sub>4</sub> .
Liaw <sup>20</sup>	Biosolid	Drop-tube/ Fixed-bed reactor	1100–1300 °C	Little P is released at 1100 °C while P is almost completely released at 1300 °C.
Hossain <sup>136</sup>	Biosolid	Fixed-bed reactor	300–700 °C	No inorganic P is released under experimental conditions.
Jiang <sup>135</sup>	Plant biomass	Drop-tube/ Fixed-bed reactor	350–600 °C	P is released at 350 °C and higher temperature leads to enhanced P release.
Wu <sup>4</sup>	Rice bran	Tube reactor	300–900 °C	Little P is released at T < 900 °C
<b>Combustion</b>				
Wu <sup>4</sup>	Rice bran	Tube reactor	500–1100 °C	P is released at T > 700 °C in form of KPO <sub>3</sub> . The addition of Ca species has little influence on P release.
Beck <sup>56,129</sup>	Biosolid and MBM	Industrial boiler	Unknown	Organic P is released at T < 500 °C while inorganic P might be transferred into the gas phase by reacting with H <sub>2</sub> SO <sub>4</sub> and generating gaseous H <sub>3</sub> PO <sub>4</sub> at higher temperatures.

- **Temperature**

Temperature is the dominating factor governing P transformation and release during pyrolysis and combustion of P-containing solid fuels.<sup>134</sup> Jiang et al.<sup>135</sup> investigated P

release during pyrolysis of algae biomass and found that P release starts at ~ 350 °C and higher pyrolysis temperatures lead to enhanced P release. Liaw et al.<sup>20</sup> found that little P is released during biosolid pyrolysis at 1100 °C while complete release of P is achieved at 1300 °C in a drop-tube/fixed-bed reactor. Wu et al.<sup>4</sup> concluded that release of P increases with temperature increase above 700 °C during rice bran combustion in a horizontal tube reactor. It seems that the effect of temperature on P release is contradictory in different studies, possibly due to the different biomass properties and reactor configurations.

- **Atmosphere**

Based on the reaction pathways of the P-containing species during biomass combustion shown in Figure 2-4, H<sub>2</sub>O, O<sub>2</sub> and SO<sub>2</sub> in the atmosphere can significantly enhance P release during pyrolysis and combustion of P-containing solid fuels.<sup>4</sup> Other gases such as CH<sub>4</sub> and CO are also reported to increase P release during biosolid pyrolysis at high temperatures.<sup>66</sup> However, an investigation into the thermal treatment of biosolid under N<sub>2</sub>, CO<sub>2</sub> and air atmospheres found that atmosphere conditions had limited effect on P transformation at 400–800 °C.<sup>127</sup>

- **Occurrence of phosphorus**

Different occurrence forms of P present different volatilities. Generally, organic P can be released at relatively low temperatures during pyrolysis, while the release of inorganic P occurs at high temperatures. For example, the pyrolysis of biosolid in a tube reactor at 900–1300 °C found that organic P could be released at temperature lower than 1100 °C while inorganic P could only be released at temperature higher than 1200 °C.<sup>66</sup>

- **Other inorganic species**

Potassium (K) is considered as the most important inorganic element influencing P release during pyrolysis or combustion.<sup>26,33</sup> Wu et al.<sup>4</sup> concluded that the distribution of P-containing species in flue gas is sensitive to the molar ratio of the released K/P. When the molar ratio of the released K/P is below 1 at temperatures above 500 °C,  $KPO_3$  and  $P_4O_{10}$  are the main inorganic species present in flue gas, while only  $KPO_3$  would present in the gas phase when the molar ratio is above 2 (see Figure 2-4).<sup>4</sup> Ca-containing minerals can effectively inhibit the release of P by forming P-containing minerals.<sup>4,57,129,137</sup> As shown in Figure 2-4, S in biomass could significantly affect P release. For example,  $SO_2$  could react with  $KH_2PO_4$  or  $K_3PO_4$  to form volatile  $KPO_3$  or  $P_2O_5$  under oxidation conditions.<sup>4</sup>  $SiO_2$  is also likely to enhance P release under reducing atmospheres.<sup>66</sup> The roles of other inorganic elements in P release have been rarely investigated.

### **2.6.3 Summary**

Although there have been several studies on the transformation and release of P, the specific mechanisms are still largely unclear. More importantly, some contradictory conclusions are found in different studies possibly due to different biomass properties, various P occurrence forms in biomass and reactor configurations used, as described above. Therefore, further systematic investigations need to be conducted to understand the P transformation and release during biomass pyrolysis and combustion.

### **2.7 PM<sub>10</sub> emission during combustion of P-containing solid fuels**

Solid fuel combustion is an important contributor to significant PM emissions in stationary applications. Extensive studies have been carried out on the formation and emission of PM during solid fuel combustion. This section will give a brief review on the formation mechanisms and characteristics of PM, with emphasis on the distribution and occurrence of phosphorus in PM<sub>10</sub> during P-containing solid fuel combustion under different atmospheres. Additionally, this section also summarizes

the indirect evidence for the effect of volatile–char interactions on PM<sub>10</sub> emission during solid fuel combustion and finally identifies the research gaps.

### 2.7.1 The mechanisms of PM<sub>10</sub> emission during combustion of P-containing solid fuels

The mechanisms of PM<sub>10</sub> formation during fuel combustion in different combustion systems have been well documented, as is shown in Figure 2-5. More specifically, the PM<sub>10</sub> produced from solid fuel combustion consists of submicron aerosol (PM with the aerodynamic diameter < 1 μm, known as PM<sub>1</sub>) and supermicron aerosol (PM with the aerodynamic diameter between 1 and 10 μm, known as PM<sub>1-10</sub>). PM<sub>1</sub> and PM<sub>1-10</sub> have different formation mechanisms and characteristics during solid fuel combustion, which are briefly discussed as follows.

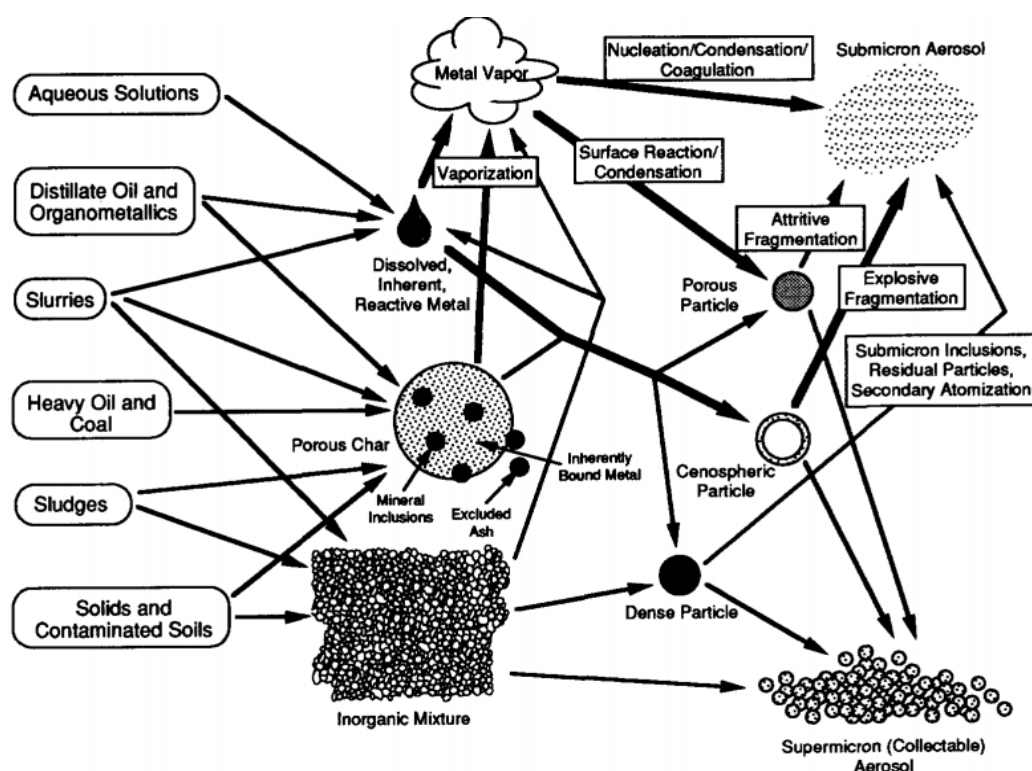


Figure 2-5 Possible controlling mechanisms for PM emission in a combustion system<sup>138</sup>

**Formation mechanism of inorganic PM<sub>1</sub>.** It is well-known that inorganic PM<sub>1</sub> are mainly formed via the “solid-vapour-particle” process.<sup>139</sup> This process includes vaporization of volatile elements and gas-phase reaction, followed by homogeneous nucleation and/or heterogeneous condensation/reaction on the existing particles. The vaporization of volatile elements relies on the volatilities and occurrence forms of these elements as well as the combustion conditions (e.g. combustion temperature and atmospheres).<sup>140</sup> Generally, organic-bound minerals, S, Cl and part of P could be easily released during solid fuel combustion,<sup>139,141</sup> while those metallic elements associated with aluminosilicate are difficult to be released.<sup>141</sup> Na and K are well-known as volatile elements during combustion.<sup>142</sup> However, high particle temperatures and reducing environments within the solid fuel particles could also enhance the volatilization of other inorganic species such as Ca, Mg, Si, Al and Fe in forms of sub-oxides and/or metal elements.<sup>139,140</sup> Those released metallic species would further react with oxygen, steam, and other acidic vapours (e.g. HCl and/or SO<sub>2</sub>) in the gas phase,<sup>21,61,139</sup> and then start to generate spherical and/or aggregate-like PM<sub>1</sub> particles via homogeneous nucleation, followed by the coagulation, agglomeration, heterogeneous condensation on the pre-existing particles, and particle growth.<sup>143</sup> There are also other hypothesized mechanisms for PM<sub>1</sub> formation, such as surface ash shedding,<sup>144,145</sup> convective transport of minerals,<sup>146</sup> bubble bursting of cenospheres<sup>147</sup> and direct carryover of submicron coal particles minerals.<sup>148</sup>

**Formation mechanism of inorganic PM<sub>1-10</sub>.** PM<sub>1-10</sub> are mainly contributed by the refractory elements such as Mg and Ca, and are generally considered to be formed via the “solid-to-particle” process during solid fuels combustion.<sup>144</sup> Such process includes mineral coalescence and particle fragmentation. Specifically, mineral coalescence only takes place when (1) temperature is higher than the melting points of the minerals; (2) the molten or semi-melting mineral droplets have the chance to coagulate together on the burning surface of the same solid fuel particle.<sup>149,150</sup> A large particle in PM<sub>1-10</sub> will then be generated after cooling and condensation. It is worth noting that mineral

coalescence does not occur for excluded mineral or minerals in different solid fuel particles due to the few chances for them to be connected.<sup>151</sup> Consequently, this process is highly relevant to particle temperature, occurrence of mineral species as well as their particle size distributions and chemical compositions.<sup>145</sup>

Particle fragmentation is a process that breaks one piece of solid fuel or mineral particle into several or hundreds of smaller pieces during pyrolysis and combustion.<sup>145,152,153</sup> Consequently, subsequent minerals coalescence would also generate a relatively small ash particle.<sup>145</sup> On the other hand, particle fragmentation could also affect mineral coalescence via reducing the quantity of mineral pieces in the new small fuel particle.<sup>154</sup> For some excluded mineral particles, this process might be accompanied by mineral decompositions, gas release and gas-solid reactions.<sup>155</sup> Furthermore, particle fragmentation also depends on combustion conditions such as heating rate, temperature and the structures of the char formed during devolatilization process.<sup>146,154,156</sup> Generally, increase in combustion temperature, heating rate and char macroporosity would enhance char fragmentation and thus increase PM<sub>1-10</sub> emission.<sup>145</sup>

### **2.7.2 PM<sub>10</sub> emission under oxyfuel combustion conditions**

In recent years, new combustion technologies have been developed to reduce the greenhouse gas emission from fuel-fired power generation. Among those technologies, oxyfuel combustion has been considered as one of the major options for future clean fuel technology and the most competitive carbon capture technologies in existing coal-fired power plants.<sup>25</sup> Figure 2-6 illustrates the flowsheet of oxyfuel combustion for power generation with CO<sub>2</sub> capture and storage. Briefly, instead of using air as oxidant, pure oxygen or a mixture of oxygen and recycled flue gas is used to produce CO<sub>2</sub>-rich product gas that is ready for sequestration and storage after removing impurities such as water vapor, HCl, SO<sub>2</sub> and aerosols.<sup>157-159</sup> However, during oxyfuel

combustion, using the same oxygen concentration as in traditional air combustion would considerably reduce flame temperature due to the higher heat capacity of  $\text{CO}_2$  and lower diffusion rate of  $\text{O}_2$  in  $\text{CO}_2$ .<sup>58</sup> Therefore, oxyfuel combustion usually uses increased oxygen concentration, so as to achieve the similar flame temperature and temperature profiles in the boilers. However, the significantly high content of  $\text{CO}_2$  and the impurities in the recycled flue gas can still substantially vary the emission and characteristics of  $\text{PM}_{10}$  emission during oxyfuel combustion.

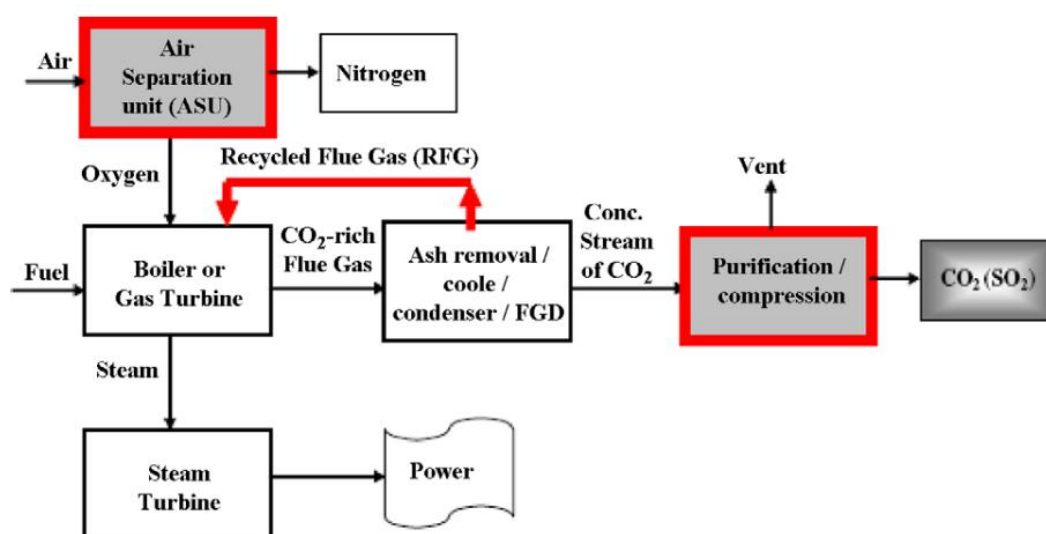


Figure 2-6 Flowsheet of oxyfuel combustion for power generation with  $\text{CO}_2$  capture and storage<sup>25</sup>

Extensive studies have been carried out on  $\text{PM}_{10}$  emission during simulated oxyfuel combustion via mixing  $\text{O}_2$  with  $\text{CO}_2$ . One of the approaches is direct substitution of  $\text{N}_2$  in air with pure  $\text{CO}_2$ . It was found that this substitution would lead to the reduction in the yields of  $\text{PM}_1$  and the shift of the fine mode diameter to the smaller size due to the reduced volatilization of inorganic species and char fragmentation caused by the lower combustion temperature.<sup>58,160-162</sup> The reduce char fragmentation also decreases  $\text{PM}_{1-10}$  emission and its particle size.<sup>163</sup> However, the lower combustion temperature also results in the mitigation of mineral coalescence and thus generates more larger

particles.<sup>164</sup> The char-CO<sub>2</sub> gasification also generates more developed pore structure of the burning char particles and might improve char fragmentation.<sup>163</sup> Thus, the exact influence of replacement of N<sub>2</sub> by CO<sub>2</sub> on PM<sub>1-10</sub> emission highly depends on the fuel properties, especially ash compositions and char structure. If a similar combustion temperature is achieved by increasing oxygen concentration in the oxyfuel combustion atmospheres, both PM<sub>1</sub> and PM<sub>1-10</sub> emission are enhanced with its fine mode peak shifting to larger sizes and the coarse mode peak to smaller sizes.<sup>163</sup> This is due to the increased combustion temperature, vaporization of inorganic species, and char fragmentation and burnout.<sup>165</sup> Especially, when increasing oxygen concentration to ~30%, the combustion profile is similar to that under air condition, which then leads to similar PM<sub>10</sub> emission profile.<sup>20</sup> In addition, it is reported that high oxygen contents during oxyfuel combustion would also affect the reactions among different minerals and the melting behaviours of some minerals,<sup>166</sup> especially the inherent minerals in solid fuels.

On the other hand, impurities in the recycled flue gas such as water vapor, HCl and SO<sub>2</sub> can also exert significant effect on PM emission during oxyfuel combustion. The concentration of water vapor in oxyfuel combustion atmosphere can reach 10–30% or even higher.<sup>25</sup> However, the effect of water vapor on ash chemistry during oxyfuel combustion has mainly been investigated using coal samples. For example, the presence of water vapor could vary the limestone desulfurization and the sintering of the Ca- and Mg-containing species,<sup>167</sup> and significantly improve the pore structures of the sulfation products during coal combustion under oxyfuel conditions.<sup>159</sup> Consequently, the presence of water vapour could significantly influence PM<sub>10</sub> emission.<sup>168</sup> Specifically, water vapor enhances the emission of PM, especially PM<sub>1</sub>, while decreases the concentrations of trace elements in PM during oxyfuel coal combustion.<sup>169</sup> Another study pointed out that the presence of water vapor may have enhanced vaporization of SiO<sub>2</sub> via increasing particle temperature and H<sub>2</sub> partial pressure in the coal char particles, thereby increasing PM<sub>1</sub> emission during oxyfuel



coal combustion.<sup>168</sup> SO<sub>2</sub> in the oxyfuel combustion atmosphere has little effect on total PM yield, although it could decrease the concentration of trace elements in the PM.<sup>169</sup> The presence of SO<sub>2</sub> could enhance the sulfation of metal species,<sup>170</sup> thus varying the composition of other inorganic species in PM.<sup>171</sup> However, HCl is the most crucial factor promoting the vaporization of metals including trace elements,<sup>172</sup> alkali species and organically bound Al and Ti via chlorination in the oxyfuel combustion atmospheres.<sup>170</sup> However, the effect of HCl on PM emission might be mitigated by the presence of water vapours.<sup>172</sup> Overall, the presence of water vapor, SO<sub>2</sub> and HCl in oxyfuel atmospheres could significantly affect ash chemistry and PM emission during practical oxyfuel combustion.<sup>171,172</sup>

### **2.7.3 Distribution and occurrence of phosphorus in PM<sub>10</sub> during combustion of P-containing solid fuels**

Phosphorus is a critical inorganic species for generating PM<sub>10</sub> during solid fuel combustion.<sup>20</sup> Comprehensive studies have been conducted to investigate PM<sub>10</sub> emission during P-containing solid fuel combustion or its co-combustion with coal. Ninomiya et al.<sup>67</sup> found that the P in aerosols is mainly present in PM<sub>1</sub>, especially PM<sub>0.1</sub> (PM with aerodynamic diameter <0.1 μm) during co-combustion of coal with biosolid, although most of the P in the solid fuels is retained in coarse ash associated with refractory metals (such as Mg, Ca, Al and Si). Interestingly, the melt P-containing minerals in ash can capture those vaporized trace elements, thereby decreasing their contents and shifting their particle size distribution to larger values in PM<sub>10</sub>. Zhang et al.<sup>21</sup> investigated P distributions in PM during coal and biosolid combustion at 1200–1450 °C. The results indicated that both the organically bound P and inorganic P in a complex form containing refractory elements could readily vaporize and contribute to PM<sub>1</sub> emission in forms of phosphorus oxides and alkali phosphate. While P in PM<sub>1-10</sub> mainly consists of apatite (Ca<sub>3</sub>(PO<sub>4</sub>)<sub>2</sub>) and condensed melting phase, which might be formed through direct liberation of inherent apatite

and the shedding of melting P-containing minerals from char surface.<sup>21</sup> However, other investigations into the co-combustion of coal with meat and bone meal<sup>56,129</sup> or sewage sludge<sup>57</sup> show that P mainly bonds with Ca in PM<sub>1</sub> via condensation of phosphates on small Ca particles or the transformation of apatite. A recent study<sup>20</sup> on the combustion of *in situ* volatiles and char from biosolid suggested that P is mainly present in PM<sub>1</sub> in forms of P<sub>4</sub>O<sub>10</sub> and alkali metaphosphates generated during combustion of *in situ* volatiles. Evidence also shows that the vapours of P<sub>4</sub>O<sub>10</sub> and alkali metaphosphates could react with the alumina reactor tube to form alkali aluminophosphate glass at 1300 °C, thus reducing the yield of P in PM<sub>1</sub>.<sup>12</sup> However, during char combustion, alkali metaphosphates and alkaline phosphates are the primary phosphorus species in PM<sub>1</sub> and PM<sub>1-10</sub>, respectively. Notably, combustion atmospheres have different influences on the occurrence of P in PM<sub>1</sub> and PM<sub>1-10</sub>.<sup>20</sup> For example, when switching air to oxyfuel conditions during biosolid char combustion, the volatilized P might react with CaO to form non-volatile Ca<sub>3</sub>PO<sub>4</sub>, thus reducing the content of P in PM<sub>1</sub>, while it has little influence on alkaline phosphates in PM<sub>1-10</sub>.<sup>20,21</sup>

Overall, P could present in both PM<sub>1</sub> and PM<sub>1-10</sub> during combustion of P-containing solid fuels. Fuel types and combustion conditions are the two key factors governing the vaporization of P and the transformation of inherent ash,<sup>129</sup> thus varying the occurrences and distributions of P in PM<sub>10</sub>.

#### **2.7.4 Indirect evidence on roles of volatile–char interactions in PM<sub>10</sub> emission**

During solid fuel combustion in any system, pyrolysis is the first step that produces volatiles and char for subsequent combustion. As described in Section 2.5.1, the volatile–char interactions during pyrolysis of solid fuel can exert significant effect on the release of alkali species, char structure and char reactivity. Recently, Wu et al.<sup>12,19</sup> investigated the PM emission during combustion of *in situ* volatiles and char from

biomass and biosolid using a two-stage reactor system (as shown in Figure 2-7). These studies have implied that volatile–char interactions might also influence PM emission.

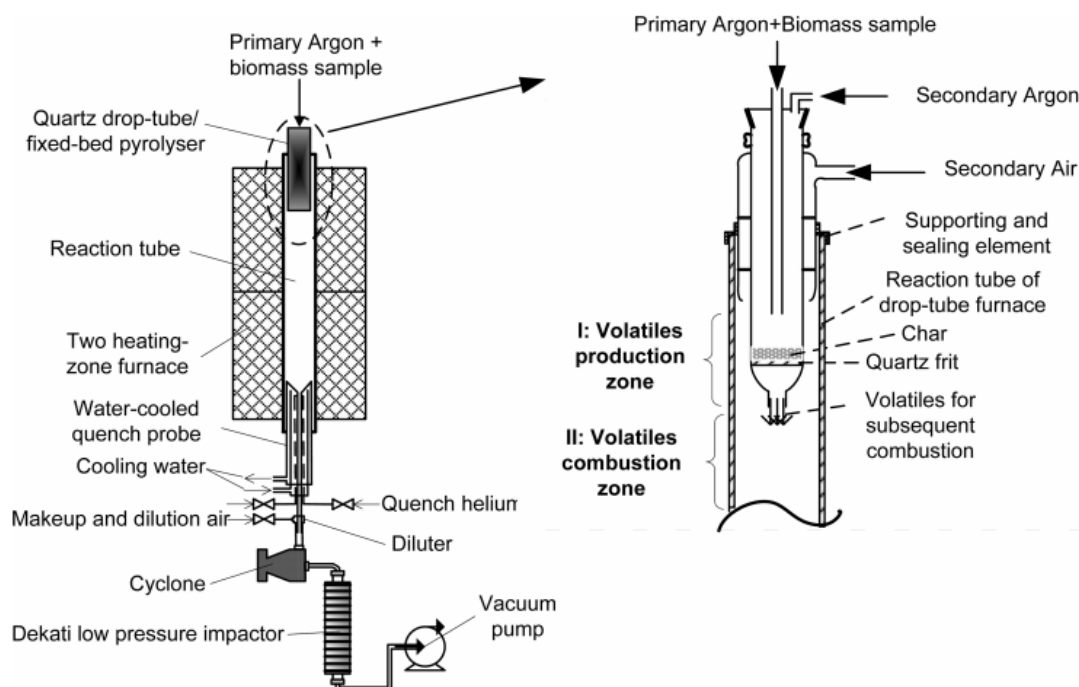


Figure 2-7 Schematic diagram of the two-stage pyrolysis/combustion reactor system used for combustion of *in situ* biomass volatiles<sup>19</sup>

Specifically, the aggregated PM<sub>10</sub> yields (PM<sub>10</sub> from volatiles combustion plus that from char combustion) and the elemental yields of Na and K in PM<sub>10</sub> are slightly higher from the separated combustion of *in situ* volatiles (generated at the pyrolysis temperature of 800–1000 °C) and char from biomass at 1300 °C, compared to those from the direct combustion of whole biomass at 1300 °C.<sup>19</sup> Another study using biosolid found that the separated combustion of *in situ* volatiles and char under the same condition leads to lower yields of PM<sub>10</sub> and significant differences in the distribution and yields of trace elements (especially As, Cd, Pb, Co, Cr and V) in PM<sub>10</sub>, compared to direct combustion of raw biosolid.<sup>23</sup> Notably, one of the major differences between the two combustion conditions (the separated combustion of *in situ* volatiles and char vs the direct combustion of whole biomass or biosolid) is whether the

volatiles could continuously be generated and react with the char particles retained on the quartz frit. Therefore, those studies have provided an indirect evidence that the continuous volatile–char interactions could potentially affect PM emission during solid fuel combustion. However, there are still some unsolved questions, e.g. why opposite observations were found in those two studies and what are the respective effect of volatile–char interaction on PM emission during subsequent *in situ* volatiles combustion and char combustion. Therefore, further investigation needs to be conducted to reveal the direct evidence on volatile–char interactions and more importantly their mechanistic roles in PM emission during solid fuel combustion.

### **2.7.5 Summary**

The mechanism of PM emission during combustion of P-containing solid fuels has been briefly reviewed in this section. Previous studies revealed various factors that could significantly affect the characteristics of PM emission, including fuel properties, combustion temperatures and combustion atmospheres etc. However, some of the influencing factors were only investigated during coal combustion, e.g. the effect of water vapours on PM emission and trace elements in PM. In consideration of the significant differences between coal and biomass in terms of ash compositions, volatiles component and char structures, it is largely unknown whether the conclusions based on coal combustion could be extrapolated to biomass combustion. Furthermore, the fundamental effect of water vapours on PM emission during combustion of *in situ* volatiles and char is still unclear. In addition, although the possible effect of volatile–char interactions on PM<sub>10</sub> emission have been speculated, further investigation is needed to directly investigate the fundamental roles of volatile–char interactions on PM emission during solid fuels combustion.

## 2.8 Conclusions and research gaps

Based on the above literature review, several critical conclusions are summarized as following along with the proposed research gaps:

- **Firstly**, phosphorus presents in solid fuels in various occurrence forms. Understanding the occurrence forms of P-containing species is environmentally important for the thermochemical utilization of P-containing solid fuels. However, the existing methods for quantifying phosphorus with different forms are unreliable;
- **Secondly**, several studies have been conducted to investigate the transformation and release of phosphorus during pyrolysis and combustion of P-containing solid fuels, which is closely related with the characteristics of char combustion and PM emission. However, some conclusions are contradictory in these studies due to different pyrolysis or combustion conditions, fuel types, occurrence of phosphorus and reactor configurations;
- **Thirdly**, as an indispensable inorganic species, phosphorus could exert significant influence on the pyrolysis of solid fuels in terms of the pyrolytic decomposition of solid fuel and the distributions of pyrolysis products. However, the effect of different forms of phosphorus on the structure and reactivity of char samples is still unclear. Moreover, the effect of coexistence of phosphorus and other inorganic species such as AAEMs on char structure and char reactivity also needs to be unravelled.
- **Fourthly**, previous studies using single volatiles generated from brown coal revealed that volatile–char interactions could substantially vary char structure and char reactivity. However, in practical combustion or pyrolysis systems, volatiles generated from different solid fuels or different types of biomass may have distinctly-different chemistry. Therefore, investigation into the effect of various *in situ* volatiles with distinctly-different chemistry on char structure and

char reactivity is necessary;

- **Fifthly**, PM emission during combustion of P-containing solid under oxyfuel conditions is a significant issue and extensive studies have investigated the factors affecting PM emission under oxyfuel conditions, including the presence of impurities such as water vapours, HCl and SO<sub>2</sub> and particulate matter. Nevertheless, those studies are mainly on coal combustion and the fundamental effect of those impurities on PM emission during respective combustion of volatiles and char remains unravelled;
- **Sixthly**, indirect evidences suggest that volatile–char interactions could potentially affect PM emission during solid fuel combustion. To explore the mechanism of such effect, individual combustion of *in situ* volatiles and char should first be figured out via purposely-designed reactor system.

In summary, further investigations are required to fill the research gaps in the field of pyrolysis and combustion of P-containing solid fuels in aspects of char structure, char reactivity and PM emission.

## 2.9 Research objectives of current study

As listed in the section 2.8, several research gaps in the field have been identified from the literature review. Nevertheless, it is practically impossible to fill all the research gaps due to the limited timeframe of the PhD study. Thus, the scope of this thesis aims to achieve seven objectives as follows:

- (1) To develop a method for quantifying phosphorus in various occurrence forms in solid fuels;
- (2) To investigate the transformation and release of phosphorus during pyrolysis of P-containing biomass under different conditions;
- (3) To study the effect of different forms of phosphorus on structure and reactivity of char samples prepared from biomass pyrolysis;

- (4) To investigate the roles of *in situ* volatiles with distinctly-different chemistry played in char structure and char reactivity during volatile–char interactions;
- (5) To examine the effect of water vapours on PM emission during combustion of *in situ* volatiles and char from contaminated biomass with high contents of trace elements;
- (6) To find out the direct evidence on the effect of volatile–char interactions on PM emission during combustion of *in situ* volatiles from biosolid;
- (7) To investigated the effect of volatile–char interactions on PM emission during combustion of different biosolid char samples under different combustion conditions.

## CHAPTER 3 RESEARCH METHODOLOGY AND ANALYTICAL TECHNIQUES

### 3.1 Introduction

This chapter describes the research methodology employed to achieve the individual objectives outlined in Chapter 2. Details of experimental and analytical techniques are presented in the following sections.

### 3.2 Methodology

A series of P-containing solid fuels were used in this PhD project, i.e. mallee wood and leaf, rice bran, biosolid, biosolid char, chicken litter, algae, meat and bone meal. Accordingly, a set of systematic experiments was carried out to achieve the objectives listed in Section 2.9, including:

- Samples preparation, such as acid-washing to elute the inorganic species from solid fuels;
- Pyrolysis of P-containing solid fuels in various reactor systems to produce char samples with different properties;
- Combustion experiments in a drop-tube furnace, including combustion of P-containing solid fuels and separated combustion of *in situ* volatiles and char generated from P-containing solid fuels under air or oxyfuel conditions;
- Characterization of solid and liquid samples using an array of analytical instruments, including elemental analyser, Raman spectroscopy, ion chromatography, inductively coupled plasma-optical emission spectroscopy and thermogravimetric analyser etc.

In this project, experiments or instrumental analyses were at least duplicated to



ensure reproducibility of results. Figure 3-1 illustrates the overall methodology map along with the proposed research objectives in Chapter 4–10. The specific experiments conducted to achieve each objective are then summarized in the following subsections 3.2.1–3.2.7.

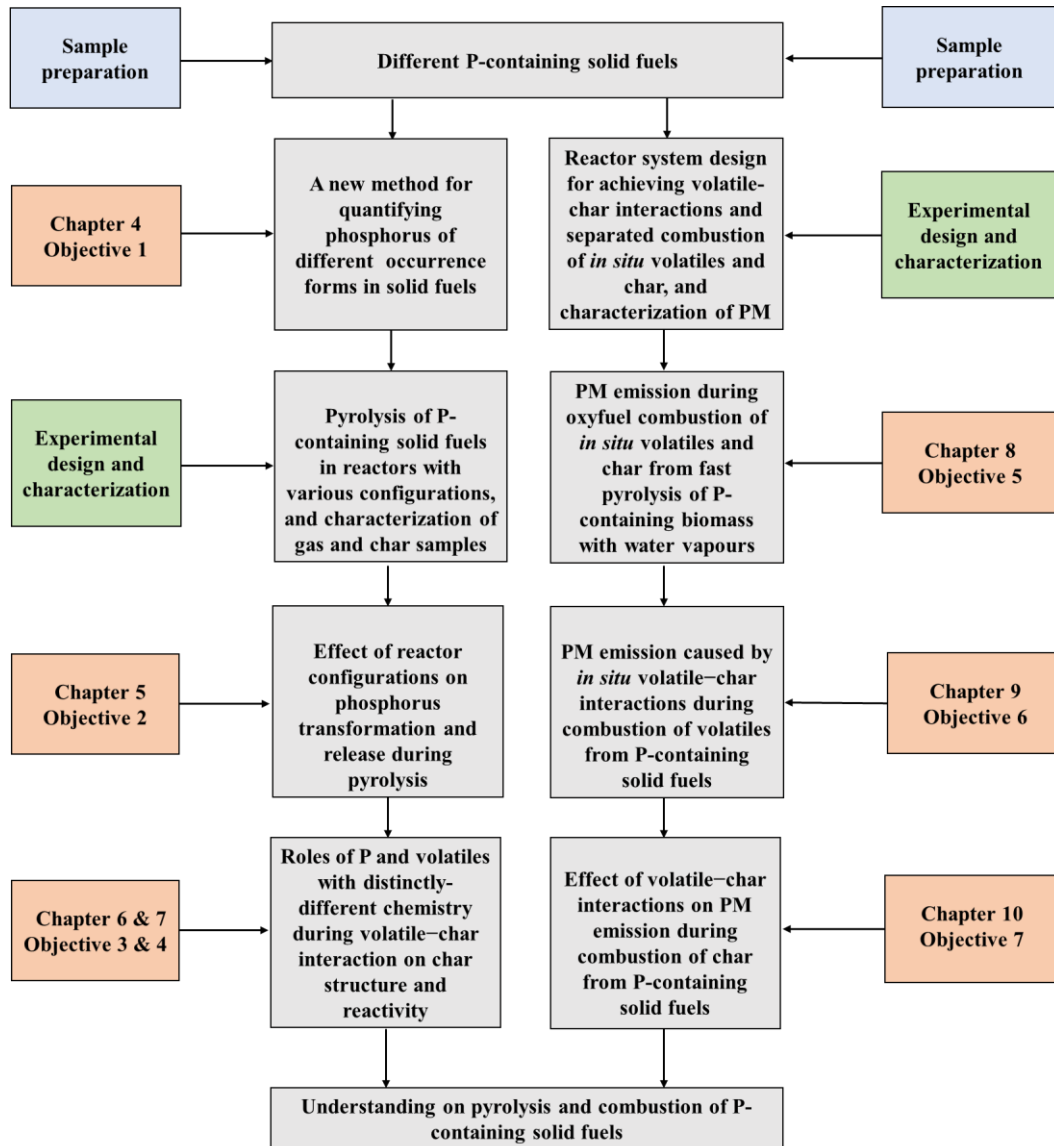


Figure 3-1 Research methodology linked with the research objectives in this thesis

### **3.2.1 A New method for quantifying phosphorus of various occurrence forms in solid fuels**

Three acid-washed samples (i.e. acid-washed mallee wood, acid-washed rice bran and double-acid washed biosolid) were prepared as P-free substrates and then loaded with different P-containing chemicals as P-containing standards to validate the existing SMT method (see Section 2.4.1) and a new method for quantifying phosphorus of different occurrence forms in solid fuels. Seven P-containing solid fuels (i.e. biosolid, meat and bone meal, chicken litter, rice bran, algae, mallee leaf and biosolid char) were also subjected to the application of these methods. Thereinto, P-containing biosolid char was prepared from slow heating pyrolysis of biosolid in a fixed bed reactor (see Section 3.3.1) at 800 °C. The ultimate and proximate composition of solid fuel and char samples were analysed according the method detailed in Section 3.4.1. The contents of inorganic species in solid fuel samples were analysed using the methods described in Section 3.4.2. The detailed procedure, validation and application of the newly-developed method for quantification of different forms of phosphorus are described in Chapter 4.

### **3.2.2 Transformation and release of phosphorus during pyrolysis of P-containing biomass in reactors with different configurations under various conditions**

A typical P-rich biomass i.e. rice bran was used to investigate the effect of reactor configurations on transformation and release of phosphorus under different conditions at 400–900 °C. The pyrolysis experiments were conducted in three different reactor systems including slow heating pyrolysis in a fixed bed reactor and fast heating pyrolysis in drop-tube/fixed-bed reactors with either continuous feeding or pulse feeding (see Section 3.3.2). A bubbler system was connected to the pyrolysis reactors for collecting phosphorus oxides via 0.1 M sodium hydroxide (NaOH) solution and phosphine by 0.1 M sodium hypochlorite in volatiles. Another

two-stage pyrolysis/combustion reactor system was also employed to investigate the total P (including P in tar and P in gas) in volatiles. The phosphorus fractions in rice bran and char samples were determined using the method developed in Chapter 4. The results and discussions for this work are elaborated in Chapter 5.

### **3.2.3 Roles of phosphorus in evolution of char structure and char reactivity**

In Chapter 6, the effect of different forms of phosphorus on char structure and reactivity was investigated. A P-free mallee wood was prepared by HCl acid-washing and then loaded with different forms of P-containing chemicals via impregnation method (Section 3.3.1) to prepare P-loaded samples. These samples were then subjected to fast heating pyrolysis in a drop-tube/fixed-bed with pulse feeding (Section 3.3.2) and the char samples were collected for subsequent analysis, including quantification of phosphorus according to the method developed in Chapter 4, char structure using Raman spectroscopy (Section 3.4.3) and char reactivity using thermogravimetric analyser (Section 3.4.4).

### **3.2.4 Volatile–char interactions: roles of *in situ* volatiles with distinctly-different chemistry in determining structure and reactivity of char from P-containing biosolid**

Firstly, a two-stage reactor system (see Figure x in Section 3.3.3) was purposely designed to achieve the direct evidence of *in situ* volatile–char interactions in Chapter 7. Then, a biosolid with little inorganic species was prepared via double acid-washing process (Section 3.3.1) and subjected to fast heating pyrolysis with pulse feeding at 1000 °C to prepare a char sample. Afterwards, the collected char was subjected to the interactions with volatiles with distinctly-different chemistry generated *in situ* from pyrolysis of cellulose, polyethylene (PE), double-acid washed biosolid (DAWB) and polyethylene glycol (PEG) in a newly-designed reactor (Figure 3-3, Section 3.3.3). Subsequently, the char samples before and after

volatile–char interactions were subjected to various analyses, including elemental analysis (Section 3.4.1), char structure (section 3.4.3) and char reactivity (Section 3.4.4). In addition, the contents of inorganic species in all solid samples were analysed using the method described in Section 3.4.2.

### **3.2.5 Effect of water vapour on PM<sub>10</sub> emission during combustion of *in situ* volatiles and char from fast pyrolysis of P-containing contaminated wood**

In Chapter 8, chromated-copper-arsenate-treated (CCAT) wood was used to investigate the effect of water vapour on PM<sub>10</sub> emission during the individual combustion of *in situ* volatiles and char samples generated from fast pyrolysis. CCAT wood is P-containing contaminated wood with abundant trace elements. A new two-stage pyrolysis/combustion system (Figure 3-4, Section 3.3.4) was deployed to achieve the generation and combustion of *in situ* volatiles at the same temperature (1300 °C) in the presence of different contents of water vapours under oxyfuel conditions. The contents of inorganic species in CCAT wood, char and PM<sub>10</sub> were determined using the method described in Section 3.4.2.

### **3.2.6 Effect of *in situ* volatile–char interactions on PM emission during the combustion of volatiles from P-containing biosolid**

In Chapter 9, a three-stage pyrolysis/combustion reactor system (Figure 3-5, Section 3.3.4) was purposely designed for *in situ* generating fresh volatiles to interact with the prepared biosolid char then realising the immediate combustion of the resultant volatiles. The biosolid char was prepared from slow heating pyrolysis of biosolid using a fixed bed reactor (Section 3.3.2). The *in situ* volatiles generated in the three-stage pyrolysis/combustion reactor system came from fast pyrolysis of cellulose, polyethylene and a acid-washed biosolid sample. Similarly, the contents of inorganic species in the solid samples were determined using the method detailed in Section 3.4.2.

### 3.2.7 Effect of volatile–char interactions on PM<sub>10</sub> emission during combustion of P-containing biosolid chars under air and oxyfuel conditions

To investigate the influence of volatile–char interactions on PM<sub>10</sub> emission during char combustion, slow heating char was prepared in a fixed-bed reactor while fast heating char was prepared in a fixed-bed/drop-tube reactor (Section 3.3.2) at 1000 °C. These char samples were then reacted with the volatiles produced *in situ* from the pyrolysis of polyethylene (PE) and double acid-washed biosolid (DAWB) in the aforementioned two-stage volatile–char interactions reactor (Figure 3-3, Section 3.2.4) at 1000 °C. After volatile–char interactions, the char samples were then subjected to the air and oxyfuel combustion in a drop-tube furnace combustion system, which will be elaborated in Section 3.3.4. The contents of inorganic species in biosolid, char samples and in PM<sub>10</sub> were analyzed using the method described in Section 3.4.2. The macroporosity of char samples were analyzed according to the method detailed in Section 3.4.5. The detailed results on this subject are reported in Chapter 10.

## 3.3 Experimental

### 3.3.1 Sample preparation

**P-containing solid fuels.** Several P-containing solid fuels were used in this study. Specifically, biosolid used in Chapter 4, 7, 9 and 10 are sourced from a waste water treatment plant in Western Australia (WA). The bulk biosolid sample was dried for 12 h in an oven at 105 °C, crushed and then sieved to yield the biosolid sample with a size fraction of 90–150 µm in Chapter 7, 9 and 10 and a size fraction of 70–120 µm in Chapter 4. Chicken litter (in Chapter 4), rice bran (in Chapter 4 and 5) and algae sample (in Chapter 4) were purchased from local stores in WA. Mallee wood (in Chapter 4 and 6) and leaf (in Chapter 4) was separated from mallee trees harvested in Narrogin, WA. All those samples were cut/ground and then sieved to 70–120 µm

then air dried at 80 °C for 48 h. The prepared samples were sealed in plastic containers and stored in a freezer under -4 °C prior to further analysis or experiment. The preparation of char samples under different pyrolysis conditions would be elaborated in each chapter along with their analyses.

**Acid-washed solid fuel samples.** Acid-washing was conducted in this thesis to elute major inorganic species in solid fuels including single acid-washing and double-acid washing. Briefly, during single acid-washing of solid samples, samples were soaked in 1 M HCl solution (solid to liquid ratio of 1:200) for 24 hours, and then repeatedly filtered and rinsed with deionised water until no Cl<sup>-</sup> was detected in the filtrate via ion chromatography (IC, model: Dionex ICS-1100) equipped with IonPac AS22-fast column. The recovered solid samples were dried at 80 °C or 105 °C for acid-washed biosolid samples to yield the acid-washed samples. Single acid-washed mallee wood samples were used in Chapter 4 and 5 while single acid-washed rice bran and biosolid were used in Chapter 4 and Chapter 9, respectively.

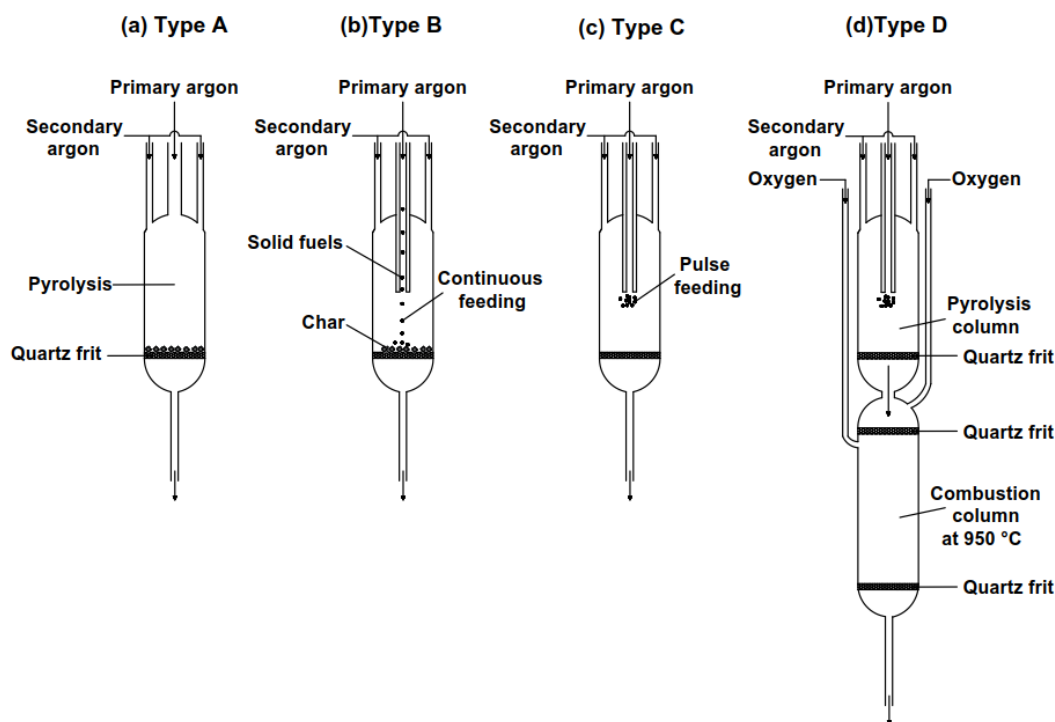
A double acid-washed biosolid (DAWB) was also used in Chapter 4, 7 and 10. Specifically, the prepared biosolid was first leached with 1 M HCl solution at solid to liquid ratio of 1:200 for 24 h before it was filtrated. The recovered solid was leached with 20 wt% HF solution at 80 °C in a sealed Teflon vial for 12 h then the acid solution was evaporated. The recovered samples were once again subjected to leaching with the HCl and HF solutions before it was repeatedly rinsed with ultrapure water and filtrated until no Cl<sup>-</sup> and F<sup>-</sup> was detected in the filtrate via IC. The recovered solid samples were dried at 105°C to yield the DAWB samples. The characterization of the acid-washed samples was carried out prior to experiments and the results are presented in each chapter.

**Loading of P-containing chemicals into acid-washed samples.** Briefly, ~ 5g acid-washed sample (wood, rice bran or biosolid) was first soaked in the solutions

(PH  $\approx$  6.2) containing a desired amount of P-containing species such as phytic acid, orthophosphoric acid and polyphosphoric acid as well as ultrapure water in a 100 ml container. The mixtures were then stirred at room temperature for 24 h and then heated at 50 °C to evaporate the liquid in the container. The collected P-loaded samples were then further dried at 60 °C for 24 h. This method is specifically used in Chapter 6 to prepare P-loaded wood samples.

**Other chemicals used in this study.** Cellulose, polyethylene (PE), and polyethylene glycol (PEG), sodium hexametaphosphate [(NaPO<sub>3</sub>)<sub>6</sub>], sodium pyrophosphate tetrabasic (Na<sub>4</sub>P<sub>2</sub>O<sub>7</sub>), sodium triphosphate pentabasic (Na<sub>5</sub>P<sub>3</sub>O<sub>10</sub>), ammonium phosphate [(NH<sub>4</sub>)<sub>3</sub>PO<sub>4</sub>], hydroxyapatite [Ca<sub>5</sub>(OH)(PO<sub>4</sub>)<sub>3</sub>], aluminium phosphate (AlPO<sub>4</sub>), phytic acid sodium salt hydrate (C<sub>6</sub>H<sub>18</sub>O<sub>24</sub>P<sub>6</sub>·xNa<sup>+</sup>·yH<sub>2</sub>O), 1,2-dioleoyl-sn-glycero-3-phosphoric acid sodium salt, adenosine 5'-monophosphate monohydrate, cytidine-5' triphosphate disodium salt, deoxyribonucleic acid sodium salt and D-fructose 6-phosphate disodium salt hydrate were sourced from Sigma Aldrich. In Chapter 4, calcium phosphate silicate, not available commercially, was produced using a method detailed elsewhere<sup>72</sup> as the model compound for P-silicate in solid fuels. Briefly, SiO<sub>2</sub> gel, which was prepared from tetraethoxysilane and the mixed solvent of C<sub>2</sub>H<sub>5</sub>OH and H<sub>2</sub>O, was mixed with calcium phosphate solution and heated to 1200 °C in a Pt crucible in air for 4 h. After cooling down to room temperature, the mixture was washed with 1M HCl solution to remove the calcium phosphate until no P was detected in the filtrate. The acid-insoluble P-containing residue was finally dried and ground to < 10 μm prior to analysis and utilization. other chemicals, such as high-purity analytical-grade methanol, chloroform, acetone, hydrofluoric acid, orthophosphoric acid, perchloric acid, nitric acid, hydrofluoric acid, hydrogen peroxide, sodium hypochlorite, KOH powder and NaCl powder were purchased from Chem-Supply.

## 3.3.2 Reactor systems for pyrolysis experiments

Figure 3-2 Pyrolysis reactor systems used in this thesis<sup>104</sup>

As shown in Figure 3-2, four pyrolysis reactor systems were used in this study. The detailed procedures of these pyrolysis experiments are shown in the following text. The heating rate and the gas residence time in Type A, Type B and Type C reactor system in Chapter 6 are shown in Table 3-1.

Table 3-1 A summary of heating rate and residence time in the isothermal zone of the reactors shown in Figure 3-2

Reactors	Type A	Type B	Type C
Heating rate, °C /s	0.17	1000	1000
Gas residence time, s	1.5	1.5	1.5



**Type A: Pyrolysis in a fixed bed reactor.** Briefly, 5 g of solid fuel was loaded onto the frit of a quartz fixed-bed reactor with an internal diameter of 60 mm. The reactor was then heated in a vertical tube furnace to the desired temperature at 10 °C/min using argon (1 L/min) as the sweep gas. The reactor was held at the desired temperature for a further 15 minutes before it was lifted from the furnace and allowed to cool to ambient temperature with the argon flow continuing to flow through the reactor.

**Type B: Pyrolysis in a drop-tube/fixed bed reactor with continuous feeding.** First, the reactor was preheated to the desired temperature, then ~1.0 g of solid fuel sample was continuously fed into the reactor via a stream of primary argon (1.0 L/min) at ~0.05 g/min. Solid fuel particles fed in the Type B reactor underwent rapid pyrolysis at an estimated heating rate of around 1000 °C/s. Under such conditions, *in situ* volatiles generated continuously interacted with the nascent char particles that were produced from solid fuel particles previously fed into the reactor and remained on the quartz frit, leading to the enhanced volatile–char interactions.<sup>104</sup>

**Type C: Pyrolysis in a drop-tube/fixed bed reactor with pulse feeding.** To minimise volatile–char interactions, pyrolysis experiments could be carried out in the Type C reactor system where ~0.1 g of solid fuel was fed into the reactor in a single shot via a pulse feeder using a stream of primary argon (1.0 L/min).<sup>104</sup> For experiments in Type B and Type C reactor systems, the reactor was further held for 10 min at the pyrolysis temperatures after feeding was completed. In each pyrolysis experiment in these reactor systems, the temperature in the isothermal zone of the quartz reactor was monitored by a thermocouple and controlled by a temperature controller for all pyrolysis experiments. In addition, by adjusting the flow rate of secondary argon, the gas residence time in Type A, Type B and Type C reactor was kept as ~1.5 s in Chapter 5. After a pyrolysis experiment was completed, the reactor was lifted out of the furnace for cooling, with argon gas being continuously flowing

through the reactor. After a pyrolysis experiment was completed, the reactor was lifted out of the furnace for cooling, with argon gas continuously flowing through the reactor.

**Type D: Pyrolysis/combustion in a two-stage reactor system.** To recover the total phosphorus in volatiles, experiments were conducted in a two-stage pyrolysis/combustion reactor system (Type D reactor system) in Chapter 5. The two-stage reactor system was a combination of a pyrolysis reactor (first stage) and a combustion reactor (second stage) in series. The first stage pyrolysis reactor was operated as a fixed-bed reactor (Type A) or a drop-tube/fixed-bed reactor with either continuous feeding (Type B) or pulse feeding (Type C), same as those described above. During pyrolysis in the pyrolysis reactor, the fresh volatiles flew through the frit in the first stage reactor, entered into the second stage reactor, mixed with a stream of primary oxygen gas (0.5 ml/L) then entered (via the top frit) into the second stage combustion reactor that was preheated at 950 °C. A stream of secondary oxygen (0.5 L/min) was also injected (below the top frit) into the combustion reactor to assist the complete combustion of volatiles. In such cases, all P (including phosphine) in the volatiles were converted into phosphorus oxides and captured by 0.1 M NaOH solutions after *in situ* volatiles combustion, realising the quantification of total P in volatiles.

### 3.3.3 Reactor system for *in situ* volatile–char interactions

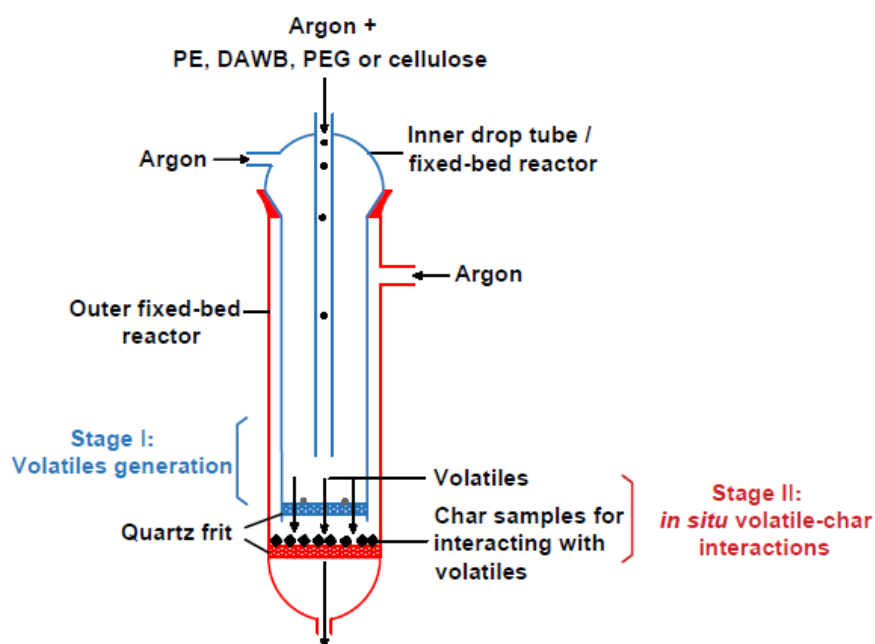


Figure 3-3 Two-stage reactor systems for *in situ* volatile-char interactions

A two-stage quartz reactor was employed in Chapter 7 and Chapter 10 for studying the *in situ* volatile–char interactions at 1000 °C. As showed in Figure 3-3, the reactor consists of an inner drop-tube/fixed-bed quartz reactor (Stage I) cascaded into an outer fixed-bed reactor (Stage II). Briefly, 0.3 g char was first loaded into the outer fixed-bed reactor, followed by inserting the inner reactor into the outer reactor. The cascaded two-stage reactor was pre-heated to 1000 °C in a vertical furnace. A suitable amount of polyethylene (PE), double-acid washed biosolid (DAWB), polyethylene glycol (PEG) and cellulose was then fed into the inner reactor for 20 mins via an entrained sample feeder using a stream of argon (1 L/min) as feeding gas. The char produced from the rapid pyrolysis of PE, PEG, DAWB or cellulose, if any, was retained on the frit in the inner reactor while the fresh volatiles generated *in situ* passed through the frit of inner reactor to immediately interact with the pre-loaded char sample on the frit of the outer reactor. Two streams (0.5 and 0.3 L/min) of argon were introduced through the annulus between the feeding tube and the inner reactor

and that between the inner and outer reactors, respectively, to prevent the back flow of volatiles. The residence time of *in situ* volatiles in the reactor is estimated to be ~0.6 s. Upon the completion of feeding, the reactor was held for a further 2 min and then immediately lifted out of the furnace for rapid cooling to ambient temperature (with the argon continuously flowing through the reactor). While the volatiles generated *in situ* from PE, DAWB, PEG and cellulose have different oxygen and hydrogen contents, the feeding rate was adjusted so that the total molar flow rates of O and H in the volatiles are maintained at 0.0054 mol/min in all experiments. Separate experiments were also conducted to hold the char sample in Stage II without feeding any sample into Stage I, i.e. producing the char without volatile–char interactions.

### 3.3.4 Combustion reactor and PM collection system

**A novel two-stage pyrolysis/combustion reactor system.** As shown in Figure 3-3, a novel two-stage pyrolysis/combustion system<sup>12</sup> was employed in Chapter 8 to achieve the *in situ* generation and combustion of volatiles from P-containing contaminated wood at the same temperature (1300 °C) in presence of water vapour under oxyfuel conditions. Briefly, an inner alumina tube (OD: 25 mm) as Stage I for *in situ* volatiles generation is cascaded via a water-cooled probe into an outer alumina tube (OD: 65 mm) that is also the reactor tube of drop-tube furnace (DTF) and acts as stage II for *in situ* volatiles combustion. The top end of the inner tube is fully-open and connected with sample feeding system, through which wood particles are fed into Stage I for rapid pyrolysis. The bottom end is rounded open with a 3-mm hole, above which a layer of yttria-stabilized-zirconia (YSZ) felt is loaded for retaining the char produced during rapid pyrolysis while allowing the *in situ* volatiles to pass through the hole for subsequent Stage II combustion in the DTF. In an experiment, 1 L/min of ultra-high purity argon flow was used as the carrier gas to entrain the wood particles via the sample feeder into stage I at 0.05 g/min for 20 min.

An additional 0.45 L/min argon was introduced through the annulus between the feeding tube and the small alumina tube to prevent the backflow of the volatiles to inner tube headspace. The required oxyfuel gas was supplied through annulus between the water-cooled probe and the inner tube. Delivered by an HPLC pump (Model 626), a steady flow of deionised water was injected into the heated zone of the furnace through a 1.6mm stainless-steel tubing. The water injection tubing was swirled around the top section of the inner alumina tube to ensure the complete vaporization of the water and homogeneous mixing of water vapour with pre-mixed CO<sub>2</sub>/O<sub>2</sub> gas before reaching the tip of the inner alumina tube. Simulations using computation fluid dynamics showed that homogeneous mixing of water vapour and CO<sub>2</sub>/O<sub>2</sub> gas was achieved in the annulus at the tip of inner alumina tube under various conditions. The gas temperatures around the tip of the inner alumina tube after steam-gas mixing under various conditions, measured by a thermocouple, were 1300 °C. The water flow rates are 0.33 and 0.99 mL/min, corresponding to equivalent 10% and 30% water vapour content at 1300 °C in this study. The oxygen content was maintained at 30% in all combustion experiment in Chapter 8.

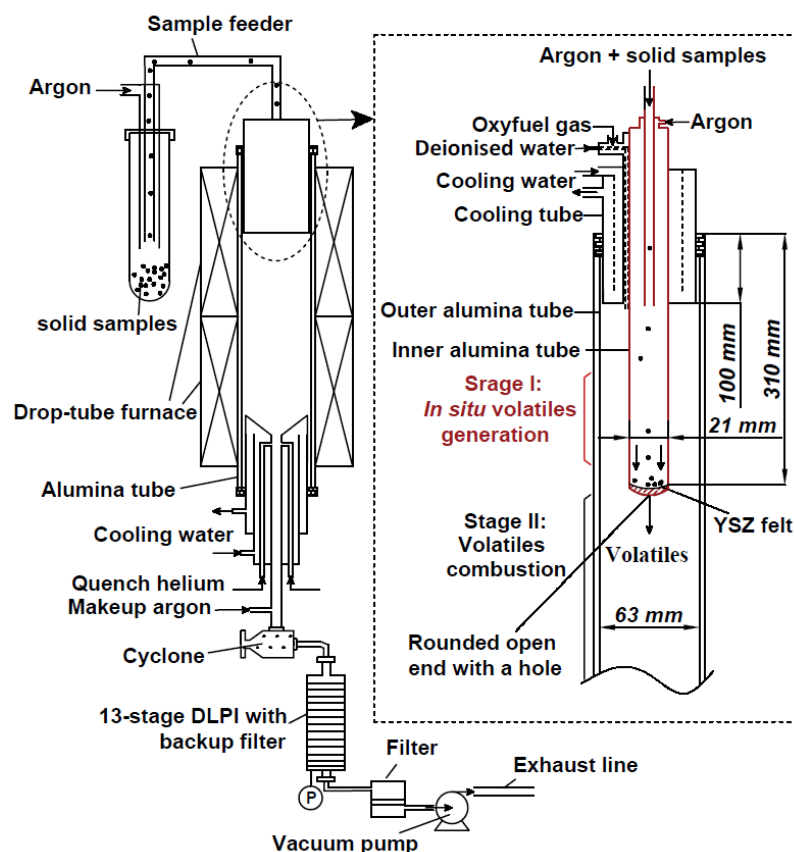


Figure 3-4 Schematic diagram of the two-stage pyrolysis/combustion reactor system<sup>12</sup>

In Chapter 10, pyrolysis experiments were carried out to prepare char from contaminated wood at 1300 °C using the DTF in another configuration. Briefly, a 19 mm OD alumina tube is inserted into the 65 mm OD alumina tube through two water-cooled probes at the top and bottom of the furnace. Contaminated wood particles were fed into the DTF that was preheated at 1300 °C for rapid pyrolysis in argon. Helium was used for quenching the hot flue gas and makeup argon was introduced to ensure the total flow rate of the gas be 10 L/min before entering a Dekati cyclone for char collection.

During char combustion experiment in Chapter 8, ~0.5 g char was fed into the DTF

by 1 L/min pre-mixed CO<sub>2</sub>/O<sub>2</sub> into the alumina reactor tube using an entrained sample feeder through a water-cooled probe. Another 3.45 L/min of the water vapour (corresponding to 0, 10 or 30% of water vapour content at 1300 °C) and CO<sub>2</sub>/O<sub>2</sub> gas mixture was introduced for combustion. However, in Chapter 10, char combustion was conducted under both air and oxyfuel (30% O<sub>2</sub> in CO<sub>2</sub>). Therefore, 1 L/min instrument-grade air for air combustion or 30% O<sub>2</sub> in CO<sub>2</sub> for oxyfuel combustion was used as entrain gas for carrying char samples into the alumina reactor tube. An additional 4.6 L/min of instrument grade air (for air combustion) or 30% O<sub>2</sub> in CO<sub>2</sub> (for oxyfuel combustion) was supplied through the water-cooled probe for complete char combustion.

**A novel three-stage pyrolysis/combustion reactor system.** In Chapter 9, to simulateously achieve the *in situ* generation of fresh volatiles, *in situ* volatile-char interactions as well as the immediate combustion of the resulting volatiles is the key for the experimental design. Accordingly, it was achieved by cascading the two-stage quartz reactor for volatile-char interactions (shown in Figure 3-3) into the DTF (shown in Figure 3-4) to establish a novel three-stage pyrolysis/combustion reactor system, as shown in Figure 3-5. Specifically, the two-stage quartz reactor is an inner drop-tube/fixed bed reactor inserted into an outer fixed-bed reactor. The inner reactor serves as a pyrolyser for *in situ* generation of fresh volatiles (Stage I) from desired samples, retaining the char on the quartz frit and only allowing the fresh volatiles to enter the next stage. The outer fixed-bed reactor (Stage II) enables the incoming fresh volatiles generated *in situ* in Stage I to pass through the bed of preloaded chars for volatile-char interactions. The volatiles after interactions with char then pass the quartz frit of Stage II and enter the DTF for immediate combustion in air at 1300°C (Stage III).

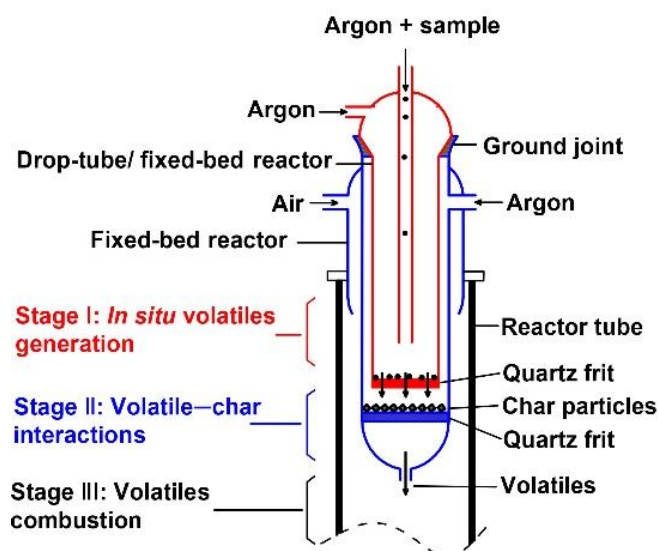


Figure 3-5 Schematic diagram of the three-stage pyrolysis/combustion reactor system

In an experiment in Chapter 9,  $\sim 0.3$  g of char prepared from slow heating pyrolysis in the fixed-bed reactor at  $800$  °C or  $1000$  °C was pre-loaded into the outer fixed-bed reactor (Stage II). The assembled two-stage quartz reactor (Stages I and II) was cascaded into the DTF that was then heated up to  $1300$  °C. The position for the quartz reactor to be inserted was predetermined prior to experiments to ensure that the quartz frits of Stage II was maintained at  $800$  °C or  $1000$  °C which was the same temperature for preparing the slow heating biosolid chars. The distance between the two quartz frits was  $\sim 1$  cm and the difference in the measured temperatures of the two quartz frits was minimal. About 1 g of cellulose, polyethylene or acid-washed biosolid was then fed into the inner reactor (Stage I) via a feeder using argon (1 L/min, UHP) as the carrier gas at a feeding rate of 0.05 g/min. As the fuel particles were injected into the inner reactor, fast pyrolysis took place and the fresh volatiles and char were generated. A second stream of argon (0.3 L/min) was used to assist in sweeping the fresh volatiles through the quartz frit of the inner reactor, while the char was retained by the quartz frit. The volatiles leaving Stage I then passed the bed of slow heating biosolid char particles that were pre-loaded onto the quartz frit of the outer reactor. Similarly, an additional stream of argon (0.5 L/min) was introduced to



push the volatiles after reacting with char particles through the quartz frit and ejected into the volatile combustion zone in the DTF. A stream of instrument grade air (4.7 L/min) was supplied for subsequent complete combustion of the volatiles. Blank experiments for the combustion of cellulose, polyethylene (PE), and AW biosolid volatiles were also conducted without pre-loading the biosolid char into the outer reactor (Stage II).

**PM sampling system.** The PM samples generated from solid fuel or its components were collected and fractionated using a sampling system that comprises of a quench sampling probe, a cyclone with a cutting size of 10  $\mu\text{m}$ , a 13-stage Dekati low-pressure impactor coupled with backup filter and a vacuum pump, as shown in Figure 3-4. The quench sampling probe enables the rapid quenching of flue gas particles with the aid of cooling water and helium. The dilution of the flue gas stream to 10 L/min and rapid quenching with helium significantly minimizes the interaction among particles and forces the nucleation of vaporized species. Notably, in order to avoid the condensation of acidic gases (e.g.,  $\text{SO}_3$  and  $\text{HCl}$ ) in the flue gas,<sup>61</sup> the temperature of the flue gas at the outlet of sampling probe and the PM sampling line was kept at 115 °C. In Chapter 8, it was further increased to 120 °C due to the increase in the dew point of  $\text{SO}_3$  in presence of water vapours in the oxyfuel combustion atmospheres.<sup>61</sup> Sequentially, the coarse particles in the flue gas would first be separated by the cyclone and the PM with aerodynamic diameters less than 10  $\mu\text{m}$  were then collected by the backup filter and the 13-stage Dekati low-pressure impactor (DLPI) with the working pressure inside the DLPI being controlled by the vacuum pump. The average particle size of the PM collected in backup filter and stage 1 to 13 of the DLPI is 0.010, 0.022, 0.043, 0.077, 0.138, 0.248, 0.373, 0.612, 0.957, 1.627, 2.442, 4.094, 6.863 and 10.189  $\mu\text{m}$ , respectively. Accordingly, in this thesis, PM collected in DLPI and backup filter with aerodynamic diameters of <0.1, 0.1–1, 0.1–10, <1, 1–10, <2.5 and <10  $\mu\text{m}$  hereafter is termed as  $\text{PM}_{0.1}$ ,  $\text{PM}_{0.1-1}$ ,  $\text{PM}_{0.1-10}$ ,  $\text{PM}_1$ ,  $\text{PM}_{1-10}$ ,  $\text{PM}_{2.5}$  and  $\text{PM}_{10}$ , respectively.

It should be noted that in this thesis for all combustion experiments, the ratios of the actual air-fuel ratio/stoichiometric air-fuel ratio were over 12 to ensure the complete combustion of solid fuels or volatiles. In addition, no unburned carbon was detected in the PM samples by the thermogravimetric analysis and no organic carbon was found in the leachates from water washing of the PM samples during the total organic carbon analysis. These evidences proved that complete combustion was indeed achieved during all combustion experiments in this thesis.

### **3.4 Instruments and analytical techniques**

#### **3.4.1 Proximate and ultimate analysis**

The ultimate analysis of P-containing solid fuels and the derived char samples was conducted using a CHN elemental analyser (PerkinElmer 2400 series II model). The proximate analysis of solid samples was conducted using a thermogravimetric analyser (TGA; Mettler TGA/DSC 1 STAR model), following the procedure described in ASTM E870-82.

#### **3.4.2 Quantification of inorganic species in solid fuels and PM**

**Quantification of AAEMs, P and trace elements.** The analysis of AAEMs in solid samples (excluding char and PM samples) involves acid digestion and quantification. Briefly, ~0.1 g digested in a mixture of HF/HNO<sub>3</sub>/H<sub>2</sub>O<sub>2</sub> in a Teflon vial at 120 °C for 16 hours. Subsequently, the solution after acid digestion was evaporated at 120 °C to remove residue acids. Once the Teflon vial was cooling down, 10 ml 20 mM methanesulfonic acid (MSA) was added to dissolve the residue prior to the quantification of AAEM species using an ion chromatography (IC) (model: ICS 3000, column: CS12A, eluent: 20 mM MSA). For quantification of P and trace elements (including As, Cr, Cd, Cu, Co, Ni, Pb, Zn, V and Mn), 2% HNO<sub>3</sub> solution was used instead of MSA to dissolve the residue in the Teflon vial. Phosphorus and trace

elements were then quantified using inductively coupled plasma optical emission spectrometry (ICP-OES, model: PerkinElmer Optima 8300) and an inductively coupled plasma-mass spectrometry (ICP-MS, model: PerkinElmer NexION 350D), respectively.

For the quantification of these elements in PM<sub>10</sub> samples with no organic carbon, the PM<sub>10</sub> along with the polycarbonate substrate on each DLPI stage and backup filter were digested in HNO<sub>3</sub>/HF acids mixture prior to analysis using ICP-OES and ICP-MS. However, for the quantification of these elements in char, char was first ashed in a platinum (Pt) crucible at 600 °C in a Muffle furnace according to a temperature-time program described elsewhere.<sup>173</sup> The resulted ash was then subjected to the HNO<sub>3</sub>/HF acid digestion prior the quantification using IC, ICP-OES or ICP-MS.

**Quantification of Si, Al and Fe and.** For quantification of Si, Al and Fe, the samples after ashing at 600 °C<sup>173</sup> was mixed with X-ray flux (mass ratio of flux to ash, 30:1) and then fused at 950 °C for 2 h in a Pt crucible with a lid in Muffle furnace.<sup>174</sup> The residue was then dissolved in 2% HNO<sub>3</sub> solution and subjected to the quantification using ICP-OES.

**Quantification of S and Cl.** The contents of S and Cl were determined using a recently developed method.<sup>175</sup> Specifically, ~ 30 mg solid samples were first mixed with ~50 mg Eschka flux (sodium carbonate and magnesium oxide, Sigma Aldrich, 00166) and then further covered by ~100 mg Eschka flux on top of the mixed samples in a Pt crucible. For quantification of Cl, the crucible containing mixed sample was placed in the Muffle furnace and heated to 675 °C,<sup>175</sup> held for 2 h and then dissolved by ultrapure water prior to the quantification of Cl using IC (model: Dionex ICS-1100) equipped with an IonPac AS22 fast analytical column. While for determining contents of S in solid samples, the mixture in the crucible was heated to

800 °C instead of 675 °C to ensure the complete transformation of S in solid samples, according to Australian Standard AS 1038.6.3.1.

### 3.4.3 Char structure

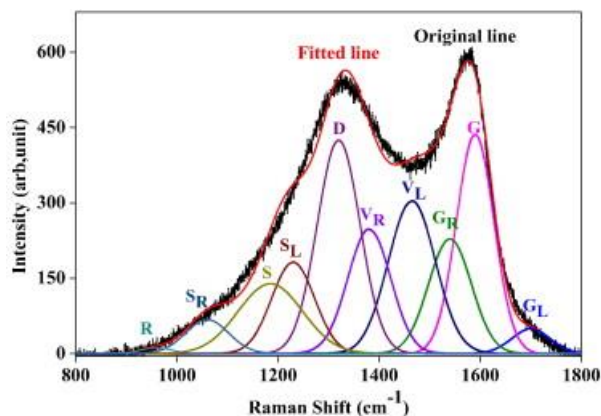


Figure 3-6 Schematic diagram of Raman peak deconvolution for a low-rank solid fuel char samples<sup>142</sup>

The char carbon structure was characterised using Raman spectroscopy in Chapter 6 and Chapter 7. Specifically, as shown in Figure 3-5, Raman spectra in the range of 800–1800  $\text{cm}^{-1}$  were recorded then deconvoluted into 10 Gaussian bands using GRAMS/AI software according to the procedure detailed elsewhere.<sup>11</sup> Each band represents the typical structures in chars produced from low-rank fuels. Especially, G band at 1590  $\text{cm}^{-1}$  represents aromatic ring quadrant breathing and the graphite  $E_2^{2g}$  vibration while D band located at 1300  $\text{cm}^{-1}$  represents defect structures in highly-ordered carbonaceous material with no less than 6 aromatic rings. The  $G_r$  (1540  $\text{cm}^{-1}$ ),  $V_1$  (1465  $\text{cm}^{-1}$ ) and  $V_r$  (1380  $\text{cm}^{-1}$ ) between the D and G bands represent typical structures in amorphous carbon such as aromatics with 3-5 rings. This study considers three key parameters, including the fraction of the combined ( $G_r + V_1 + V_r$ ) band in the total area of Raman spectrum, i.e.  $S_{(G_r + V_1 + V_r)}/S_{\text{all}}$ , the fraction of D band in the total area of Raman spectrum, i.e.  $S_D/S_{\text{all}}$ , and the ratios between the two fractions, i.e.  $S_{(G_r + V_1 + V_r)}/S_D$ , for characterising char carbon structure. The three Raman parameters gives

key information on char structure in terms of the relative amounts of large or small aromatic structures in char. Higher  $S_{(Gr+Vl+Vr)}/S_{all}$  and  $S_{(Gr+Vl+Vr)}/S_D$ , and accordingly, lower  $S_D/S_{all}$  suggest more small aromatic ring systems in the char sample.

### 3.4.4 Char reactivity

In Chapter 6 and 7, isothermal char reactivity was measured using a thermogravimetric analyser (TGA, model: Mettler Toledo). Specifically, about 10 mg of char was loaded into a platinum sample pan and then the sample temperature rose from 30 °C to 110 °C in argon (ultra high purity) and held for 30 min at 110 °C so as to fully remove moisture in char samples. Subsequently, char was further heated at the speed of 50 °C/min to 410 or 500 °C in argon atmospheres. After keeping at the desired temperature for 5 min, the atmosphere was switched to air and the reactivity measurement was commenced under kinetic control regime. Optimal reaction parameters (i.e. gas flow rate, particle size and bed depth) were chosen to ensure that the reactor can be regarded as a differential reactor with respect to the reactive gas. The specific reactivity ( $R$ ,  $\text{min}^{-1}$ ) of a char at any time was calculated from the differential mass loss data ( $dW/dt$ ) according to  $R = -(1/W) \times (dW/dt)$ , where  $W$  is the mass (dry-ash-free) of the char at any time  $t$  (min).<sup>142</sup>

### 3.4.5 X-ray photoelectron spectroscopy measurement

The X-ray Photoelectron spectroscopy (XPS) measurements of char samples were conducted using 5700C model Physical Electronics apparatus equipped with hemispherical analyser (SES R4000) under ultrahigh vacuum condition. The Mg  $K\alpha$  X-ray source at 1253.6 eV was applied to generate core excitation and the  $C_{1s}$  peak position was set at 284.5 eV for calibration with an energy step of 0.025 eV. XPS peak was deconvolution using GRAMS/AI software with Gaussian-Lorentzian curves and Shirley type background line.<sup>126</sup> The  $P_{2p}$  spectrum was divided into four bands and each band represents a typical P bonding type.<sup>125,126</sup> Specifically, the band

at binding energy of 134.0 eV was assigned to C-O-P type bonds where P atom is bonded to four O atom by one double bond or three single bonds, such as in C-O-PO<sub>3</sub>, (CO)<sub>2</sub>PO<sub>2</sub> and (CO)<sub>3</sub>PO groups. A second band at binding energy of 133.2-133.4 eV is characteristic of C-P bonding as in C-PO<sub>3</sub> groups. The third band observed at 132.3 ± 0.2 eV is associated to the reduced phosphorus compounds as C<sub>3</sub>-PO. And a fourth band is located at 131.0 eV representing C<sub>3</sub>-P groups.

### 3.4.6 Surface area of char samples

The surface area analysis of char samples was conducted using Micromeritics Tri-star II Model 3020. About 100 mg char samples were first degassed at 120 °C for 12 h and the weight loss during degassing was measured. The Brunauer Emmett-Teller (BET) N<sub>2</sub> surface area analysis was conducted using N<sub>2</sub> as adsorbate at liquid nitrogen temperature. The surface area was calculated with Micromeritics ASAP 3020 software using BET equation at the linear range of the isotherm.<sup>176</sup> The range of P/P<sub>0</sub> was between 0.05 and 0.35.

### 3.4.7 Particle size distributions and macroporosity of char samples

The particle size distributions of char samples were measured using a particle size analyser (model: Malvern Mastersizer 2000). In order to analyse the macroporosity of char samples, each char sample was set in epoxy resin, solidified, polished and then coated with carbon before the cross-section of the char samples was observed and imaged under a scanning electron microscope (SEM). The SEM images were then processed in an image analyser, Digimizer, to determine the macropores size. The detailed description of sample preparation and data processing can be found elsewhere.<sup>177</sup> In this study, the char macroporosity is given by  $A_p/A_{char}$ , where  $A_p$  is the total cross-sectional pore area with pore diameter being more than 1 μm while  $A_{char}$  represents the total char cross-sectional particle area.

### 3.4.8 Conclusions

To achieve the objectives listed in Section 2.9, series experiments including acid-washing, pyrolysis and combustion of P-containing solid fuels have been conducted. A suitable method was established to quantify phosphorus with various occurrence forms in solid fuels and applied for subsequent analysis of P in char prepared from P-containing solid fuels. Various pyrolysis reactor systems were employed to investigate the pyrolysis behaviour of P-containing solid fuels. Especially, a novel two-stage reactor was employed to achieve the simultaneous generation of volatiles and *in situ* volatile–char interactions. Based on this two-stage reactor, a three-stage pyrolysis/combustion reactor system was further developed and the combustion of volatiles after *in situ* volatile–char interactions was achieved. More importantly, in this study, the generation and combustion of *in situ* volatiles at 1300 °C were realized via a two-stage pyrolysis/combustion reactor system. Various instrumental analyses were conducted to determine the properties of solid fuel and its derived products.

## CHAPTER 4 A NEW METHOD FOR QUANTIFYING PHOSPHORUS OF VARIOUS OCCURANCE FORMS IN P-CONTAINING SOLID FUELS

### 4.1 Introduction

Thermochemical utilisation of P-containing solid fuels, has become increasingly important for combating climate change and reducing fossil fuel consumption.<sup>6,7,26,178</sup> However, thermal utilization of P-containing solid fuels could face various process challenges and environmental problems. The occurrence forms of P in solid fuels varies significantly and dictates P transformation during fuel thermochemical processing. As described in Section 2.6, organic P is likely to be released into gaseous phase during combustion or gasification of solid fuels<sup>4,66</sup> while some inorganic P species can be transformed into refractory mineral and thus retained in the ash.<sup>66</sup> Meanwhile, different forms of P in the by-products (i.e. char, ash and fly ash) from thermochemical processing of these solid fuels have different mobilities and bioavailabilities once they are discharged into environment.<sup>89</sup> Therefore, a thorough understanding of the distribution and transformation of P is critical for optimizing operation conditions during thermochemical utilisation of P-containing solid fuels.

As detailed in Section 2.4.1, several methods have been developed to separate and analyse the form of P in various solid fuels over the last several decades. Particularly, the standards, measurements and testing (SMT) method based on sequential extraction is most commonly used to quantify organic and inorganic P in solid fuels. Unfortunately, those methods have significant disadvantages and might not be successfully applied to quantify phosphorus of various occurrence forms in solid fuels, as detailed in Section 2.4.2. Consequently, this chapter aims to develop a new



method for quantifying different forms of P in solid fuels via chemical extraction and acid digestion techniques, in combination with the analysis of phosphorus using IC and ICP-OES. The new method has been validated using a series of P standards with known contents and forms. It has also been successfully applied for analysing the contents and forms of P in a wide range of seven solid fuels including biosolid, meat and bone meal, chicken litter, rice bran, algae, mallee leaf and biosolid char (hereafter termed as BS, MBM, litter, RB, algae, leaf and BSC, respectively), with far better accuracies than those determined using the conventional SMT method. The properties of those solid fuels and their contents of inorganic species are shown in Table 4-1 and Table 4-2, respectively.

Table 4-1 Proximate and ultimate analyses of solid fuels used in this study

Samples	Moisture (wt%, ar <sup>a</sup> )	Proximate (wt%, db b)			Ultimate (wt%, daf <sup>e</sup> )			
		Ash	VM <sup>c</sup>	FC <sup>d</sup>	C	H	N	O <sup>f</sup>
BS	4.2	19.5	67.4	13.1	53.78	8.15	9.98	28.09
RB	3.5	9.2	35.9	54.9	46.82	7.90	2.35	42.93
MBM	2.6	21.6	12.9	65.5	42.37	6.28	9.04	42.31
Algae	3.9	4.3	39.4	56.3	48.92	6.90	9.02	35.16
Litter	4.6	31.2	26.9	41.9	40.87	3.42	17.28	38.43
Leaf	7.8	3.9	74.8	21.3	56.21	7.29	1.49	35.01
BSC	1.8	56.2	4.2	39.6	94.10	0.22	4.68	1.00

<sup>a</sup> air dried; <sup>b</sup> dry basis; <sup>c</sup> VM–volatile matter; <sup>d</sup> FC–fixed carbon; <sup>e</sup> daf–dry ash free; <sup>f</sup> by difference.

Table 4-2 Contents (mg/kg<sub>solid fuels, db</sub>) of inorganic species in solid fuels

	BS	RB	MBM	Algae	Litter	Leaf	BSC
Na	1346.2 ± 18.2	129.1 ± 12.3	14761.3 ± 22.1	780.7 ± 12.5	8849.9 ± 81.1	5537.5 ± 4.9	4200.3 ± 3.2
K	2008.6 ± 20.3	17563.9 ± 26.3	7440.2 ± 32.9	9139.5 ± 71.1	17763.3 ± 92.1	3780.6 ± 6.7	5302.1 ± 9.5
Ca	20652.3 ± 26.9	426.6 ± 10.6	70191.5 ± 99.8	1332.2 ± 15.9	32293.1 ± 94.2	7633.0 ± 9.6	70120.1 ± 4.1
Mg	4852.6 ± 36.9	8489.2 ± 22.8	1768.4 ± 37.8	2865.2 ± 44.2	5463.6 ± 41.1	1418.5 ± 2.4	16052.6 ± 11.2
Cl	892.4 ± 2.9	526.2 ± 3.2	8182.5 ± 21.1	1970.2 ± 12.9	5569.1 ± 32.1	1852.6 ± 12	15.6 ± 3.4
S	8548.9 ± 29.7	2026.9 ± 15.9	4687.6 ± 36.9	4428.6 ± 26.9	2218.6 ± 3.6	1184.6 ± 12	5302.6 ± 5.2
Fe	3158.9 ± 48.5	87.5 ± 2.9	928.3 ± 55.8	2.6 ± 0.3	1492.6 ± 9.6	142.6 ± 0.4	10625.6 ± 11.8
P	21887.6 ± 99.7	11532.6 ± 29.7	45532.5 ± 23.6	15282.9 ± 3.6	18259.6 ± 32.9	1613.3 ± 2.6	60155.2 ± 14.9
Si	19007.9 ± 69.4	298.6 ± 7.8	5543.2 ± 32.4	127.7 ± 5.2	18793.1 ± 32.7	504.7 ± 8.2	61425.2 ± 24.0
Al	6708.9 ± 48.7	52.6 ± 2.9	554.7 ± 5.6	109.7 ± 9.5	3002.3 ± 69.3	198.7 ±	28125.6 ± 9

## 4.2 Evaluation of the SMT method for quantifying different forms of phosphorus in solid fuels

In this section, experiments were carried out to evaluate the effectiveness of the SMT method for quantifying different forms of phosphorus in solid fuels. It is known that five typical organic P-containing components (i.e., A: D-fructose 6-phosphate disodium salt hydrate representing sugar phosphate; B: Phytic acid sodium salt hydrate representing phytate; C: Adenosine 5'-monophosphate monohydrate representing nucleotides; D: 1,2-Dioleoyl-sn-glycero-3-phosphoric acid sodium salt representing phospholipid; E: Deoxyribonucleic acid sodium salt representing nucleic acids.) are commonly presented in solid fuels. Following the SMT method (See Section 2.4.1), these organic P-containing components were first extracted using 1M HCl for 16h, the residue was later burned in a Pt crucible at 450 °C and then the solid residue in the Pt crucible was extracted using 1M HCl for 16h. The phosphate contents in the final extracts were quantified and the recoveries of organic P (as per SMT method) in these organic phosphates are presented in Figure 4-1. The results in Figure 4-1 clearly shows that no P in sugar phosphate, phytic acid and nucleotide is recovered because these organic phosphates are acid-soluble and thus present in acid-soluble fractions. Analysis of the first extract solution using ICP-OES confirmed that all P in these three organic phosphates are recovered in the solution. In addition, the recoveries of P from phospholipid and nucleic acids are ~76-82%, indicating significant portions of P in phospholipids and nucleic acids are also lost during thermal treatment. This can be attributed to the formation of phosphorus pentoxide which sublimates at 300 °C<sup>179</sup> during thermal treatment. Clearly, the SMT method is unable to quantify organic phosphorus in biomass. Therefore, none of the existing methods can be applicable to various solid fuels for accurately quantifying both organic and inorganic phosphorus in solid fuels. Consequently, a new method must be developed to achieve this purpose.

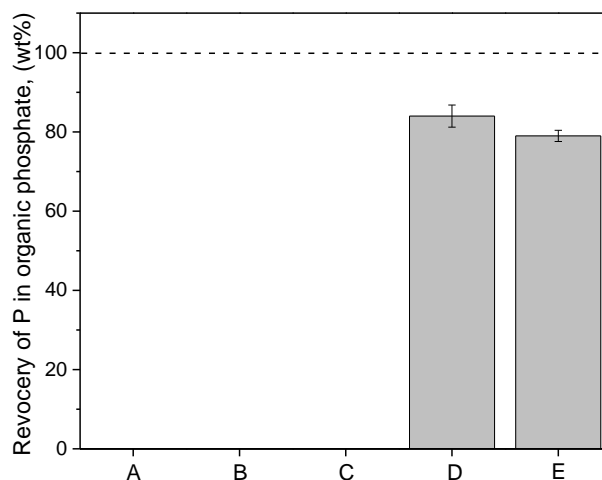


Figure 4-1 Recovery of P in organic phosphate after sequential extraction according to the SMT method. A: D-fructose 6-phosphate disodium salt hydrate; B: Phytic acid sodium salt hydrate; C: Adenosine 5'-monophosphate monohydrate; D: 1,2-Dioleoyl-SN-glycero-3-phosphoric acid sodium salt; E: Deoxyribonucleic acid sodium salt

### 4.3 A new method for quantifying P of various forms in solid fuels

#### 4.3.1 Overview of the new method

Figure 4-2 illustrates the proposed new method for quantifying P of various forms in solid fuels. The method fractionates the total P ( $P_t$ ) in solid fuels into five fractions of P. These consists of two inorganic P fractions [i.e., acid-soluble inorganic P ( $P_{as-in}$ ) and acid-insoluble inorganic P ( $P_{ai-in}$ )] and three organic P fractions [i.e., acid-soluble organic P ( $P_{as-or}$ ) and two-acid insoluble organic P including P in phospholipids ( $P_{li}$ ) and P in other acid-insoluble organic structures such as nucleic acids ( $P_{na}$ )]. The new method consists of three extraction steps, including extraction and quantification of  $P_{as-or}$  and  $P_{as-in}$  (Step 1),  $P_{li}$  (Step 2) as well as  $P_{na}$  and  $P_{ai-in}$  (Step 3). The total P ( $P_t$ ) in solid fuels is determined using ICP-OES after HF/HNO<sub>3</sub>/H<sub>2</sub>O<sub>2</sub> digestion.<sup>174</sup> The details of key steps of the proposed new method are described as follows.

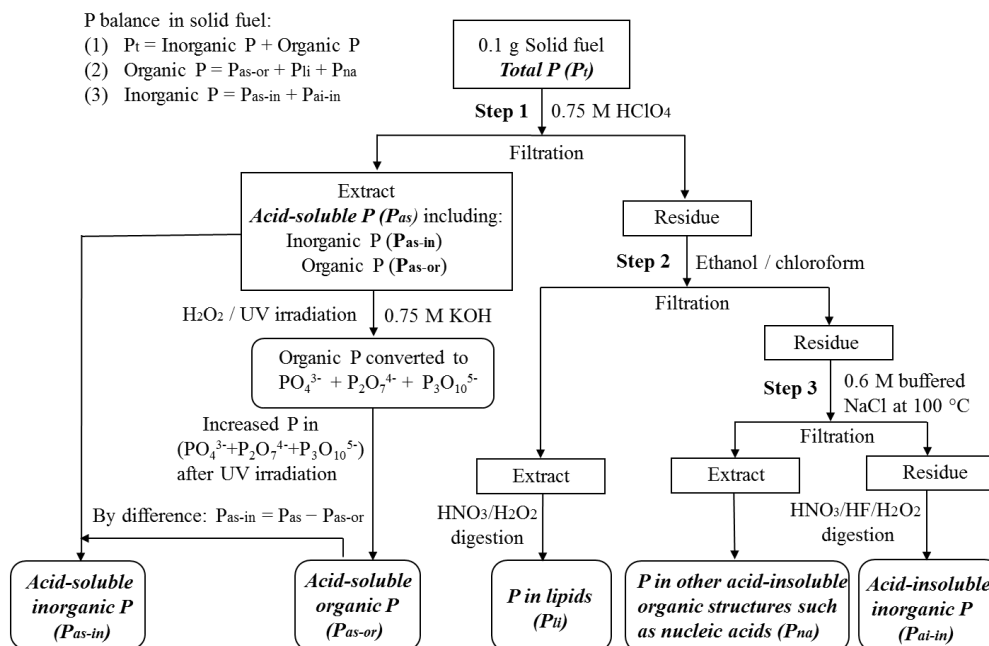


Figure 4-2 A schematic diagram of the new method for fractionation and quantification of P with various occurrence forms in solid fuels.  $P_t$  and  $P_{\text{as}}$  represent total phosphorus and acid-soluble phosphorus in solid fuel, respectively.  $P_{\text{as-in}}$  and  $P_{\text{ai-in}}$  represent acid-soluble inorganic P and acid-insoluble inorganic P, respectively.  $P_{\text{as-or}}$ ,  $P_{\text{li}}$  and  $P_{\text{na}}$  represent acid-soluble organic P, P in phospholipids and P in other acid-insoluble organic structures such as nucleic acids, respectively

### 4.3.2 Key steps of the new method

**Step 1: Extraction and quantification of  $P_{\text{as-or}}$  and  $P_{\text{as-in}}$ .** The new method starts with extraction of solid fuels with cold perchloric acid (PCA) to quickly destruct all phosphatases which otherwise can rapidly hydrolyse the organic phosphorus into inorganic phosphorus.<sup>7</sup> Briefly, ~ 0.1g solid fuel was immersed into 15 ml (~ 4 °C) 0.75 M PCA in a 60 ml perfluoroalkoxy alkanes (PFA) vial, followed by stirring the mixture at room temperature for 1 h. The mixture was then vacuum filtered using a 2  $\mu\text{m}$  polytetrafluoroethylene (PTFE) filter (45mm diameter) mounted on a glass vacuum filtration funnel. The filtrate was collected and solid residue on the PTFE filter was further washed with deionised water until the pH of the filtrate was close to 7.

During acid extraction, acid-soluble inorganic phosphorus (e.g. alkali, alkaline and iron phosphates) can be extracted from the fuel.<sup>92</sup> For organic phosphorus, sugar phosphate, inositol phosphate and nucleotides can be extracted without degradation while phospholipid and nucleic acids are retained as residue.<sup>7,98</sup> The excess PCA in the filtrate should be neutralised immediately to prevent the hydrolysis of organic phosphorus under acid conditions. This was done via pipetting and mixing 10 ml of the filtrate with 10 ml 0.75 M KOH in a 60 ml PFA vial and keeping the mixture at 4 °C for 2 h to neutralize the acid solution, forming KClO<sub>4</sub> precipitates. The neutralised solution was filtered with a 0.45 µm membrane filter prior to quantification of PO<sub>4</sub><sup>3-</sup>, P<sub>2</sub>O<sub>7</sub><sup>4-</sup> and P<sub>3</sub>O<sub>10</sub><sup>5-</sup> ions using an IC and acid-soluble P content (P<sub>as</sub>) using an ICP-OES. The use of KOH is favoured due to low solubility of KClO<sub>4</sub> in water, effectively removing significant portion of perchlorate ion in the sample matrix prior to IC analysis.

Separation of the organic phosphorus in solution is the key to quantify the acid-soluble organic or inorganic phosphorus in the acid-extract. However, this proves to be challenging. Previous research pointed out that exposure of sea-water to ultra-violet (UV) irradiation in presence of 3% hydrogen peroxide (H<sub>2</sub>O<sub>2</sub>) can rapidly liberate the organic phosphate via breaking P–O–C and P–C bonds as inorganic phosphate while the P–O–P bonds remained intact.<sup>73,180</sup> Consequently, organic phosphates in solutions can be selectively converted to orthophosphate (PO<sub>4</sub><sup>3-</sup>), pyrophosphate (P<sub>2</sub>O<sub>7</sub><sup>4-</sup>) and tripolyphosphate (P<sub>3</sub>O<sub>10</sub><sup>5-</sup>) while inorganic phosphorus including all condensed phosphates remain unchanged. Therefore, the acid-soluble organic phosphorus content (P<sub>as-or</sub>) in the solutions can be determined from the difference in PO<sub>4</sub><sup>3-</sup>, P<sub>2</sub>O<sub>7</sub><sup>4-</sup> and P<sub>3</sub>O<sub>10</sub><sup>5-</sup> ion content in the solution before and after UV irradiation. This method is adopted in this study for quantification of organic phosphorus in solution after PCA extraction. To ensure the complete conversion of organic phosphorus during UV irradiation, the solution is diluted using deionised water and hydrogen peroxide ensure the total acid-soluble P content (P<sub>as</sub>) in the solution in < 10 mg/L while keeping the

content of H<sub>2</sub>O<sub>2</sub> in solution at 3% (v/v). Briefly, 10 ml of the diluted solution was then stirred in a Pyrex glass reactor and irradiated under a 300 W Mercury-Xenon lamp (UXM-502MD, Ushio) for 8 h at a constant distance (~30 cm) while the temperature of the reactor was maintained at 25 °C by continuously passing chilled water through the reactor. Subsequently, the PO<sub>4</sub><sup>3-</sup>, P<sub>2</sub>O<sub>7</sub><sup>4-</sup> and P<sub>3</sub>O<sub>10</sub><sup>5-</sup> ion concentration in solution pre- and post- UV irradiation are quantified using an IC equipped with IonPac AS11-HC column. The increased P contents in integrated (PO<sub>4</sub><sup>3-</sup> + P<sub>2</sub>O<sub>7</sub><sup>4-</sup> + P<sub>3</sub>O<sub>10</sub><sup>5-</sup>) ions after UV irradiation equal to the contents of acid-soluble organic P (P<sub>as-or</sub>) in solid fuel. Consequently, acid-soluble inorganic P (P<sub>as-in</sub>) can be calculated by subtracting P<sub>as-or</sub> from acid-soluble P (P<sub>as</sub>) in solid fuels.

**Step 2: Extraction and quantification of P in phospholipids (P<sub>li</sub>).** Phospholipids in solid fuels can be separately extracted by different solutions after PCA extraction. To extract the phospholipids,<sup>99</sup> the residue from Step 1 was stirred (100 r/min) in 10 ml ethanol and chloroform mixture (v/v, 1:1) in a 60 ml PFA container at room temperature for 2 h, followed by vacuum filtration using a 2 μm PTFE filter. Subsequently, 5 ml of the filtrate was transferred into a 15 ml PFA vial and dried at 60 °C in an extracted oven for 4 h to fully evaporate the solvents prior to digestion in HNO<sub>3</sub>/H<sub>2</sub>O<sub>2</sub> at 120 °C and quantification of P in phospholipids (P<sub>li</sub>) using ICP-OES.

**Step 3: Extraction and quantification of P<sub>ai-in</sub> and P in other acid-insoluble organic structures such as nucleic acids (P<sub>na</sub>).** Following the extraction of phospholipids, the remaining organic P in the residue is in forms of other acid-insoluble organic structures such as nucleic acids (i.e. P<sub>na</sub>). These acid-insoluble organic P can be extracted using buffered NaCl solution (0.6 M NaCl in 0.1 M sodium acetate at pH 4.0) with minimum extraction of other P-containing species.<sup>181</sup> Briefly, the residue from Step 2 was transferred into a 15 ml PFA vial, which was then sealed and heated at 100 °C for 30 min after the addition of 10 ml buffered NaCl solution. After the solution was cooled down to room temperature, the suspension was vacuum

filtrated and the P in the filtrate was then quantified as  $P_{na}$  using an ICP-OES. It is noted that strong alkaline solutions were also used to extract P in the forms of nucleic acids from plant tissue in previous studies.<sup>49</sup> However, some inorganic phosphorus species such as  $AlPO_4$ <sup>182</sup> and long-chain condensed phosphates<sup>130</sup> can be dissolved in alkaline solutions so that alkaline solutions should not be used for such extractions and determination of  $P_{na}$  in solid fuels.

The residue after the extraction using buffered NaCl solution contains little organic phosphorus and the remaining P is mainly consist of acid-insoluble inorganic phosphorus ( $P_{ai-in}$ ), such as calcium phosphate silicate and long-chain condensed phosphates.<sup>100</sup> These P-containing species can only be liberated through digestion in concentrated HF/ $HNO_3$  mixture at 120 °C. The detailed procedure is described elsewhere.<sup>174</sup>

#### 4.4 Validation and application of the new method

##### 4.4.1 Standard samples for validation

Table 4-3 Contents (mg/kg\_solid fuels, db) of inorganic species in acid-washed samples

	AWMW	AWRB	DAWB
Na	6.2 ± 1.0	4.9 ± 1.1	1.3 ± 0.4
K	2.6 ± 0.3	3.3 ± 0.3	0.9 ± 0.2
Ca	6.3 ± 2.5	6.6 ± 1.7	2.5 ± 0.5
Mg	5.6 ± 0.9	5.0 ± 0.6	1.9 ± 0.7
Cl	0	0	0
S	0.9 ± 0.5	0	0.4 ± 0.3
Fe	2.8 ± 0.5	5.6 ± 0.4	0.5 ± 0.2
P	1.6 ± 0.7	4.6 ± 0.5	2.3 ± 0.5
Si	17.9 ± 4.5	114.3 ± 10.1	744.9 ± 71.1
Al	8.9 ± 1.7	119.6 ± 2.3	454.9 ± 51.8

Two categories of (a total of 28) P-containing standards were purposely prepared via loading known amounts of one or more P-containing chemical compound(s) into P-free samples. Accordingly, acid-washed mallee wood (AWMW), acid-washed rice bran (AWRB) and double-acid washed biosolid (DAWB) were prepared as substrates with the contents of inorganic species in those samples shown in Table 4-3. Clearly, little P is present in those acid-washed samples.

The information on the P-containing standards are listed in Table 4-4. Category I standards consist of 25 standards with a single phosphorus occurrence form (i.e.  $P_{as-in}$ ,  $P_{ai-in}$ ,  $P_{as-or}$ ,  $P_{li}$  or  $P_{na}$ ) at a wide range of P contents, prepared by loading different but known amounts of P-containing model compounds into AWMW sample. Briefly, the desired amounts of P-containing model compounds and about 1 g AWMW were weighted in a 50 ml polyethylene container and then manually mixed for 60 min to yield the P-loaded standard samples. Hydroxyapatite/sodium hexametaphosphate mixture (1:1, w/w), aluminium phosphate/calcium phosphate silicate mixture (1:1, w/w), adenosine 5'-monophosphate monohydrate/phytic acid sodium salt hydrate/D-fructose 6-phosphate disodium salt hydrate mixture (1:1:1,w:w:w), 1,2-Dioleoyl-sn-glycero-3-phosphoric acid sodium salt and deoxyribonucleic acid sodium salt were respectively loaded to represent  $P_{as-in}$ ,  $P_{ai-in}$ ,  $P_{as-or}$ ,  $P_{li}$  and  $P_{na}$  in solid fuels. Based on the typical range of concentrations of different forms of phosphorus in solid fuels,<sup>7,89,90,100</sup> the content of  $P_{as-in}$ ,  $P_{ai-in}$ ,  $P_{as-or}$ ,  $P_{li}$  and  $P_{na}$  are ~500–100,000 mg/kg in SA1–SA5 standard samples, ~200–10,000 mg/kg in SB1–SB5 standard samples, ~200–15,000 mg/kg in SC1–SC5 standard samples, ~200–1,500 mg/kg in SD1–SD5 standard samples and ~200–2,500 mg/kg in SE1–SE5 standard samples, respectively.

Category II standards include 3 standards samples (SF, SG and SH) containing a mixture of different P occurrence forms via selectively loading various P-containing model compounds with multiple phosphorus forms into AWMW, AWRB and DAWB



substrates, respectively. These P occurrence forms represent P in typical woody biomass, seed-originated biomass and biosolid.<sup>7,91</sup> As listed in Table 5, SF and SH standards contain dominantly inorganic P while organic P in nucleotides and inositol phosphate are the main phosphorus occurrence forms in SG sample.

Table 4-4 Contents and recovery of P with different forms in standards SF, SG and SH samples determined by SMT and the proposed new method

Standard	P content (mg/kg)	P form	P-containing model compounds loaded	Substrate used
<b>Category I: Standards with P of a single occurrence form</b>				
SA1	520.8	P <sub>as-in</sub>	Hydroxyapatite	AWMW
SA2	19794.2		and sodium hexametaphosphate mixture	
SA3	50914.8		(1:1, w/w)	
SA4	81836.1			
SA5	105182.9			
SB1	197.4	P <sub>ai-in</sub>	Aluminium phosphate	AWMW
SB2	1764.0		and calcium phosphate silicate mixture	
SB3	4214.0		(1:1, w/w)	
SB4	6921.2			
SB5	9601.3			
SC1	184.8	P <sub>as-or</sub>	Adenosine 5'-monophosphate monohydrate,	AWMW
SC2	2140.7		phytic acid sodium salt hydrate and	
SC3	5031.2		D-fructose 6-phosphate disodium salt hydrate	
SC4	9476.1		mixture (1:1:1, w:w:w)	
SC5	14760.8			
SD1	189.3	P <sub>li</sub>	1,2-Dioleoyl-SN-glycero-3-phosphoric acid	AWMW
SD2	433.5		sodium salt	
SD3	766.3			
SD4	1199.5			
SD5	1548.7			
SE1	214.2	P <sub>na</sub>	Deoxyribonucleic acid sodium salt	AWMW
SE2	684.2			
SE3	1177.3			
SE4	1864.5			
SE5	2408.6			
<b>Category II: Standards with P of multiple occurrence forms</b>				
SF	4526.5	P <sub>as-in</sub>	Ammonium phosphate	AWMW
			and sodium pyrophosphate tetrabasic mixture (1:1, w/w)	
	259.9	P <sub>ai-in</sub>	Aluminium phosphate and calcium phosphate	

			silicate mixture (1:1, w/w)	
	1704.9	P <sub>as-or</sub>	D-fructose 6-phosphate disodium salt hydrate and cytidine-5' triphosphate disodium salt mixture (1:1, w/w)	
	356.1	P <sub>li</sub>	1,2-Dioleoyl-sn-glycero-3-phosphoric acid sodium salt	
	263.8	P <sub>na</sub>	deoxyribonucleic acid sodium salt	
SG	1053.5	P <sub>as-in</sub>	Ammonium phosphate and sodium pyrophosphate tetrabasic mixture (1:1, w/w)	
	672.2	P <sub>ai-in</sub>	Aluminium phosphate and calcium phosphate silicate mixture (1:1, w/w)	
	8943.9	P <sub>as-or</sub>	Adenosine 5'-monophosphate monohydrate and phytic acid sodium salt hydrate mixture (1:1, w/w)	AWRB
	1422.1	P <sub>li</sub>	1,2-Dioleoyl-sn-glycero-3-phosphoric acid sodium salt	
	1723.2	P <sub>na</sub>	Deoxyribonucleic acid sodium salt	
SH	46506.2	P <sub>as-in</sub>	Hydroxyapatite and sodium hexametaphosphate mixture (1:1, w/w)	
	5689.7	P <sub>ai-in</sub>	Aluminium phosphate and calcium phosphate silicate mixture (1:1, w/w)	
	532.6	P <sub>as-or</sub>	Adenosine 5'-monophosphate monohydrate and phytic acid sodium salt hydrate mixture (1:1, w/w)	DAWB
	322.5	P <sub>li</sub>	1,2-Dioleoyl-sn-glycero-3-phosphoric acid sodium salt	
	843.7	P <sub>na</sub>	Deoxyribonucleic acid sodium salt	

#### 4.4.2 Validation of the new method

To demonstrate the proposed method can accurately quantify and classify P fractions in solid fuels, this method is verified through three validation experiments. First, as the conversion of organic phosphorus into inorganic phosphorus by UV irradiation is only tested for sea water samples with low organic P concentration (<0.1 mg/L) in previous study,<sup>73,180</sup> four organic P-containing model compounds (A: adenosine 5'-monophosphate monohydrate; B: cytidine 5'-triphosphate disodium salt; C: phytic

acid sodium salt hydrate; D: D-fructose 6-phosphate disodium salt hydrate) and two condensed phosphates salts (E: sodium hexametaphosphate, F: sodium pyrophosphate tetrabasic) are respectively dissolved in cold PCA solution and the solutions are processed according to the procedure described above. The conversions of organic phosphorus to  $\text{PO}_4^{3-}$ ,  $\text{P}_2\text{O}_7^{4-}$  and  $\text{P}_3\text{O}_{10}^{5-}$  before and after UV irradiation are shown in Figure 4-3. Clearly, after UV irradiation, organic P species are completely converted into  $\text{PO}_4^{3-}$ ,  $\text{P}_2\text{O}_7^{4-}$  and  $\text{P}_3\text{O}_{10}^{5-}$  while condensed phosphates are unchanged, indicating that organic phosphorus can be selectively converted with UV irradiation. These results suggest that UV irradiation is very effective in converting acid-soluble organic phosphorus into orthophosphate, pyrophosphate and tripolyphosphate.

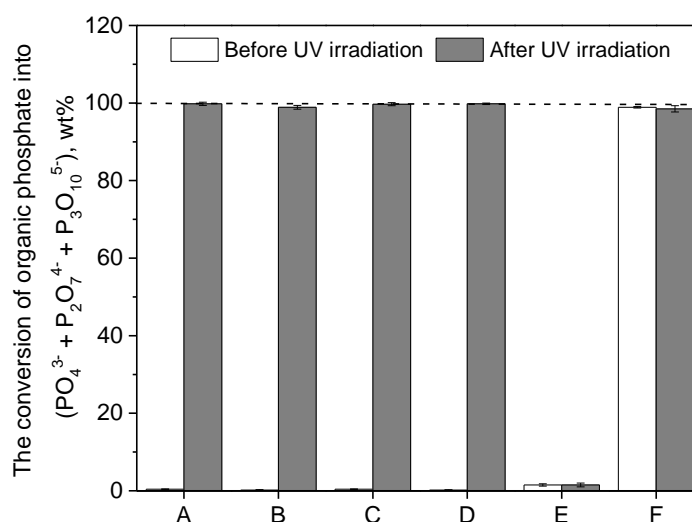


Figure 4-3 Conversion of organic phosphorus to  $\text{PO}_4^{3-}$ ,  $\text{P}_2\text{O}_7^{4-}$  and  $\text{P}_3\text{O}_{10}^{5-}$  by UV irradiation for 8 h. A: adenosine 5'-monophosphate monohydrate; B: Cytidine 5'-triphosphate disodium salt; C: phytic acid sodium salt hydrate; D: D-fructose 6-phosphate disodium salt hydrate; E: sodium hexametaphosphate; F: sodium pyrophosphate tetrabasic

Second, to validate whether SMT method and the proposed method can quantitatively determine phosphorus in solid fuels, standard samples SA1–SA5 containing  $\text{P}_{\text{as-in}}$ , SB1–SB5 containing  $\text{P}_{\text{ai-in}}$ , SC1–SC5 containing  $\text{P}_{\text{as-or}}$ , SD1–SD5

---

containing  $P_{li}$  and standard samples SE1–SE5 containing  $P_{na}$  were analysed using the new method and SMT method with the results shown in Figure 4-4. Clearly, both inorganic and organic P loaded in the AWMW samples cannot be fully recovered (P balance well below 80 %) using SMT method, especially for acid-soluble organic P (see Figure 4-4c). However, the contents of P loaded in those standard samples are significantly matched with the contents of P quantified with the new method with minimal errors (<3%), suggesting that the new method is effective in quantifying single P fraction in solid fuels.

Third and last, to validate whether the proposed method can effectively separate different occurrence forms of phosphorus in solid fuels, SF, SG and SH standard samples were analysed using the proposed method and existing SMT method. The determined contents of P and recovery of P in those standard samples analysed by SMT and the proposed method are shown and compared in Table 4-5. The results again demonstrate that SMT method is unable to accurately quantify both organic and inorganic P in these standard samples, especially organic P where the recoveries are low (15-40%). However, both organic and inorganic P species were successfully extracted and quantified by the proposed method with high recovery (> 95%) and good repeatability which further proves the effectiveness of the proposed method in quantification of different forms of phosphorus in solid fuels.

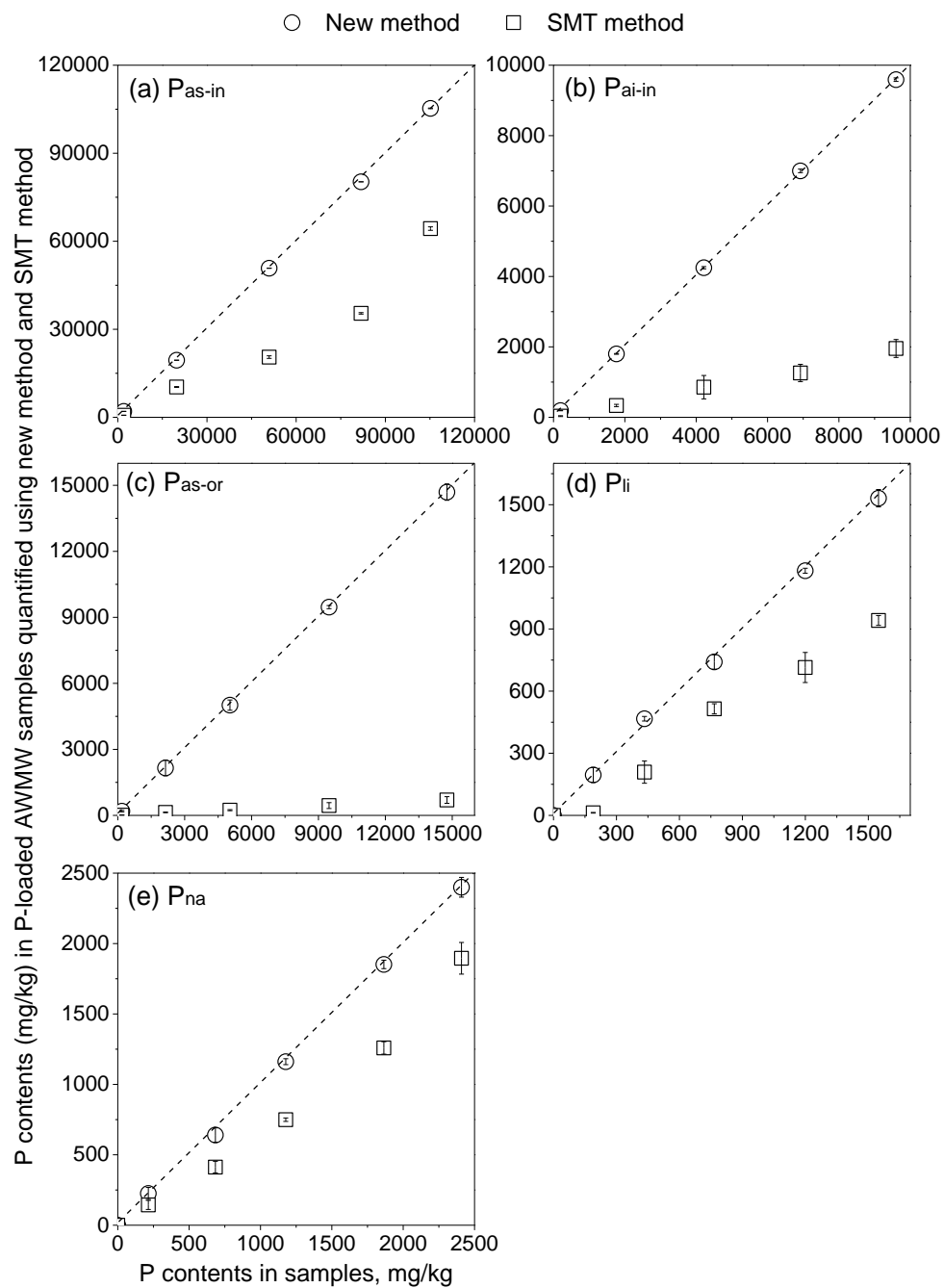


Figure 4-4 Contents of phosphorus in P-loaded AWMW samples, quantified using the new method (open circle) and existing SMT method (open square); (a)  $P_{as-in}$  in Standards SA1-SA5; (b)  $P_{ai-in}$  in Standards SB1-SB5; (c)  $P_{as-or}$  in Standards SC1-SC5; (d)  $P_{li}$  in Standards SD1-SD5; (e)  $P_{na}$  in Standards SE1-SE5

Table 4-5 Contents and recovery of P with different forms in standards SF, SG and SH samples determined by SMT and the proposed new method

Standard	P forms	P content	SMT method	Recovery, wt%	New method	Recovery, wt%	
SF	P <sub>as-in</sub>	4526.5			4580.3 ± 44.2	101.2	
	P <sub>ai-in</sub>	259.9			254.2 ± 12.6	97.8	
	<b>Total inorganic P</b>	<b>4786.4</b>	<b>2874.8 ± 89.4</b>	<b>60.1</b>	<b>4834.5 ± 40.2</b>	<b>101.0</b>	
	P <sub>as-or</sub>	1704.9			1685.9 ± 44.2	98.9	
	P <sub>li</sub>	356.1			349.5 ± 10.2	98.1	
	P <sub>na</sub>	263.8			242.9 ± 5.9	95.9	
	<b>Total organic P</b>	<b>2324.8</b>	<b>358.4 ± 38.7</b>	<b>15.4</b>	<b>2278.3 ± 34.8</b>	<b>98.0</b>	
	SG	P <sub>as-in</sub>	1053.5			1042.6 ± 142.3	99.0
		P <sub>ai-in</sub>	672.2			642.9 ± 22.1	95.6
		<b>Total inorganic P</b>	<b>1725.7</b>	<b>985.6 ± 77.2</b>	<b>57.1</b>	<b>1685.5 ± 100.2</b>	<b>97.7</b>
P <sub>as-or</sub>		8943.9			8812.6 ± 142.3	98.5	
P <sub>li</sub>		1422.1			1400.1 ± 33.0	98.5	
P <sub>na</sub>		1723.2			1731.9 ± 22.6	100.5	
<b>Total organic P</b>		<b>12089.2</b>	<b>2541.9 ± 88.1</b>	<b>21.0</b>	<b>11944.6 ±</b>	<b>98.8</b>	
SH	P <sub>as-in</sub>	46506.2			46463.1 ± 13.9	99.9	
	P <sub>ai-in</sub>	5689.7			5587.1 ± 127.2	98.2	
	<b>Total inorganic P</b>	<b>52195.9</b>	<b>38475.6 ± 95.3</b>	<b>73.7</b>	<b>52050.2 ± 59.6</b>	<b>99.7</b>	
	P <sub>as-or</sub>	532.6			513.9 ± 13.9	96.5	
	P <sub>li</sub>	322.5			308.9 ± 33.4	95.8	
	P <sub>na</sub>	843.7			810.9 ± 24.7	96.1	
	<b>Total organic P</b>	<b>1698.8</b>	<b>687.5 ± 54.1</b>	<b>40.5</b>	<b>1633.7 ± 27.9</b>	<b>96.2</b>	

## 4.4.3 Application of the new method

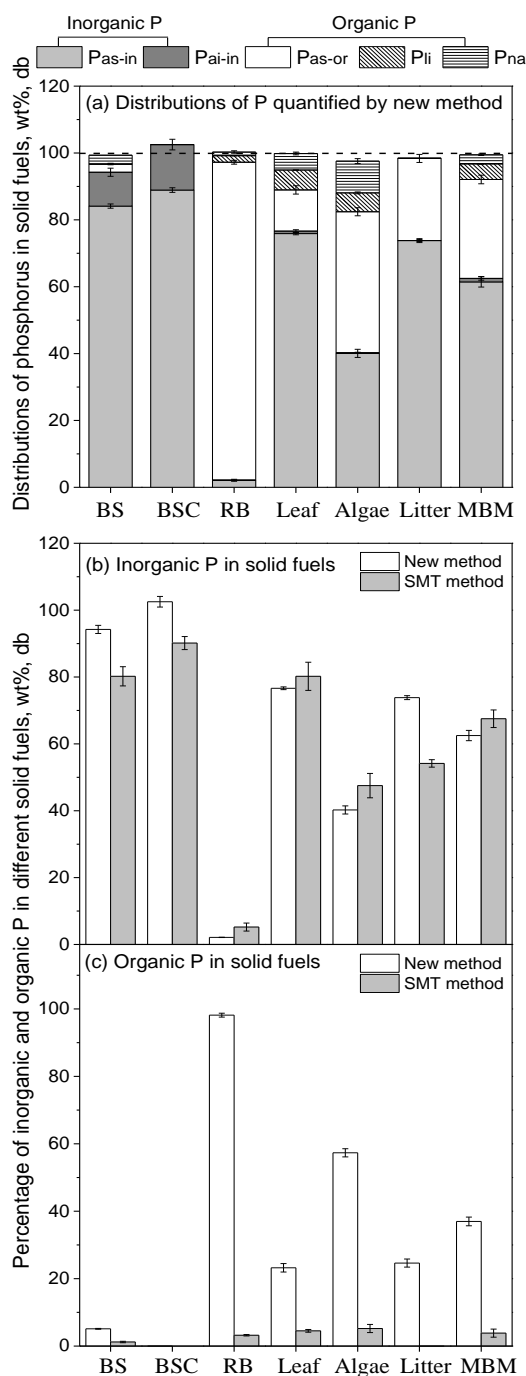


Figure 4-5 Comparison of P with various forms in seven different solid fuel samples, quantified using the SMT method and the new method proposed in this study, including (a) distribution of P in these solid fuels determined by the new method; the percentages of (b) inorganic and (c) organic P in these solid fuels quantified using the new method and SMT method

The distributions of phosphorus in 7 different solid fuels were then determined using the proposed new method in this study, with the results presented in Figure 4-5a. It can be seen that over 95% of P in all solid fuels can be recovered and quantified using the proposed new method, which demonstrates good repeatability and minimal errors. Four important observations can also be made based on the results in Figure 4-5. First, compared to biosolid, no organic phosphorus was found in slow heating biosolid char prepared at 800 °C, implying that organic phosphorus is thermally unstable during pyrolysis.<sup>8</sup> Second, except in biosolid and its derived char, little acid-insoluble inorganic phosphorus is found in other solid fuels. This can be attributed to the presence of  $\text{AlPO}_4$  and P-containing silicates in biosolid sample, which has considerably high concentrations of Al and Si. Third, the distributions of phosphorus in different biomass (rice bran, leaf and algae) are significantly different. Organic P only accounts for ~25% of total P in mallee leaf. However, it accounts for >95% and ~60% of total P in rice bran and algae, respectively. Reasonably, organic phosphorus (such as inositol phosphate and nucleotides) plays important roles in growth of seed<sup>7</sup> and algae,<sup>183</sup> resulting in the presence of large proportion of organic phosphorus in these samples. The extract from  $\text{HClO}_4$  extraction of rice bran was also analyzed in an IC and the result confirms that ~95% P in rice bran is phytic acid (an inositol phosphate). Fourth, both organic and inorganic P are present in two animal wastes, i.e. chicken litter and meat and bone meal (MBM). Some organic P-containing species such as inositol phosphate cannot be digested by animal's digestion system, thus remaining in chicken litter<sup>74</sup> while for meat and bone meal, acid-soluble nucleotides, phospholipids and other P-containing organic structures (including nucleic acids) are the main organic P components. In addition, it is also known that hydroxyapatite is the major component of tooth enamel and bone mineral.<sup>76</sup> Therefore, hydroxyapatite may be abundant in meat and bone meal, considering the high contents of Ca (see Table 4-2).

Further efforts were also made to compare the new method with the SMT method in quantification of inorganic P in these solid fuels, with the results presented in Figure



4-5b. It is clearly seen that the SMT method reports considerably lower inorganic P in biosolid, biosolid char and chicken litter because the method can only determine acid-soluble orthophosphate. In addition, compared with the new method, excessive acid extraction (16h) also hydrolyses part of organic P into orthophosphate, leading to slightly higher inorganic P contents in leaf, algae and meat and bone meal, reported by the SMT method. Similarly, the SMT method can only detect acid-insoluble organic phosphorus species (i.e., phospholipids, nucleic acids and other acid-insoluble P-containing organic structures), and thus significantly under-reports the acid-soluble organic P such as phytic acid in rice bran, as shown in Figure 4-5c.

In sum, the results clearly demonstrate that the SMT method is unreliable. The new method proposed in this study is proven to be capable of determining the distributions of P with various forms in solid fuels and achieves phosphorus mass balance.

#### **4.5 Conclusions**

A new method is proposed in this study to extract different forms of phosphorus in solid fuels via three-step sequential extraction, followed by phosphorus quantification in each fraction using IC and ICP-OES. Three organic phosphorus fractions (i.e. acid-soluble organic P, P in phospholipids and P in other acid-insoluble organic structures such as nucleic acids) and two inorganic P fractions (acid-soluble inorganic P and acid-insoluble inorganic P) in solid fuels can be extracted and determined using the new method. To validate the proposed new method, samples loaded with different forms and concentrations of phosphorus were extracted and quantified using the new method with complete P being recovered. Compared with the poor performance of the conventional SMT method, the application of this new method in quantifying different forms of phosphorus in seven different solid fuels achieves high P mass balance and is suitable for quantifying P of various forms in solid fuels.

*Reprinted with permission from (Xujun Chen, Sui Boon Liaw, and Hongwei Wu. A New Method for Quantifying Phosphorus of Various Occurrence Forms in Solid Fuels, Energy & Fuels 2019, 33, 3311-3321). Copyright (2019) American Chemical Society.*

---

# CHAPTER 5 EFFECT OF REACTOR CONFIGURATIONS ON TRANSFORMATION AND RELEASE OF PHOSPHORUS DURING P-RICH BIOMASS PYROLYSIS UNDER VARIOUS CONDITIONS

## 5.1 Introduction

Thermochemical utilisation of P-containing biomass is an important strategy for sustainable supply of energy and green chemicals.<sup>59</sup> Practically, seed-originated biomass resources such as grain,<sup>28,29</sup> bran<sup>4</sup> and rapeseed meal or cake<sup>2</sup> from biodiesel industry, are increasingly utilized in grate-fired or fluidized bed combustion or gasification systems<sup>4</sup>. The high contents of phosphorus in those biomass play an important role in ash transformation reactions<sup>2,8,31,62</sup> and fly ash chemistry<sup>4,27-29,132,184</sup> during their thermochemical utilization. Consequently, as described in Section 2.2, thermochemical utilization of these P-rich biomass faces various process challenges and leads to undesired environmental impacts. Clearly, fundamental understanding on the transformation of P during thermochemical utilisation of P-rich biomass is critical to optimizing operation conditions, reducing equipment maintenance costs and mitigating P emission.

During combustion or gasification of P-rich biomass, some P species are known to be released in forms of P-containing gases, such as  $\text{PH}_3$ ,  $\text{PO}$ ,  $\text{PO}_2$ ,  $\text{P}_2$ <sup>13,66</sup> and  $\text{KPO}_3$ .<sup>4</sup> Practically, during biomass combustion, it first experiences pyrolysis and rapidly decomposes into biochar and volatiles. It is reported that P was mainly released with volatiles during pyrolysis of P-containing solid fuels.<sup>66</sup> The retained P in char during pyrolysis could be stabilised by forming mineral phosphates via associations with alkali/alkaline earth metallic (AAEM) species, Fe and Al<sup>66</sup> or by forming complexes

with organic carbon fraction of biochar<sup>132</sup>, resulting in different mobilities and bioavailabilities<sup>89</sup> when char product is used as soil amendments<sup>14</sup>. Therefore, pyrolysis is the critical step for P release and transformation during thermal treatment of P-rich biomass.<sup>66</sup> As elaborated in Section 2.6, several studies have investigated the transformation and release of P during combustion or gasification in horizontal tube reactors<sup>4,66</sup>, fixed-bed reactors<sup>39</sup> and fluidized bed reactors.<sup>2,31,62,133</sup> These reports on P release are sometimes in discrepancies, possibly due to the significant differences in the hydrodynamics of different reactors. Therefore, a systematic study into the role of reactor configurations in P transformation and release during P-rich biomass pyrolysis is lacking and highly desired. Most importantly, the underlying reaction mechanisms governing P transformation and release due to different reactor configurations are still largely unknown. Consequently, this chapter aims to investigate the transformation and release of P during pyrolysis of a typical P-rich biomass at 400–900 °C in three reactor configurations. In addition, distributions of P in volatiles are successfully quantified using the two-stage pyrolysis/combustion reactor system and the evolution of P in char during pyrolysis in different reactor configurations were analysed using the new method developed in Chapter 4.

Table 5-1 The properties of rice bran used in Chapter 5

Moisture (wt%, ar <sup>d</sup> )	Proximate (wt%, db)			Ultimate (wt%, daf <sup>d</sup> )			
	Ash	VM <sup>b</sup>	FC <sup>c</sup>	C	H	N	O <sup>e</sup>
3.8	9.1	35.7	55.2	46.70	7.83	2.37	43.10
Major elements (mg/kg_rice bran, db)							
Al	48.1 ± 1.7			Ca	444.6 ± 12.1		
Fe	92.8 ± 1.2			Cl	563.2 ± 1.6		
Na	132.1 ± 14.4			P	18848.6 ± 52.4		
K	18596.9 ± 45.9			S	2004.5 ± 13.2		
Mg	8498.6 ± 33.2			Si	293.4 ± 1.2		

<sup>a</sup>as received; <sup>b</sup>VM–volatile matter; <sup>c</sup>FC–fixed carbon; <sup>d</sup>daf–dry ash free; <sup>e</sup>by difference;

## 5.2 Changes in char chemistry during pyrolysis under various conditions

As shown in Figure 3-2, three reactor systems were used in this chapter, including Type A: a fixed-bed reactor, Type B: a drop-tube/fixed-bed reactor with continuous feeding and Type C: a drop-tube/fixed-bed reactor with pulsed feeding. In this chapter, char samples produced from the three types of reactors are denoted as “Type A-char-XXX”, “Type B-char-XXX”, and “Type C-char-XXX”, respectively, where “XXX” represents the pyrolysis temperature.

Table 5-2 lists the elemental analysis of rice bran and char samples produced from rice bran pyrolysis at 400–900 °C in the three types of reactors. It clearly shows that reactor configuration has an important effect on char chemistry. While the differences in the chemistry in slow- and fast-heating chars are well known, there are two new findings in the chemistry of chars produced from Type B and Type C reactors. One is that the C content in chars produced in Type B reactor at temperatures below 700 °C is slightly higher than those produced in Type C reactor. This can be attributed to the unique feature of Type B reactor where at temperatures below 700 °C, the fresh volatiles generated from the continuous feeding of rice bran constantly cracks into soot that subsequently deposits on the surface of nascent char particles, leading to increasing char C content. This is also evident by the slightly-increased char yields, as shown in Figure 5-1. Second, H and O contents in chars prepared from Type B reactor system at temperature above 700 °C are interestingly higher than those in chars prepared in Type C reactor system. For examples, the H and O contents in Type C-char 900 are 0.84 and 6.41, respectively, while they increased to 0.99 and 6.63 in Type B-char 900. It is noted that pyrolysis in Type B reactor can be considered as an initial fast heating pyrolysis with pulse feeding (same as that in Type C reactor), followed by continuous interactions between the formed char with the volatiles produced in situ from the next batch pulse feeding. Clearly, the key difference in reactor configurations is that Type B reactor results in extensive volatile–char

interactions that are minimised (even eliminated) in Type C reactor. Therefore, the differences in char chemistry must be caused by the volatile–char interactions, which also result in decreases in char yields (see Figure 5-1) in Type B reactor during rice bran pyrolysis. It is further noted that the O/H molar ratios of the volatiles generated *in situ* from pyrolysis in Type C reactor is  $0.34 \pm 0.1$  at 800 and 900 °C. This is consistent with the studies in Chapter 7 that volatile–char interactions can increase O and H contents in char when the O/H molar ratio of the volatiles is higher than 0.25. Pyrolysis in Type B reactor generates significant amount of O-containing reactive species, which continuously interact with char particles. Volatile–char interactions are known to mitigate the carbon structure from condensing into large aromatic ring systems via forming C–O complex oxides,<sup>185</sup> thus increasing H and O contents in char. These results suggest that both reactor configuration and pyrolysis temperature play important roles in char chemistry during rice bran pyrolysis.

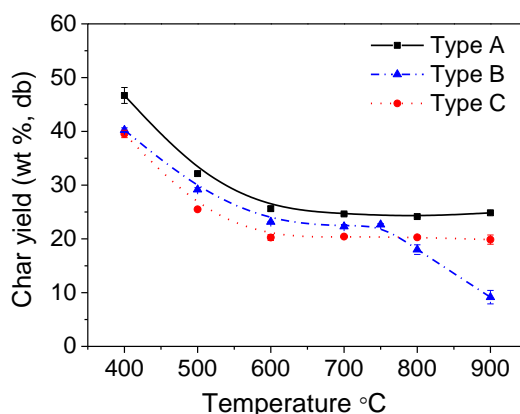


Figure 5-1 Char yields at different pyrolysis temperatures during pyrolysis in (a) Type A, fixed-bed reactor; (b) Type B, drop-tube/fixed-bed reactor with continuous feeding; (c) Type C, drop-tube/fixed-bed reactor with pulsed feeding

Table 5-2. Ultimate analyses of char samples prepared from rice bran pyrolysis in reactors with different configurations

Char samples	Ultimate analysis (wt%, daf <sup>a</sup> )			
	C	H	N	O <sup>b</sup>
Type A-Char-400	65.32 ± 0.07	3.36 ± 0.02	1.15 ± 0.03	30.17 ± 0.07
Type A-Char-500	64.59 ± 0.08	3.30 ± 0.06	1.13 ± 0.02	30.98 ± 0.08
Type A-Char-600	82.87 ± 0.10	2.38 ± 0.07	1.02 ± 0.05	13.81 ± 0.10
Type A-Char-700	87.56 ± 0.07	1.29 ± 0.06	0.94 ± 0.03	10.21 ± 0.07
Type A-Char-800	89.25 ± 0.05	1.30 ± 0.05	0.92 ± 0.01	8.53 ± 0.05
Type A-Char-900	92.59 ± 0.09	0.72 ± 0.02	0.77 ± 0.04	5.92 ± 0.09
Type B-Char-400	72.01 ± 0.02	2.08 ± 0.04	1.08 ± 0.02	24.83 ± 0.08
Type B-Char-500	74.12 ± 0.05	1.96 ± 0.01	0.98 ± 0.04	22.94 ± 0.05
Type B-Char-600	86.71 ± 0.02	1.61 ± 0.04	0.89 ± 0.06	10.79 ± 0.06
Type B-Char-700	89.10 ± 0.10	1.44 ± 0.01	0.86 ± 0.03	8.60 ± 0.10
Type B-Char-800	89.29 ± 0.02	1.42 ± 0.02	0.81 ± 0.04	8.48 ± 0.08
Type B-Char-900	92.44 ± 0.02	0.99 ± 0.03	0.74 ± 0.06	6.63 ± 0.06
Type C-Char-400	71.09 ± 0.01	2.13 ± 0.02	1.24 ± 0.01	25.54 ± 0.06
Type C-Char-500	72.21 ± 0.03	2.02 ± 0.03	1.18 ± 0.03	24.59 ± 0.08
Type C-Char-600	86.29 ± 0.05	1.77 ± 0.04	1.03 ± 0.06	10.91 ± 0.06
Type C-Char-700	88.05 ± 0.02	1.64 ± 0.01	0.89 ± 0.04	9.42 ± 0.06
Type C-Char-800	89.66 ± 0.01	1.30 ± 0.02	0.84 ± 0.02	8.20 ± 0.02
Type C-Char-900	91.95 ± 0.07	0.84 ± 0.03	0.80 ± 0.01	6.41 ± 0.07

<sup>a</sup> daf—dry ash free; <sup>b</sup> by difference; Type A-Char-XXX stands for the char prepared under a fixed-bed reactor configuration at XXX °C; Type B-Char-XXX and Type C-Char-XXX represent char samples prepared under drop-tube/fixed-bed configuration at XXX °C with a continuous feeding and pulse feeding, respectively.

### 5.3 Release and distributions of P during rice bran pyrolysis

Based on char yield and the contents of P in char and rice bran, the release of P during pyrolysis of rice bran in the three types of reactors can be calculated, with the results presented in Figure 5-2. Clearly, little P was released during slow heating pyrolysis in Type A reactor at 400–900 °C. There are small but appreciable amounts (less than 5%)

of P released during fast heating pyrolysis in Type B and Type C reactors at 500–700 °C. Compared with low heating rate ( $\sim 0.17$  °C/s) in Type A reactor high heating rates ( $\sim 1000$  °C/s) enhance the release of P during pyrolysis in Type B and C reactors. Specifically, higher heating rate could significantly suppress the intra-particle secondary reactions of volatiles and the transformation of the volatile inorganic species into char bonded forms, thus enhancing the release of P during pyrolysis in Type B and Type C reactors. This effect could be further enhanced with pyrolysis temperature rising from 700 °C to 900 °C, resulting in the increased P release by 8.1 % in Type C reactor. However, P release increased by 22.4 % in Type B reactor at the same temperature range (from 700 °C to 900 °C). The significant difference in P release in Type B and Type C reactor can be attributed to the unique feature of Type B reactor. During pyrolysis in Type B reactor with continuous volatile–char interactions, the released volatiles could induce strong reducing conditions around char particles on the quartz frit, which favours the reduction of phosphorus compounds in char to P-containing gases,<sup>129</sup> thus substantially enhancing P release in Type B reactor.

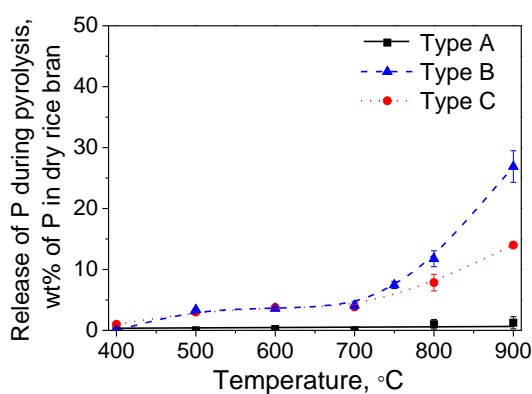


Figure 5-2 The release of P during pyrolysis of rice bran at different temperatures in a fixed-bed reactor (Type A) and in drop-tube/fixed-bed reactor with continuous feeding (Type B) and pulse feeding (Type C)



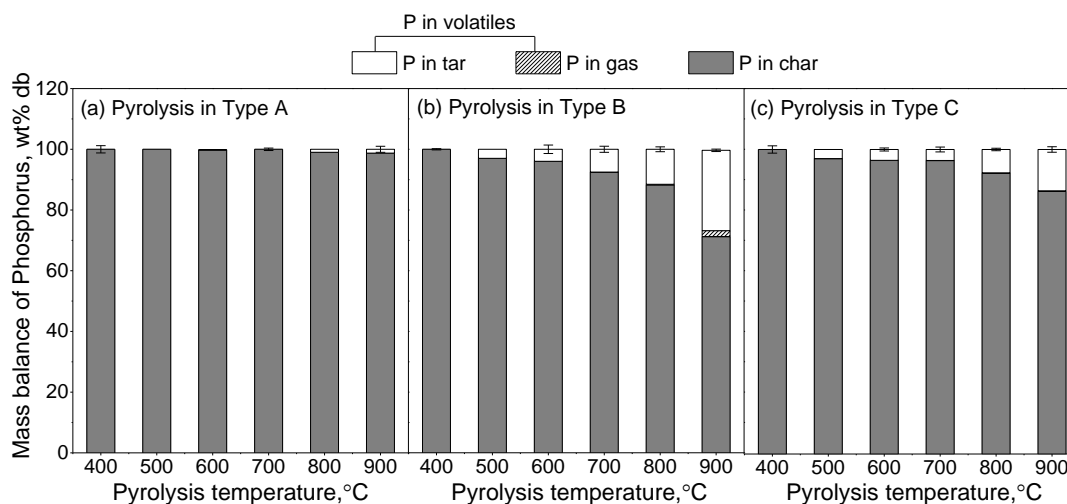


Figure 5-3 The mass balance of P during pyrolysis of rice bran in a fixed-bed reactor (Type A) and in drop-tube/fixed-bed reactor with continuous feeding (Type B) and pulse feeding (Type C). The P in volatiles includes P in gas and P in tar. The P in tar is calculated by P contents in char and in gas

Figure 5-3 shows the distributions of P in tar, gas and char produced from pyrolysis of rice bran in the three types of reactors at 400-900 °C. It should be noted that P in gas was collected by a bubbler system and P in tar is defined as water-insoluble P species in volatiles, which is calculated by subtracting P in char and P in gas from total P in rice bran. It was reported that P could be released in different forms of gases, including elemental phosphorus ( $P_4$ ), phosphorus oxides ( $P_2O_3$ ,  $P_2O_4$  and  $P_2O_5$ , etc.), phosphine ( $PH_3$ )<sup>66</sup> and condensed phosphates<sup>4</sup> during thermal treatment of P-containing solid fuels. However, the release of elemental phosphorus and condensed phosphates only occurs at temperatures higher than 1000 °C,<sup>4,13</sup> thus it is not taken into consideration under current experimental conditions. Consequently, P released in form of phosphorus oxides and  $PH_3$  was collected by 0.1 M NaOH and 0.1 m NaOCl solutions, respectively. As clearly seen from Figure 5-3, the majority of P remains in char during pyrolysis in all three types of reactors at the temperature range studied. For example, the P is nearly 100% distributed in char during pyrolysis in Type A reactor, while P

retention in char are ~ 70 and 82 % in Type B and Type C pyrolysis reactors at 900 °C.

For the P released from pyrolysis in Type B and Type C reactors, little P is present in gas phase except the case of pyrolysis in Type B reactor at 900 °C where ~ 2% P was found in gas. Two possible reasons are responsible for this observation: (1) the majority of P in volatiles might be in organically-bound form as water-insoluble species, thus not being collected in gas; (2) the released P might interact with the quartz reactor at the studied temperatures, thus reducing the amounts of P captured in gas phase. To clarify this, further experiments were designed to *in situ* burn the released volatiles in the Type D reactor systems (see Figure 3-2 d) with either continuous feeding (same as Type B) or pulse feeding (same as Type C). The P in volatile was recovered by combustion and captured in 0.1 M NaOH were shown in Figure 5-4. Clearly, the recovery of P in volatile is more than 95%, which rules out the second possibility of P depositing in reactor system after interacting with quartz reactor. Therefore, the results indicate that P in volatiles is dominantly organically bound in tar as water-insoluble species. In addition, part of the organically-bound P species could be formed as a result of reactions between gaseous P species and reactive organic species in volatiles.

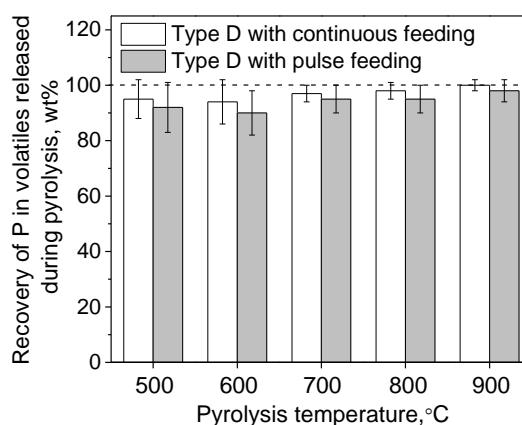


Figure 5-4 Recovery of P via combustion of volatiles produced *in situ* from rice bran pyrolysis in Type D reactor system with either continuous feeding and pulse feeding at 500–900 °C

#### 5.4 Transformation of phosphorus in char during pyrolysis in different reactor systems

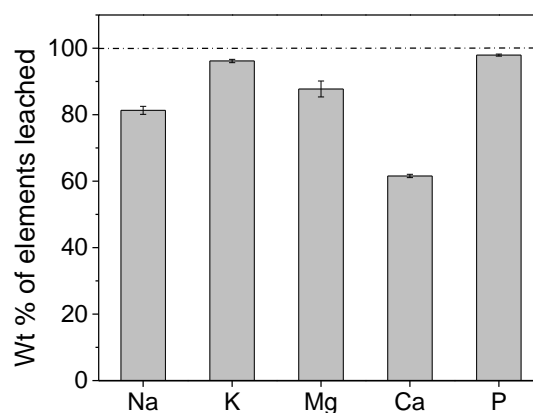


Figure 5-5 Mass percentage of water-soluble inorganic species leached from rice bran via water leaching

As discussed in Section 5.4, the majority of P is retained in char during pyrolysis under studied conditions. Therefore, efforts were made to understand the occurrence of P in char. To start with, the occurrence of P in original rice bran was investigated. Figure 5-5 presents the percentage of P and major cation (i.e. alkali and alkaline earth metallic, AAEM) species in the water leachate of rice bran in a semi-continuous leaching apparatus (details of the apparatus given elsewhere<sup>186</sup>) which prevents the contact of leachate (such as organic acid in rice bran) and rice bran samples being leached. It shows that 80% of Na, 95% of K, 85% of Mg, 60% of Ca and 98% of P are water-soluble, indicating that most AAEM species and almost all P in rice bran exist as either free ions in aqueous solution and/or deposit as discrete water-soluble salt particles. The leachate from water leaching of rice bran was further subjected to anion analysis. The qualitative results shown in Figure 5-6 demonstrate that phytic acid is the major P-containing specie in the leachate. Further quantitative analysis using various concentrations of phytic acid as standards revealed that ~ 98% of P in leachate (equals to ~96% of P in rice bran) is in the form of phytic acid. It is reported that phytic acid tends to combine with metallic ions, especially AAEM and Fe species in

biomass.<sup>7</sup> However, Ca, Mg and Fe phytates are water-insoluble,<sup>7,187</sup> then the significant water-soluble P in rice bran is most likely in the form of Na/K phytate. Considering the significantly high content of K (18596.9 mg/kg) and relatively low content of Na (132.1 mg/kg) in rice bran (see Table 5-1), phosphorus in rice bran could dominantly exist as potassium phytate. The molar ratio of K/P in leachate is less than 1 (0.78), also implying that part of hydrogen ions in the molecule of phytic acid are substituted by K.

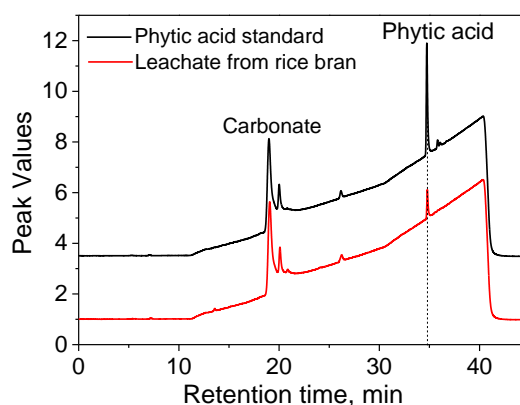


Figure 5-6 Qualitative analysis of water-soluble P in leachate from rice bran using IC

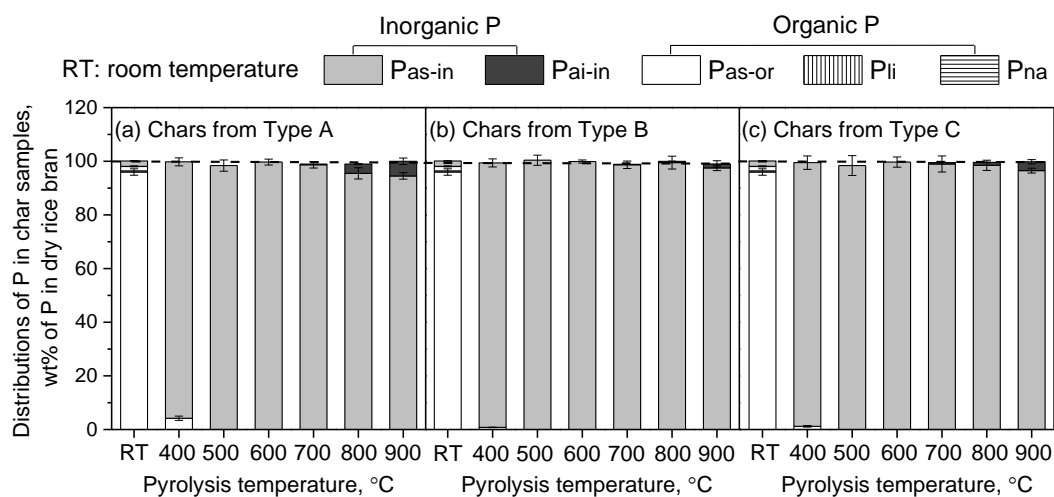


Figure 5-7 Distributions of P in char samples produced from pyrolysis in (a) fixed-bed reactor (Type A) and in drop-tube/fixed-bed reactors with (b) continuous feeding (Type B) and (c) pulse feeding (Type C) under different temperatures. RT represents

rice bran sample prepared at room temperature

Subsequently, char samples prepared under different pyrolysis conditions were processed using a new three-step extraction method to divide phosphorus species into two inorganic species [acid-soluble inorganic P ( $P_{as-in}$ ) and acid-insoluble inorganic P ( $P_{ai-in}$ )] and three organic species [acid-soluble organic P ( $P_{as-or}$ ), P in lipids ( $P_{li}$ ) and P in other acid-insoluble organic structures such as nucleic acids ( $P_{na}$ )]. The forms of occurrence of P in char samples are shown in Figure 5-7, normalised to the total P in dry rice bran. Clearly, after pyrolysis in all reactor systems at 400–900 °C, the vast majorities of organic P in rice bran are converted into acid-soluble inorganic P in chars. Even at temperatures as low as 400 °C, P in rice bran (mostly organically-bound) are thermally unstable. It should also be noted that ~5% P in char prepared at 400 °C in Type A reactor system is acid-soluble organic P (see Figure 5-7 a), while little phytic acid was detected with further analysis using IC. This can be contributed to the decomposition of phytate into lower inositol phosphates (also an acid-soluble organic P) during pyrolysis in Type A reactor (this was also reported previously under slow pyrolysis conditions<sup>188</sup>). However, little acid-soluble organic P was found in chars prepared from Type B and Type C reactor systems (see Figure 5-7 b and c) with high heating rates at 400 °C. The results indicate that fast heating conditions enhance the conversion of potassium phytate into acid-soluble inorganic P species during pyrolysis. It is also noteworthy that increasing pyrolysis temperature to 500–700 °C in all three pyrolysis reactor systems leads to complete transformation of organic P into acid-soluble inorganic P. Acid-soluble inorganic P in char often associates with Ca or Mg in forms of orthophosphates and condensed phosphates such as pyrophosphates or metaphosphates.<sup>4</sup> The significantly high contents of Mg in rice bran (see Table 5-1) or char (< ~3% is released under all conditions) indeed could provide abundant source for P recombination in char during pyrolysis. Nevertheless, further increasing pyrolysis temperature above 700 °C results in the formation of acid-insoluble inorganic P in chars. This is especially the case for the

chars prepared in Type A reactor system due to a lengthy residence time during slow heating pyrolysis. At high temperatures, acid-soluble inorganic P might react with other inorganic species to form acid-insoluble inorganic P species such as aluminophosphates.<sup>12</sup>

## 5.5 Conclusions

This chapter systematically investigated the transformation and release of P during rice bran pyrolysis at 400–900 °C in three reactor system under different conditions. Reactor configurations significantly influence P release and transformation during pyrolysis. Under current pyrolysis conditions, little P is released during slow heating pyrolysis in a fixed-bed reactor. Below 700 °C, small but appreciable P is released into volatiles during pyrolysis in a drop-tube/fixed-bed reactor either with continuous feeding or pulse feeding. High heating rate in a drop-tube/fixed-bed reactor with pulse feeding increases P release by 8.1% when increasing pyrolysis temperature from 700 °C to 900 °C. However, P release significantly increases by 22.4% during pyrolysis in a drop-tube/fixed-bed reactor with continuous feeding when increasing temperature from 700 °C to 900 °C due to the enhanced volatile–char interactions. *In situ* combustion of volatiles at 950 °C in a two-stage pyrolysis/combustion reactor system could effectively convert more than 95% of P in volatiles (dominantly P in tar) into water-soluble P species. P in rice bran is mainly organic phosphorus in form of potassium phytate. This organic phosphorus can be substantially transformed into acid-soluble inorganic P even at temperatures as low as 400 °C during pyrolysis and high heating rate could accelerate this transformation. Above 800 °C, acid-soluble inorganic P reacts with other inorganic species in char and generates acid-insoluble inorganic P during rice bran pyrolysis.

*Reprinted with permission from (Xujun Chen and Hongwei Wu. Transformation and release of phosphorus during rice bran pyrolysis: Effect of reactor configurations*

*under various conditions, Fuel 2019, 255, 115755). Copyright (2019). Published by Elsevier Inc.*

---

## CHAPTER 6 EFFECTS OF PHOSPHORUS ON CHAR STRUCTURE AND REACTIVITY OF BIOCHARS PREPARED FROM ACID-WASHED BIOMASS LOADED WITH P OF VARIOUS FORMS

### 6.1 Introduction

As listed in Section 2.8, the effect of different forms of inherent phosphorus in biomass on char structure and char reactivity is an important research gap in terms of the thermal utilization of P-containing solid fuels. Therefore, this chapter reports the effect of three P-containing species including phytic acids, orthophosphoric acid and polyphosphoric acid on structure and intrinsic reactivity of biomass char. For this purpose, a wood sample containing little inorganic species was first prepared via HCl washing (see Section 3.3.1) to eliminate the interference from other inorganic species in biomass and then P-loaded wood samples were prepared via impregnation method (See section 3.3.1). These wood samples were subsequently subjected to fast pyrolysis at 1000 °C with a pulse feeder (Type C, Figure 3-2) to prepare char samples with the occurrences of phosphorus in char, char structure and char intrinsic reactivity being analysed using a newly-developed extraction method, thermogravimetric analyser (TGA) and Raman spectroscopy, respectively. The properties of the acid-washed mallee wood used in this chapter are shown in Table 6-1. In this chapter, the acid-washed wood sample, acid-washed wood samples loaded with phytic acid, orthophosphoric acid and polyphosphoric acid is termed as AW-wood, Ph-A wood, Or-A wood and Po-A wood, respectively, and the char prepared from these wood samples are termed as AW-char, Ph-A char, Or-A char and Po-A char, accordingly. The total content of P in dry Ph-A wood, Or-A wood and Po-A wood is 8084.2 mg/kg, 8125.4 mg/kg and



8145.9 mg/kg, respectively.

Table 6-1 The properties of acid-washed mallee wood used in Chapter 6

Moisture (wt%, ar <sup>a</sup> )	Proximate (wt%, db)			Ultimate (wt%, daf <sup>d</sup> )			
	Ash	VM <sup>b</sup>	FC <sup>c</sup>	C	H	N	O <sup>e</sup>
3.6	0.1	84.0	15.9	54.32	7.41	0.18	38.09
Major elements (mg/kg_rice bran, db)							
Al	9.6 ± 1.3			Ca	2.6 ± 0.7		
Fe	1.6 ± 0.4			Cl	0		
Na	2.9 ± 1.1			P	0		
K	1.3 ± 0.3			S	0.7 ± 0.4		
Mg	2.0 ± 0.6			Si	3.4 ± 1.2		

<sup>a</sup>as received; <sup>b</sup>VM–volatile matter; <sup>c</sup>FC–fixed carbon; <sup>d</sup>daf–dry ash free; <sup>e</sup>by difference;

## 6.2 Char yield during biomass pyrolysis and phosphorus retention in char

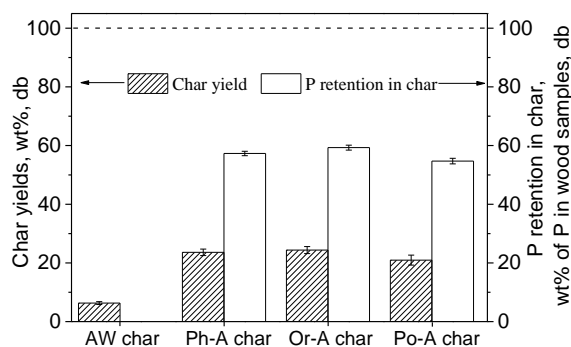


Figure 6-1 Char yields during pyrolysis of wood samples (left Y axis) and phosphorus retention (right Y axis) in char samples prepared from fast pyrolysis at 1000 °C

The char yields and P retention in char prepared from fast pyrolysis of acid-washed wood and P-loaded wood samples at 1000 °C are shown in Figure 6-1. Clearly, the presence of both organic and inorganic P-containing species in P-loaded wood samples significantly improves char yields. Specifically, the yields for AW char was 6.2%, while it substantially increases to ~26.0 % for Ph-A char and Or-A char, and to

~ 23.0% for Po-A char. During biomass pyrolysis at 1000 – 1500 °C, P is known to be released in forms of various P-containing gases.<sup>4,13</sup> However, in this study, after the pyrolysis of P-containing AW wood at 1000 °C, the results in Figure 6-1 show that the majority (~ 60%) of P is retained in char. Considering the low contents of inorganic species in acid-washed wood (see Table 6-1), phosphorus is unlikely to exist as metal phosphates in char. To investigate the occurrence of P in char samples, char samples was extracted using the recently-developed method in Chapter 4 to quantify the contents of P with various occurrence forms, with the results listed in Table 6-2. Surprisingly, ~100% of P in Or-A char, Ph-A char and Po-A char samples are presented in the category of P in either nucleic acids or other acid-insoluble organic structures ( $P_{na}$ ). In this study, as nucleic acids are not possible to survive at in char after pyrolysis at 1000 °C, the P in the char samples must be present in the form of P in acid-insoluble organic structures. It is known that P-containing organic structures such as phosphate and polyphosphate esters in biochar could significantly enhance crosslinking and reduce bond cleavage and depolymerization,<sup>189</sup> thus preventing the further condensation/graphitization of carbon structure during pyrolysis (see discussion in Section 6.5). Phosphorous was also reported to inhibit the formation of some volatile organic species (e.g. levoglucosan<sup>189</sup>) during biomass thermal treatment. Therefore, it is not surprising to see that the char yield increases after the AW wood is loaded with P. Those results also demonstrate that the enhanced crosslinking by P-containing organic structures in biochar could potentially affect char structure (as further elaborated in Section 6.5).

Table 6-2 Distributions of different forms of P in char samples and ultimate analysis of char after pyrolysis and partially-converted char samples after oxidation

Char samples	Occurrences of P in char, wt % of P					Ultimate (wt%, daf <sup>a</sup> )			
	in char					C	H	N	O <sup>b</sup>
I	II	III	IV	V					
AW char	0	0	0	0	0	72.47 ± 0.13	0.88 ± 0.06	0.54 ± 0.06	26.11 ± 0.10
AW char (0)	0	0	0	0	0	72.49 ± 0.11	0.87 ± 0.05	0.55 ± 0.08	26.09 ± 0.09
AW char (20)	0	0	0	0	0	80.21 ± 0.12	0.65 ± 0.04	0.40 ± 0.01	18.74 ± 0.08
AW char (40)	0	0	0	0	0	85.31 ± 0.12	0.44 ± 0.04	0.28 ± 0.01	13.97 ± 0.10
AW char (60)	0	0	0	0	0	88.62 ± 0.21	0.30 ± 0.02	0.19 ± 0.02	10.89 ± 0.11
AW char (80)	0	0	0	0	0	92.58 ± 0.19	0.21 ± 0.04	0.12 ± 0.01	7.09 ± 0.04
Ph-A char	0	0	0	0	100.2 ± 1.1	76.51 ± 0.07	1.28 ± 0.03	0.38 ± 0.02	21.83 ± 0.07
Ph-A char (0)	0	0	0	0	99.7 ± 2.4	76.55 ± 0.02	1.01 ± 0.04	0.29 ± 0.01	22.15 ± 0.10
Ph-A char (20)	0	0	0	0	98.8 ± 1.0	80.42 ± 0.04	0.84 ± 0.02	0.25 ± 0.01	18.49 ± 0.08
Ph-A char (40)	0	0	0	0	99.9 ± 2.1	83.25 ± 0.06	0.51 ± 0.03	0.21 ± 0.04	16.03 ± 0.10
Ph-A char (60)	0	0	0	0	101.1 ± 0.2	86.21 ± 0.11	0.30 ± 0.01	0.14 ± 0.01	13.35 ± 0.07
Ph-A char (80)	0	0	0	0	103.7 ± 2.5	89.41 ± 0.12	0.14 ± 0.02	0.05 ± 0.01	10.40 ± 0.06
Or-A char	0	0	0	0	101.8 ± 0.9	76.33 ± 0.05	1.44 ± 0.08	0.28 ± 0.06	21.95 ± 0.07
Or-A char (0)	0	0	0	0	98.4 ± 1.9	76.34 ± 0.14	1.44 ± 0.02	0.28 ± 0.01	21.94 ± 0.14
Or-A char (20)	0	0	0	0	97.9 ± 1.4	81.25 ± 0.11	0.87 ± 0.03	0.23 ± 0.01	17.65 ± 0.02
Or-A char (40)	0	0	0	0	98.6 ± 2.7	84.33 ± 0.05	0.54 ± 0.03	0.19 ± 0.04	14.94 ± 0.11
Or-A char (60)	0	0	0	0	103.4 ± 2.9	87.01 ± 0.04	0.28 ± 0.02	0.12 ± 0.02	12.59 ± 0.03
Or-A char (80)	0	0	0	0	102.1 ± 3.4	90.12 ± 0.11	0.11 ± 0.01	0.04 ± 0.02	9.73 ± 0.04
Po-A char	0	0	0	0	100.6 ± 0.8	75.07 ± 0.04	1.41 ± 0.02	0.44 ± 0.05	23.08 ± 0.05
Po-A char (0)	0	0	0	0	99.6 ± 3.1	75.12 ± 0.08	1.40 ± 0.05	0.44 ± 0.01	23.04 ± 0.12
Po-A char (20)	0	0	0	0	101.2 ± 2.0	81.05 ± 0.05	0.92 ± 0.06	0.25 ± 0.01	17.78 ± 0.01
Po-A char (40)	0	0	0	0	97.9 ± 3.0	83.69 ± 0.09	0.60 ± 0.04	0.18 ± 0.03	15.53 ± 0.07
Po-A char (60)	0	0	0	0	101.7 ± 1.8	87.15 ± 0.10	0.24 ± 0.05	0.11 ± 0.02	12.50 ± 0.10
Po-A char (80)	0	0	0	0	98.8 ± 2.2	89.95 ± 0.05	0.12 ± 0.01	0.03 ± 0.01	9.90 ± 0.13

I: acid-soluble inorganic P (P<sub>as-in</sub>); II: acid-insoluble inorganic P (P<sub>ai-in</sub>); III: acid-soluble organic P (P<sub>as-or</sub>);

IV: P in lipids (P<sub>li</sub>); V: P in other acid-insoluble organic structures such as nucleic acids (P<sub>na</sub>); <sup>a</sup>daf-dry ash free;

<sup>b</sup>by difference

### 6.3 Effect of phosphorus on chemistry of char sample prepared from biomass pyrolysis

Table 6-3 presents the contents of inorganic species in those char samples prepared from pyrolysis of AW wood or P-loaded wood samples. For the inorganic species (except P) in all these char samples, only trace amounts of AAEM species and Fe are present while Si and Al are the dominant inorganic species. However, the contents of the inorganic species (except P) in Ph-A char, Or-A char and Po-A char are almost four times lower than those in AW char due to the enhanced char yields in presence of phosphorus. Further calculations also show that during wood pyrolysis, all inorganic species (except P) are retained in these char samples, proving that these inorganic species are indeed in the forms of aluminosilicates or silicates. Therefore, the char samples could be safely considered as free of catalytically-active metallic species.

Table 6-3 Contents (mg/kg, dry basis) of inorganic species in char samples prepared from fast pyrolysis of wood samples at 1000 °C

Char samples	AW char	Ph-A char	Or-A char	Po-A char
P	0	21556.8 ± 13.5	18959.3 ± 22.1	21528.6 ± 16.8
Na	52.9 ± 13.2	12.8 ± 3.7	15.3 ± 3.1	14.7 ± 1.9
K	20.1 ± 2.2	5.3 ± 1.7	5.2 ± 2.1	4.5 ± 1.3
Ca	44.1 ± 5.2	10.4 ± 1.0	12.5 ± 0.8	12.2 ± 3.1
Mg	38.1 ± 2.1	7.5 ± 2.1	8.4 ± 1.8	7.2 ± 2.2
Fe	27.7 ± 3.7	7.5 ± 1.4	7.3 ± 0.9	7.6 ± 0.8
Si	178.6 ± 4.1	44.4 ± 9.7	40.7 ± 7.4	50.6 ± 9.6
Al	166.7 ± 12.6	40.3 ± 2.5	46.7 ± 5.6	49.7 ± 5.5
P/C molar ratio	0	0.011 ± 0.001	0.010 ± 0.001	0.011 ± 0.001

Except the significantly high contents of phosphorus in char samples prepared from P-loaded AW wood samples, the presence of phosphorus in biomass also exerts substantial influence on the chemistry of the resultant char samples. For examples, the content of C and H in AW char is 72.47 and 0.88, respectively; however, it

increased 76.33 and 1.44 in Or-A char, respectively. The pronounced increases in C and H contents are also observed for other char samples prepared from Ph-A wood and Po-A wood. The increases in the contents of C and H can be attributed to the enhanced crosslinking of C- and H-containing polymer chains (e.g. polyethylene linkages [15]). Accordingly, the contents of N and O in chars prepared from pyrolysis of wood samples with phosphorus are decreased. Notably, though P contents in Or-A is slightly lower, the molar ratios of P/C are similar at 0.011 for the char samples prepared from P-loaded wood samples. Nevertheless, those results clearly demonstrate that the presence of either organic or inorganic P species in biomass plays important roles in altering char chemistry during biomass pyrolysis.

#### **6.4 Effect of phosphorus with different occurrence forms on char reactivity**

Figure 6-2a presents the reactivity of chars measured in air at 500 °C using TGA with char conversion ranging from 20 to 80%. Measured under the conditions of a differential reactor and kinetic control regime, the char reactivity is the truly intrinsic reactivity of char. Also as discussed above, all char samples are free of catalytically-active metallic species, so the intrinsic char reactivity measured in this study should be governed by the carbon structure of the char samples and/or the presence of P. Three important observations can be made from the experimental results presented in Figure 6-2a.

First, during the whole char conversion, the intrinsic reactivities of char samples with P are overlapped, indicating that the organic P (i.e., phytic acid) and two inorganic P (i.e., orthophosphoric acid and polyphosphoric acid) exert same effect on char reactivity in this study, which could also be evidenced by the similar char chemistry such as similar P/C molar ratio in char (see Table 6-3). Second, the char samples with phosphorus reached the highest char reactivities at char conversion of 40%, while the reactivity of AW char increased with increasing char conversion to 80%, indicating

different evolution routes of physico-chemical structures of char samples during char reactivity measurement. Third, at char conversion less than 60%, the reactivities of char samples with phosphorus are higher than that of AW char; however, this trend is reversed at higher char conversion.

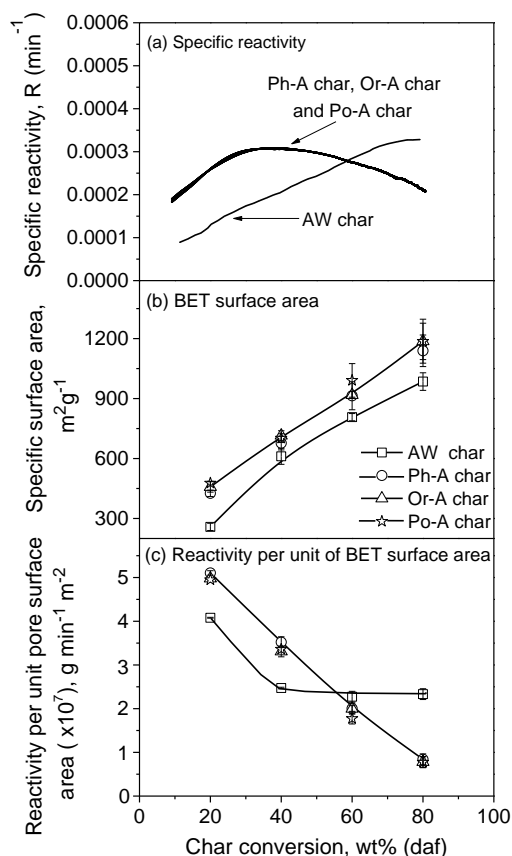


Figure 6-2 (a) Specific reactivities of char samples measured at 500 °C in air by TGA. The relative experimental error for char reactivity measurement is 3%; (b) BET pore surface area of char samples; (c) Reactivity per unit pore surface area of char samples

To interpret the changes in char reactivity in Figure 6-2a, the measurement of char reactivity at 500 °C in TGA was terminated at specific char conversion (dry ash free basis), i.e., 0%, 20%, 40%, 60% and 80%, and the char samples [termed as char (x) with x representing char collected at x% char conversion (wt, daf)] were then cooled

down to room temperature and collected for further analysis. Notably, char with 0% char conversion [see char (0) in Table 6-2] represents the char sample that was heated to 500 °C under argon but not subjected to the oxidation in air according to the measurement procedure of char reactivity in TGA. Figure 6-2b shows the BET surface areas of char samples as a function of char conversion. Notably, some micropores might not be taken into account for initial chars from pyrolysis due to the molecular-sieve effect during determination of BET surface area using N<sub>2</sub> absorption technique, however, such effect could be diminished as combustion or gasification proceeds.<sup>190</sup> Therefore, Figure 6-2b only shows the BET surface area for char samples with no less than 20% of char conversion. Clearly, total pore surface area increases with char conversion for all char samples, indicating that char conversion in air leads to the formation of new pores or the opening of the closed pores.<sup>11</sup> Especially, at lower char conversion (< 20%), the surface area of chars prepared from P-loaded wood are higher than that of char prepared from acid-washed wood due to less tar generated during pyrolysis of P-loaded wood and thus less soot condensed in the pore structures of the resulting chars. The increasing pore surface area for AW char from 278 m<sup>2</sup>/g to 985 m<sup>2</sup>/g with char conversions rising from 20% to 80% result in the increased intrinsic reactivity of AW char at higher char conversion, as shown in Figure 6-2a. However, the similarly increasing pore surface area is accompanied with decreasing char reactivity for P-containing chars at char conversion higher than 40%.

On the other hand, the specific reactivity of char samples in Figure 6-2a is the “overall” reactivity of active sites under kinetic control regime. Attempts were also taken to investigate the important role of carbon structure in char reactivity by normalizing this “overall” reactivity by total surface area, i.e., specific reactivity per unit of pore surface area, which can be considered as an indication of the average intrinsic reactivity,<sup>11</sup> as shown in Figure 6-2c. For AW char, the reactivity per unit pore surface area significantly decreases with char conversion increasing from 20%

to 40%, then levelled off at higher char conversion. This result suggests that average intrinsic reactivity of carbon active sites in the reacting AW char decreases with char conversion at char conversion less than 40%, while it is unchanged at higher char conversion. Previous study<sup>11</sup> revealed that under noncatalytic conditions, the reactive components in AW char with highly heterogeneous carbon structure are consumed at lower char conversion while the inner ones are remained at higher conversions, resulting in the “selective conversion” for AW chars at lower char conversion. However, for the chars prepared from P-loaded acid-washed wood, the average intrinsic reactivity decreased with increasing char conversion from 20% to 80%, suggesting that “selective conversion” occurred in presence of P during the whole char conversion investigated. Those results indicate that phosphorus can significantly affect char reactivity and might plays different roles in the evolution of char structure at various char conversions.

### **6.5 Effect of phosphorus with different occurrence forms on char carbon structure**

To clarify the significant differences observed in the evolution of the reactivity per unit pore surface area for AW char and char with P, efforts were then taken to characterise the carbon structure of chars with different char conversions using Raman spectroscopy. Figure 6-3 presents the results on the three key parameters, i.e.  $S_{(Gr + VI + Vr)}/S_{all}$ ,  $S_D/S_{all}$  and  $S_{(Gr + VI + Vr)}/S_D$ . Clearly, the carbon structure of char samples prepared from acid-washed wood loaded with P is more active than that of AW char due to the enhanced cross-linking of reactive carbon structures and reduced condensation by P-containing structures during pyrolysis.

During low-temperature oxidation, for AW char at lower char conversion (< 60%), char structure becomes more inert with higher  $S_D/S_{all}$  (see Figure 6-3a) and lower  $S_{(Gr + VI + Vr)}/S_{all}$  (see Figure 6-3b) with rising char conversion due to the “selective



conversion” of carbon structures<sup>11,105</sup>, while the “selective conversion” weakens at higher char conversion with dominantly inert carbon structures in char. Carbon structure of char samples prepared from P-loaded wood samples are similar when char conversion ranging from 0–80%, in coincidence with char reactivities shown in Figure 6-2a. When char conversion is less than 60%, the carbon structures of char samples from P-loaded wood are more active than that of AW char with lower char reactivity due to the crosslinking of P-containing groups and reduced condensation of char structure during wood pyrolysis.<sup>189,191</sup> With the increasing of char conversion, the reactive structure crosslinked by P-containing groups would be further consumed<sup>125,189</sup>, leading to the more condensed char structure and reduced char reactivity though higher surface area can still be observed for char samples with higher char conversions. At higher char conversion above 60%, the carbon structure of all char samples with or without P tends to be similar. However, in comparison with P-containing char samples, AW char sample shows higher char reactivity, indicating that the presence of P somehow reduced char reactivity at higher char conversion.

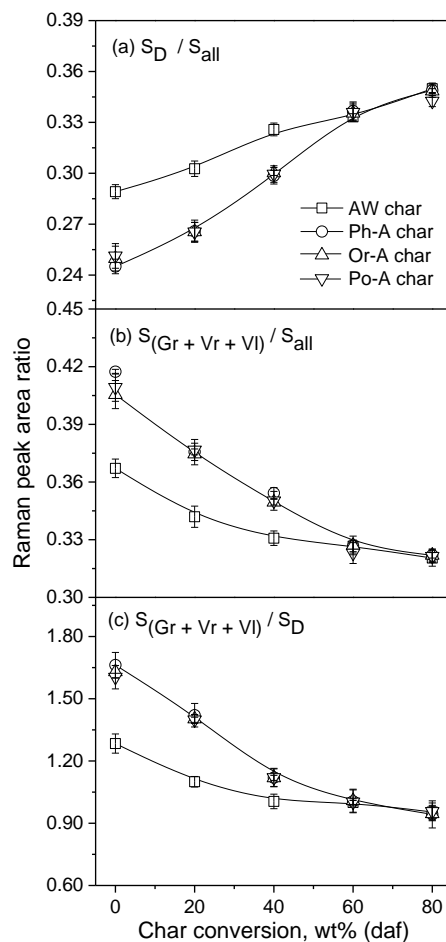


Figure 6-3 Peak fractions of (a) D band and (b) ( $G_r + V_l + V_r$ ) band out of the total peak area, and (c) peak area ratio of  $S_{(G_r + V_l + V_r)}/S_D$  (c) in chars with different char conversions

Figure 6-4a illustrates the retention of P in char samples with various char conversions. Clearly, little P is released at char conversion less than 40% while it tends to be significantly volatilized at higher char conversions, enabled by the scission of P-containing groups.<sup>189</sup> The loss of P-containing groups would further lead to the condensation of aromatic ring systems,<sup>189</sup> making char structure more inert. Therefore, the increased P release above 40% char conversion results in the gradual decrease of intrinsic reactivity for P-containing char samples. However, P release is not proportional to the conversion of P-containing chars, as shown in Figure 6-4b. For example, more than 40% of P is retained in these P-containing chars

at 80% char conversion and the P/C molar ratios keep increasing at higher char conversions for all P-containing char samples. Further analysis in Table 6-2 shows that all P retained in char are acid-insoluble organic structure ( $P_{na}$ ), suggesting that those unconsumed P-containing species are still combined with carbon structure in char.

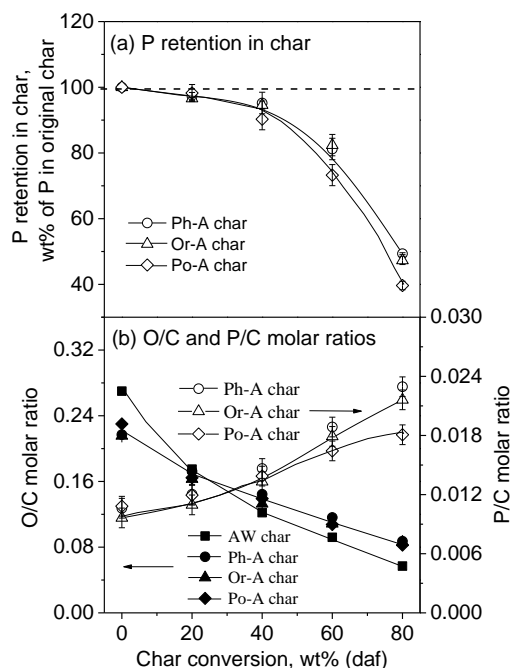


Figure 6-4 (a) Phosphorus retention and (b) O/C and P/C molar ratios in chars with different char conversions

To investigate the evolution of P-containing groups associated with carbon structure in char, char samples with different char conversions were further analysed using XPS with the result shown in Table 6-4. Clearly, C-O-P structure and C-PO<sub>3</sub> groups are the major P-containing groups while little C<sub>3</sub>-PO and no C<sub>3</sub>-P groups are observed in char with various char conversions. However, with the increasing of char conversion, C-O-P bond is becoming increasingly dominate (i.e., more than 95% of P) in Ph-A char, Or-A char and Po-A char due to the release of P from P-containing groups and/or the oxidation of C<sub>3</sub>-PO and C-PO<sub>3</sub> groups to C-O-P bond.<sup>125</sup>

However, C-O-P bond can block the active carbon sites from reacting with oxygen,<sup>125,126,192</sup> thus significantly reduce char reactivity. With the increasing char conversion above 60% for P-containing chars, C-O-P bond becomes more concentrated with creasing P/C molar ratios (see Figure 6-4b), resulting in lower char reactivity, compared with AW char regardless of the similar carbon structures. Notably, the breakage of polyphosphates groups [such as C-O-(PO<sub>3</sub>H)<sub>n</sub>] also result in enhanced P release,<sup>126</sup> leading to the lower P retention in Po-A char, compared with that in Ph-A char and Or-A char, as shown in Figure 6-4a.

Table 6-4 Distributions of P groups associated with carbon structure in char samples with different char conversions

Char samples	% of P groups in P <sub>2p</sub> spectrum			
	C-O-P	C-PO <sub>3</sub>	C <sub>3</sub> -PO	C <sub>3</sub> -P
Ph-A char (0)	24.0 ± 1.2	75.8 ± 1.2	0.2 ± 0.1	0
Ph-A char (20)	51.4 ± 3.1	48.5 ± 3.0	0.1 ± 0.1	0
Ph-A char (40)	60.3 ± 2.9	39.7 ± 2.9	0	0
Ph-A char (60)	69.2 ± 3.1	30.8 ± 3.1	0	0
Ph-A char (80)	97.2 ± 2.4	2.8 ± 2.4	0	0
Or-A char (0)	27.2 ± 3.1	72.7 ± 3.0	0.1 ± 0.1	0
Or-A char (20)	53.6 ± 1.3	46.3 ± 1.2	0.1 ± 0.1	0
Or-A char (40)	58.9 ± 2.8	41.1 ± 2.8	0	0
Or-A char (60)	72.6 ± 1.9	27.4 ± 1.9	0	0
Or-A char (80)	96.9 ± 2.6	3.1 ± 2.6	0	0
Po-A char (0)	33.7 ± 2.2	66.0 ± 2.3	0.3 ± 0.1	0
Po-A char (20)	56.4 ± 4.1	43.5 ± 4.1	0.1 ± 0.1	0
Po-A char (40)	63.8 ± 2.3	36.2 ± 2.3	0	0
Po-A char (60)	68.9 ± 3.0	31.1 ± 3.0	0	0
Po-A char (80)	98.2 ± 0.4	1.8 ± 0.4	0	0

It should also be noted that the presence of P in char also has significant effect on char chemistry during char conversion. As shown in Figure 6-4c, the O/C molar ratio

in AW char is higher than that in P-containing char samples due to the lower oxygen content in chars prepared from P-loaded wood at low char conversion ( $\leq 20\%$ ). While at higher char conversion, O/C molar ratios for P-containing char samples are slightly higher due to the presence of P associated with oxygen in char. Nevertheless, the decreased O/C molar ratio at higher char conversion also indicate the selective consumption of reactive O-containing structures during char oxidation.<sup>193</sup>

## 6.6 Conclusions

This chapter reports a systematic investigation into the effect of phosphorus on char structure and reactivity of char prepared from the fast pyrolysis of purposely-prepared P-loaded biomass samples at 1000 °C in absence of other inorganic species. Experimental results show that both organic and inorganic P substantially increase char yields during biomass pyrolysis due to the enhanced crosslinking by P-containing structures in char, leading to increases in the char C and H contents and a decrease in char O content. The presence of P in biochars plays an important role in the evolution of char structure and intrinsic reactivity measured during low-temperature oxidation at 500 °C in air under chemical-reaction-controlled regime. After pyrolysis and subsequent char oxidation, all P in biomass either as organic or inorganic P are found to be present in the form of acid-insoluble organic structures. For char prepared from acid-washed wood, char reactivity increases with char conversion due to the increasing pore surface area at higher conversion. Comparatively, for char prepared from acid-washed wood loaded with various P at char conversion below 60%, the presence of P increases char intrinsic reactivity due to the enhanced crosslinking and reduced condensation of char structures. However, at higher char conversions, P-containing species in char leads to a significant decrease in char reactivity, due to the formation of abundant C-O-P bonds, that is highly resistant to the oxidation in air, in the reacting chars.

**CHAPTER 7 VOLATILE–CHAR INTERACTIONS: ROLES OF  
*IN SITU* VOLATILES WITH DISTINCTLY-DIFFERENT  
CHEMISTRY IN DETERMINING STRUCTURE AND  
REACTIVITY OF CHAR PREPARED FROM P-CONTAINING  
BIOSOLID**

### **7.1 Introduction**

Combustion and gasification are important technologies for utilizing P-containing solid fuels.<sup>38</sup> In a gasifier or combustor, solid fuel particles first experience rapid devolatilisation to produce char and volatiles.<sup>34</sup> Char conversion is the rate-limiting step, therefore, char reactivity is a critical consideration in reactor design.<sup>194,195</sup> As elaborated in Section 2.5.1, during rapid devolatilisation, fresh volatiles can significantly interact with char particles, resulting in the volatile–char interactions.<sup>15</sup> Previous literatures<sup>15,16,18</sup> report that volatile–char interactions could substantially reduce char reactivity during coal pyrolysis in fluidised bed, using a single volatile produced from acid-washed brown coal. However, fuels vary widely in fuel chemistry so that the volatiles generated *in situ* during pyrolysis can be distinctly-different in chemistry. Such volatiles with distinctly-different chemistry may play different roles in altering char structure and char reactivity during volatile–char interactions. Currently, there have been no investigation on this important aspect. Therefore, this chapter reports the different roles that *in situ* volatiles with distinctly-different chemistry may play during volatile–char interactions under non-catalytic conditions in determining char structure and reactivity.

## 7.2 Distinct differences in chemistry of volatiles produced for *in situ* volatile–char interactions

For preparing char samples used for volatile–char interactions, double acid-washed biosolid (DAWB) was produced (detailed description can be found in Section 3.3.1) and then subjected to fast heating pyrolysis in Type C reactor with pulse feeding in Figure 3-2c to produce DAWB char with minimised volatile–char interactions at 1000 °C. Polyethylene (PE), DAWB, polyethylene glycol (PEG) and cellulose were used to generate *in situ* volatiles. The properties of samples used in this chapter are shown in Table 7-1 while the contents of inorganic species in DAWB and DAWB char are shown in Table 7-2. Clearly, as shown in Table 7-1, cellulose, PEG and PE samples are free of inorganic species and the DAWB sample is almost inorganics-free with only 0.3% ash. More importantly, those solid samples have distinctly-different fuel chemistry. Table 7-2 further shows that the DAWB sample contains little AAEMs and Fe, and only trace amounts of Si and Al, indicating the remaining inorganic species being aluminosilicates/silicates. Therefore, the DAWB sample can be considered as free of catalytically-active inorganic species. Those samples were then subjected to the novel two-stage reactor (see Figure 3-3) for *in situ* volatile–char interactions at 1000 °C with the detailed description given in Section 3.3.3. Hereafter, the chars collected after interactions with the volatiles generated *in situ* from PE, DAWB, PEG and cellulose volatiles are termed as Char-PE, Char-DAWB, Char-PEG and Char-Cellulose, respectively. Another DAWB char was also subjected to the same procedure but without feeding any volatiles into the inner reactor (i.e., without volatile–char interactions) as a reference. Hereafter, this char is termed as Char-holding.

Table 7-1 The properties of samples used in Chapter 7

Samples	Moisture (wt%, ar <sup>a</sup> )	Proximate (wt%, db)			Ultimate (wt%, daf <sup>d</sup> )			
		Ash	VM <sup>b</sup>	FC <sup>c</sup>	C	H	N	O <sup>e</sup>
DAWB	3.8	0.3	80.4	19.3	73.61	9.17	2.87	14.35
Cellulose	1.7	0.0	90.5	9.5	43.68	6.11	0.00	50.21
PEG	0.1	0.0	100.0	0.0	54.54 <sup>g</sup>	9.09 <sup>g</sup>	0.00	36.37 <sup>g</sup>
PE	0.1	0.0	100.0	0.0	85.71 <sup>g</sup>	14.29 <sup>g</sup>	0.00	0.00 <sup>g</sup>
DAWB char	1.2	3.4	0.3	96.3	97.33	1.09	0.46	1.12

<sup>a</sup>as received; <sup>b</sup>VM–volatile matter; <sup>c</sup>FC–fixed carbon; <sup>d</sup>daf–dry ash free; <sup>e</sup>by difference;

Table 7-2 The concentrations (mg/kg, dry basis) of inorganic species in DAWB and DAWB char

	DAWB	DAWB char
Na	1.3 ± 0.3	12.9 ± 3.2
K	0.9 ± 0.2	10.1 ± 1.2
Ca	2.7 ± 0.9	32.1 ± 5.7
Mg	1.6 ± 0.4	18.1 ± 2.3
Cl	0 <sup>a</sup>	0 <sup>a</sup>
S	0.4 ± 0.2	0 <sup>a</sup>
P	2.3 ± 0.5	19.4 ± 3.4
Si	749.6 ± 72.4	9068.6 ± 94.1
Al	459.2 ± 65.4	5557.7 ± 27.6
Fe	0.3 ± 0.1	2.7 ± 0.7

<sup>a</sup> not detected

Containing little inorganic species, PE, DAWB, PEG and cellulose produce *in situ* volatiles that contain essentially organic species and are free of catalytically-active inorganic species. Table 7-3 shows that the char yields during rapid pyrolysis of PE, DAWB, PEG and cellulose in Stage I reactor at 1000 °C are 0.0, 8.9, 0.0, and 0.0 wt%, respectively. In other words, the yields of *in situ* volatiles are 91.1 wt% for DAWB and 100 wt% for PE, PEG or cellulose, respectively.



Table 7-3 The char yields of PE, DAWB, PEG and cellulose after *in situ* volatiles generation

Samples	Char yield (wt %, dry basis)
PE	0.0 <sup>a</sup>
DAWB	8.9 ± 0.4
PEG	0.0 <sup>a</sup>
Cellulose	0.0 <sup>a</sup>

<sup>a</sup> no char is produced during pyrolysis

Considering the data on char yield and the chemistry of char generated during *in situ* volatiles generation and the parent feedstock, the chemical compositions of the volatiles generated *in situ* from PE, DAWB, PEG and cellulose can be calculated. As shown in Figure 7-1a, these volatiles are distinctly different in chemistry. For example, the volatiles generated *in situ* from PE pyrolysis contain only H and C but free of oxygen. The volatiles generated *in situ* from DAWB, PEG and cellulose contain not only C and H but also O and that from DAWB also contains negligible N. As shown in Figure 7-1b, on a molar basis, H is a major contributor in all the volatiles, followed by C and O. The C content of the volatiles generated from DAWB is 41 mol% while those from PE, PEG and cellulose are similar (~32–36 mol%). The molar contents of oxygen are in the order of PE volatile (0%) < DAWB volatiles (5.1%) < PEG volatiles (14.3%) < cellulose volatiles (24.3%). Figure 7-1c further presents the molar ratios of O/H and H/C in the volatiles. The O/H molar ratios are 0, 0.12, 0.25 and 0.51 in PE, DAWB, PEG and cellulose volatiles, respectively. PE and PEG volatiles have the highest H/C molar ratio (2.0), followed by cellulose (1.7) and DAWB volatiles (1.3).

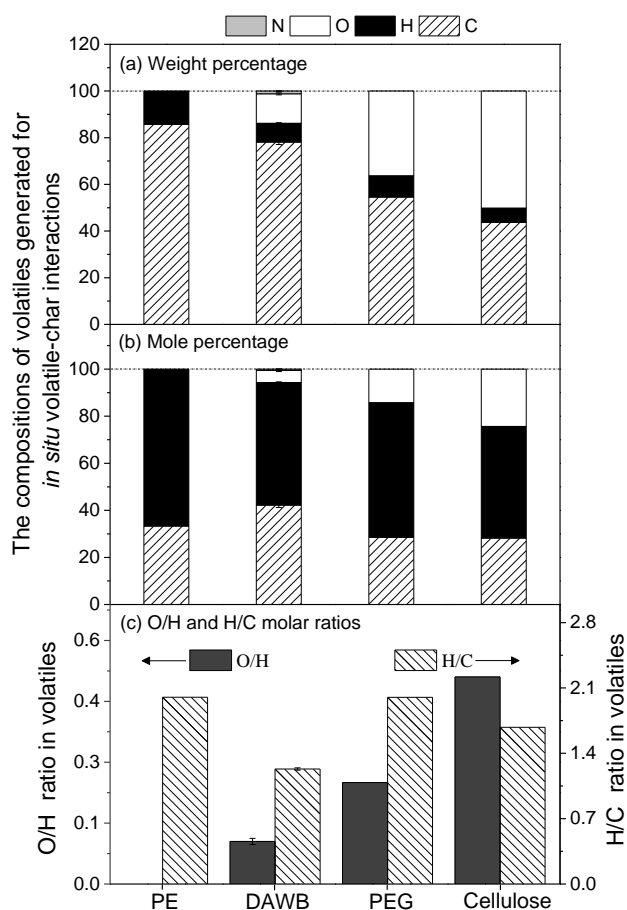


Figure 7-1 Chemistry of volatiles generated *in situ* from PE, DAWB, PEG and cellulose for *in situ* volatile–char interactions at 1000 °C, including (a) weight percentage and (b) mole percentage of elemental compositions and (c) O/H and H/C molar ratios

### 7.3 Variations in char chemistry during *in situ* volatile–char interactions

Figure 7-2 shows that the char yields after holding at 1000 °C or *in situ* interactions with PE, DAWB, PEG and cellulose volatiles are 100%, indicating that the holding or *in situ* volatile–char interactions result in little weight change of the chars. Table 7-3 further presents the concentrations of inorganic species in the DAWB char, Char-holding and chars after *in situ* volatile–char interactions. All chars contain trace amounts of AAEM species and Fe and the main inorganic species are Si and Al. Calculations show that all inorganic species during char holding or *in situ*

volatile–char interactions are retained in the char. These trace amount of inorganic species in DAWB char are in the forms of aluminosilicates or silicates which are catalytically inactive.

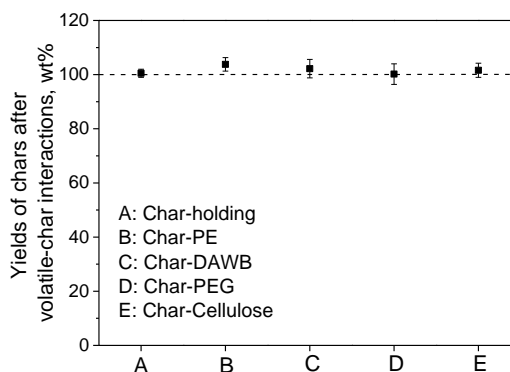


Figure 7-2 Char yields after holding or *in situ* volatile–char interactions at 1000 °C in Stage II reactor

Table 7-4 The content (mg/kg, dry basis) of inorganic species in char in the absence or presence of *in situ* volatile–char interactions

	DAWB char	Char-holding	Char-PE	Char-DAWB	Char-PEG	Char-Cellulose
Na	12.9 ± 3.2	12.2 ± 2.1	11.3 ± 2.1	12.7 ± 1.9	11.9 ± 1.1	13.0 ± 1.2
K	10.1 ± 1.2	9.3 ± 0.7	10.2 ± 2.1	9.5 ± 1.1	11.3 ± 2.1	11.2 ± 0.4
Ca	32.1 ± 5.7	30.4 ± 4.4	32.5 ± 6.8	32.2 ± 5.1	33.1 ± 4.2	33.0 ± 3.8
Mg	18.1 ± 2.3	17.5 ± 2.1	18.4 ± 2.3	17.2 ± 4.2	18.6 ± 1.1	18.5 ± 2.4
Fe	2.7 ± 0.7	2.5 ± 0.4	2.3 ± 0.5	2.6 ± 0.3	2.6 ± 0.5	2.6 ± 0.4
Si	9068.6 ± 94.1	9054.4 ± 99.7	9150.7 ± 87.4	9250.6 ± 79.6	9109.8 ± 58.4	9104.7 ± 88.2
Al	5557.7 ± 27.6	5558.3 ± 12.5	5436.7 ± 75.6	5499.7 ± 59.5	5472.3 ± 99.3	5498.7 ± 75.7

Table 7-5 lists the ultimate analysis of the DAWB char, Char-holding and chars after *in situ* volatile–char interactions. Surprisingly, the content of H in Char-PE is slightly lower than those in Char-holding, but the contents of H and O in Char-Cellulose are higher than those in Char-holding, indicating that the volatiles with distinctly-different chemistry exert different effect on char chemistry. Furthermore, the results in Figure 7-2 and Table 7-5 show that although the substantial amounts of C as part of volatiles are input into the reactor, the net changes in the carbon in the

DAWB char before and after volatile–char interaction are negligible.

Table 7-5 Ultimate analysis of DAWB char, Char-holding and chars after *in situ* volatile–char interactions

Char samples	Ultimate (wt%, daf <sup>a</sup> )			
	C	H	N	O <sup>b</sup>
DAWB Char	97.33 ± 0.15	1.09 ± 0.04	0.46 ± 0.03	1.12 ± 0.10
Char-holding	97.44 ± 0.10	1.05 ± 0.05	0.45 ± 0.02	1.06 ± 0.08
Char-Cellulose	96.92 ± 0.08	1.44 ± 0.04	0.33 ± 0.01	1.31 ± 0.07
Char-PEG	97.18 ± 0.04	1.23 ± 0.04	0.35 ± 0.02	1.24 ± 0.09
Char-DAWB	97.57 ± 0.07	1.01 ± 0.06	0.34 ± 0.03	1.08 ± 0.04
Char-PE	97.87 ± 0.15	0.89 ± 0.07	0.36 ± 0.05	0.88 ± 0.15

<sup>a</sup> daf–dry ash free; <sup>b</sup> by difference

#### 7.4 Effect of volatiles chemistry on char reactivity after *in situ* volatile–char interactions

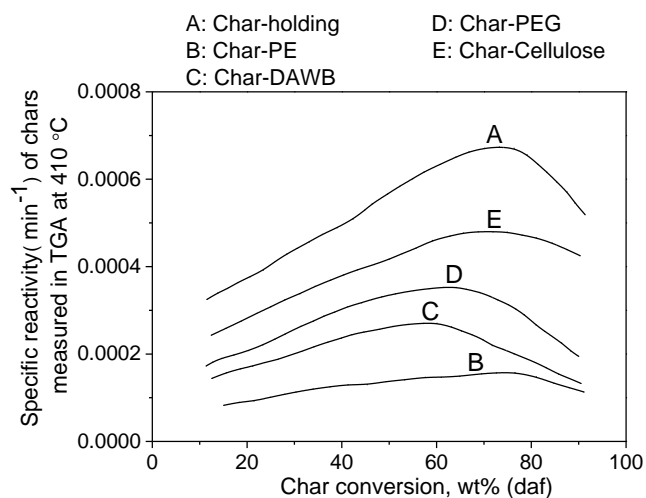


Figure 7-3 Specific reactivities of Char-holding and chars after interactions with different *in situ* volatiles at 410 °C in air determined by TGA

Figure 7-3 presents the reactivity of chars measured in air at 410 °C using the TGA that was operated as a differential reactor and the relative experimental error for char reactivity measurement is 3%. Such conditions ensure char reactivity be measured

---

under kinetic control regime and also eliminate the changes in char structure during reactivity measurement so that the measured reactivity is truly intrinsic reactivity reflecting char structure. In addition, all chars have gone through the same thermal annealing time during *in situ* volatile–char interactions (or char holding) so that any differences observed in the char reactivity are due to the volatile–char interactions.

There are three important observations in Figure 7-3. First, the specific reactivities of the chars after interactions with volatiles are considerably lower than that of Char-holding (see curve A). This is expected because some reactive species in volatiles can react with char and reduce char reactivity.<sup>16</sup> Second, the specific reactivities of the chars after volatile–char interactions are strongly dependent on the *in situ* volatiles, indicating that the chemistry of volatiles plays a significant role in determining char reactivity. Third and most importantly, the reactivity of chars after volatile–char interactions increases with increasing O/H molar ratio of the volatiles. As the O/H molar ratio of the volatiles increases from zero of PE volatiles to 0.12 of DAWB volatiles, 0.25 of PEG volatiles and 0.51 of cellulose volatiles, the maximal reactivity of char increases from  $0.00015 \text{ min}^{-1}$  for Char-PE, to  $0.00028 \text{ min}^{-1}$  for Char-DAWB,  $0.00034 \text{ min}^{-1}$  for Char-PEG and  $0.00053 \text{ min}^{-1}$  for Char-cellulose. The results indicate that both H-containing and O-containing reactive species play important roles in determining char reactivity during *in situ* volatile–char interactions. Because these chars are free of catalytically-active inorganic species, such significant differences in char reactivity must be due to the differences in char carbon structure.

### 7.5 Effect of volatiles chemistry on char carbon structure after *in situ* volatile–char interactions

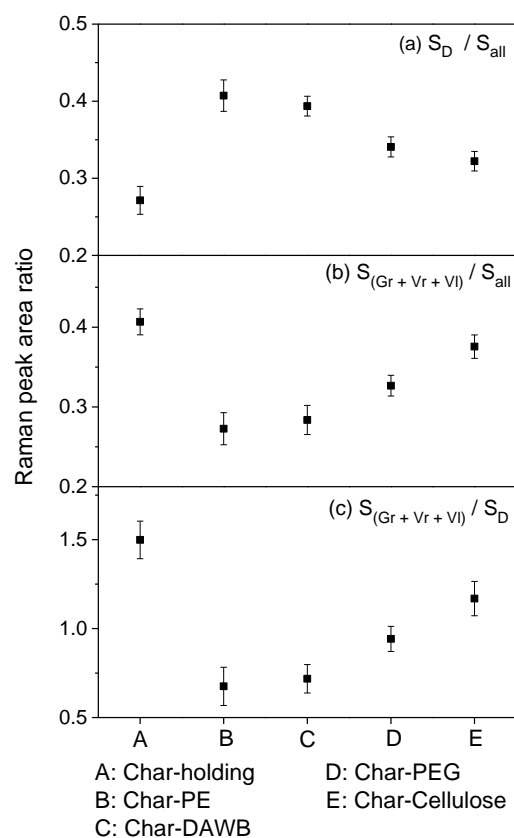


Figure 7-4 Peak fractions of (a) D band and (b) (Gr + V1 + Vr) band out of the total peak area, and (c) peak area ratio of  $S_{(Gr + V1 + Vr)}/S_D$  (c) in chars in the absence or presence of *in situ* volatile–char interactions

Further efforts were then taken to characterise the carbon structure of chars before and after *in situ* volatile–char interactions using Raman spectroscopy. Figure 7-4 presents the results on the peak fractions of the combined (Gr + V1 + Vr) band and D band out of the total peak area and their peak area ratio, i.e.  $S_{(Gr + V1 + Vr)}/S_{all}$ ,  $S_D/S_{all}$  and  $S_{(Gr + V1 + Vr)} / S_D$ , respectively. It is important to note that D band represents defect structures with no less than 6 aromatic rings in highly ordered carbonaceous while the combined (Gr + V1 + Vr) band represents typical structures in amorphous

carbon with 3-5 aromatic rings.<sup>11</sup> Therefore, the three Raman parameters gives key information on char structure in terms of the relative amounts of large or small aromatic structures in char. Three important observations can be made from the results presented in Figure 7-4. First, *in situ* volatile–char interactions significantly increase  $S_D/S_{all}$  (see Figure 7-4a) and decreases  $S_{(Gr + VI + Vr)}/S_{all}$  (see Fig. 5b) and  $S_{(Gr + VI + Vr)}/S_D$  (see Figure 7-4c). The results are in consistence with the char reactivity presented in Figure 7-3 and clearly indicate that more larger aromatic structures are formed during *in situ* volatile–char interactions. This is understandable because during *in situ* volatile–char interactions, the small H-containing reactive species<sup>11,16</sup> are able to penetrate deep into the char matrix and intensify the ring condensation reactions and convert small aromatic ring systems into large ones,<sup>15</sup> thus making the carbon structure less reactive and accordingly decreasing the char reactivity.

Second, Figure 7-4 further show that among all the chars after interactions with various volatiles, Char-PE has the most inert structures, indicating the importance of H-containing reactive species in condensing the aromatic structures in char. However, Char-DAWB has larger aromatic structures than that of Char-PEG though the H content of the DAWB volatiles is lower than that of the PEG volatiles (see Figure 1b), indicating that H-containing reactive species in the volatiles are not the only decisive factor governing the evolution of char carbon structure during *in situ* volatile–char interactions. As shown in Figure 7-4c, the  $S_{(Gr + VI + Vr)}/S_D$  ratio of the chars after *in situ* volatile–char interactions increases with the O/H molar ratio of the volatiles. The results clearly indicate that O-containing reactive species in volatiles also play important role in altering char carbon structure. The O-containing reactive species are known to attack the zig-zag face of carbonaceous materials at temperatures up to 1000 °C and form stable C-O complex oxides, such as carbonyl, ether, anydride or lactone complexes.<sup>196</sup> Oxygen is also known to intercalate into the graphite layers.<sup>197</sup> Those C-O complex oxides are known to mitigate the graphitization of the carbon structure of char during thermal treatment at 900–1200 °C.<sup>185</sup> Therefore, in this study,

similar C-O complex oxides can be formed as results of the interactions between O-containing reactive species in volatiles and the DAWB char hence effectively prevent the carbon structure from further graphitization, clearly supported by the substantial increase in  $S_{(Gr + V_I + V_r)}/S_D$  with increasing oxygen content in volatiles.

Third and last, the changes in char structure directly affect the content of H in the chars after *in situ* volatile–char interactions. For example, PE volatiles are dominated by H-containing reactive species which lead to the most intense condensation of aromatic carbon structure during *in situ* volatile–char interactions. Table 7-5 shows that such structural condensation is also accompanied by the slight decline in H content in char. With increasing O/H molar ratio in volatiles, the mitigating effect of C-O complex oxides on char chemistry is gradually enhanced. For example, compared with PE volatiles, the DAWB volatiles with an O/H molar ratio of 0.12 have little effect on the H content in char. However, when the O/H molar ratio of volatiles becomes higher (e.g. 0.51 for cellulose volatiles), the formation of C-O complex oxides becomes more pronounced, thus leading to the chars with increasing H and O contents and less condensed carbon structures.

## 7.6 Conclusions

This chapter investigates the roles of volatiles, generated from DAWB, PE, PEG or cellulose and distinctly-different in chemistry, in determining char intrinsic reactivity and char structures during *in situ* volatile–char interactions in a two-stage reactor at 1000 °C. Experimental results show that *in situ* volatiles–char interactions substantially reduce char reactivity. It is interesting to see that char reactivity increases with increasing O/H molar ratio of the volatiles for *in situ* volatile–char interactions. The results show that both H- and O-containing reactive species in volatiles play important but different roles during *in situ* volatile–char interactions. H-containing reactive species substantially induce the condensation of the aromatic



ring systems in char and consequently decrease H content in char, thus making the char structure more inert. However, O-containing reactive species in volatiles react with char particles to form C-O complex oxides which mitigates the carbon structure from condensing into larger aromatic ring systems and increases O and H contents in char, thus effectively increasing char reactivity.

*Reprinted with permission from (Xujun Chen and Hongwei Wu. Volatile-char interactions: Roles of in situ volatiles with distinctly-different chemistry in determining char structure and reactivity, Proceedings of the Combustion Institute 2019, 37, 2749-2755). Copyright (2018) The Combustion Institute. Published by Elsevier Inc*

# CHAPTER 8 EFFECT OF WATER VAPOUR ON PM EMISSION DURING COMBUSTION OF *IN SITU* VOLATILES AND CHAR FORM FAST PYROLYSIS OF P-CONTAINING CONTAMINATED WOOD

## 8.1 Introduction

Combustion is a key strategy to process P-containing contaminated biomass such as chromated-copper-arsenate-treated (CCAT) wood.<sup>45</sup> Oxy-fuel combustion replaces conventional air combustion via the use of oxygen and recycled flue gas to produce CO<sub>2</sub>-dominated flue gas and sequestration ready,<sup>198</sup> and thus achieves carbon negativity.<sup>58</sup> However, oxyfuel atmosphere containing substantial water vapour (10–30% or even higher<sup>25</sup>) results in significant variations in heat and mass transfer, flame temperature and burnout of the combustion process.<sup>199</sup> There is still considerable gap for systematic research into the effect of water vapour on PM emission during oxyfuel combustion for at least three reasons. First, there are only scattered reports available on the topic.<sup>158,159,169</sup> Particularly, contaminated biomass, such as CCAT wood contains abundant toxic trace elements but the only study into the effect of water vapour on trace elements emission in PM was under oxy-coal combustion conditions.<sup>168,169</sup> It is unknown if such knowledge can be extrapolated to the emission of trace elements during combustion of contaminated biomass. Second, the current understanding on the effect of water vapour on PM emission during oxyfuel combustion is only based on the combustion of the whole fuel. As solid fuel particles are injected into the furnace, the first step is rapid pyrolysis that generates char and volatiles. Our previous studies<sup>19,23,24</sup> revealed the distinct differences in the pathways of volatiles and char combustion to PM emission, via a novel two-stage

pyrolysis/combustion system. However, the effect of water vapour on PM emission via such individual char or volatiles combustion is still unknown. Third and last, limited by the working temperature of the quartz reactor for generating *in situ* volatiles, those studies only considered the volatiles generated at temperatures (800–1000 °C) lower than the combustion temperature (1300 °C). It is highly desired to investigate the effect of water vapour on PM emission behaviour during the combustion of *in situ* volatiles and char produced at the same temperature of combustion. Unfortunately, this important aspect has not been investigated.

Consequently, this chapter investigated the fundamental mechanisms governing the effect of water vapour on PM emission during separate oxy-fuel combustion of char and *in situ* volatiles generated from CCAT wood at 1300 °C in a novel two-stage pyrolysis/combustion system<sup>12</sup> (see Figure 3-4 in Section 3.3.4).

Table 8-1 Properties of the P-containing contaminated wood used in Chapter 8

Moisture (wt%, ar <sup>a</sup> )	Proximate (wt%, db)			Ultimate (wt%, daf <sup>d</sup> )			
	Ash	VM <sup>b</sup>	FC <sup>c</sup>	C	H	N	O <sup>e</sup>
2.3	0.6	48.9	50.5	49.49	5.90	0.45	44.16
Major elements (mg/kg_CCAT_wood)				Trace elements (mg/kg_CCAT_wood)			
Al	93.3 ± 9.7			As	15.382 ± 0.917		
Fe	144.2 ± 15.7			Cr	21.882 ± 0.089		
Na	418.5 ± 34.4			Ni	1.032 ± 0.044		
K	342.6 ± 14.6			Cu	18.921 ± 1.002		
Mg	233.4 ± 24.6			Pb	4.304 ± 0.099		
Ca	1074.4 ± 99.9			Mn	34.383 ± 0.129		
Cl	278.3 ± 12.5			Ti	154.004 ± 13.200		
P	149.6 ± 2.4						
S	79.2 ± 3.2						
Si	391.2 ± 25.2						

<sup>a</sup>as received; <sup>b</sup>VM–volatile matter; <sup>c</sup>FC–fixed carbon; <sup>d</sup>daf–dry ash free;

## 8.2 Effect of water vapour on the properties of PM<sub>10</sub> during the combustion of *in situ* volatiles and char

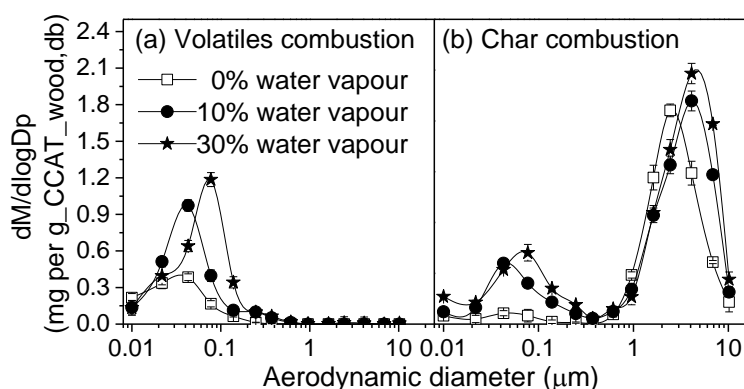


Figure 8-1 PSDs of PM collected during the combustion of (a) *in situ* volatiles and (b) char under oxyfuel conditions at 1300 °C and different water vapour contents

Figure 8-1 presents the PSDs of PM<sub>10</sub> collected during char and *in situ* volatiles combustion in absence or presence of water vapour, normalised to the mass of the CCAT wood. Blank experiment was also conducted with water vapour and oxy-fuel gas injecting into the drop-tube furnace (DTF) without volatiles or char feeding and the results show that no PM<sub>10</sub> was produced. The Stage I and Stage II alumina tubes (see Figure 3-4) were also washed by diluted sulfuric acid and deionised water before each experiment to prevent the release of any inorganic species pre-deposited on the reactor tube of the DTF to distort the measurement of PM<sub>10</sub> emission.<sup>200</sup> Three important observations can be made in Figure 8-1. First, *in situ* volatiles combustion in either presence or absence of water vapour only produces PM<sub>1</sub> with a unimodal size distribution. Second, the mode diameter of PM samples collected during volatiles combustion without water vapour and 10% water vapour content is 0.042 μm and 0.077 μm with water vapour increasing to 30%, indicating that the increased impinging of water molecules<sup>201</sup> at high water vapour contents could enhance the growth of nuclei, condensation of inorganic species on existing nuclei or/and coagulation of fine particles. Third, PM<sub>10</sub> generated during char combustion without

the addition of water vapour have bimodal distributions that include a fine mode at  $0.043\ \mu\text{m}$  and a coarse mode at  $2.44\ \mu\text{m}$ . Similarly, the mode diameter of the fine mode shifts to  $0.077\ \mu\text{m}$  when the water vapour content increases to 30%. Interestingly, the mode diameter of the coarse mode also shifts to a larger size of  $4.094\ \mu\text{m}$  when the water vapour content increases from 10% and 30%. The results suggest that water vapour also enhances the coalescence or/and agglomeration of coarse particles because water vapour could accelerate the sintering rate of  $\text{Ca}^{202}$  and Mg-bearing species,<sup>157</sup> thus enhancing the agglomeration of those species.

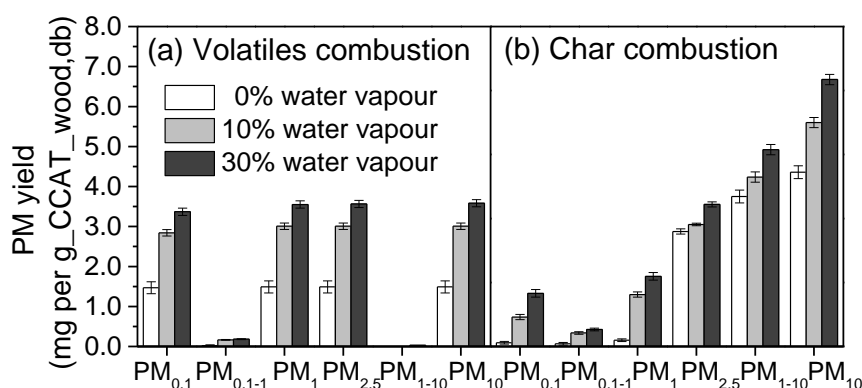


Figure 8-2 Yields of PM collected during combustion of (a) *in situ* volatiles and (b) char under oxyfuel conditions at 1300 °C and different water vapour contents

Figure 8-2a further shows that volatiles combustion only generates PM<sub>1</sub>, especially PM<sub>0.1</sub>. The introduction of water vapour substantially increases the PM<sub>1</sub> yield from 1.5 (in absence of water vapour) to 3.0 (at 10% water vapour content) and 3.8 mg/g\_CCAT\_wood (at 30% water vapour content), respectively. Figure 8-2b shows in absence of water vapour char combustion produces very low PM<sub>1</sub> yield (0.2 mg/g\_CCAT\_wood) because most of volatile inorganic species would have been released into the volatiles during char preparation at 1300 °C. Again, the addition of water vapour into the combustion atmosphere also significantly increases PM<sub>1</sub> yield, from 0.2 (in absence of water vapour) to 1.5 (at 10% water vapour content) and 2.0 mg/g\_CCAT\_wood (at 30% water vapour content), respectively. The addition of

water vapour also significantly increases the  $PM_{1-10}$  yield during char combustion, from 3.8 (in absence of water vapour) to 4.6 (at 10% water vapour content) and 5.2  $mg/g\_CCAT\_wood$  (at 30% water vapour content), respectively.

### 8.3 Effect of water vapour on the emission of major elements in $PM_{10}$ during the combustion of *in situ* volatiles and char

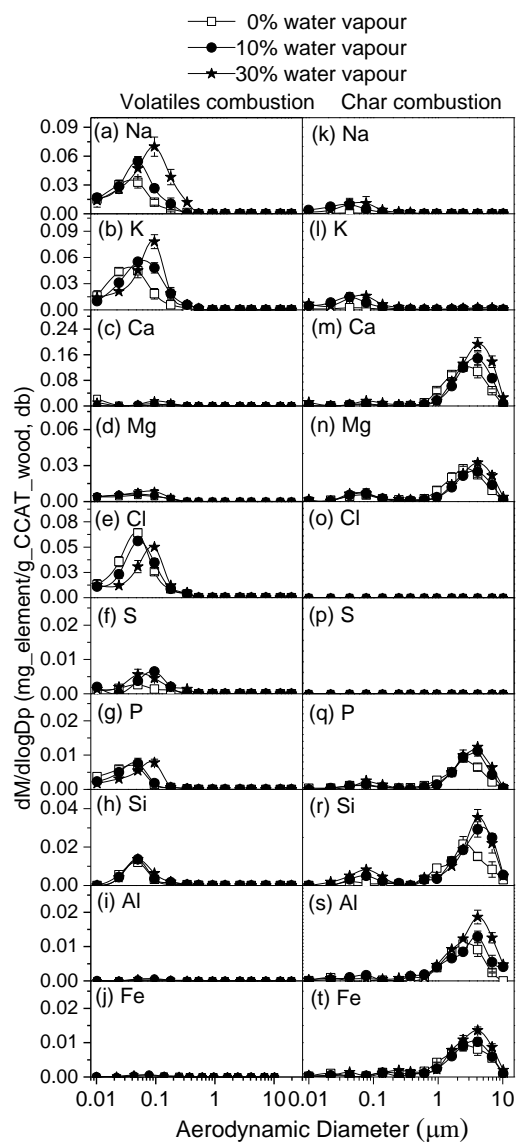


Figure 8-3 PSDs of major elements in the PM collected during combustion of (a–j) *in situ* volatiles and (k–t) char under oxyfuel conditions with different water vapour contents

Figure 8-3 presents the PSDs of major elements in PM<sub>10</sub> collected during the combustion of *in situ* volatiles and char, with the respective elemental yields shown in Figure 8-4. For volatiles combustion, PM<sub>1</sub> indeed contains dominantly volatile species (including Na, K, Cl, S and P). Interestingly, there are also small amounts of refractory Mg and Si in PM<sub>1</sub>. Considering the combustion temperature is 1300 °C and the presence of P and S, the most likely pathway for the release of Mg to form PM<sub>1</sub> is in the forms of magnesium sulphate and magnesium phosphate that have low melting points of 1124 and 1184 °C, respectively. The presence of Si in PM<sub>1</sub> can be attributed to the reduction of SiO<sub>2</sub> by reducing agents (e.g. C, CO, H<sub>2</sub>) which are produced abundantly during pyrolysis to generate gaseous SiO under reducing conditions,<sup>168</sup> resulting in the release of some Si into the gaseous phase during pyrolysis and then re-oxidised into SiO<sub>2</sub> as part of PM<sub>1</sub> during subsequent combustion. Figure 8-4 shows that water vapour has little effect on the P yield during volatiles combustion. However, the introduction of water vapour leads to slight decrease in Cl and slight increase in S in the PM<sub>1</sub>. However, the molar yields of (S + Cl) in PM<sub>1</sub> remain unchanged, irrespective of water vapour content in the combustion atmospheres, suggesting that water vapour facilitates the transformation between chloride and sulphide. Specifically, H<sub>2</sub>O-derived OH radical can combine with SO<sub>2</sub> to form intermediate HOSO<sub>2</sub>, which could subsequently react with chlorides to form sulphates<sup>30</sup> and release HCl, thus possibly reducing the yield of Cl and increasing that of S in PM<sub>1</sub> during *in situ* volatiles combustion.

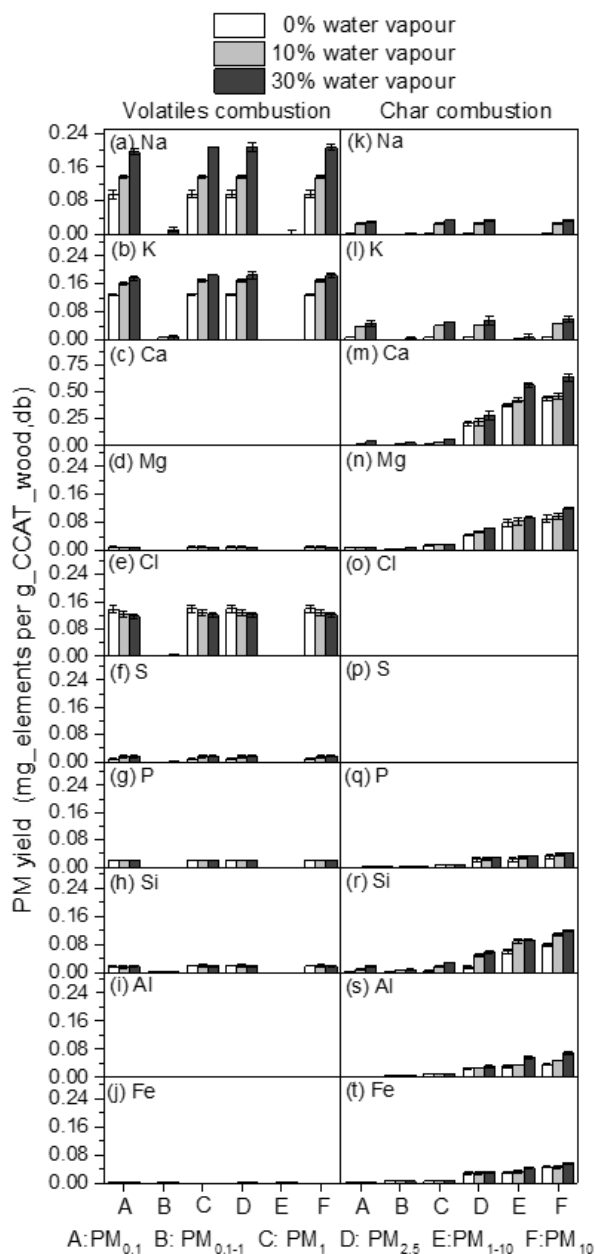


Figure 8-4 Yields of major elements in PM collected during combustion of (a–j) in situ volatiles and (k–t) under oxyfuel conditions with different water vapour contents

The results in Figure 8-4 clearly show that increasing water vapour content leads to substantial increases in the yields of Na and K in PM<sub>0.1</sub> (hence the total yield of PM<sub>0.1</sub> as shown in Figure 8-2) generated during *in situ* volatiles combustion. In addition to chlorides and sulphates, alkalis are also known to be released as alkali



metaphosphates e.g. (Na,K)PO<sub>3</sub> during solid fuel combustion.<sup>20</sup> Further efforts were taken to calculate the (Na+K+2Mg)/(Cl+2S+P) molar ratios in PM<sub>0.1</sub> during volatiles combustion under various combustion conditions. Without the addition of water vapour, the (Na+K+2Mg)/(Cl+2S+P) molar ratio is 1.08, proving that Na, K and Mg are indeed dominantly present in the forms of chloride, sulphate or metaphosphate in PM<sub>0.1</sub>. However, it increased to 1.81 and 2.70 at 10% and 30% water vapour content, respectively. Because the addition of water vapour leads to little increases in the yields of anion species (Cl, S and P), as shown in Figure 8-4, an increase in the (Na+K+2Mg)/(Cl+2S+P) molar ratio indicates that the increased Na and K in PM<sub>0.1</sub> are in chemical forms other than chloride, sulphate or metaphosphate. Most likely, water vapour favours the reaction between Na (and K) and H<sub>2</sub>O-derived OH radical to form NaOH which is the most stable forms,<sup>203</sup> instead of reacting with reactor tube wall and retaining in the DTF, leading to the significant increase in the yields of Na and K in PM<sub>0.1</sub>. Vapours of alkali hydroxides can react with the alumina reactor tube of the DTF to form water-soluble alkali aluminates (NaAlO<sub>2</sub> and KAlO<sub>2</sub>) during combustion at 1300 °C, via the following overall reactions:<sup>200</sup>



The net consequences of Reaction R1 and R2 are that Na and K are captured by the alumina reactor tube, instead of being collected in PM. Both reactions may be reversible so that increasing water vapour content would hinder the formation of alkali aluminates, hence less Na and K would be captured by the alumina reactor tube. The alumina reactor tubes after volatiles combustion at different water vapour concentrations were then washed using deionized water and the amounts of Na, K and Al in the washed solutions were quantified. As shown in Table 8-2, the molar ratios of (Na+K)/Al in all the solutions from water washing of the alumina reactor tubes are ~1.0, proving that (Na, K)AlO<sub>2</sub> were formed on the alumina reactor tube. The total

amount of Na or K captured in PM and the outer alumina reactor tube remains unchanged under all conditions. Considering the amounts of Na and K (0.045 and 0.041 mg/g CCAT wood, respectively) retained in the inner alumina tube and the YSZ felt (see Figure 3-4) during pyrolysis, the mass balances of Na and K in the reactor system achieve over 90%. The results demonstrate that both reactions R1 and R2 do proceed and are indeed reversible under the combustion conditions in this study. Increasing water vapour addition hinders the formation of alkali aluminates by the reactions between the alkali vapours and the reactor wall. Such mechanisms can also explain the increase in the yield of PM<sub>0.1</sub> during char combustion as water vapour addition increases. Increasing water vapour addition might also enhance the volatilisation of Na, K and Si from char, contributing to the increased yields of those elements in PM<sub>1</sub> (see Figure 8-4k, 4l and 4r) during char combustion.

Table 8-2 Yields of Na and K in PM<sub>1</sub> and the alumina reactor tube during volatiles combustion and Al in the solutions from water washing of the alumina reactor tube of the DTF

	Water vapor content	Yield (mg per g CCAT wood)		
		(A) in PM <sub>1</sub>	(B) in the solution <sup>b</sup>	(A+B) total
Na	0%	0.093	0.150	0.243
	10%	0.137	0.096	0.233
	30%	0.224	0.014	0.238
K	0%	0.101	0.103	0.204
	10%	0.150	0.042	0.192
	30%	0.164	0.034	0.198
Al <sup>c</sup>	0%	-	0.236	-
	10%	-	0.142	-
	30%	-	0.041	-
(Na+K)/Al molar ratio in the solution, <sup>b</sup> calculated		0% water vapour		1.0
		10% water vapour		1.0
		30% water vapour		1.0
<sup>a</sup> experimental errors are within $\pm 0.005$ mg per g CCAT wood for the analyses of Na, K and Al; <sup>b</sup> refers to the solution from water washing of the alumina reactor tube; <sup>c</sup> refers to Al present in the solutions.				

The increases in the yields of PM<sub>1-10</sub> (see Figure 8-2) and refractory elements including Ca, Mg, Al, Fe, Si in PM<sub>1-10</sub> (see Figure 8-4) with increasing water vapour content is most likely due to enhanced char fragmentation during char combustion in presence of water vapour. Considering the oxygen content was maintained at 30% for all combustion experiments, the effect of water vapour on char particle temperature is insignificant.<sup>204</sup> However, the reactions between H<sub>2</sub>O and char prefer to form more mesoporous and macroporous structures<sup>205</sup> even with a limited char conversion,<sup>206</sup> which are expected to enhance char fragmentation hence increase the yields of PM<sub>2.5</sub> and PM<sub>1-10</sub>. Surprisingly, traceable Si is also presented in the PM<sub>1</sub> produced during char combustion and its yield increases with increasing water vapour content. This can be attributed to the reactions between SiO<sub>2</sub> and H<sub>2</sub>O to form gaseous SiO(OH)<sub>2</sub>, Si(OH)<sub>4</sub> and/or Si<sub>2</sub>O(OH)<sub>6</sub> (known to take place at high temperature<sup>168</sup>), resulting in the release of Si as part of PM<sub>1</sub>.

### 8.4 Effect of water vapour on the emission of trace elements during the combustion of *in situ* volatiles and char

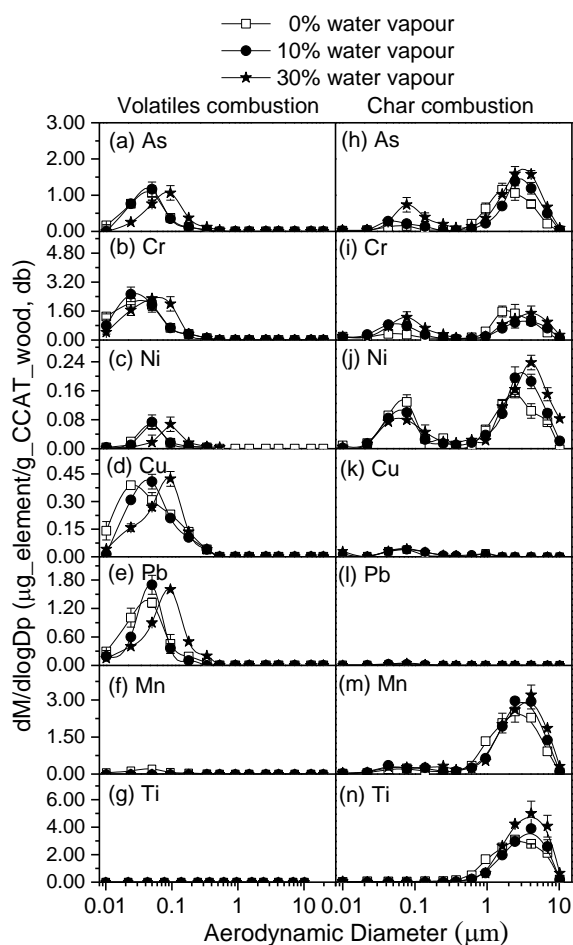


Figure 8-5 PSDs of trace elements in PM collected during the combustion of (a–g) *in situ* volatiles and (h–n) char under oxyfuel conditions with different water vapour contents

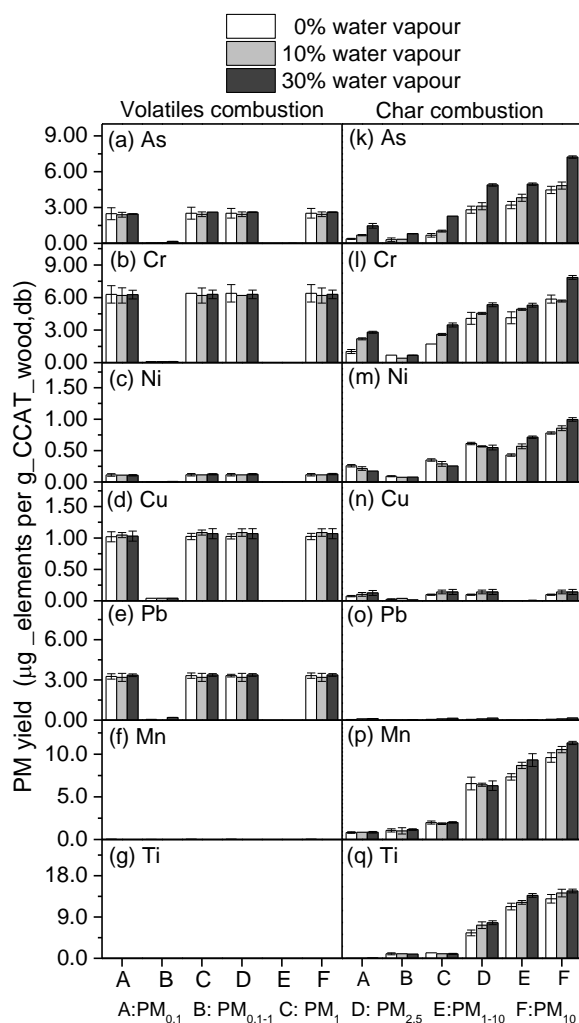


Figure 8-6 Yields of trace elements in PM collected during the combustion of (a–g) in situ volatiles and (h–n) char under oxyfuel conditions with different water vapour contents

The PSDs of trace elements in PM collected during the combustion of *in situ* volatiles and char are presented in Figure 8-5 and the yields of individual trace elements are shown in Figure 8-6. Several important observations can be made based on the results in these two figures. First, the results in the panels a–g of Figure 8-5 and Figure 8-6 show that during the combustion of *in situ* volatiles, As, Cr, Ni, Cu and Pb are only presented in PM<sub>1</sub> and the introduction of water vapour alters the PSDs, but has little effect on the yields of these trace elements in PM<sub>1</sub>. Second, As,

Cr, Cu and Ni are present in both PM<sub>1</sub> and PM<sub>1-10</sub> while the non-volatile Mn and Ti are only present in PM<sub>1-10</sub> during char combustion. Increasing water vapour content increases the yields of As, Cr, Cu, Ni, Mn and Pb in PM<sub>1-10</sub> due to the possibly enhanced char fragmentation during char combustion. Third, it is interesting that the yields of As and Cr in PM<sub>1</sub> increase with increasing water vapour content during char combustion. Under current experimental conditions, arsenic is mostly likely present in the char as calcium arsenate or arsenic oxides<sup>207</sup> and it is reported that under less oxidising conditions, all As could be converted to AsO(s) and sublimated.<sup>208</sup> In presence of water vapour, despite the limited char gasification under current conditions, the reactions between H<sub>2</sub>O and char is much more intense than that between CO<sub>2</sub> and char,<sup>209</sup> thus promotes a less oxidised conditions locally and enhances the evaporation of As. Chromium is mostly likely present in char as Cr<sub>2</sub>O<sub>3</sub> that is the most thermally stable form,<sup>208</sup> while Cr<sub>2</sub>O<sub>3</sub> could react with water vapour to generate gaseous oxyhydroxides such as CrO(OH), CrO<sub>2</sub>(OH), and CrO(OH)<sub>2</sub> at high temperatures,<sup>208</sup> resulting in an increase in Cr condensed in PM<sub>1</sub>. Fourth and last, the yield of Ni in PM<sub>1</sub> decreases with increasing water vapour content, as higher water vapour could hinder the Ni chlorination reaction  $[\text{NiO}(\text{cr}) + 2\text{HCl}(\text{g}) \rightleftharpoons \text{NiCl}_2(\text{g}) + \text{H}_2\text{O}(\text{g})]$  and favours NiO formation.<sup>208</sup>

## 8.5 Conclusions

This chapter deployed a two-stage pyrolysis/combustion system for investigating the effect of water vapour on PM emission during the separate combustion of *in situ* volatiles and char generated from P-containing CCAT wood at 1300 °C. During *in situ* volatiles combustion, water vapour could significantly enhance the nucleation, coagulation and condensation of fine particles and increases the PM<sub>0.1</sub> yield. During char combustion, water vapour might also enhance char fragmentation hence increases the PM<sub>1-10</sub> yield. For trace elements, volatile trace elements (As, Cr, Ni, Cu and Pb) are only presented in PM<sub>1</sub> during *in situ* volatiles combustion. Water vapour shifts the

PSDs, but has little effect on the yields of these trace elements. During char combustion, As, Cr, Cu and Ni are present in both  $PM_1$  and  $PM_{1-10}$  while non-volatile Mn and Ti are only present in  $PM_{1-10}$ . Water vapour increases the yields of As, Cr, Cu, Ni, Mn and Ti in  $PM_{1-10}$  due to possibly enhanced char fragmentation. With the addition of water vapour, the yields of As and Cr in  $PM_{0.1}$  are increased but that of Ni in  $PM_{0.1}$  is decreased during char combustion, most likely due to water vapour facilitating the conditions that enhance the release of As and the generation of gaseous chromium oxyhydroxides but inhibits the production of volatile  $NiCl_2$ .

*Reprinted with permission from (Xujun Chen, Sui Boon Liaw and Hongwei Wu. Effect of water vapour on particulate matter emission during oxyfuel combustion of char and in situ volatiles generated from rapid pyrolysis of chromated-copper-arsenate-treated wood, Proceedings of the Combustion Institute 2019, 37, 4319–4327). Copyright (2018) The Combustion Institute. Published by Elsevier Inc*

---

# CHAPTER 9 IMPORTANT ROLE OF VOLATILE-CHAR INTERACTIONS IN ENHANCING PM<sub>1</sub> EMISSION DURING COMBUSTION OF VOLATILES FROM P-CONTAINING BIOSOLID

## 9.1 Introduction

Combustion of biosolid featuring in high P contents is considered as one of the important technologies for volume reduction, destruction of toxic matters, and energy recovery.<sup>5,48</sup> However, as described in Section 2.7, it could generate significant PM, especially PM<sub>2.5</sub> and PM<sub>10</sub><sup>21,210</sup> that have adverse impacts on process operations and the environment.<sup>4,22,58,151,163,211,212</sup> As elaborated in Section 2.5.1 and 2.7.4, during biosolid combustion, volatiles and char may experience strong interactions during devolatilization (the first step of combustion) and such volatile-char interactions may affect the transformation of inorganic species. Our recent studies<sup>19,23</sup> also show that volatile-char interactions might play an important role in PM emission during solid fuels combustion. Unfortunately, thus far, there has been no direct evidence on this important aspect.

Therefore, this chapter aims to provide direct evidence on this important issue using a three-stage reactor system (detailed description given in Section 3.3.4 and Figure 3-5). It is noted that due to the working temperature limit (below 1100 °C) of the quartz reactor, experiments were carried out for *in situ* generation of volatiles (hence volatile-char interactions) at 800 and 1000 °C, which are lower than the temperature of volatiles combustion (1300 °C). Nevertheless, the series of experiments are sufficient to prove the potentially important role of volatile-char interactions in PM emission during biosolid combustion.



## 9.2 Properties of char and samples used for generating volatiles with *in situ* volatile–char interactions

In this chapter, three samples are used for generating *in situ* volatiles, namely, cellulose, polyethylene (PE) and single acid-washed biosolid (AW-biosolid). The detailed description for the preparation of AW-biosolid could be found in Section 3.3.1. The properties of the biosolid and AW biosolid samples are listed in Table 9-1. The retentions of major and trace elements in biosolid after acid-washing are presented in Figure 9-1, which clearly shows that the majority of the AAEMs, S, P and trace elements such as As, Ni, Co, Pb, and Cu were removed during acid-washing, while significant Al, Fe, Si, Cr and Cd were retained. It is also noted that the biosolid sample has a low Cl content and the AW biosolid contains little Cl.

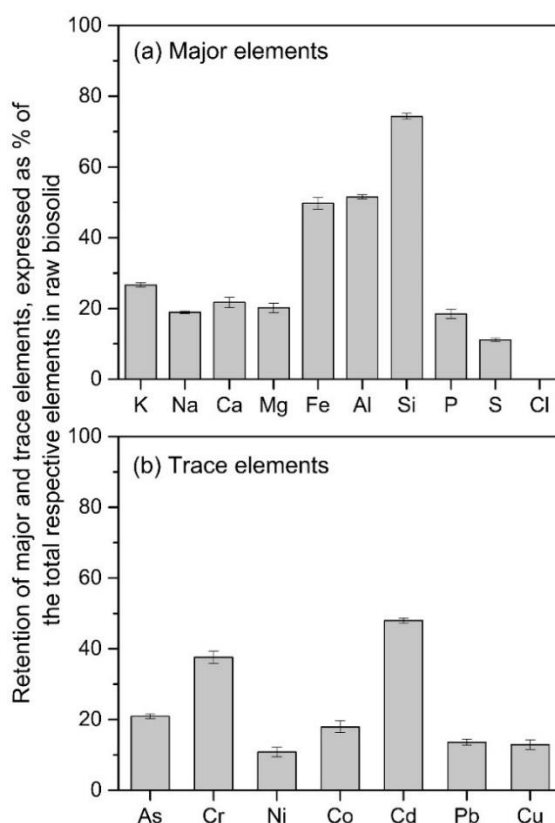


Figure 9-1 Retention of (a) major and (b) trace elements in acid-washed biosolid after acid-washing of the biosolid sample, expressed as % of those in biosolid

Table 9-1 Properties of biosolid, acid-washed biosolid, cellulose, polyethylene and slow heating biosolid chars prepared at 800°C and 1000°C, respectively.

Samples	Biosolid	AW Biosolid	Cellulose	Polyethylene	BSH800 Char <sup>g</sup>	BSH1000 Char <sup>h</sup>
Moisture (wt % ad <sup>a</sup> )	5.3	3.7	4.0	0.1	1.3	1.4
Proximate Analysis (wt% db <sup>b</sup> )						
Volatile Matter	67.1	74.4	90.7	100.0	4.2	2.8
Fixed Carbon	13.2	17.9	9.3	0.0	39.5	35.6
Ash	19.7	7.7	0.03	0.0	56.3	61.6
Ultimate Analysis (wt% daf <sup>c</sup> )						
C	52.82	61.47	43.74	85.71 <sup>e</sup>	94.20	96.30
H	6.98	11.92	6.07	14.29 <sup>e</sup>	0.29	0.11
N	9.33	3.72	0.00	0.00	4.71	3.12
O <sup>d</sup>	30.87	22.89	50.19	100	0.8	0.47
Major Elements (mg/kg, db <sup>b</sup> )						
Si	19008.7 ± 584.2	9042.6 ± 325.2	n.d. <sup>g</sup>	n.d. <sup>f</sup>	63402.8 ± 302.2	67084.9 ± 229.9
Al	6782.2 ± 68.4	2237.3 ± 29.7	<1.0	<1.0	21792.4 ± 30.6	23637.5 ± 39.1
Fe	3277.6 ± 47.8	1044.2 ± 15.7	11.4 ± 2.8	7.2 ± 3.4	10627.7 ± 23.7	11241.2 ± 14.4
K	2007.8 ± 18.7	342.6 ± 14.6	<5.0	<5.0	5367.2 ± 12.4	5894.5 ± 16.0
Na	1389.8 ± 16.2	168.5 ± 4.4	41.7 ± 5.5	20.6 ± 7.1	4218.7 ± 4.4	4217.3 ± 8.7
Ca	20668.3 ± 389.6	2874.4 ± 106.8	<5.0	<5.0	70960.4 ± 210.0	76344.2 ± 273.4
Mg	4901.7 ± 44.6	633.4 ± 24.6	<5.0	<5.0	16019.3 ± 26.6	17006.5 ± 35.0
P	18228.9 ± 188.4	2149.6 ± 98.4	n.d. <sup>g</sup>	n.d. <sup>g</sup>	61079.9 ± 110.5	63465.2 ± 208.7
Cl	882.4 ± 5.5	n.d. <sup>g</sup>	<5.0	<5.0	20.1 ± 3.2	11.4 ± 2.7
S	8592.2 ± 74.2	612.4 ± 46.8	<5.0	6.8 ± 0.1	5314.3 ± 38.4	4714.8 ± 45.6

Table continued in next page

Trace Elements (mg/kg, db<sup>b</sup>)

As	2.852 ± 0.144	0.382 ± 0.017	n.d. <sup>g</sup>	n.d. <sup>g</sup>	5.866 ± 0.181	2.097 ± 0.093
Cr	32.776 ± 0.998	7.882 ± 0.089	<1.000	n.d. <sup>g</sup>	102.001 ± 0.929	105.321 ± 1.989
Co	3.469 ± 0.078	0.398 ± 0.021	0.062 ± 0.040	0.038 ± 0.026	10.669 ± 0.089	11.431 ± 0.114
Ni	19.204 ± 0.143	1.328 ± 0.044	<0.200	<0.200	60.882 ± 1.177	64.691 ± 2.296
Cu	492.4 ± 7.8	40.7 ± 2.4	n.d. <sup>g</sup>	n.d. <sup>g</sup>	1577.5 ± 6.5	1725.1 ± 8.4
Cd	2.384 ± 0.099	0.732 ± 0.034	<0.100	<0.100	5.770 ± 0.221	1.148 ± 0.104
Pb	14.003 ± 1.275	1.218 ± 0.068	0.482 ± 0.042	0.306 ± 0.051	18.667 ± 0.348	4.125 ± 0.239

<sup>a</sup> ad = air dried; <sup>b</sup> db = dry basis; <sup>c</sup> daf = dry and ash free; <sup>d</sup> by difference; <sup>e</sup> calculated values; <sup>f</sup> n.d. = non-detected; <sup>g</sup> BSH800 Char = biosolid char prepared from slow heating pyrolysis of the raw biosolid in a fixed-bed at 800 °C; <sup>h</sup> BSH1000 Char = biosolid char prepared from slow heating pyrolysis of the raw biosolid in a fixed-bed at 1000 °C.

However, some inorganic species are still present in the AW samples. To understand the release of the inorganic species in the volatiles generated *in situ* from AW biosolid fast pyrolysis, separate pyrolysis experiments were carried out at 800 °C and 1000 °C in a drop-tube/fixed-bed reactor (Type B, in Figure 3-2) under the same conditions. As shown in Figure 9-2, during *in situ* volatiles generation from AW biosolid at 800 and 1000 °C, small proportions of Na, K and P, >90% of S and some of the trace elements (i.e. As, Cr, Cd, and Pb) were released into the AW biosolid volatiles. In addition, cellulose and polyethylene with size <200 μm were also used to *in situ* generate volatiles of different characteristics for interacting with the chars. As shown in Table 9-1, cellulose sample is almost inorganics-free (ash content: 0.03%) so that its rapid pyrolysis generates volatiles containing essentially organic species. Only containing C and H, polyethylene pyrolysis produces volatiles consisting of purely hydrocarbon and free of oxygen-containing species.

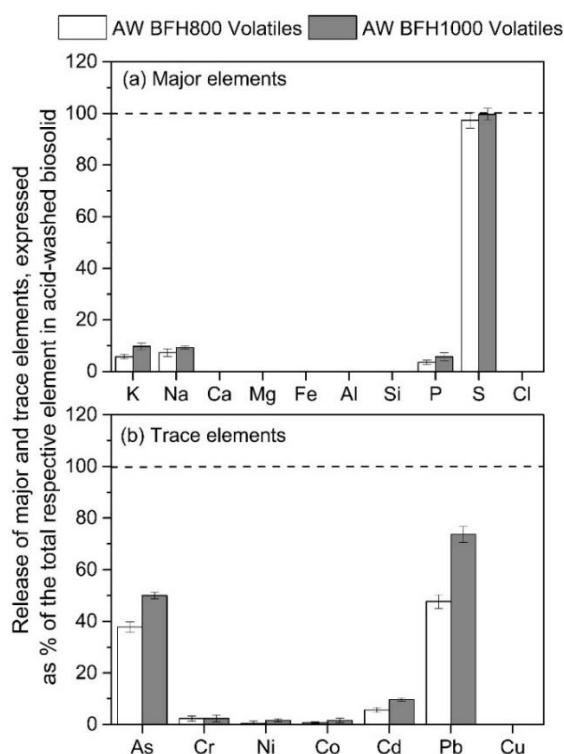


Figure 9-2 Release of (a) major and (b) trace elements in the volatiles generated *in situ*

from the fast heating pyrolysis of acid-washed biosolid. The AW BFH800 volatiles and AW BFH1000 volatiles are generated *in situ* from fast heating pyrolysis of acid-washed biosolid at 800 and 1000 °C, respectively, for volatile–char interactions experiment

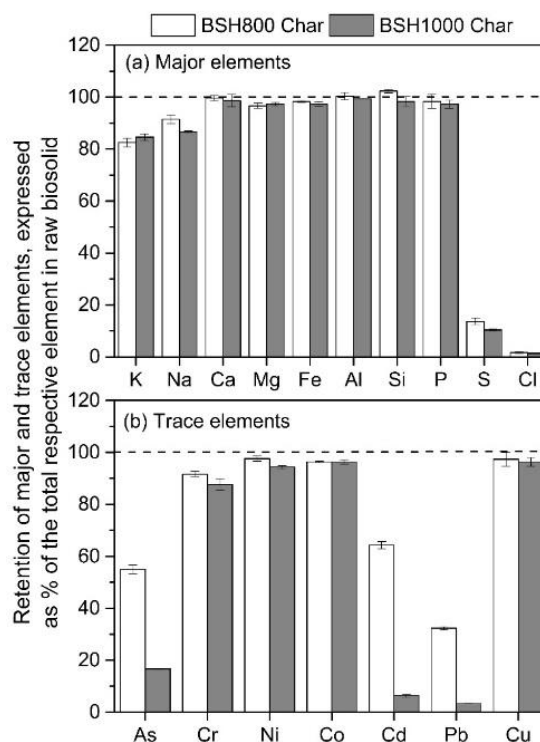


Figure 9-3 Retention of (a) major and (b) trace elements in chars produced from slow heating pyrolysis of biosolid at 800 (BSH800 Char) and 1000 °C (BSH1000 Char)

As inorganic PM is originated from inorganic matter in the parent fuels, it is highly desired to prepare char samples of high inorganic concentrations for the experiments to illustrate the importance of volatile–char interactions. For this reason, slow heating pyrolysis of biosolid were conducted at 800 and 1000 °C at a heating rate of 10 °C/min in fixed-bed reactor (See Figure 3-2a) to prepare two biochar samples, referred to as “BSH800 char” and “BSH1000 char”, respectively, for subsequent volatile–char interactions. The contents and retentions of inorganic species in these slow heating chars are presented in Table 9-1 and Figure 9-3, respectively. The

majorities of Na, K and P and almost all Ca, Mg, Fe, Al, and Si are retained in the chars, while only a small proportion of S and little Cl are retained in the chars. Meanwhile, significant As, Cd, and Pb were released into the gaseous phase during slow pyrolysis and the respective retentions in char are  $< 20\%$  at  $1000\text{ }^{\circ}\text{C}$ .

### 9.3 Direct Evidence on the importance of Volatile–char Interactions in PM Emission

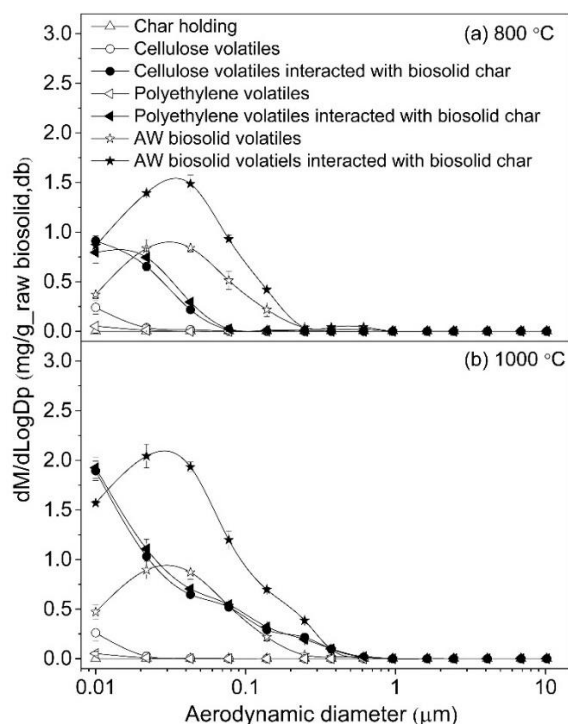


Figure 9-4 The PSDs of PM collected from the combustion of fresh volatiles generated from cellulose, polyethylene and AW biosolid without or with interactions with slow heating biosolid char at (a)  $800\text{ }^{\circ}\text{C}$  and (b)  $1000\text{ }^{\circ}\text{C}$ , respectively

Figure 9-4 presents the particle size distributions (PSDs) of the  $\text{PM}_{10}$  released during combustion of volatiles generated from cellulose, polyethylene, and AW biosolid, without or with interactions with the bed of slow heating biosolid char at  $800\text{ }^{\circ}\text{C}$  and  $1000\text{ }^{\circ}\text{C}$ , respectively, normalised to equivalent biosolid. There are two cases for experiments in absence of volatile–char interactions. One is the blank experiment

where the bed of char is held at the temperature without volatiles passing through the char bed. The results in Figure 9-4 clearly show that no  $PM_{10}$  is produced in that case, ruling out the possibility of self-volatilisation of inorganic species in the char during char holding at both 800 and 1000 °C. The other is the combustion of volatiles only without the presence of the bed of char. The combustion of cellulose and polyethylene volatiles produces very little fine PM (except a traceable amount of  $PM_{0.01}$ ) which is expected because the cellulose and polyethylene used are almost inorganic-free. The combustion of AW biosolid volatiles produces some  $PM_{10}$  which has a unimodal size distribution with a fine mode of 0.043  $\mu m$ . The combustion of volatiles alone is known to produce  $PM_1$ <sup>19</sup> of a fine mode which is apparently due to the presence of remaining volatile inorganic species (e.g. Na and K) in the AW biosolid (see Table 9-1 and Figure 9-2) even after acid-washing of the biosolid.

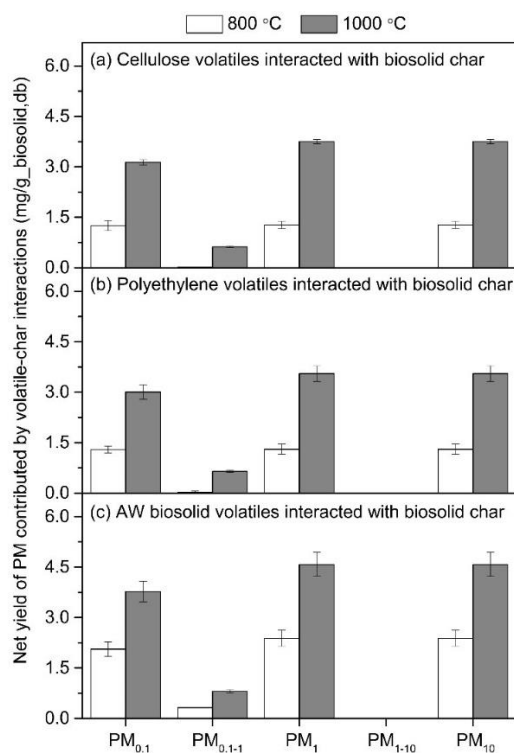


Figure 9-5 Net yield of PM during volatiles combustion, contributed by the interactions between volatiles generated from (a) cellulose, (b) polyethylene, (c) AW biosolid and chars at 800 °C and 1000 °C, respectively

The most interesting results are presented in Figure 9-4 for the experiments under the conditions in presence of volatile–char interactions. After experiencing reactions with the preloaded chars, combustion of the resulting volatiles leads to substantial increases in  $PM_{10}$  emission. The results clearly demonstrate that volatile–char interactions indeed exerted significant influence on  $PM_{10}$  emission during volatiles combustion. Figure 9-5 further presents the net yield of the  $PM_1$  as a direct result of volatile–char interactions, calculated via the subtraction of the yield of  $PM_1$  from the combustion of fresh volatiles from the yield of  $PM_1$  from the combustion of volatiles after interactions with the slow heating biosolid char. Four important observations can be made in Figure 9-5. First, volatile–char interactions result in only  $PM_1$  (dominantly  $PM_{0.1}$ ) emission. Second, although more inorganic elements are retained in the BSH800 Char than the BSH1000 Char (see Figure 9-3), the interactions between fresh volatiles generated *in situ* at 1000 °C and BSH1000 Char lead to more PM than those at 800 °C and the BSH800 Char. Clearly, the effect of volatile–char interactions on PM emission is dependent on temperature. Overall, the data in Figure 9-4 and Figure 9-5 indicate that increasing temperature leads to the intensified volatile–char interactions. Third, the net yields of PM contributed by the interactions between cellulose volatiles and slow heating biosolid chars are similar to those from the interactions between polyethylene volatiles and slow heating biosolid chars, although the pyrolysis of cellulose produces oxygen-containing species in the volatiles while that of polyethylene does not. Fourth, the net yields of PM contributed by the interactions between char and the AW biosolid volatiles are considerably higher than those between the same char and the cellulose volatiles or polyethylene volatiles. In addition, the interactions of chars with the volatiles produced from cellulose, polyethylene or AW biosolid leads to the emission of unimodal PM with considerably different mode diameters. As shown in Figure 9-4, the PM emitted from the interactions between chars and cellulose or polyethylene volatiles has a fine mode diameter of 0.01  $\mu\text{m}$  in comparison to 0.043  $\mu\text{m}$  for the PM



emitted from the interactions between chars and AW biosolid volatiles. However, such model sizes are similar to those for the PM emitted from volatiles combustion alone in absence of volatile–char interactions. Such differences are apparently due to the dissimilarity in the volatiles produced from either cellulose, polyethylene, or AW biosolid. For instance, volatiles produced from cellulose or polyethylene are essentially free from inorganic species but part of the inorganic species remained in AW biosolid are released in the volatiles (see Figure 9-2). It appears that subsequent combustion of AW biosolid volatiles result in considerably higher concentrations of inorganic species in the gaseous phase, leading to intensified homogeneous and heterogeneous condensation, hence producing PM<sub>1</sub> with a larger mode diameter.

### 9.4 Changes in major and trace elements distributions in PM due to volatile–char interactions

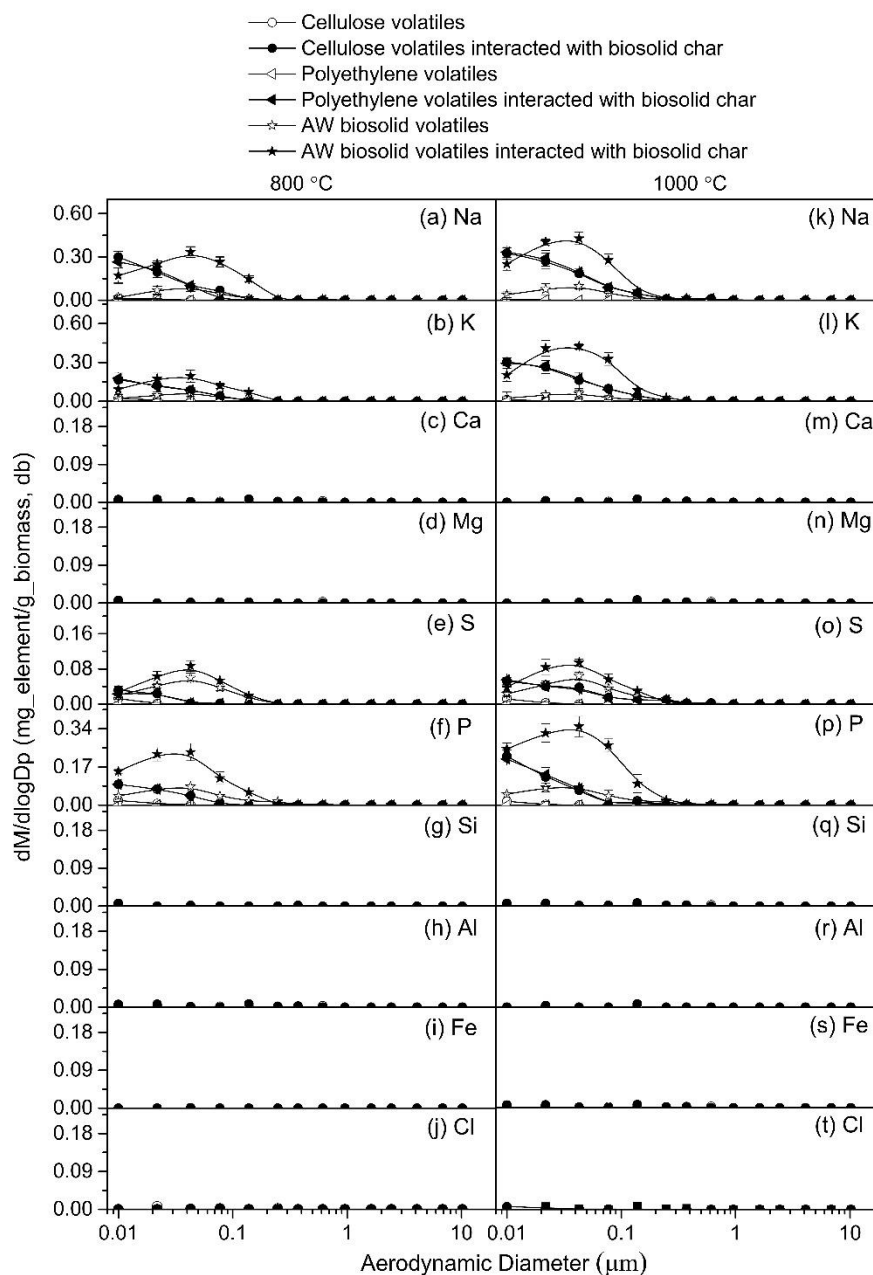


Figure 9-6 PSDs of major elements in PM collected from the combustion of fresh volatiles generated from cellulose, polyethylene, AW biosolid and the respective volatiles after interactions with slow heating biosolid char at (a-j) 800 °C and (k-t) 1000 °C, respectively

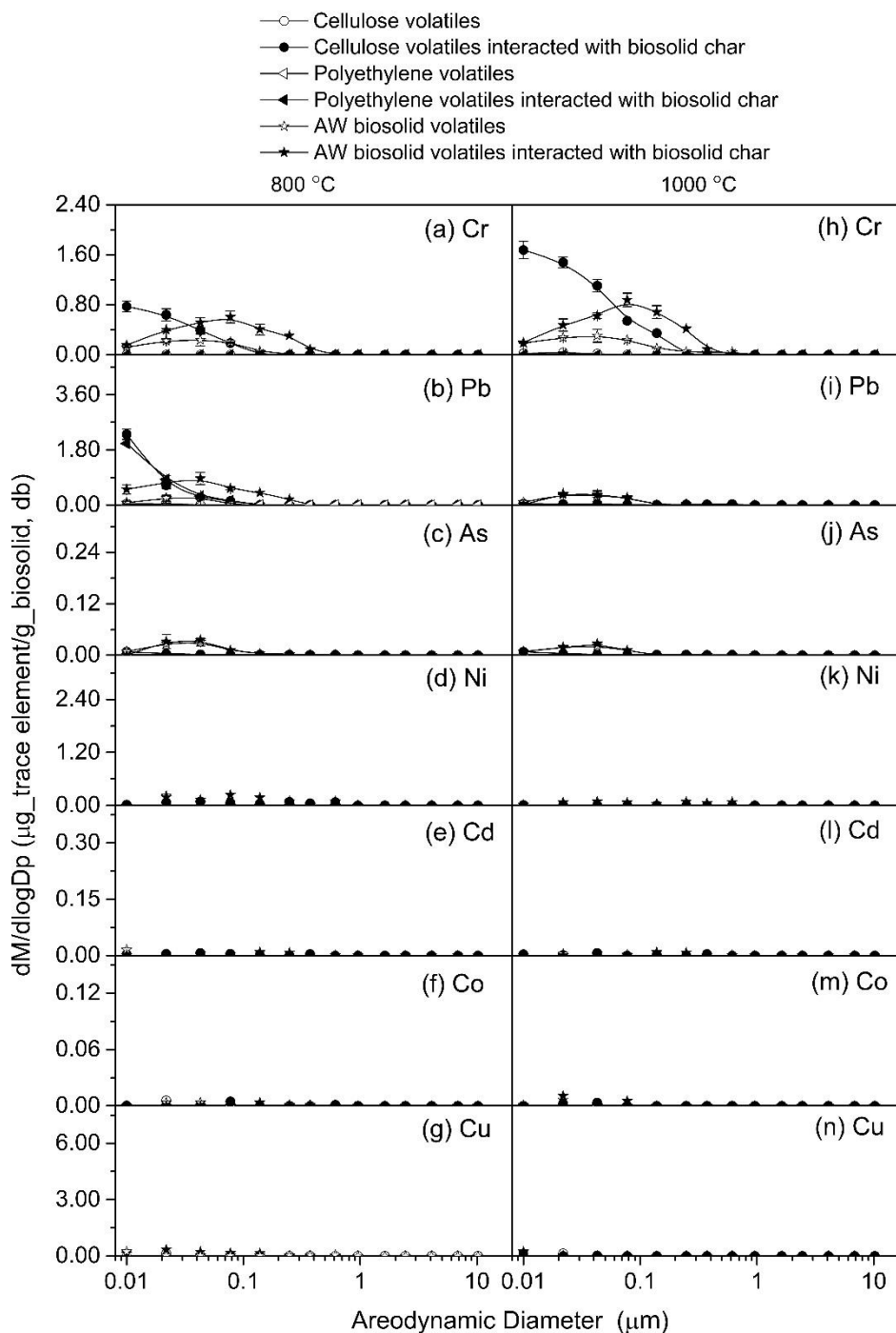


Figure 9-7 PSDs of trace elements in PM collected from the combustion of fresh volatiles generated from cellulose, polyethylene and AW biosolid and the respective volatiles after interactions with slow heating biosolid char at (a-g) 800 °C and (h-n) 1000 °C, respectively

Efforts were further taken to examine the effect of volatile–char interactions on the elemental PSDs of the major and trace elements in the PM, with the results presented in Figure 9-6 and Figure 9-7, respectively. As only PM<sub>1</sub> is produced, the net yields of major and trace elements in PM<sub>0.1</sub>, PM<sub>0.1-1</sub> and PM<sub>1</sub> are then presented in Figure 9-8. The release of the monovalent alkali metallic species (i.e. Na and K) are enhanced by volatile–char interactions to form PM<sub>1</sub> during combustion. There are little divalent alkaline earth metallic species (i.e. Ca and Mg) presented in the PM and volatile–char interactions have little effect on the release of those species. The PM<sub>1</sub> also contains little other refractory elements such as Fe, Al and Si. In addition, Cl is also absent from the PM<sub>1</sub>, owing to the removal of Cl in the AW biosolid via acid-washing and little Cl retained in biosolid slow heating chars (see Table 9-1). Furthermore, S and P in PM<sub>1</sub> are also enhanced by volatile–char interactions, following similar trends of Na and K in PM<sub>1</sub>. Such enhancements are intensified at 1000 °C in comparison to 800 °C. It is also noteworthy that Na, K, S and P as the key elements in PM<sub>1</sub> formed from volatile–char interactions are dominantly presented in PM<sub>0.1</sub>, as shown in Figure 9-8. Such observations suggest that the presence of Na, K, S and P in PM<sub>1</sub> are interrelated as a result of volatile–char interactions (further discussion on this aspect is given in the next section).

Although trace elements only contribute to less than 0.5% (by mass) of the total PM emission during the biosolid combustion,<sup>23</sup> the release of trace elements cannot be ignored due to the toxicity of these elements. It is interesting to see in Figure 9-7 that the presence of Cr and Pb in PM is also enhanced by volatile–char interactions. It is noted that Pb emission in the PM was only enhanced by volatile–char interactions at 800 °C but not at 1000 °C. Interestingly, although the interactions between cellulose volatiles or AW biosolid volatiles and char resulted in Cr emission, such behaviour is not observed for interactions between polyethylene volatiles and char. As polyethylene volatiles are free of oxygenated species as opposed to cellulose volatiles or AW biosolid volatiles, such an observation suggests that the property of volatiles can have

an important role in the release of inorganic species resulted from volatile–char interactions. In addition, there is also an appreciable amount of As present in  $PM_{10}$  (dominantly  $PM_{0.1}$ ) from the combustion of AW biosolid but the presence of As in the PM is not influenced by volatile–char interactions. Furthermore, there is little Ni and Co in the PM emitted from the combustion of volatiles, with or without volatile–char interactions. As shown in Figure 9-8, the net yields of these elements (except Pb) in  $PM_{0.1}$ ,  $PM_{0.1-1}$  and  $PM_{10}$  contributed by volatile–char interactions increase with the temperature of volatile–char interactions, in consistence with the observation on the total net PM yields (see Figure 9-5).

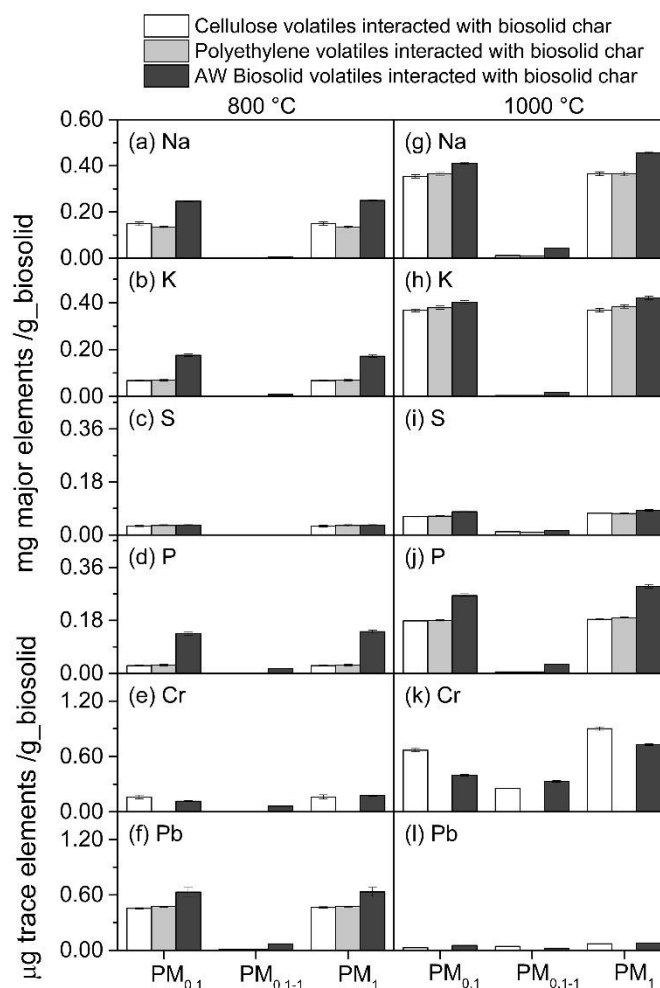


Figure 9-8 Net yields of (a-d and g-j) major and (e-f and k-l) trace elements in PM from the combustion of volatiles from cellulose, polyethylene and AW biosolid,

contributed by the volatile-char interactions at (a-f) 800 °C and (g-l) 1000 °C, respectively

### 9.5 Further discussion

It is clearly shown in Figure 9-6 and Figure 9-7 that Na, K, S and P are the key elements in the net PM<sub>1</sub> emission as a result of volatile-char interactions. To better understand the occurrence of the inorganic species in the net PM<sub>1</sub> yielded from volatile-char interactions, the PM samples were washed with ultrapure water and further analysed. It is found that all the Na, K, P, and S in the PM were water-soluble. Because there is little Cl in the net PM yielded from volatile-char interactions (see Figure 9-6) and the net PM<sub>1</sub> released is dominantly PM<sub>0.1</sub> (see Figure 9-5), the molar ratios of (Na+K) to the (P+2S) bounded to major elements in the net PM collected in DLPI backup filter and stage 1-3 are then calculated and presented in Figure 9-9. Since Na, K, S and P contributed to >99.5% of the total net PM<sub>0.1</sub> released from volatile-char interactions, the molar ratio (*MR*) can be approximated by the molar ratio of (Na+K) to total (P+2S) as shown in Eq. (1):

$$MR = \frac{(Na+K)}{(P+2S)_{ME}} \approx \frac{(Na+K)}{(P+2S)_{ME}+(P+2S)_{TE}} = \frac{(Na+K)}{(P+2S)_{Total}} \quad (1)$$

where *ME*, *TE*,  $(P+2S)_{ME}$ ,  $(P+2S)_{TE}$ ,  $(P+2S)_{Total}$  denote major elements, trace elements, P and S bound with major elements, P and S bound with trace elements, total P and S in the PM, respectively.  $(P+2S)_{Total}$  is determined directly by experiments and  $(P+2S)_{Total} = (P+2S)_{ME} + (P+2S)_{TE}$ . The amount of P and S associated with trace elements i.e.  $(P+2S)_{TE}$  is very small and can be ignored in the calculation so that we have  $(P+2S)_{Total} \approx (P+2S)_{ME}$ . Therefore, it is possible to estimate the molar ratio of (Na + K)/(P+2S) in the PM based on Eq. (1) based on experimental data. As shown in Figure 9-9, the molar ratio of (Na+K)/(P+2S) in the net PM<sub>0.1</sub> formed by volatile-char interactions is around 1.0, suggesting that the Na, K, S, and P released during volatile-char interactions are presented in PM<sub>0.1</sub> as sodium or potassium sulphate and

metaphosphate. Unfortunately, such approximation cannot be extended to trace elements to provide an indication for the occurrence of Pb and Cr in the net  $PM_{0.1}$  released from volatile–char interactions.

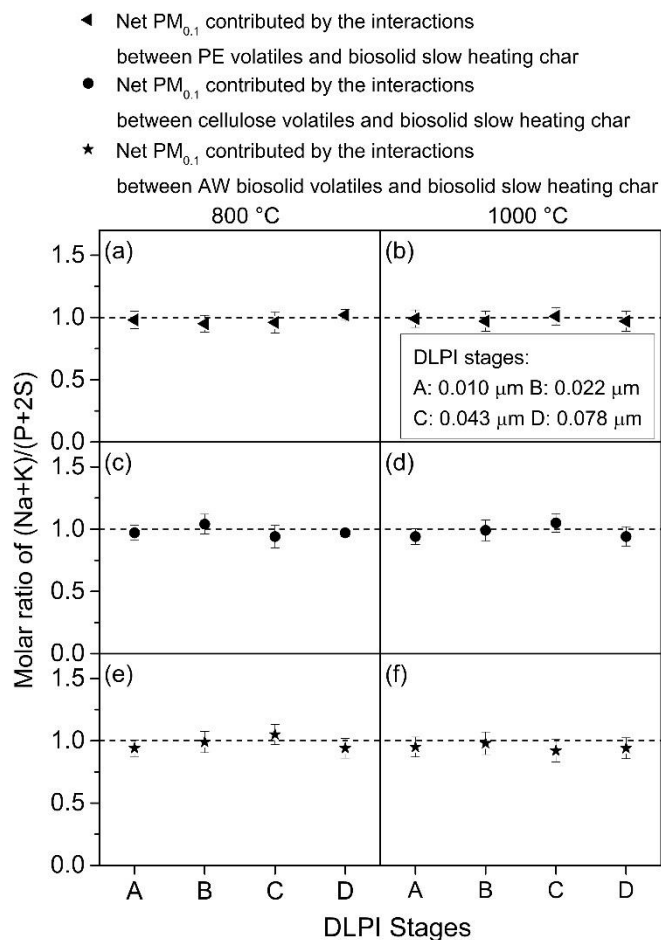


Figure 9-9 Molar ratios of  $(\text{Na}+\text{K})/(\text{P}+2\text{S})$  in the net  $PM_{0.1}$  released due to volatile–char interactions. Stages A–D represent  $PM_{0.1}$  collected from the backup filter and stage 1–3 of the DLPI, respectively

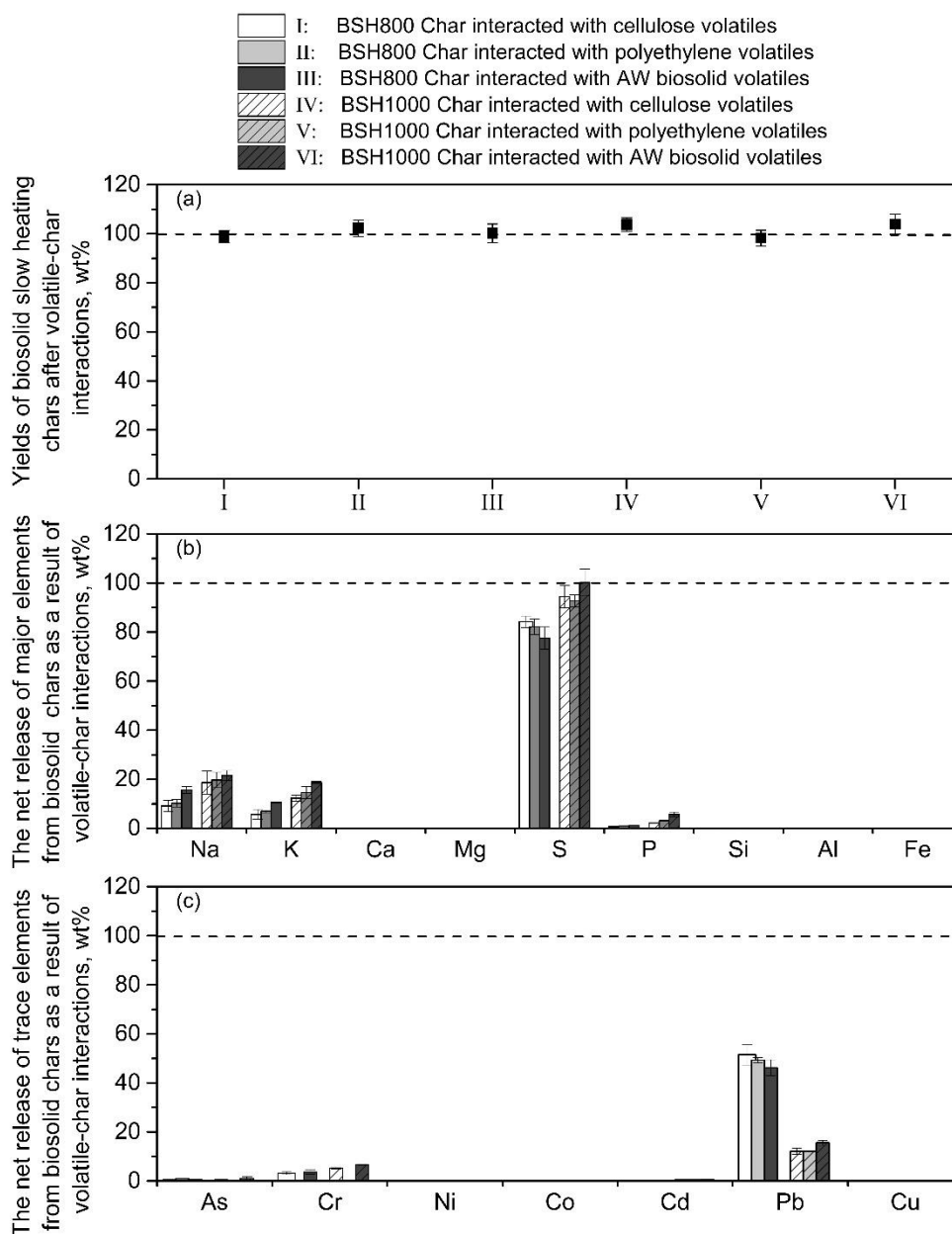


Figure 9-10 (a) Yields of biosolid slow heating chars after volatile–char interactions; and the net release of (b) major and (c) trace elements from the biosolid slow heating chars as a result of volatile–char interactions



Further analyses of the BSH800 and BSH1000 chars before and after volatile–char interactions were also conducted to examine the changes in char mass and the release of key major and trace elements during volatile–char interactions. As shown in Figure 9-10a, volatile–char interactions lead to little change in the char yields. Figure 9-10b and 10c show that Na, K, S, P, Cr and Pb in the char were released during volatile–char interactions and contributed to the formation of PM<sub>1</sub> during the combustion of the resulting volatiles. In addition, the molar ratios of (Na+K)/(P+2S) released from biosolid slow heating chars during volatiles-char interactions and the collection efficiencies of these released elements in DLPI were then calculated and presented in Figure 9-11. Clearly, the molar ratios are ~1.0 and the collection efficiencies of all key elements are over 90%. Therefore, the inorganic species released from the chars during volatile–char interactions are indeed responsible for these inorganic species in the net PM emitted from the combustion of volatiles that have experienced the volatile–char interactions. The results also demonstrate the high collection efficiencies of PM<sub>1</sub> in the reactor system.

The reactive species in volatiles may include steam, CO<sub>2</sub> and/or other reactive species such as free radical species (that are known to be produced abundantly during solid fuels pyrolysis<sup>213,214</sup>). These reactive species may react with the char, results in the release of these inorganic species during volatile–char interactions. Figure 9-10a shows little change in char mass is observed during volatile–char interactions. Calculations also show that the inorganic species released during volatile–char interactions contributed to less than 0.5 wt% (on dry basis) of the biosolid slow heating chars so that the release of these inorganic species has little effect on the weight loss of chars (if any). Therefore, the little weight loss of chars during volatile–char interactions suggests that gasification reactions (char-steam and/or char-CO<sub>2</sub>, if any) in the fresh volatiles generated *in situ* is insignificant. Considering that polyethylene contains only C and H, pyrolysis of polyethylene produces volatiles that are free of oxygen-containing reactive species (e.g. CO<sub>2</sub>, steam or other oxygen-containing free

radicals). The similar release of key inorganic species during the interactions between cellulose or polyethylene volatiles with char further suggests that oxygen-containing reactive species such as CO<sub>2</sub>, steam and oxygen-containing free radicals are unlikely to be the reactive species responsible for the release of inorganic species during volatile-char interactions. Therefore, the release of inorganic species which lead to enhanced PM<sub>1</sub> emission as a result of volatile-char interactions is caused by other non-oxygen-containing reactive species that are most likely free radicals that can be formed from volatiles thermal cracking. Such reactive species appears to react with char particles to enhance the release of monovalent inorganic species (e.g. Na) but not divalent inorganic species (e.g. Mg and Ca) because the release of divalent species requires multiple bonds to be broken simultaneously.<sup>15</sup> The results reported in this study are consistent with those observations because the net yields of multi-valent species (including Mg, Ca, Fe, Al, Si, As, Cd, Ni, Cu and Co) in the PM formed by volatile-char interactions are little. In addition, the reactions between these non-oxygen-containing reactive species and char during volatile-char interactions lead to little weight (and carbon) losses of the chars during volatile-char interactions (see Figure 9-10a). Therefore, such non-oxygen-containing reactive species must be small, most likely H radicals that are highly mobile and reactive.

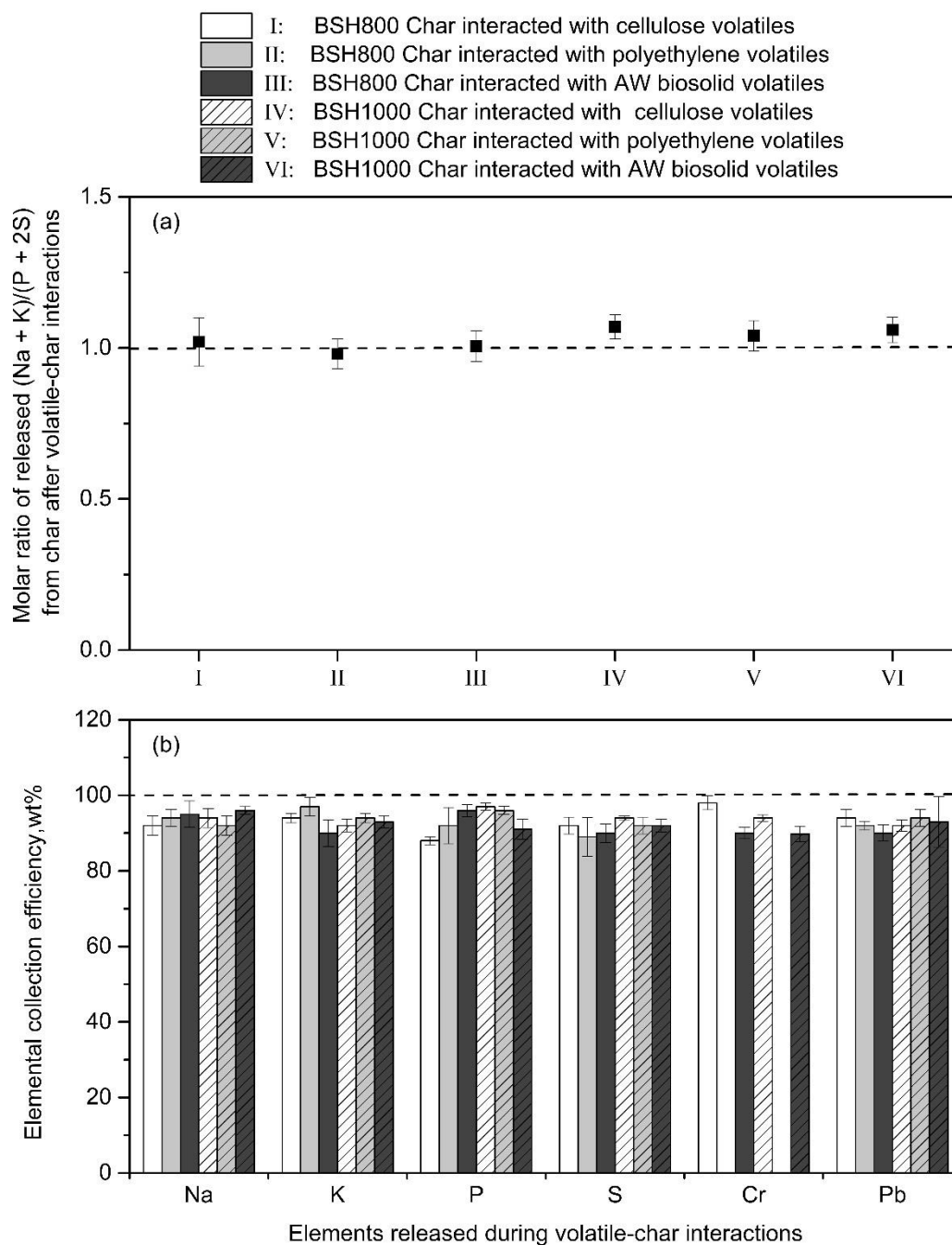


Figure 9-11 (a) Molar ratios of (Na+K)/(P+2S) for the net elements released from the chars as a result of volatile-char interactions; (b) collection efficiency for the net elements released from chars as a result of volatile-char interactions as  $PM_{0.1}$

Furthermore, during slow pyrolysis of biosolid, the organic phosphorous species are volatilised while the mineral species that are less volatile are retained in the char.<sup>4</sup> The results of this study clearly show that the interactions between these chars and the volatiles generated from pyrolysis of cellulose, polyethylene or AW biosolid can also facilitate the release of P and S into the gaseous phase. It was reported that under reducing conditions induced by volatiles, phosphorus compounds can be reduced to volatile phosphorus compounds (e.g.  $P_2O_3$ ).<sup>129,215</sup> Likewise, the S retained in char might be transformed into gaseous sulphur products (e.g.  $SO_2$ )<sup>167,216</sup> under reducing conditions. For instance,  $CaSO_4$  in the char may form CaO thus lead to the liberation of  $SO_2$ . These volatile phosphorus and sulphur compounds would then undergo oxidation and reactions with metallic vapours (e.g. Na and K) in the gaseous phase during volatiles combustion, followed by homogeneous and heterogeneous condensations to produce  $PM_{10}$ .<sup>21</sup> The molar ratio of the net  $(Na+K)/(P+2S)$  released from volatile-char interactions are  $\sim 1.0$  (see Figure 9-11). However, the majority of Na and K are associated with P ( $> 77\%$ ) on molar basis while  $< 23\%$  of them are associated with S. The results suggest that the free radicals present in the volatiles may facilitate the release of these species which are otherwise stable in the char.

It is also important to note that trace elements such as Pb and Cr were also released during volatile-char interactions. As these trace elements are multi-valance species, their release is unlikely to result from the reaction between free radicals and char. The Pb emission is only enhanced by the volatile-char interactions at 800 °C but not 1000 °C. This is apparently due to the fact that  $\sim 35\%$  of Pb was retained in the biosolid char produced at 800 °C (i.e. BSH800 Char), while there is only  $< 4\%$  of Pb retained at 1000 °C (i.e. BSH1000 Char), as shown in Figure 9-3. Under slow heating conditions, pyrolysis of the raw biosolid at 1000°C leads to the little Pb retained in the char.<sup>217</sup> The release of Pb from volatile-char interactions at 800 °C was probably due to the reducing atmosphere created by fresh volatiles. Under such conditions, the Pb compounds such as PbO which is stable at 800 °C can be reduced to  $Pb(g)$ <sup>208</sup> which is

released during volatile–char interactions. Interestingly, although Cr is released as  $PM_{10}$  resulted from the interactions of cellulose or AW biosolid volatiles with char, the interactions between polyethylene volatiles and char do not. The release of Cr from volatile–char interactions may be attributed to the formation of volatile chromium oxyhydroxides<sup>218</sup> under reducing conditions. The lack of oxygen-containing species in polyethylene volatiles leads to no formation of chromium oxyhydroxides and Cr is not released from the interactions between polyethylene volatiles and char. This in turn supports that Cr is released in the form of chromium oxyhydroxides during volatile–char interactions. Furthermore, while Pb and Cr are likely to be released in the forms of elemental lead and chromium oxyhydroxides, respectively, this does not mean that Pb and Cr collected in  $PM_{10}$  are present in these forms because at least part of the elemental Pb for example, may undergo gas phase reaction to form PbO during combustion.

## 9.6 Conclusions

This chapter demonstrates the importance of volatile–char interactions in the  $PM_{10}$  emission during the combustion of biosolid volatiles using a unique three-stage reactor system. Volatile–char interactions significantly change the PSDs of PM during the combustion of volatiles both produced from ash-free cellulose or polyethylene and acid-washed biosolid. The volatile–char interactions only enhance the emission of  $PM_{10}$  (mainly  $PM_{0.1}$ ) and are intensified at a higher temperature. The reactive volatiles can react with biosolid char and enhance the release of Na, K, P and S during volatile–char interactions but lead to little change in the yields of biosolid chars. As far as  $PM_{10}$  emission is concerned during volatiles combustion, oxygen-containing reactive species in volatiles play an unimportant role in volatile–char interactions. The molar ratios of  $(Na+K)/(P+2S)$  for both  $PM_{10}$  and the net release of these key elements from the chars are also found to be  $\sim 1.0$ , suggesting these key elements are released from the chars then react to form alkali metaphosphate and sulphate in  $PM_{10}$

during volatiles combustion. The experimental results also show that volatile–char interactions can transform part of the Pb and Cr in the chars into more volatile forms, which are subsequently released and contributed to PM<sub>1</sub> emission. The absence of Cr release during interactions between polyethylene volatiles and char further suggests that Cr is released in the form of chromium oxyhydroxides during volatile–char interactions.

*Reprinted with permission from (Xujun Chen, Sui Boon Liaw and Hongwei Wu. Important role of volatile–char interactions in enhancing PM<sub>1</sub> emission during the combustion of volatiles from biosolid, Combustion and Flame 2017, 182, 90-101). Copyright (2017) The Combustion Institute. Published by Elsevier Inc*

## CHAPTER 10 EFFECT OF VOLATILE–CHAR INTERACTIONS ON PM<sub>10</sub> EMISSION DURING THE COMBUSTION OF P-CONTAINING BIOSOLID CHARS UNDER AIR AND OXYFUEL CONDITIONS

### 10.1 Introduction

Chapter 9 provided direct experimental evidence for demonstrating the significant role of volatile–char interactions in enhancing PM<sub>0.1</sub> emission from the combustion of biosolid volatiles. While the potential volatile–char interactions may also influence the transformation of inorganic species in char and the structure of char hence PM<sub>10</sub> emission during char combustion. The fundamental research question is “Does the exposure of char to reactive volatiles potentially influence the transformation of inorganic species in and the structure of char hence PM<sub>10</sub> emission during the subsequent combustion of the char?”, of which the answer is largely unknown.

This chapter is a fundamental investigation to answer the aforementioned key research question, i.e. providing experimental evidence to demonstrate that exposure of chars to reactive volatiles produced *in situ* from rapid pyrolysis can influence char properties hence PM<sub>10</sub> emission during subsequent char combustion. Despite the constraints of the quartz reactor, nevertheless, the experimental results in this study show that volatile–char interactions not only enhance the release of the inorganic species from char particles, but also alter the pore structures of the chars, both of which affect PM<sub>10</sub> emission during char combustion.

### 10.2 The properties of char samples used for volatile–char interactions

Table 10-1 Properties of biosolid, polyethylene (PE), double acid-washed biosolid (DAWB) and char samples

	Biosolid	DAWB	PE	SHC	SHC-holding	SHC-PE	SHC-DAWB	FHC	FHC-holding	FHC-PE	FHC-DAWB
	Moisture (wt% ad <sup>a</sup> )										
	5.1	3.6	0.1	3.8	3.4	3.2	2.7	4.1	3.9	3.8	3.5
	Proximate Analysis (wt% db <sup>b</sup> )										
VM <sup>c</sup>	65.4	80.2	100.0	3.0	2.9	2.8	2.6	3.9	3.7	3.6	3.4
FC <sup>d</sup>	14.9	19.5	0.0	38.3	38.5	40.0	39.5	31.2	31.1	32.1	32.6
A <sup>e</sup>	19.7	0.3	0.0	58.7	58.6	57.2	57.9	64.9	65.2	64.3	64.0
	Ultimate Analysis (wt% daf <sup>f</sup> )										
C	54.33	73.58	85.71 <sup>g</sup>	95.78	95.82	96.54	96.25	93.13	93.26	95.04	93.60
H	7.02	9.14	14.29 <sup>g</sup>	0.13	0.12	0.02	0.09	1.45	1.41	0.51	1.35
N	9.41	2.77	0.00	3.06	3.06	2.77	2.61	3.49	3.44	3.21	3.13
O <sup>h</sup>	29.24	14.51	0.00	1.03	1.00	0.67	1.05	1.93	1.89	1.24	1.92
	Major Elements (mg/kg, db <sup>b</sup> )										
Si	18476.1 ± 471.2	882.3 ± 32.1	n.d. <sup>i</sup>	66482.1 ± 252.2	66478.2 ± 521.9	66474.2 ± 247.4	66492.2 ± 279.8	69412.0 ± 423.8	69436.4 ± 337.2	69431.4 ± 580.8	69443.0 ± 271.7
Al	6287.2 ± 44.1	497.3 ± 15.1	n.d. <sup>i</sup>	28334.1 ± 354.2	28365.4 ± 521.5	28344.4 ± 652.8	28362.0 ± 244.6	29763.0 ± 625.4	29778.4 ± 544.9	29799.9 ± 330.1	29787.0 ± 325.2
Fe	3007.6 ± 45.4	0.7 ± 0.2	7.2 ± 3.1	19357.1 ± 256.4	19352.7 ± 325.2	19359.1 ± 364.1	19363.8 ± 289.9	20385.0 ± 554.2	20401.0 ± 485.3	20389.8 ± 369.4	20395.4 ± 441.7
K	2017.6 ± 18.7	1.4 ± 0.4	n.d. <sup>i</sup>	5687.6 ± 44.6	5695.6 ± 82.1	4660.9 ± 47.8	4435.8 ± 110.2	4619.8 ± 21.2	4632.7 ± 36.9	4157.1 ± 89.2	3972.4 ± 33.9
Na	1481.7 ± 16.2	1.6 ± 0.2	9.8 ± 1.1	4287.2 ± 26.8	4278.8 ± 66.3	3715.6 ± 14.9	3486.1 ± 48.5	3717.8 ± 23.5	3721.9 ± 46.3	3382.4 ± 22.9	3122.9 ± 32.7
Ca	20048.2 ± 389.1	3.8 ± 0.6	n.d. <sup>i</sup>	81145.4 ± 159.7	81215.4 ± 327.9	81158.0 ± 289.9	81167.8 ± 327.0	83354.2 ± 446.5	83285.0 ± 501.1	83368.4 ± 428.2	83378.1 ± 603.0

Table continued in next page



Mg	4814.4 ± 44.3	2.0 ± 0.4	n.d. <sup>i</sup>	18236.8 ± 110.0	18262.0 ± 163.1	18263.0 ± 189.4	18288.2 ± 145.8	18942.4 ± 136.0	18904.7 ± 188.8	18972.2 ± 203.0	18998.8 ± 217.4
P	18725.1 ± 188.2	6.6 ± 1.9	n.d. <sup>i</sup>	63971.0 ± 331.2	63985.4 ± 298.7	59493.0 ± 274.2	57573.0 ± 306.6	77478.9 ± 398.9	77484.1 ± 442.4	70912.4 ± 403.7	64930.0 ± 601.3
Cl	804.6 ± 15.5	n.d. <sup>i</sup>	n.d. <sup>i</sup>	n.d. <sup>i</sup>	n.d. <sup>i</sup>	n.d. <sup>i</sup>	n.d. <sup>i</sup>	n.d. <sup>i</sup>	n.d. <sup>i</sup>	n.d. <sup>i</sup>	n.d. <sup>i</sup>
S	8023.1 ± 74.2	n.d. <sup>i</sup>	n.d. <sup>i</sup>	4106.8 ± 33.6	4038.0 ± 47.6	87.6 ± 18.1	64.8 ± 12.3	525.6 ± 26.9	519.8 ± 36.5	32.9 ± 12.2	27.8 ± 11.9
Trace Elements (mg/kg, db <sup>b</sup> )											
As	2.930 ± 0.101	0.180 ± 0.021	n.d. <sup>i</sup>	2.870 ± 0.190	2.850 ± 0.131	2.672 ± 0.220	2.820 ± 0.194	1.770 ± 0.210	1.781 ± 0.230	1.651 ± 0.190	1.705 ± 0.150
Cr	43.820 ± 0.991	0.331 ± 0.190	n.d. <sup>i</sup>	128.001 ± 0.922	127.362 ± 1.690	130.981 ± 6.980	92.450 ± 3.215	147.871 ± 4.770	142.114 ± 5.908	149.425 ± 8.205	104.594 ± 9.210
Co	4.000 ± 0.072	0.211 ± 0.032	n.d. <sup>i</sup>	13.000 ± 0.081	12.884 ± 0.090	12.879 ± 0.215	13.115 ± 0.100	15.451 ± 0.980	14.089 ± 0.081	15.679 ± 0.091	15.328 ± 0.160
Ni	16.922 ± 0.142	0.300 ± 0.041	n.d. <sup>i</sup>	57.325 ± 1.285	58.001 ± 1.320	55.235 ± 2.010	69.450 ± 2.151	70.391 ± 1.581	69.211 ± 1.605	70.481 ± 0.982	71.002 ± 1.021
Cu	492.4 ± 7.8	10.8 ± 2.4	n.d. <sup>i</sup>	1672.2 ± 42.1	1682.4 ± 41.2	1682.5 ± 36.6	1681.7 ± 26.5	2042.5 ± 3.6	2029.3 ± 11.6	2049.6 ± 0.2	2038.9 ± 13.2
Cd	2.381 ± 0.091	0.231 ± 0.010	n.d. <sup>i</sup>	1.224 ± 0.185	1.181 ± 0.110	1.281 ± 0.210	1.201 ± 0.220	1.244 ± 0.190	1.104 ± 0.140	1.250 ± 0.061	1.231 ± 0.050
Pb	14.002 ± 1.284	0.511 ± 0.082	n.d. <sup>i</sup>	3.181 ± 0.300	3.254 ± 0.320	n.d. <sup>i</sup>	n.d. <sup>i</sup>	n.d. <sup>i</sup>	n.d. <sup>i</sup>	n.d. <sup>i</sup>	n.d. <sup>i</sup>
Zn	958.0 ± 9.8	7.7 ± 1.7	n.d. <sup>i</sup>	8.4 ± 0.8	8.2 ± 0.5	8.0 ± 0.7	7.9 ± 0.1	n.d. <sup>i</sup>	n.d. <sup>i</sup>	n.d. <sup>i</sup>	n.d. <sup>i</sup>
V	1.641 ± 0.532	0.7012 ± 0.211	n.d. <sup>i</sup>	5.411 ± 0.982	5.150 ± 1.024	5.434 ± 0.660	5.291 ± 0.980	7.000 ± 1.001	6.991 ± 0.480	6.921 ± 0.720	6.894 ± 0.840
Mn	28.721 ± 12.200	3.000 ± 0.501	n.d. <sup>i</sup>	98.441 ± 14.504	97.900 ± 11.542	95.300 ± 12.741	100.100 ± 3.411	124.700 ± 9.300	122.119 ± 2.201	119.200 ± 8.600	119.211 ± 6.601

<sup>a</sup> ad = air dried; <sup>b</sup> db = dry basis; <sup>c</sup> VM = volatile matter, <sup>d</sup>FC=fixed carbon; <sup>e</sup>A= ash; <sup>f</sup>daf=dry and ash free; g, calculated values; <sup>h</sup> by difference; <sup>i</sup> n.d. = non-detected. SHC and FHC represent the biosolid chars prepared via slow heating pyrolysis and fast heating char at 1000 °C, respectively. SHC-PE and SHC-DAWB represent the SHC interacted with PE and DAWB volatiles at 1000 °C, respectively. FHC-PE and FHC-DAWB represent the FHC interacted with PE and DAWB volatiles at 1000 °C, respectively. SHC-holding and FHC-holding represent SHC and FHC being held in Stage II without volatile-char interactions

To study the effect of volatile–char interactions on PM<sub>10</sub> emission during char combustion, two chars were prepared, including a slow-heating char (SHC) and a fast-heating char (FHC). The SHC was prepared using a fixed-bed quartz reactor (Type A, Figure 3-2a) under slow pyrolysis conditions at 1000 °C and the FHC was prepared using a fixed-bed/drop-tube reactor (Type C, Figure 3-2c) under fast pyrolysis conditions at 1000 °C with minimised interactions between char and volatiles during the preparation of fast heating char. The char yields of SHC and FHC are ~28.2% and ~22.4% on a dry basis (db), respectively. On the other hand, polyethylene (PE) with a size <200 μm and demineralised biosolid were used to generate oxygen-free and oxygen-containing volatiles *in situ*, respectively, to interact with SHC and FHC chars. Double acid-washed biosolid (thereafter, termed as DAWB) was also prepared used the method detailed in Section 3.3.1. Table 10-1 lists the properties of the biosolid (different batch from the one used in Chapter 9), PE, DAWB, SHC and FHC samples used in this study. The DAWB has a low ash content of 0.3 wt % (on a dry basis) and contains little S and Cl. As shown in Table 10-1, PE only contains C and H, while DAWB also contains 14.51% of O and 2.77% N.

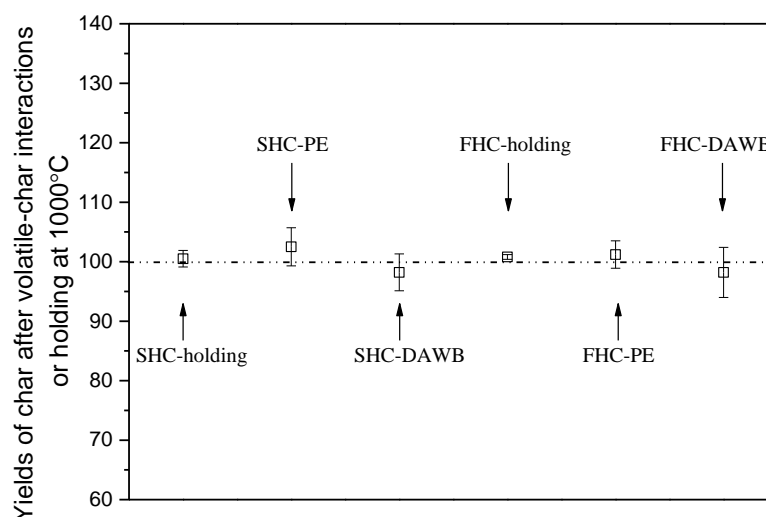


Figure 10-1 Yields of chars after volatile–char interactions or holding at 1000°C in the Stage II of the two-stage quartz reactor

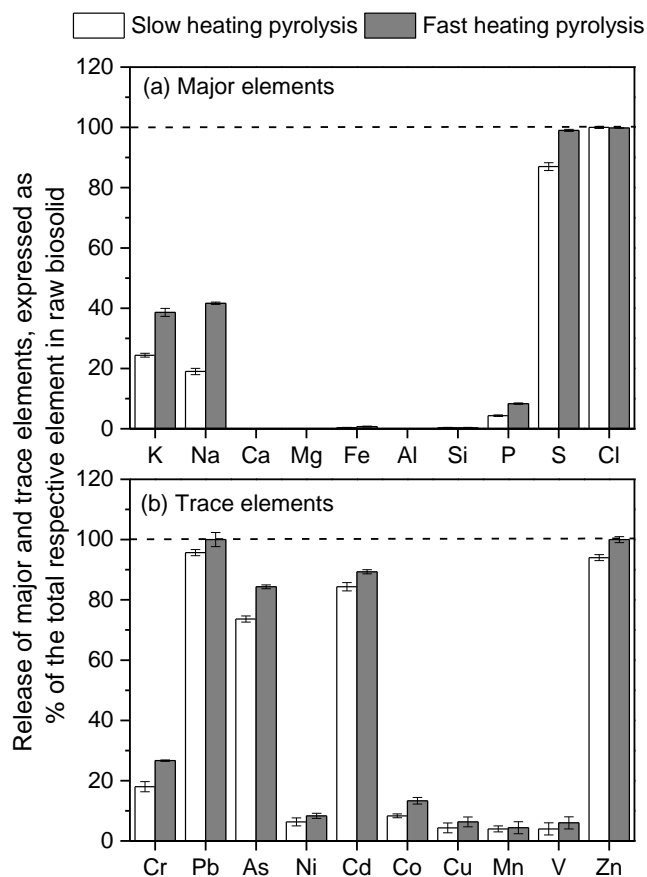


Figure 10-2 Release of (a) major and (b) trace elements during slow and fast heating pyrolysis for the preparation of chars at 1000°C

The interactions between char and *in situ* volatiles are conducted in a two-stage reactor system (see Figure 3-3) at 1000 °C with the detailed procedure given in Section 3.3.3. The chars collected after the interactions between SHC and PE (or DAWB) volatiles were termed as SHC-PE (or SHC-DAWB) while those between FHC and PE (or DAWB) volatiles were termed FHC-PE (or FHC-DAWB), respectively. SHC and FHC were also held in Stage II (see Figure 3-3) without the generation of volatiles in Stage I, thus producing chars without *in situ* volatile–char interactions (hereafter termed as SHC-holding and FHC-holding, respectively). Figure 10-1 presents the char yields after volatile–char interactions with respect to the char without being subjected to the two-stage reactor, which clearly shows that

volatile–char interactions result in little weight loss (in the order of  $\pm 2\%$ ) in chars for all experiments in this study. As shown in Table 10-1, the biosolid sample used in this study contains abundant P but a trace amount of Cl and a low content of S. Figure 10-2 further presents the release of major and trace elements during slow and fast heating pyrolysis for char preparation at 1000 °C. As shown in Figure 10-2a, all Cl and the majority of S are released to gaseous phase during slow and fast heating pyrolysis, leading to the SHC and FHC chars containing no Cl and low concentrations of S but dominantly P.

### 10.3 Effect of *in situ* volatile–char interactions on PM<sub>10</sub> emission during char combustion in air

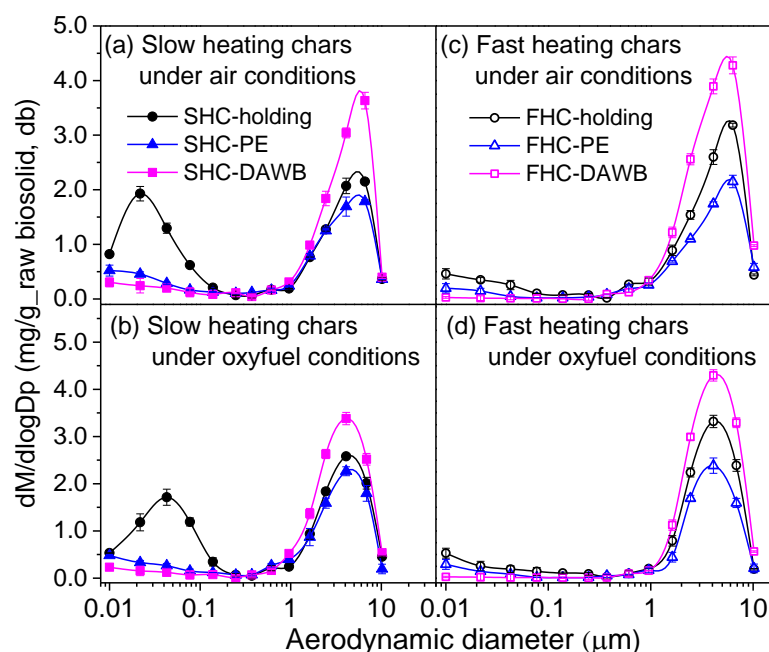


Figure 10-3 PSDs of PM<sub>10</sub> from the combustion of (a and b) slow heating char and (c and d) fast heating char and its volatile–interacted char under (a and c) air and (b and d) oxyfuel conditions

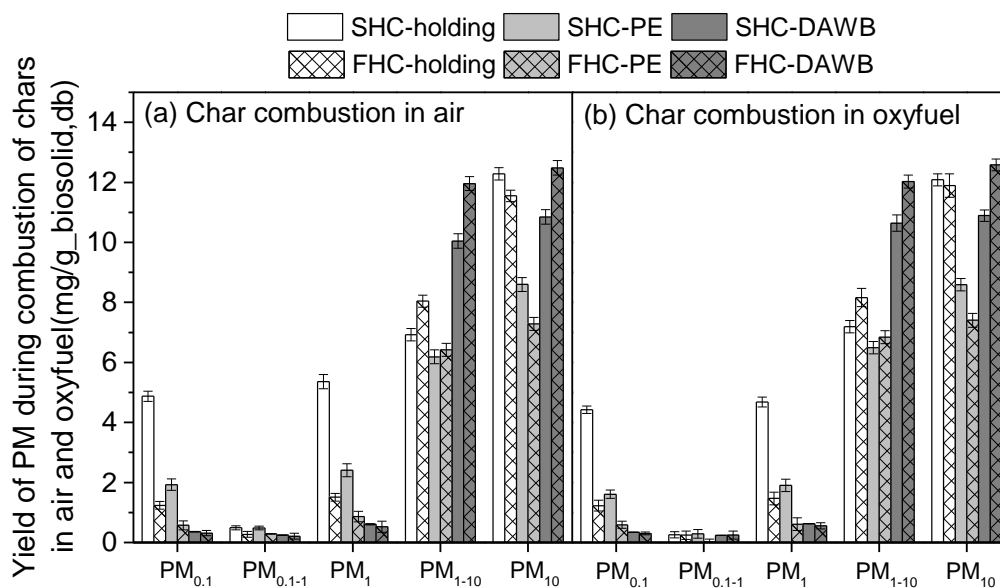


Figure 10-4 PSDs of  $PM_{10}$  from the combustion of (a and b) slow heating char and (c and d) fast heating char and its volatile–interacted char under (a and c) air and (b and d) oxyfuel conditions

Figure 10-3 and Figure 10-4 present the particle size distributions (PSDs) and the yields of the  $PM_{10}$  released during combustion of various chars (with and without experiencing volatile–char interactions) under air and oxyfuel conditions, respectively. To enable direct comparison, the yields of  $PM_{10}$  are normalised on the same basis of total biosolid fed into the reactor in this study. The results in Figure 10-3 clearly show that the volatile–char interactions significantly affect the PSDs of  $PM_{10}$  in all cases. As shown in Figure 10-3a, the PSDs of  $PM_{10}$  generated from the combustion of the SHC without experiencing *in situ* volatile–char interactions (SHC-holding) exhibit a bimodal distribution with a fine and coarse mode of  $\sim 0.022 \mu\text{m}$  and  $\sim 6.8 \mu\text{m}$ , respectively. The identical coarse mode of  $6.8 \mu\text{m}$  is also observed for the combustion of the SHC experiencing *in situ* volatile–char interactions (i.e. SHC-PE and SHC-DAWB) in air. However, the peak intensities for the fine mode of the combustion of those chars are significantly reduced. Indeed, as shown in Figure 10-4a, there is a substantial reduction in the yields of  $PM_1$  (dominantly  $PM_{0.1}$ ) from the combustion of

the SHC-PE and SHC-DAWB compared to that from the combustion of the SHC-holding. Interestingly, the combustion of the SHC-DAWB leads to an increase in  $PM_{1-10}$  formation while a reduction in the  $PM_{1-10}$  formation from the combustion of the SHC-PE is observed.

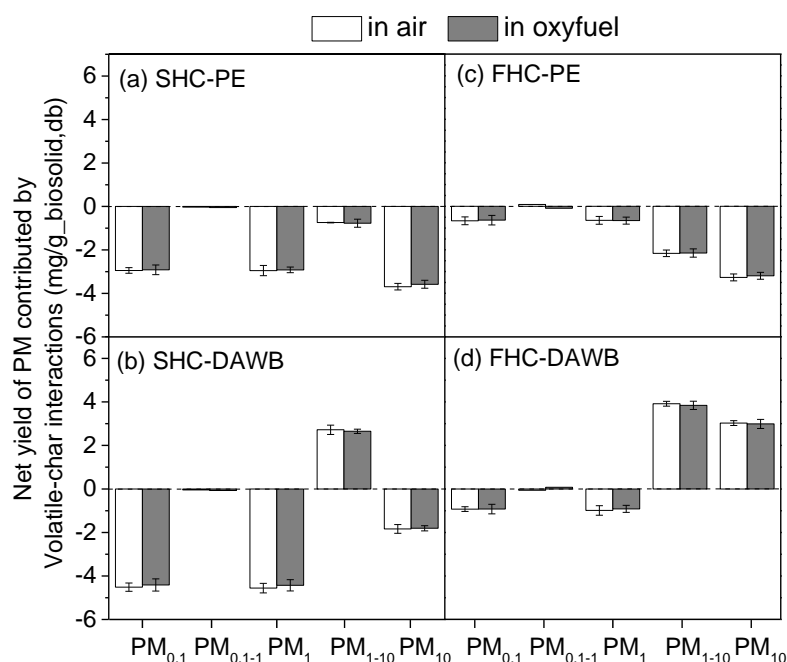


Figure 10-5 The net yields of PM contributed by the interactions (a) between slow heating char (SHC) and polyethylene volatiles; (b) between SHC and double acid-washed biosolid volatiles; (c) between fast heating char (FHC) and polyethylene volatiles; and (d) between FHC and double acid-washed biosolid volatiles

In order to quantify the effect of *in situ* volatile–char interactions on PM emission during char combustion, the net yields of PM caused by *in situ* volatile–char interactions are calculated from the PM yields of chars after interacted with the volatiles and that of SHC-holding, with the results presented in Figure 10-5. Figures 10-5a and 5b clearly demonstrate that after interactions with the PE and DAWB volatiles, the air combustion of the resultant SHCs leads to substantial reductions in the yields of  $PM_{0.1}$ . Specifically, the net reductions in  $PM_{0.1}$  are 2.8 and 4.3 mg/g

biosolid for the combustion of the SHC-PE and SHC-DAWB, respectively, indicating that the DAWB volatiles exhibiting a more significant effect on the reduction in  $PM_{10}$  emission during subsequent char combustion. In addition, interactions with the oxygen-free PE volatiles also leads to a slight decrease in the yield of  $PM_{1-10}$  during the combustion of the resultant SHC, with a net reduction of 0.8 mg/g biosolid in  $PM_{1-10}$  yield. However, interactions with the oxygen-containing DAWB volatiles result in a substantial increase in  $PM_{1-10}$  yield during the combustion of the resultant char, with a net increase in the  $PM_{1-10}$  yield of 2.9 mg/g biosolid. The results clearly indicate the different roles played by oxygen-free and oxygen-containing reactive species in the emission of  $PM_{1-10}$ .

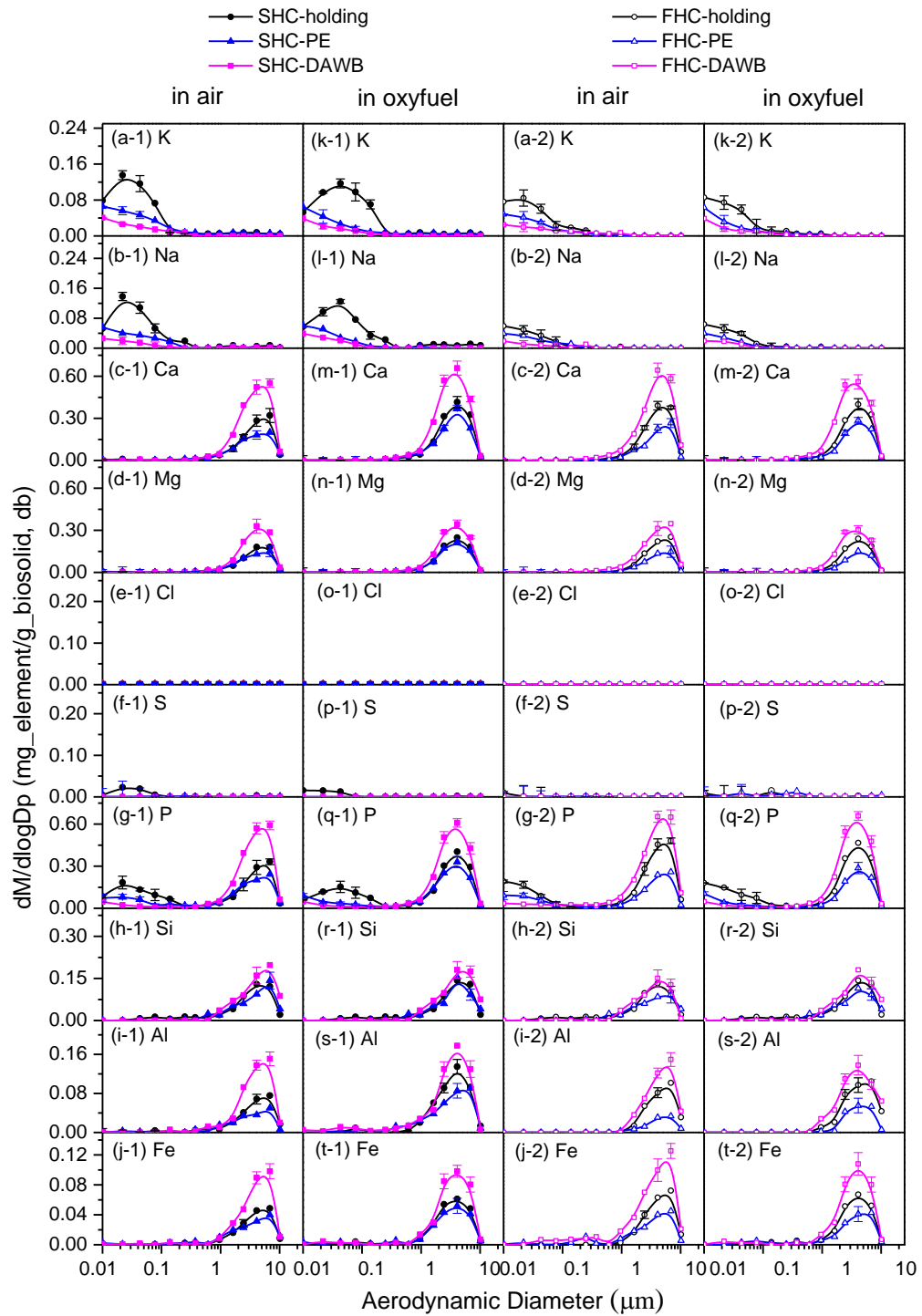


Figure 10-6 PSDs of major elements in PM<sub>10</sub> during char combustion. The left two columns represent results from the combustion of SHCs under air and oxyfuel conditions while the right two columns represent the results from the combustion of FHCs under air and oxyfuel conditions, respectively



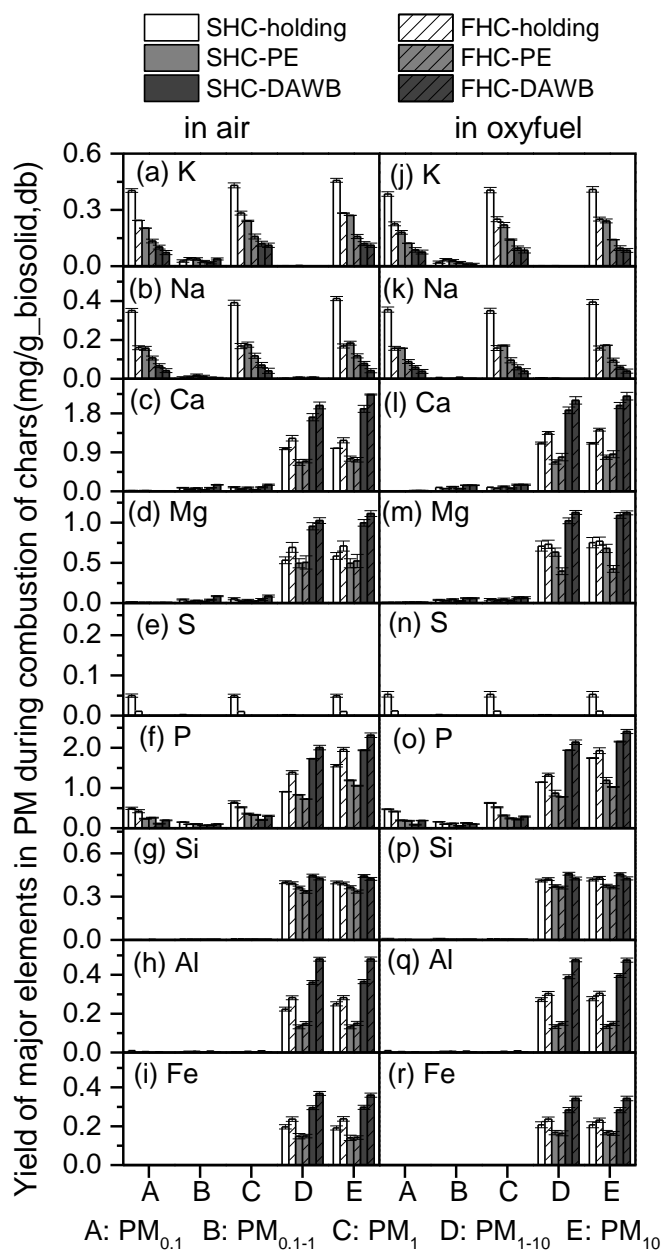


Figure 10-7 Yields of major elements during char combustion under air (left column) and oxyfuel (right column) conditions

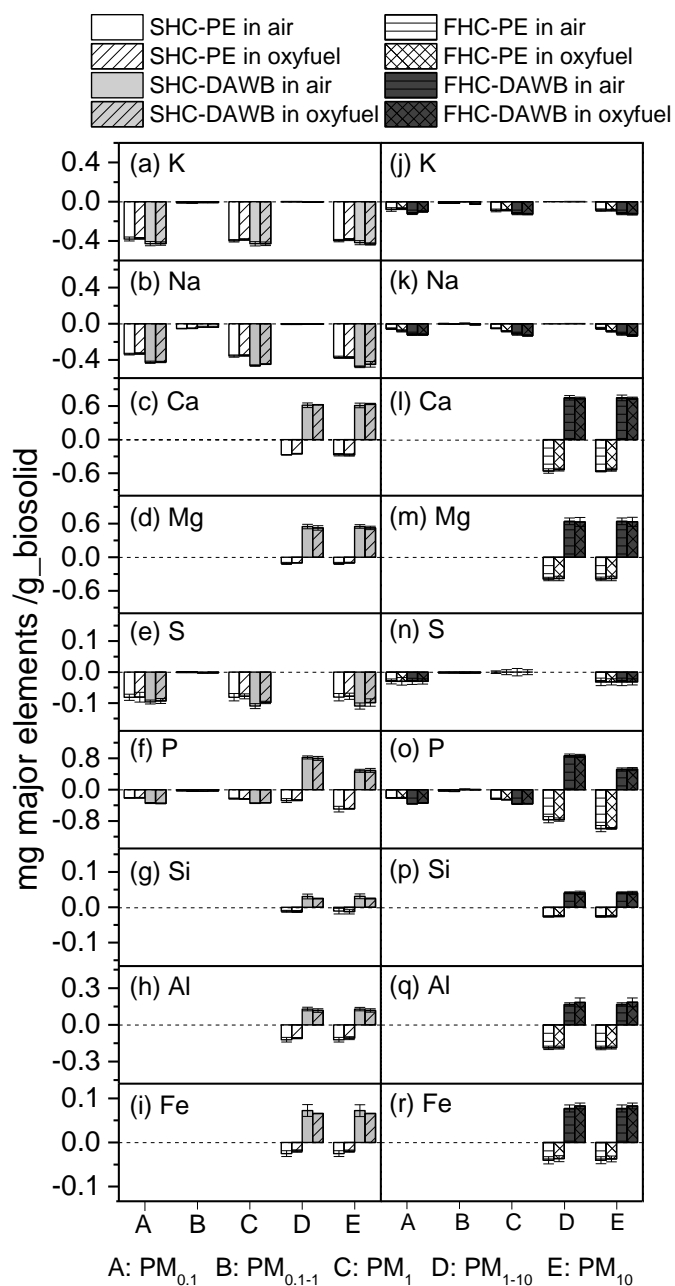


Figure 10-8 Net yields of major elements in PM contributed by volatile-char interactions

Figure 10-6 and Figure 10-7 present the experimental results on the PSDs and individual yields of major elements in PM produced during the combustion of chars, with the corresponding net yields of individual major elements contributed by volatile-char interactions shown in Figure 10-8. As shown in Figure 10-6, the

elemental PSDs of volatile elements (i.e. Na, K, P and S) have a fine mode at  $\sim 0.022$   $\mu\text{m}$  during the combustion of the SHC-holding (i.e. the char before volatile-char interactions) in air. However, the peak intensities of the fine mode are significantly reduced for these elemental PSDs of the  $\text{PM}_{10}$  produced from the combustion of the SHCs interacted with the PE or DAWB volatiles. Furthermore, as shown in the left column of Figure 10-8, the DAWB volatiles exhibit more significant effect on decreasing the yields of  $\text{PM}_{0.1}$  and volatile elements (i.e. Na, K, P and S) in  $\text{PM}_{0.1}$  than the oxygen-free PE volatiles do. For example, the net decrease in the P yield in  $\text{PM}_{0.1}$  is 0.21 mg/g biosolid for the SHC char interacted with the PE volatiles, in comparison to 0.36 mg/g biosolid for the SHC char interacted with the DAWB volatiles. As shown in Figure 10-9, the P and S retained in the chars are substantially released, along with the alkalis (Na and K), during interactions between the chars with the PE and DAWB volatiles. This is attributed to the fact that the small non-oxygenated reactive species in the fresh volatiles can significantly enhance the release of alkalis (Na and K) as well as P and S into volatiles from char particles and then enhance the emission of those elements during volatiles combustion. The results show that as results of *in situ* volatile-char interactions, the released alkalis (Na and K) as well as P and S, which eventually lead to the emission of  $\text{PM}_{0.1}$  during volatiles combustion, would otherwise emit as  $\text{PM}_1$  during subsequent char combustion. Furthermore, the significant reduction of Na, K, P and S emission from the combustion of SHC-DAWB and SHC-PE lead to reduction in nucleation of volatile inorganic matters during char combustion. Consequently, the peak intensities for the fine mode during the combustion of these chars are significantly reduced.

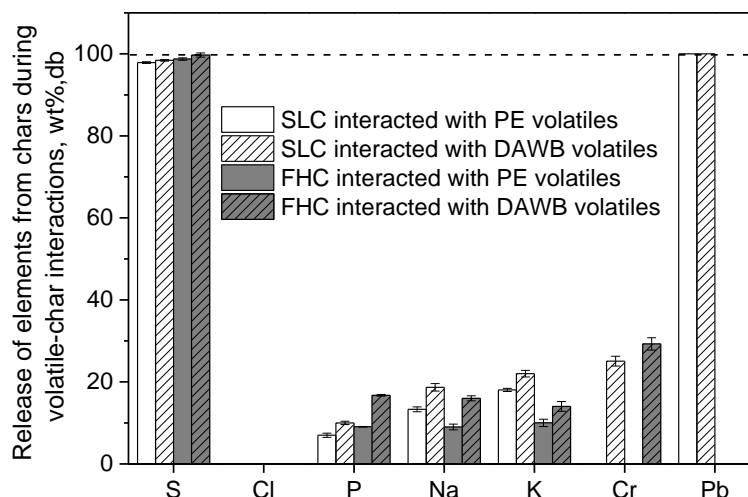


Figure 10-9 Release of key inorganic species during volatile–char interactions at 1000 °C. Release of other major elements (i.e., Ca, Mg, Fe, Al and Si) and trace elements (i.e., As, Cd, Co, Mn, V, Cu, Ni and Zn) during volatile–char interactions are negligible

For the refractory elements (i.e. Ca, Mg, P, Si, Al and Fe) in  $PM_{10}$ , the mode diameters of the coarse mode for the elemental PSDs remain unchanged at  $\sim 6.8 \mu\text{m}$ . However, the peak intensities of the coarse mode increase significantly for these elemental PSDs during the combustion of the SHC interacted with the DAWB volatiles but decrease substantially during the combustion of the SHC interacted with the oxygen-free PE volatiles. Figure 10-8 further shows that the DAWB volatiles significantly increase the  $PM_{1-10}$  yield of Ca, Mg, P, Si, Al and Fe, while the PE volatiles which is free of oxygen, slightly decrease the yields of these refractory elements in  $PM_{1-10}$ . These results reflect that the interactions between SHC and different volatiles also play important but different roles in the individual PSDs and PM yields of major elements during slow-heating char combustion in air.

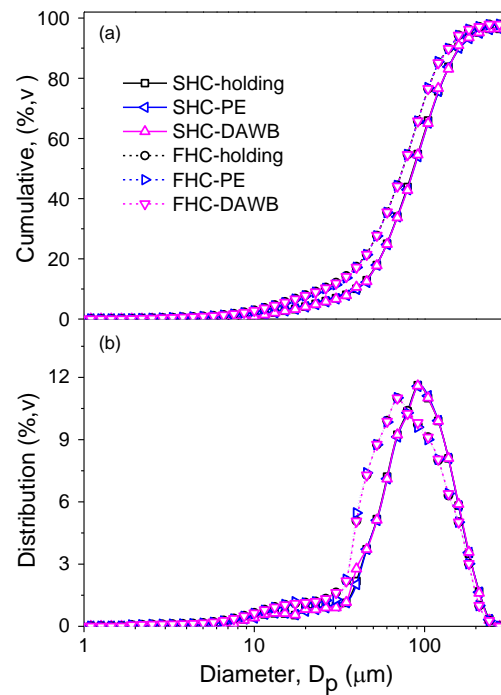


Figure 10-10 Particles size distributions (by volume) of char particles. (a) Cumulative, (b) Distribution

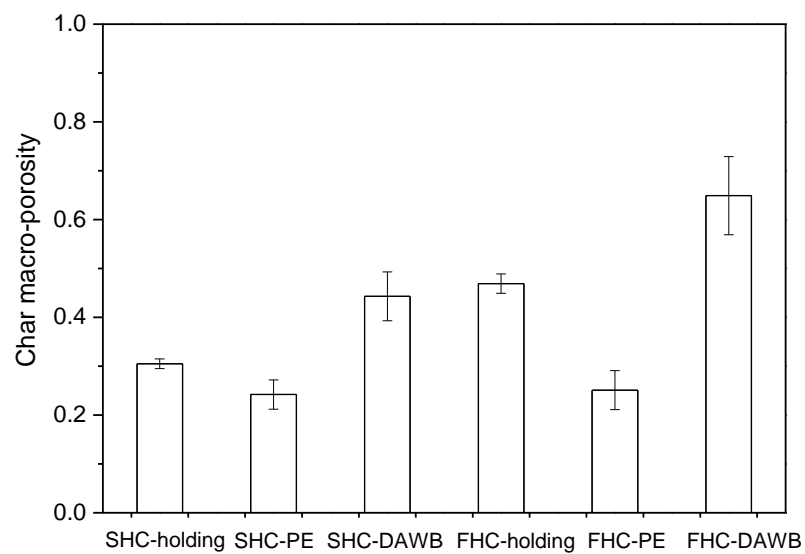


Figure 10-11 Macroporosity of char particles produced from slow heating char and fast heating char with or without volatile–char interactions

A previous study showed that the formation of  $PM_{1-10}$  is mainly governed by char

fragmentation, which is dictated by char particle size<sup>152</sup> and macroporosity.<sup>145</sup> The significant variations in the net PM<sub>1-10</sub> yield contributed by volatile-char interactions observed in this study might be caused by the changes in particle size and/or macroporosity of char samples during volatile-char interactions. Figure 10-10 and Figure 10-11 present the particle size distributions and macroporosities of chars with and without volatile-char interactions, respectively. A close match of the particle size distribution between the char with and without volatile-char interactions shown in Figure 10-10 indicates that volatile-char interactions did not alter the char particle size. However, Figure 10-11 shows the macroporosity of the chars is significantly altered by volatile-char interactions, and more importantly, the PE and DAWB volatiles play opposite roles in altering char macroporosity during volatile-char interactions. After interacting with the oxygen-free PE volatiles, the macroporosity of the SHC decreases from  $\sim 0.30$  to  $\sim 0.24$ , while it significantly increases to  $\sim 0.44$  after interacting with the DAWB volatiles. These result in a decrease in the yield of PM<sub>1-10</sub> for the SHC-PE but a substantial increase in the yield of PM<sub>1-10</sub> for the SHC-DAWB. During the interactions between the PE volatiles and char particles, volatiles could crack into soot which deposits on the surface of internal pores within the char particles,<sup>219</sup> reducing the char macroporosity. The dramatic decrease in the oxygen content (see Table 10-1) of the char (SHC-PE) after interacting with the PE volatiles also indicates that some active species in the PE volatiles may react with and eliminate the oxygen-containing species from char, thus making the char structure more condensed. However, during pyrolysis of the DAWB, the reactive O-containing species (e.g. OH-containing species<sup>220,221</sup>) can react with the char,<sup>222</sup> leading to significant pore formation and enlargement of existing pores,<sup>205</sup> thus increasing char macroporosity. Furthermore, the O-containing species in the DAWB volatiles can effectively reduce soot formation on the char surface,<sup>223,224</sup> thus alleviate the effect of soot on the reduction in char macroporosity. It is also worthwhile to point out that these reactions did not lead to significant char weight loss (see Figure 10-1). Even at 1% char conversion, it can lead

to a significant change in the char pore structure.<sup>206</sup>

The effect of the evolutions of char pore structure is not only limited to the yield  $PM_{1-10}$  from the combustion of the resultant SHCs. It can also affect the emission of  $PM_1$  during volatile–char interactions. For example, with the progress of volatile–char interactions, char particles interacted with PE volatiles are covered by soot. The reduced macroporosity hinders the contact of volatiles with char particles and gradually limiting the further progress of volatile–char interactions. However, the char particles interacted with the DAWB volatiles become more porous, which allows the DAWB volatiles to penetrate deeply into the char particle and therefore exert more severe effect on the reduction in  $PM_1$  yield during subsequent char combustion. This is supported by the experimental results in Figure 10-5 where a lower net yield of  $PM_1$  is shown from the combustion of the SHC-DAWB compared to the SHC-PE.

#### **10.4 Effect of *in situ* volatile–char interactions on the emission of trace elements in $PM_{10}$ during char combustion in air**

Figure 10-12 and Figure 10-13 present the individual PSDs and yields of trace elements in PM during the combustion of the chars and the net yields of individual trace elements contributed by volatile–char interactions are shown in Figure 10-14. Several important observations can be made in Figures 10-12, 10-13 and 10-14. First, as shown in Figures 10-11a, 10-13a and 10-14a, the yield of Cr in  $PM_{0.1}$  from the combustion the SHC interacted with the DAWB volatiles is reduced by 2.1  $\mu\text{g/g}$  biosolid compared to the SHC without interaction. However, such phenomenon is not observed for the combustion of the SHC-PE. This is because the Cr in char can react with the oxygen-containing reactive species in the fresh DAWB volatiles to form volatile chromium oxyhydroxides under reducing conditions. This results in the release of Cr from the SHC as indicated by a lower Cr in the SHC-DAWB compared to the SHC-holding. Second, Figure 10-14b indicates the combustion of the SHC

interacted with the DAWB and PE volatiles lead to a slight decrease in Pb yield as PM<sub>1</sub> compared to that without experiencing volatile–char interactions. The reducing conditions induced during volatile–char interactions can enhance the release of Pb from char,<sup>208</sup> further reducing the content of Pb in the SHC-PE and SHC-DAWB. Third, the volatile–char interactions have little effect on the PSDs and yields of volatile As, Cd and semi-volatile Ni and Cu as PM<sub>1</sub> during combustion of SHC-DAWB and SHC-PE. Lastly, a higher macroporosity of the SHC-DAWB promotes char fragmentation during char combustion thus, a significant increase in the yields of Ni, Cu, Co, Cu, Mn, V and Zn as PM<sub>1-10</sub>. However, a lower char macroporosity of the SHC-PE resulted in a decrease in the yields of these trace elements as PM<sub>1-10</sub>.



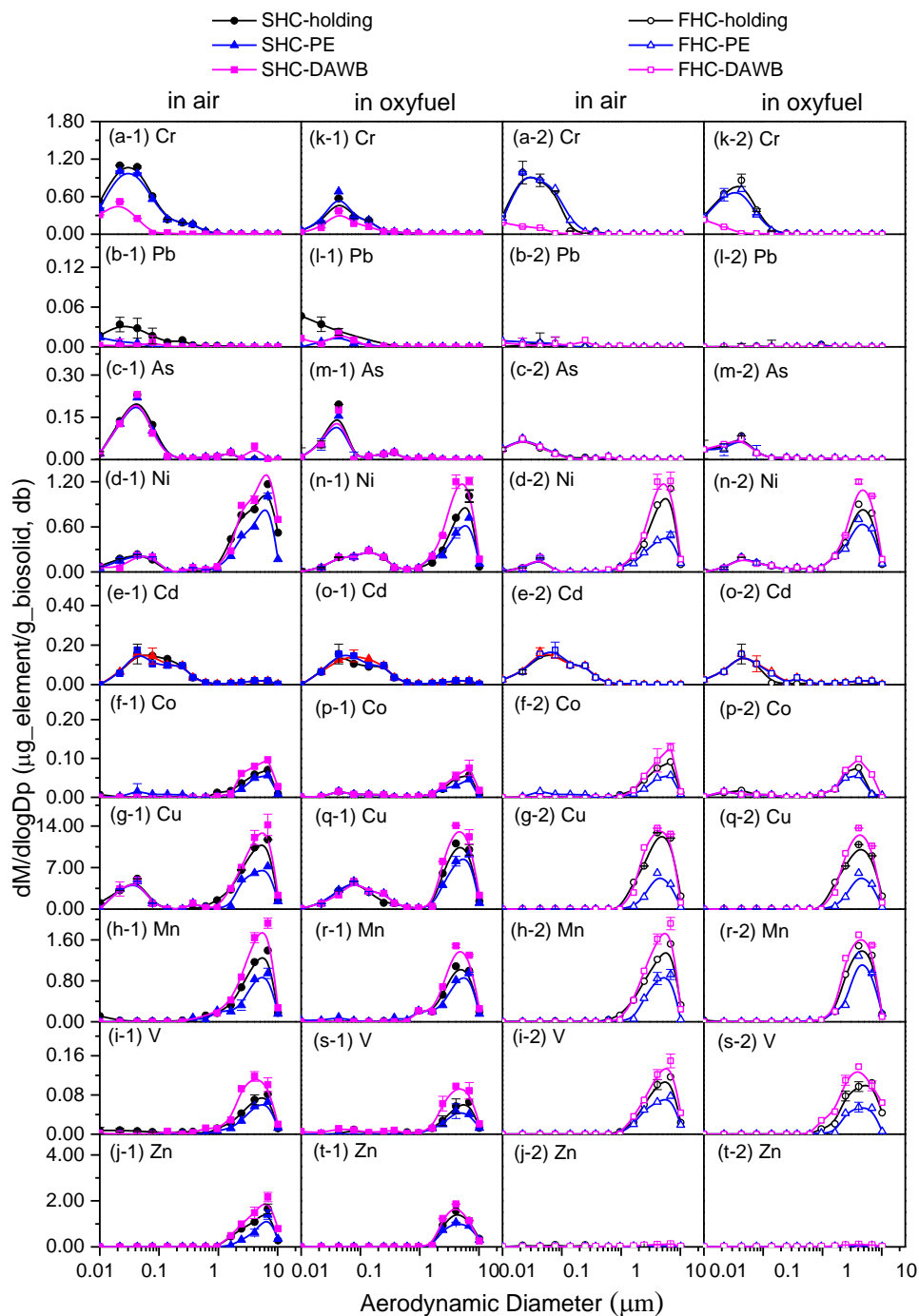


Figure 10-12 PSDs of trace elements in  $PM_{10}$  during char combustion. The left two columns represent results from the combustion of SHCs under air and oxyfuel conditions while the right two columns represent the results from the combustion of FHCs under air and oxyfuel conditions, respectively

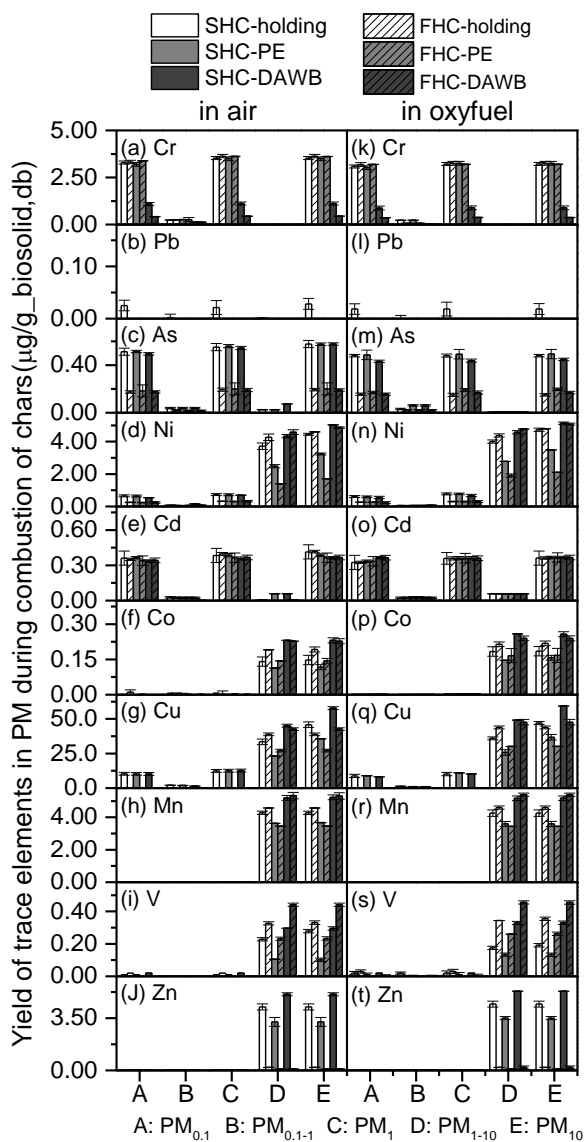


Figure 10-13 Yields of trace elements in PM during char combustion under air (left column) and oxyfuel (right column) conditions

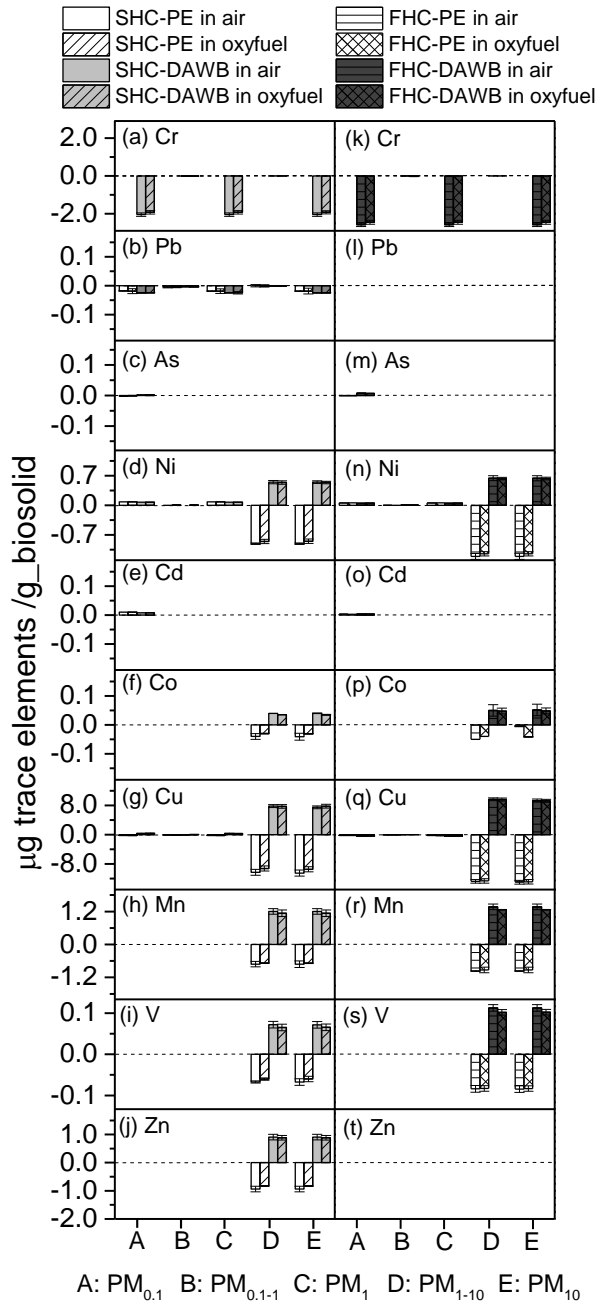


Figure 10-14 Net yields of trace elements in PM contributed by volatile-char interactions

### 10.5 Effect of pyrolysis conditions on PM<sub>10</sub> emission during the combustion of char that experienced interactions with volatiles

Compared to SHC, FHC is prepared from pulse feeding of biosolid under rapid heating

conditions. The different pyrolysis conditions result in different char properties which can affect the PM emission during char combustion. For example, as shown in Figure 10-3c, similar to the bimodal distribution observed for the PSDs of the PM<sub>10</sub> emitted from combustion of the SHC-holding in air, the PSDs of the PM<sub>10</sub> emitted from combustion of the FHC-holding in air present the same coarse mode of  $\sim 6.8 \mu\text{m}$ , while the peak intensity of the fine mode for the combustion of FHC-holding is very weak. In addition, Figure 4a shows the combustion of the FHC-holding yielded less PM<sub>1</sub> but more PM<sub>1-10</sub> compared to the SHC-holding. Compared to the SHC, while the interactions of the FHC with the DAWB and PE volatiles have little effect on PM<sub>1</sub> emission during combustion in air, such interactions have a significant effect on PM<sub>1-10</sub> emission. For example, the interactions between the PE volatiles and SHC lead to a net PM<sub>1</sub> and PM<sub>1-10</sub> yields of -2.9 mg/g biosolid and 0.8 mg/g biosolid, respectively. However, the interactions between the same volatiles and FHC lead to a net PM<sub>1</sub> and PM<sub>1-10</sub> yields of -0.9 mg/g biosolid and 2.2 mg/g biosolid, respectively.

The significantly less reduction in PM<sub>1</sub> emission from the combustion of the resultant FHC after volatile-char interactions is attributed to the low volatile species (i.e. Na, K and S) contents in the FHC (see Table 10-1) as these elements are significantly released during fast heating pyrolysis, as shown in Figure 10-2a. During biosolid pyrolysis, a higher heating rate can significantly suppress the intra-particle secondary reactions of volatiles and the transformation of the volatile inorganic species into char bonded forms.<sup>225</sup> Hence, during the fast heating pyrolysis with a high heating rate, the volatiles is swiftly released without further reaction with inherent minerals, resulting in the enhanced release of inorganic species during pyrolysis.<sup>104</sup> As shown in Figure 10-7, PM<sub>1</sub> is mainly contributed by volatile Na, K, P and S. A lower Na, K and S retention in the FHC compared to the SHC lead to a reduction in PM<sub>1</sub> formation during the combustion of the FHC-holding. This also subsequently reduced the degree of reduction in PM<sub>1</sub> formation from the combustion of the resultant FHC after volatile-char interactions. As for trace elements, the fast heating pyrolysis also

resulted in low retentions of Pb, As, Ni, Cd and Cu and thus a reduction in the release of these trace elements as  $PM_{10}$  during the FHCs combustion.

The change in  $PM_{1-10}$  yields during the combustion of the FHCs, on the other hand, is influenced by char particle size and macroporosity. As shown in Figure 10-10, the particle size of the FHCs is generally smaller than that of the SHCs, and Figure 10-11 also shows that the char macroporosity ( $\sim 0.47$ ) of the FHC-holding is substantially higher than that ( $\sim 0.30$ ) of the SHC-holding. During fast pyrolysis with pulse feeding, the thermal shock enhanced the primary char fragmentation<sup>153</sup> and the rapid release of volatiles yields chars with higher porosity.<sup>226</sup> These lead to an enhanced char fragmentation, and therefore, an increase in the yield of  $PM_{1-10}$  during the combustion of the FHCs. Consequently, the yields of major elements (Ca, Mg, P, Si, Al and Fe) and trace elements (Ni, Co, Cu, V and Mn) in  $PM_{1-10}$  generated during the combustion of the FHCs are higher compared to those from the combustion of the SHCs. Moreover, a higher FHC char porosity can significantly influence the extent of volatile–char interactions and thus affect the  $PM_{1-10}$  emission during subsequent char combustion. The more developed pore structures in the FHC can facilitate the diffusion of reactive species from volatiles into the char structure, further enhancing the effect of volatile–char interactions. More specifically, during the interaction between the FHC and the PE volatiles, increased porosity and diffusion of volatiles can lead to substantial deposition of soot within pore system and char surface, clogging the pores and resulted in reduction in char macroporosity. On the contrary, during the interaction of the FHC and the DAWB volatiles, increasing diffusion of volatiles and surface area further promote the development of char pore structure and thus result in a substantial increase in  $PM_{1-10}$  yield during the combustion of the FHC-DAWB.

### 10.6 Differences in PM<sub>10</sub> emission during the combustion of volatile–interacted chars under air and oxyfuel conditions

In order to investigate the effect of combustion atmospheres on PM emission during the combustion of the char experiencing volatile–char interactions, these chars are also combusted under oxyfuel conditions (30% O<sub>2</sub> in CO<sub>2</sub>) in this study. As shown in Figure 10-3a and b, the combustion atmospheres significantly affect the PSDs of PM<sub>10</sub> from the combustion of char. When the combustion atmospheres switched from air to oxyfuel, the fine mode diameter of PSDs of the PM<sub>10</sub> generated from the combustion of the SHCs shifts from ~0.022 μm to ~0.044 μm, while the coarse mode diameter shifts from ~6.8 μm to ~4.4 μm. It should be noted that the estimated particle temperatures under air and oxyfuel conditions is similar.<sup>20</sup> Therefore, the shift of fine mode diameter from ~0.022 μm under air to ~0.044 μm under oxyfuel conditions should be attributed to the enhanced homogeneous nucleation under oxyfuel conditions.<sup>20,227</sup> In addition, a high CO<sub>2</sub> concentration under oxyfuel conditions weakens the catalysed sintering process of Mg/Ca carbonate during combustion and hinders the growth of Mg/Ca-bearing particles,<sup>151</sup> resulting in a shift of coarse mode diameter from 6.8 μm to 4.4 μm under oxyfuel conditions. However, as shown in Figure 10-5, 10-8 and 10-14, the combustion atmospheres have little effect on the contribution of *in situ* volatile–char interactions to PM<sub>1</sub> or PM<sub>1-10</sub> emission during char combustion, because the release of the volatile species and char fragmentation during char combustion are mainly governed by char particle temperatures which are estimated to be similar under air and oxyfuel conditions.

Figure 10-7 shows that PM<sub>1</sub> is mainly contributed by Na, K, S and P, while other major elements in char, such as Ca, Mg, Si, Al, Fe and the majority of P are observed in PM<sub>1-10</sub>. For trace elements (see Figure 10-13), Cr, Pb, As, Ni, Cd and part of Cu are distributed in PM<sub>1</sub>, while Co, Cu, Mn, V and Zn are found in PM<sub>1-10</sub>. When the major elements are calculated as stable oxides (i.e., P as P<sub>2</sub>O<sub>5</sub>, Fe as Fe<sub>2</sub>O<sub>3</sub>, S as SO<sub>3</sub>), more

than 99% of the  $PM_1$  and 96% of the  $PM_{1-10}$  is accounted by the major elements analysed. However, S only exists in the  $PM_1$  generated during the combustion of the SHCs and only contributes 3% (as  $SO_3$ ) to the  $PM_1$  generated. On the other hand, alkali metals and P oxides account for  $\sim 90\%$  of the  $PM_{0.1}$  emitted and alkaline earth metals and P oxides account for  $\sim 60\%$  of the  $PM_{1-10}$  emitted, indicating that AAEM species and P are the dominant elements and play vital roles in the PM emitted from char combustion under current experimental conditions. In order to investigate the effect of volatile–char interactions on the forms of these elements in  $PM_{10}$ , the molar ratios of AAEMs over P in  $PM_{0.1}$  and  $PM_{1-10}$  are calculated and presented in Figure 10-15. Figure 10-15 clearly shows that the molar ratio of  $(Na + K) / P$  in  $PM_{0.1}$  under both atmospheres is around 1.0, suggesting that these elements are likely in the form of  $(Na, K)PO_3$  in  $PM_1$ . This is consistent with the report from equilibrium modelling of the high-phosphorus fuels combustion.<sup>4</sup> The results in Figure 10-15 also show that  $(Mg + Ca) / P$  in  $PM_{1-10}$  under both atmospheres is around 1.5, suggesting that these elements are likely in forms  $(Mg, Ca)_3(PO_4)_2$  in  $PM_{1-10}$ . Furthermore, the molar ratios of  $(Na + K)/P$  in  $PM_{0.1}$  and  $(Mg + Ca)/P$  in the  $PM_{1-10}$  generated during the combustion of chars experiencing and without experiencing volatile–char interactions remain relatively unchanged. The results indicate that volatile–char interactions have little effect on the forms of AAEMs and P in the  $PM_{10}$  released from the combustion of the resultant char. Trace elements, however, only contribute little to  $PM_{10}$  ( $< 0.5$  wt%) and the amount of P and S associated with trace elements is very small,<sup>228</sup> therefore, the same calculation for trace elements is not considered.

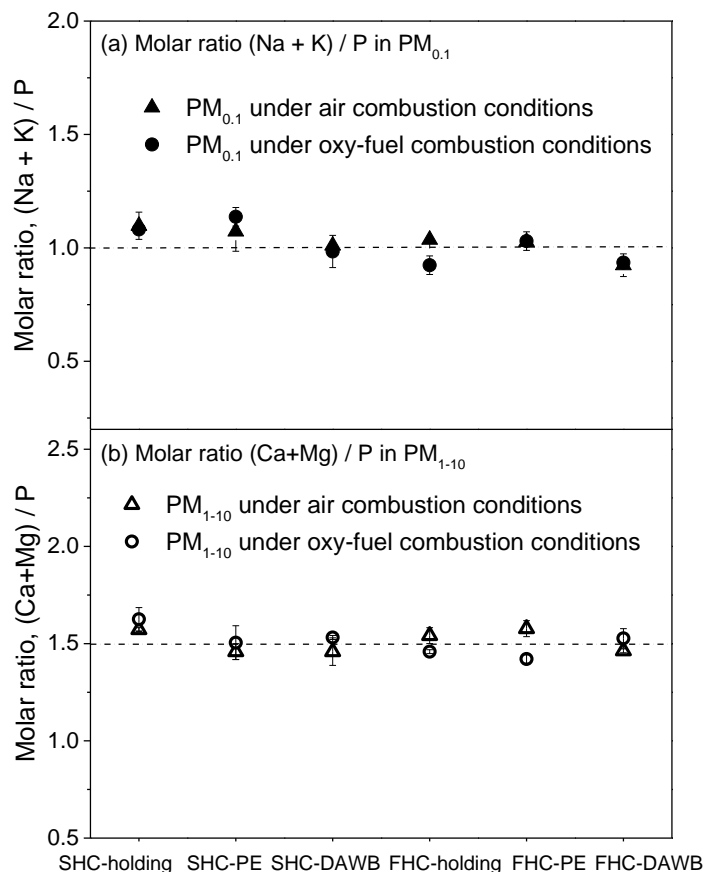


Figure 10-15 The molar ratios of (Na + K)/P in PM<sub>0.1</sub> and (Ca + Mg)/P in PM<sub>1-10</sub> generated during char combustion under air and oxyfuel conditions

## 10.7 Conclusions

This chapter investigates the effect of oxygen-free (PE) and oxygen-containing (DAWB) volatiles during volatile–char interactions on PM<sub>10</sub> emission during combustion of slow and fast heating chars under air and oxyfuel conditions at 1300 °C. The results clearly show the interactions between chars and small non-oxygenated reactive species in the PE and DAWB volatiles lead to release of Na, K, P and S thus 2.8 and 4.3 mg/g biosolid reduction in PM<sub>0.1</sub> formation during combustion of the resultant SHC-PE and SHC-DAWB in air, respectively. The interactions between oxygen-free volatiles and char can lead to a reduction in char macroporosity which in turn causes a net reduction of 0.8 mg/g biosolid in the yield of PM<sub>1-10</sub>. On the contrary,



the interactions the DAWB volatiles and char resulted in a substantial increase in char macroporosity, leading to significant increase in  $PM_{1-10}$  formation (2.9 mg/g biosolid). Compared to slow pyrolysis, fast heating pyrolysis produces char with reduced volatile species content (i.e. Na, K and S), smaller char particle size and higher macroporosity. Therefore, the effect of volatile–char interaction on net yield of  $PM_1$  emission is less profound but its effect on net yield of  $PM_{1-10}$  emission is more significant during combustion of the resultant FHCs. A net reduction of 2.2 mg/g biosolid and net increase of 3.9 mg/g biosolid in  $PM_{1-10}$  emission from the combustion of the FHC-PE and FHC-DAWB in air is observed, respectively. The combustion atmosphere is found to have little effect on the net yield of  $PM_{10}$  caused by *in situ* volatile–char interactions. The interactions of chars with oxygen-free volatiles suppress the formation of refractory major (Mg, Ca, Al, Si and Fe) and trace (Ni, Co, Cu, Mn, V and Zn) elements as  $PM_{1-10}$  but its interactions with O-containing volatiles enhance the yield of these elements in  $PM_{1-10}$ . The interactions between O-containing reactive species and chars lead to formation of volatile chromium oxyhydroxides, thus results in a substantial reduction in Cr yield in  $PM_{0.1}$  from combustion of the resultant char. Furthermore, volatile–char interactions have little effect on the forms of AAEM species and P in  $PM_1$  and  $PM_{1-10}$  generated by char combustion under air and oxyfuel conditions.

*Reprinted with permission from (Xujun Chen, Sui Boon Liaw and Hongwei Wu. Effect of volatile–char interactions on  $PM_{10}$  emission during the combustion of biosolid chars under air and oxyfuel conditions, Combustion and Flame 2018, 197, 290-303). Copyright (2018) The Combustion Institute. Published by Elsevier Inc*

## CHAPTER 11 CONCLUSIONS AND RECOMMENDATIONS

### 11.1 Introduction

This chapter summarises the key findings in this PhD study and provides some recommendations on future work in this area. Overall, this thesis has revealed new insights into the structure and reactivity of char prepared from pyrolysis of P-containing solid fuels as well as the PM emission during combustion of P-containing solid fuels through systematic investigations. First, a new method has been developed and validated for quantifying different forms of phosphorus in solid fuels. Such a method is fundamentally significant for further investigation into the behaviour and fate of P during the thermochemical processing of P-containing solid fuels. Based on this method, a systematic set of experiments were carried out to study the effect of reactor configurations on the transformation and release of phosphorus during pyrolysis under various conditions. In addition, experiments were also conducted to investigate the roles of two important factors, i.e., volatiles with distinctly-different chemistry during volatile–char interactions and the presence of different forms of phosphorus in biomass in determining char structure and char reactivity. These studies are of great significance for a P-containing solid fuel combustion system with regards to optimising combustion conditions. The last part of this thesis reports the PM emission during combustion of P-containing solid fuels, especially biosolid and contaminated biomass with abundant trace elements. The focuses are on the effect of water vapours on PM emission during solid fuel combustion under oxyfuel condition, considering the separate combustion of in situ volatiles and char generated from fast pyrolysis of P-containing contaminated biomass. More importantly, this thesis has reported, for the first time, the direct evidence on the critical roles of volatile–char interactions in governing PM emission during combustion of volatiles and char produced from P-rich biosolid. Practically,

this study enriches the fundamental understanding on char reactivity, char structure, PM emission as well as phosphorus transformation during thermochemical utilization of P-rich biomass, which is critical to optimizing operation conditions, reducing equipment maintenance costs and mitigating negative environmental impact and operational challenges caused by phosphorus.

## **11.2 Conclusions**

Several conclusions can be drawn based on the investigations in Chapter 4–10, respectively corresponding to the objective 1–7 listed in Section 2.9.

### **11.2.1 A new method for quantifying phosphorus of various occurrence forms in solid fuels**

- A new method is proposed in this study to extract different forms of phosphorus in solid fuels via three-step sequential extraction, followed by phosphorus quantification in each fraction using IC and ICP-OES;
- Three organic phosphorus fractions (i.e. acid-soluble organic P, P in phospholipids, P in nucleic acids and other acid-insoluble organic structures) and two inorganic P fractions (acid-soluble inorganic P and acid-insoluble inorganic P) in solid fuels can be extracted and determined using the new method;
- Compared with the poor performance of the conventional SMT method, the application of this new method in seven different solid fuels has achieved high P mass balance and is suitable for quantifying P of various forms in solid fuels.

---

### 11.2.2 Effect of reactor configurations on the transformation and release of phosphorus during pyrolysis under various conditions

- Both reactor configuration and pyrolysis temperature could significantly affect char yields and char chemistry during rice bran pyrolysis;
- Below 700 °C, higher heating rate in a drop-tube/fixed-bed reactor either with continuous feeding or pulse feeding enhanced P release;
- When increasing pyrolysis temperature from 700 to 900 °C, volatile–char interactions could result in substantial P release during pyrolysis in a drop-tube/fixed-bed reactor with continuous feeding;
- *In situ* combustion of volatiles at 950 °C in a two-stage pyrolysis/combustion reactor system could effectively convert more than 95% P in volatiles (dominantly P in tar) into water-soluble P species;
- P in rice bran is mainly organic potassium phytate, which can be substantially transformed into acid-soluble inorganic P even at temperatures as low as 400 °C during pyrolysis. Above 800 °C, acid-insoluble inorganic P starts to be generated during rice bran pyrolysis.

### 11.2.3 Effect of phosphorus in biomass on char structure and reactivity

- Phosphorus could substantially increase char yields during biomass pyrolysis due to the enhanced crosslinking by P-containing structures in char, leading to increases in the char C and H contents and a decrease in char O content.
- After pyrolysis and subsequent char oxidation, all P in biomass either as organic or inorganic P are found to be present in the form of acid-insoluble organic structures.
- For char prepared from acid-washed wood, char reactivity increases with char conversion due to the increasing pore surface area at higher conversion. Comparatively, for char prepared from acid-washed wood loaded with

various P at char conversion below 60%, the presence of P increases char intrinsic reactivity due to the more reactive char structures caused by enhanced crosslinking and reduced condensation of char structures.

- At higher char conversions, P-containing species in char leads to a significant decrease in char reactivity, due to the formation of abundant C-O-P bonds, that is highly resistant to the oxidation in air, in the reacting chars.

#### **11.2.4 Volatile–char interactions: Roles of *in situ* volatiles with distinctly-different chemistry in determining structure and reactivity of char prepared from P-containing biosolid**

- For the char interacted with volatiles with distinctly-different chemistry, char reactivity increases with increasing O/H molar ratio of the volatiles for *in situ* volatile–char interactions;
- Both H- and O-containing reactive species in volatiles play important but different roles during *in situ* volatile–char interactions;
- H-containing reactive species substantially induce the condensation of the aromatic ring systems in char and consequently decrease H content in char, thus making the char structure more inert;
- O-containing reactive species in volatiles react with char particles to form C-O complex oxides which mitigates the carbon structure from condensing into larger aromatic ring systems and increases O and H contents in char, thus effectively increasing char reactivity.

#### **11.2.5 Effect of water vapour on PM<sub>10</sub> emission during oxyfuel combustion of char and *in situ* volatiles generated from rapid pyrolysis of P-containing contaminated wood**

- During *in situ* volatiles combustion, water vapour could significantly enhance the nucleation, coagulation and condensation of fine particles and increases the

PM<sub>0.1</sub> yield. During char combustion, water vapour might also enhance char fragmentation hence increases the PM<sub>1-10</sub> yield;

- For trace elements, volatile trace elements (As, Cr, Ni, Cu and Pb) are only presented in PM<sub>1</sub> during *in situ* volatiles combustion. Water vapour shifts the PSDs, but has little effect on the yields of these trace elements;
- During char combustion, As, Cr, Cu and Ni are present in both PM<sub>1</sub> and PM<sub>1-10</sub> while non-volatile Mn and Ti are only present in PM<sub>1-10</sub>. Water vapour increases the yields of As, Cr, Cu, Ni, Mn and Ti in PM<sub>1-10</sub> due to possibly enhanced char fragmentation;
- With the addition of water vapour, the yields of As and Cr in PM<sub>0.1</sub> are increased but that of Ni in PM<sub>0.1</sub> is decreased during char combustion, most likely due to water vapour facilitating the conditions that enhance the release of As and the generation of gaseous chromium oxyhydroxides but inhibits the production of NiCl<sub>2</sub> (g).

### **11.2.6 Important role of volatile–char interactions in PM<sub>10</sub> emission during the combustion of volatiles from P-containing biosolid**

- Volatile–char interactions significantly change the PSDs of PM during the combustion of volatiles both produced from ash-free cellulose or polyethylene and acid-washed biosolid.
- The volatile–char interactions only enhance the emission of PM<sub>1</sub> (mainly PM<sub>0.1</sub>) and are intensified at a higher temperature. The reactive volatiles can react with biosolid char and enhance the release of Na, K, P and S during volatile-char interactions but lead to little change in the yields of biosolid chars.
- As far as PM<sub>1</sub> emission is concerned during volatiles combustion, oxygen-containing reactive species in volatiles play an insignificant role in volatile–char interactions.

- The molar ratios of  $(\text{Na}+\text{K})/(\text{P}+2\text{S})$  for both  $\text{PM}_{10}$  and the net release of these key elements from the chars are also found to be  $\sim 1.0$ , suggesting these key elements are released from the chars then react to form alkali metaphosphate and sulphate in  $\text{PM}_{10}$  during volatiles combustion.
- Volatile–char interactions can transform part of the Pb and Cr in the chars into more volatile forms, which are subsequently released and contributed to  $\text{PM}_{10}$  emission. The absence of Cr release during interactions between polyethylene volatiles and char further suggests that Cr is released in the form of chromium oxyhydroxides during volatile–char interactions

### 11.2.7 Effect of volatile–char interactions on $\text{PM}_{10}$ emission during the combustion of P-containing biosolid chars under air and oxyfuel conditions

- The interactions between chars and small non-oxygenated reactive species in volatiles lead to release of Na, K, P and S and thus reduction in  $\text{PM}_{0.1}$  formation during combustion of the volatile-interacted char in air;
- The interactions between oxygen-free volatiles and char can lead to a reduction in char macroporosity which in turn causes reduction in the yield of  $\text{PM}_{1-10}$ . On the contrary, the interactions between char and the oxygen-containing volatiles generated from double-acid washed biosolid result in a substantial increase in char macroporosity, leading to significant increase in  $\text{PM}_{1-10}$  formation;
- Compared to slow pyrolysis, fast heating pyrolysis produces char with reduced content of volatile species (i.e. Na, K and S), smaller char particle size and higher macroporosity. Therefore, the effect of volatile–char interaction on net yield of  $\text{PM}_{10}$  emission is less profound but its effect on net yield of  $\text{PM}_{1-10}$  emission is more significant during combustion of the fast heating char interacted with volatiles;
- The combustion atmosphere is found to have little effect on the net yield of  $\text{PM}_{10}$  caused by *in situ* volatile–char interactions;

- The interactions of chars with oxygen-free volatiles suppress the formation of refractory major (Mg, Ca, Al, Si and Fe) and trace (Ni, Co, Cu, Mn, V and Zn) elements as PM<sub>1-10</sub> but its interactions with O-containing volatiles enhance the yield of these elements in PM<sub>1-10</sub>;
- The interactions between O-containing reactive species and chars lead to formation of volatile chromium oxyhydroxides, thus results in a substantial reduction in Cr yield in PM<sub>0.1</sub> from combustion of the resultant char;
- Furthermore, volatile–char interactions have little effect on the forms of AAEM species and P in PM<sub>1</sub> and PM<sub>1-10</sub> generated by char combustion under air and oxyfuel conditions

### 11.3 Recommendations

Through the systematic research program, this PhD study has studied char structure, char reactivity and PM emission during pyrolysis and combustion of P-containing solid fuels. Some future investigations are recommended as below.

- 1) The phosphorus quantification method developed in Chapter 4 is effective and of high accuracy. However, the procedure is relatively complicated so that the method itself can be time-consuming. Efforts can be made to further simplify this method without jeopardising accuracy;
- 2) The majority of phosphorus are retained in char under the experimental conditions (400–900 °C) in Chapter 5, as results of the pyrolysis conditions. Future work is suggested to carry out experiments on pyrolysis at temperatures above 900 °C;
- 3) Reducing atmosphere is likely to have significant effect on P release but it is unclear how the presence of CO<sub>2</sub> and steam would affect P release during pyrolysis or gasification of P-containing solid fuels;
- 4) Inherent AAEM species play important roles in determining char reactivity. In presence of P, the potential synergetic effects between P and AAEM species on



char reactivity are unknown and should be investigated in future work;

- 5) Due to the limitation of quartz working temperature (1050 °C) in this study, the effect of volatile–char interactions on char structure and char reactivity is limited at 1000 °C. Future work should be carried out to investigate the effect of volatile–char interactions on char structure and char reactivity at temperatures of 1300 °C or above;
- 6) Similarly, due to the same limitation, there is still a lack of investigations into the roles of volatile–char interactions in the characteristics of PM emitted from subsequent combustion of P-containing solid fuels at temperatures of 1300 °C or above.

## REFERENCES

1. Ergle, D. R.; Eaton, F. M., Aspects of Phosphorus Metabolism in the Cotton Plant. *Plant Physiology* 1957, 32, (2), 106-113.
2. Piotrowska, P.; Zevenhoven, M.; Davidsson, K.; Hupa, M.; Åmand, L.-E.; Barišić, V.; Coda Zabetta, E., Fate of Alkali Metals and Phosphorus of Rapeseed Cake in Circulating Fluidized Bed Boiler Part 1: Cocombustion with Wood. *Energy & Fuels* 2010, 24, (1), 333-345.
3. Piotrowska, P.; Zevenhoven, M.; Davidsson, K.; Hupa, M.; Åmand, L.-E.; Barišić, V.; Coda Zabetta, E., Fate of Alkali Metals and Phosphorus of Rapeseed Cake in Circulating Fluidized Bed Boiler Part 2: Cocombustion with Coal. *Energy & Fuels* 2010, 24, (8), 4193-4205.
4. Wu, H.; Castro, M.; Jensen, P. A.; Frandsen, F. J.; Glarborg, P.; Dam-Johansen, K.; Røkke, M.; Lundtorp, K., Release and Transformation of Inorganic Elements in Combustion of a High-Phosphorus Fuel. *Energy & Fuels* 2011, 25, (7), 2874-2886.
5. Werther, J.; Ogada, T., Sewage sludge combustion. *Progress in Energy and Combustion Science* 1999, 25, (1), 55-116.
6. Jenkins, B. M.; Baxter, L. L.; Miles, T. R.; Miles, T. R., Combustion properties of biomass. *Fuel Processing Technology* 1998, 54, (1), 17-46.
7. Frank, A. W., *Chemistry of Plant Phosphorus Compounds*. Elsevier: Oxford, 2013.
8. Uchimiya, M.; Hiradate, S., Pyrolysis Temperature-Dependent Changes in Dissolved Phosphorus Speciation of Plant and Manure Biochars. *Journal of Agricultural and Food Chemistry* 2014, 62, (8), 1802-1809.
9. Kanno, S.; Cuyas, L.; Javot, H.; Bligny, R.; Gout, E.; Dartevelle, T.; Hanchi, M.; Nakanishi, T. M.; Thibaud, M.-C.; Nussaume, L., Performance and Limitations of Phosphate Quantification: Guidelines for Plant Biologists. *Plant and Cell Physiology* 2016, 57, (4), 690-706.
10. Wu, H.; Hayashi, J.-i.; Chiba, T.; Takarada, T.; Li, C.-Z., Volatilisation and catalytic effects of alkali and alkaline earth metallic species during the pyrolysis and gasification of Victorian brown coal. Part V. Combined effects of Na concentration and char structure on char reactivity. *Fuel* 2004, 83, (1), 23-30.
11. Wu, H.; Yip, K.; Tian, F.; Xie, Z.; Li, C.-Z., Evolution of Char Structure during the Steam Gasification of Biochars Produced from the Pyrolysis of Various Mallee Biomass Components. *Industrial & Engineering Chemistry Research* 2009, 48, (23), 10431-10438.
12. Liaw, S. B.; Deng, C.; Wu, H., A Novel Two-Stage Alumina Reactor System for Burning Volatiles Generated in Situ from Biosolid: Effect of Pyrolysis Temperature and Combustion Conditions on PM<sub>1</sub> Emission. *Energy & Fuels* 2018, 32, (9), 9438-9447.
13. Matinde, E.; Sasaki, Y.; Hino, M., Phosphorus Gasification from Sewage Sludge

- during Carbothermic Reduction. *Journal of the Iron and Steel Institute of Japan* 2008, 48, (7), 912-917.
14. Robinson, J. S.; Baumann, K.; Hu, Y.; Hagemann, P.; Kebelmann, L.; Leinweber, P., Phosphorus transformations in plant-based and bio-waste materials induced by pyrolysis. *Ambio* 2018, 47, (1), 73-82.
15. Wu, H.; Quyn, D. M.; Li, C.-Z., Volatilisation and catalytic effects of alkali and alkaline earth metallic species during the pyrolysis and gasification of Victorian brown coal. Part III. The importance of the interactions between volatiles and char at high temperature. *Fuel* 2002, 81, (8), 1033-1039.
16. Wu, H.; Li, X.; Hayashi, J.-i.; Chiba, T.; Li, C.-Z., Effects of volatile-char interactions on the reactivity of chars from NaCl-loaded Loy Yang brown coal. *Fuel* 2005, 84, (10), 1221-1228.
17. Zhang, S.; Min, Z.; Tay, H.-L.; Asadullah, M.; Li, C.-Z., Effects of volatile-char interactions on the evolution of char structure during the gasification of Victorian brown coal in steam. *Fuel* 2011, 90, (4), 1529-1535.
18. Li, X.; Wu, H.; Hayashi, J.-i.; Li, C.-Z., Volatilisation and catalytic effects of alkali and alkaline earth metallic species during the pyrolysis and gasification of Victorian brown coal. Part VI. Further investigation into the effects of volatile-char interactions. *Fuel* 2004, 83, (10), 1273-1279.
19. Gao, X.; Wu, H., Combustion of Volatiles Produced in Situ from the Fast Pyrolysis of Woody Biomass: Direct Evidence on Its Substantial Contribution to Submicrometer Particle (PM<sub>1</sub>) Emission. *Energy & Fuels* 2011, 25, (9), 4172-4181.
20. Liaw, S. B.; Wu, H., High-Phosphorus Fuel Combustion: Effect of Oxyfuel Conditions on PM<sub>10</sub> Emission from Homo- and Heterogeneous Phases. *Energy & Fuels* 2017, 31, (3), 2317-2323.
21. Zhang, L.; Ninomiya, Y., Transformation of phosphorus during combustion of coal and sewage sludge and its contributions to PM<sub>10</sub>. *Proceedings of the Combustion Institute* 2007, 31, (2), 2847-2854.
22. Linak, W. P.; Yoo, J.-I.; Wasson, S. J.; Zhu, W.; Wendt, J. O. L.; Huggins, F. E.; Chen, Y.; Shah, N.; Huffman, G. P.; Gilmour, M. I., Ultrafine ash aerosols from coal combustion: Characterization and health effects. *Proceedings of the Combustion Institute* 2007, 31, (2), 1929-1937.
23. Liaw, S. B.; Rahim, M. U.; Wu, H., Trace Elements Release and Particulate Matter Emission during the Combustion of Char and Volatiles from In Situ Biosolid Fast Pyrolysis. *Energy & Fuels* 2016, 30, (7), 5766-5771.
24. Gao, X.; Wu, H., Biochar as a Fuel: 4. Emission Behavior and Characteristics of PM<sub>1</sub> and PM<sub>10</sub> from the Combustion of Pulverized Biochar in a Drop-Tube Furnace. *Energy & Fuels* 2011, 25, (6), 2702-2710.
25. Wall, T.; Liu, Y.; Spero, C.; Elliott, L.; Khare, S.; Rathnam, R.; Zeenathal, F.; Moghtaderi, B.; Buhre, B.; Sheng, C.; Gupta, R.; Yamada, T.; Makino, K.; Yu, J., An overview on oxyfuel coal combustion—State of the art research and technology development. *Chemical Engineering Research and Design* 2009, 87, (8), 1003-1016.

26. Boström, D.; Eriksson, G.; Boman, C.; Öhman, M., Ash Transformations in Fluidized-bed Combustion of Rapeseed Meal. *Energy & Fuels* 2009, 23, (5), 2700-2706.
27. Boström, D.; Grimm, A.; Boman, C.; Björnbom, E.; Öhman, M., Influence of Kaolin and Calcite Additives on Ash Transformations in Small-Scale Combustion of Oat. *Energy & Fuels* 2009, 23, (10), 5184-5190.
28. Bäfver, L. S.; Rönnbäck, M.; Leckner, B.; Claesson, F.; Tullin, C., Particle emission from combustion of oat grain and its potential reduction by addition of limestone or kaolin. *Fuel Processing Technology* 2009, 90, (3), 353-359.
29. Lindström, E.; Sandström, M.; Boström, D.; Öhman, M., Slagging Characteristics during Combustion of Cereal Grains Rich in Phosphorus. *Energy & Fuels* 2007, 21, (2), 710-717.
30. Broström, M.; Kassman, H.; Helgesson, A.; Berg, M.; Andersson, C.; Backman, R.; Nordin, A., Sulfation of corrosive alkali chlorides by ammonium sulfate in a biomass fired CFB boiler. *Fuel Processing Technology* 2007, 88, (11), 1171-1177.
31. Grimm, A.; Skoglund, N.; Boström, D.; Öhman, M., Bed Agglomeration Characteristics in Fluidized Quartz Bed Combustion of Phosphorus-Rich Biomass Fuels. *Energy & Fuels* 2011, 25, (3), 937-947.
32. Leckner, B.; Åmand, L. E.; Lücke, K.; Werther, J., Gaseous emissions from co-combustion of sewage sludge and coal/wood in a fluidized bed. *Fuel* 2004, 83, (4), 477-486.
33. Banks, S. W.; Nowakowski, D. J.; Bridgwater, A. V., Impact of Potassium and Phosphorus in Biomass on the Properties of Fast Pyrolysis Bio-oil. *Energy & Fuels* 2016, 30, (10), 8009-8018.
34. Mohan, D.; Pittman, C. U.; Steele, P. H., Pyrolysis of Wood/Biomass for Bio-oil: A Critical Review. *Energy & Fuels* 2006, 20, (3), 848-889.
35. Asadullah, M.; Zhang, S.; Min, Z.; Yimsiri, P.; Li, C.-Z., Effects of biomass char structure on its gasification reactivity. *Bioresource Technology* 2010, 101, (20), 7935-7943.
36. Cetin, E.; Gupta, R.; Moghtaderi, B., Effect of pyrolysis pressure and heating rate on radiata pine char structure and apparent gasification reactivity. *Fuel* 2005, 84, (10), 1328-1334.
37. Huang, Y.; Yin, X.; Wu, C.; Wang, C.; Xie, J.; Zhou, Z.; Ma, L.; Li, H., Effects of metal catalysts on CO<sub>2</sub> gasification reactivity of biomass char. *Biotechnology Advances* 2009, 27, (5), 568-572.
38. Okumura, Y.; Hanaoka, T.; Sakanishi, K., Effect of pyrolysis conditions on gasification reactivity of woody biomass-derived char. *Proceedings of the Combustion Institute* 2009, 32, (2), 2013-2020.
39. Feng, Y.; Ma, K.; Yu, T.; Bai, S.; Pei, D.; Bai, T.; Zhang, Q.; Yin, L.; Hu, Y.; Chen, D., Phosphorus Transformation in Hydrothermal Pretreatment and Steam Gasification of Sewage Sludge. *Energy & Fuels* 2018, 32, (8), 8545-8551.
40. Feng, W.; Zhu, Y.; Wu, F.; He, Z.; Zhang, C.; Giesy, J. P., Forms and Lability of

- Phosphorus in Algae and Aquatic Macrophytes Characterized by Solution  $^{31}\text{P}$  NMR Coupled with Enzymatic Hydrolysis. *Scientific Reports* 2016, 6, 37164.
41. Rulkens, W., Sewage Sludge as a Biomass Resource for the Production of Energy: Overview and Assessment of the Various Options. *Energy & Fuels* 2008, 22, (1), 9-15.
42. Zhu, Y.; Wu, F.; He, Z.; Guo, J.; Qu, X.; Xie, F.; Giesy, J. P.; Liao, H.; Guo, F., Characterization of Organic Phosphorus in Lake Sediments by Sequential Fractionation and Enzymatic Hydrolysis. *Environmental Science & Technology* 2013, 47, (14), 7679-7687.
43. Vervaeke, P.; Tack, F. M. G.; Navez, F.; Martin, J.; Verloo, M. G.; Lust, N., Fate of heavy metals during fixed bed downdraft gasification of willow wood harvested from contaminated sites. *Biomass and Bioenergy* 2006, 30, (1), 58-65.
44. Stasta, P.; Boran, J.; Bebar, L.; Stehlik, P.; Oral, J., Thermal processing of sewage sludge. *Applied Thermal Engineering* 2006, 26, (13), 1420-1426.
45. Hirata, T.; Inoue, M.; Fukui, Y., Pyrolysis and combustion toxicity of wood treated with CCA. *Wood Science and Technology* 1992, 27, (1), 35-47.
46. Kakitani, T.; Hata, T.; Kajimoto, T.; Imamura, Y., Designing a purification process for chromium-, copper- and arsenic-contaminated wood. *Waste Management* 2006, 26, (5), 453-458.
47. Stals, M.; Thijssen, E.; Vangronsveld, J.; Carleer, R.; Schreurs, S.; Yperman, J., Flash pyrolysis of heavy metal contaminated biomass from phytoremediation: Influence of temperature, entrained flow and wood/leaves blended pyrolysis on the behaviour of heavy metals. *Journal of Analytical and Applied Pyrolysis* 2010, 87, (1), 1-7.
48. Fytili, D.; Zabaniotou, A., Utilization of sewage sludge in EU application of old and new methods—A review. *Renewable and sustainable energy reviews* 2008, 12, (1), 116-140.
49. Schmidt, G.; Thannhauser, S. J., A method for the determination of desoxyribonucleic acid, ribonucleic acid, and phosphoproteins in animal tissues. *Journal of Biological Chemistry* 1945, 161, 83-89.
50. Waki, M.; Tokutomi, T.; Yokoyama, H.; Tanaka, Y., Nitrogen removal from animal waste treatment water by anammox enrichment. *Bioresource Technology* 2007, 98, (14), 2775-2780.
51. Psomopoulos, C. S.; Bourka, A.; Themelis, N. J., Waste-to-energy: A review of the status and benefits in USA. *Waste Management* 2009, 29, (5), 1718-1724.
52. Hill, D. D.; Owens, W. E.; Tchounwou, P. B., Impact of Animal Waste Application on Runoff Water Quality in Field Experimental Plots. *International Journal of Environmental Research and Public Health* 2005, 2, (2), 314.
53. Sato, S.; Solomon, D.; Hyland, C.; Ketterings, Q. M.; Lehmann, J., Phosphorus Speciation in Manure and Manure-Amended Soils Using XANES Spectroscopy. *Environmental Science & Technology* 2005, 39, (19), 7485-7491.
54. Holm-Nielsen, J. B.; Al Seadi, T.; Oleskowicz-Popiel, P., The future of anaerobic digestion and biogas utilization. *Bioresource Technology* 2009, 100, (22), 5478-5484.

55. Demirbas, A., Waste management, waste resource facilities and waste conversion processes. *Energy Conversion and Management* 2011, 52, (2), 1280-1287.
56. Beck, J.; Brandenstein, J.; Unterberger, S.; Hein, K. R. G., Effects of sewage sludge and meat and bone meal Co-combustion on SCR catalysts. *Applied Catalysis B: Environmental* 2004, 49, (1), 15-25.
57. Beck, J.; Unterberger, S., The behaviour of phosphorus in the flue gas during the combustion of high-phosphate fuels. *Fuel* 2006, 85, (10), 1541-1549.
58. Toftegaard, M. B.; Brix, J.; Jensen, P. A.; Glarborg, P.; Jensen, A. D., Oxy-fuel combustion of solid fuels. *Progress in Energy and Combustion Science* 2010, 36, (5), 581-625.
59. Rabaçal, M.; Pereira, S.; Costa, M., Review of Pulverized Combustion of Non-Woody Residues. *Energy & Fuels* 2018, 32, (4), 4069-4095.
60. Otero, M.; Calvo, L. F.; Gil, M. V.; García, A. I.; Morán, A., Co-combustion of different sewage sludge and coal: A non-isothermal thermogravimetric kinetic analysis. *Bioresource Technology* 2008, 99, (14), 6311-6319.
61. Gao, X.; Wu, H., Effect of Sampling Temperature on the Properties of Inorganic Particulate Matter Collected from Biomass Combustion in a Drop-Tube Furnace. *Energy & Fuels* 2010, 24, (8), 4571-4580.
62. Grimm, A.; Skoglund, N.; Boström, D.; Boman, C.; Öhman, M., Influence of Phosphorus on Alkali Distribution during Combustion of Logging Residues and Wheat Straw in a Bench-Scale Fluidized Bed. *Energy & Fuels* 2012, 26, (5), 3012-3023.
63. Castellino, F.; Rasmussen, S. B.; Jensen, A. D.; Johnsson, J. E.; Fehrmann, R., Deactivation of vanadia-based commercial SCR catalysts by polyphosphoric acids. *Applied Catalysis B: Environmental* 2008, 83, (1), 110-122.
64. Yang, N.-z.; Guo, R.-t.; Wang, Q.-s.; Pan, W.-g.; Chen, Q.-l.; Lu, C.-z.; Wang, S.-x., Deactivation of Mn/TiO<sub>2</sub> catalyst for NH<sub>3</sub>-SCR reaction: effect of phosphorous. *RSC Advances* 2016, 6, (14), 11226-11232.
65. Conley, D. J.; Paerl, H. W.; Howarth, R. W.; Boesch, D. F.; Seitzinger, S. P.; Havens, K. E.; Lancelot, C.; Likens, G. E., Controlling Eutrophication: Nitrogen and Phosphorus. *Science* 2009, 323, (5917), 1014-1015.
66. Zhang, Q.; Liu, H.; Li, W.; Xu, J.; Liang, Q., Behavior of Phosphorus during Co-gasification of Sewage Sludge and Coal. *Energy & Fuels* 2012, 26, (5), 2830-2836.
67. Ninomiya, Y.; Zhang, L.; Sakano, T.; Kanaoka, C.; Masui, M., Transformation of mineral and emission of particulate matters during co-combustion of coal with sewage sludge. *Fuel* 2004, 83, (6), 751-764.
68. Fernandes, U.; Costa, M., Formation of Fine Particulate Matter in a Domestic Pellet-Fired Boiler. *Energy & Fuels* 2013, 27, (2), 1081-1092.
69. Pons Jr, W. A.; Guthrie, J. D., Determination of Inorganic Phosphorus in Plant Materials. *Industrial & Engineering Chemistry Analytical Edition* 1946, 18, (3), 184-186.
70. Van Wazer, J. R.; Griffith, E. J., Structure and Properties of the Condensed

- Phosphates. X. General Structural Theory. *Journal of the American Chemical Society* 1955, 77, (23), 6140-6144.
71. McCormick, L. H.; Borden, F. Y., The Occurrence of Aluminum-Phosphate Precipitate in Plant Roots<sup>1</sup>. *Soil Science Society of America Journal* 1974, 38, (6), 931-934.
72. Radev, L.; Hristov, V.; Michailova, I.; Samuneva, B., Sol-gel bioactive glass-ceramics Part I: Calcium phosphate silicate/wollastonite glass-ceramics. In *Open Chemistry*, 2009; Vol. 7, p 317.
73. Aminot, A.; K erouel, R., An automated photo-oxidation method for the determination of dissolved organic phosphorus in marine and fresh water. *Marine Chemistry* 2001, 76, (1), 113-126.
74. Seiter, J. M.; Staats-Borda, K. E.; Ginder-Vogel, M.; Sparks, D. L., XANES Spectroscopic Analysis of Phosphorus Speciation in Alum-Amended Poultry Litter. *Journal of Environmental Quality* 2008, 37, (2), 477-485.
75. Huynen, L.; Lambert, D. M., A Concentrated Hydrochloric Acid-based Method for Complete Recovery of DNA from Bone. *Journal of Forensic Sciences* 2015, 60, (6), 1553-1557.
76. Cho, G.; Wu, Y.; Ackerman, J. L., Detection of Hydroxyl Ions in Bone Mineral by Solid-State NMR Spectroscopy. *Science* 2003, 300, (5622), 1123-1127.
77. Peterson, G. L., A simplified method for analysis of inorganic phosphate in the presence of interfering substances. *Analytical Biochemistry* 1978, 84, (1), 164-172.
78. Goldenberg, H.; Fernandez, A., Simplified Method for the Estimation of Inorganic Phosphorus in Body Fluids. *Clinical Chemistry* 1966, 12, (12), 871-882.
79. King, E. J., The colorimetric determination of phosphorus. *Biochemical Journal* 1932, 26, (2), 292-297.
80. Zinzadze, C., Colorimetric Methods for the Determination of Phosphorus. *Industrial & Engineering Chemistry Analytical Edition* 1935, 7, (4), 227-230.
81. Sowden, F. J., Effects of silicon on automated methods for the determination of phosphate in water. *Canadian Journal of Soil Science* 1972, 52, (2), 237-243.
82. Toor, G. S.; Hunger, S.; Peak, J. D.; Sims, J. T.; Sparks, D. L., Advances in the Characterization of Phosphorus in Organic Wastes: Environmental and Agronomic Applications. In *Advances in Agronomy*, Academic Press: 2006; Vol. 89, pp 1-72.
83. Thomson-Bulldis, A.; Karl, D., Application of a novel method for phosphorus determinations in the oligotrophic North Pacific Ocean. *Limnology and Oceanography* 1998, 43, (7), 1565-1577.
84. Cade-Menun, B. J., Characterizing phosphorus in environmental and agricultural samples by <sup>31</sup>P nuclear magnetic resonance spectroscopy. *Talanta* 2005, 66, (2), 359-371.
85. Feng, W.; Zhu, Y.; Wu, F.; Meng, W.; Giesy, J. P.; He, Z.; Song, L.; Fan, M., Characterization of phosphorus forms in lake macrophytes and algae by solution <sup>31</sup>P nuclear magnetic resonance spectroscopy. *Environmental Science and Pollution Research* 2016, 23, (8), 7288-7297.

86. Turner, B. L.; Newman, S.; Newman, J. M., Organic Phosphorus Sequestration in Subtropical Treatment Wetlands. *Environmental Science & Technology* 2006, 40, (3), 727-733.
87. Darch, T.; Blackwell, M. S. A.; Chadwick, D.; Haygarth, P. M.; Hawkins, J. M. B.; Turner, B. L., Assessment of bioavailable organic phosphorus in tropical forest soils by organic acid extraction and phosphatase hydrolysis. *Geoderma* 2016, 284, 93-102.
88. He, Z.; Griffin, T. S.; Honeycutt, C. W., Enzymatic Hydrolysis of Organic Phosphorus in Swine Manure and Soil *Journal of Environmental Quality* 2004, 33, (1), 367-372.
89. Ruban, V.; López-Sánchez, J. F.; Pardo, P.; Rauret, G.; Muntau, H.; Quevauviller, P., Harmonized protocol and certified reference material for the determination of extractable contents of phosphorus in freshwater sediments – A synthesis of recent works. *Fresenius' Journal of Analytical Chemistry* 2001, 370, (2), 224-228.
90. Ruban, V.; Lopez-Sanchez, J.; Pardo, P.; Rauret, G.; Muntau, H.; Quevauviller, P., Selection and evaluation of sequential extraction procedures for the determination of phosphorus forms in lake sediment. *Journal of Environmental Monitoring* 1999, 1, (1), 51-56.
91. González Medeiros, J. J.; Pérez Cid, B.; Fernández Gómez, E., Analytical phosphorus fractionation in sewage sludge and sediment samples. *Analytical and Bioanalytical Chemistry* 2005, 381, (4), 873-878.
92. Ruban, V.; López-Sánchez, J. F.; Pardo, P.; Rauret, G.; Muntau, H.; Quevauviller, P., Development of a harmonised phosphorus extraction procedure and certification of a sediment reference material. *Journal of Environmental Monitoring* 2001, 3, (1), 121-125.
93. Klein, R. M., Nitrogen and Phosphorus Fractions, Respiration, and Structure of Normal and Crown Gall Tissues of Tomato. *Plant Physiology* 1952, 27, (2), 335-354.
94. Bielecki, R. L.; Young, R. E., Extraction and separation of phosphate esters from plant tissues. *Analytical Biochemistry* 1963, 6, (1), 54-68.
95. Hedley, M. J.; Stewart, J. W. B.; Chauhan, B. S., Changes in Inorganic and Organic Soil Phosphorus Fractions Induced by Cultivation Practices and by Laboratory Incubations. *Soil Science Society of America Journal* 1982, 46, (5), 970-976.
96. Bielecki, R. L., Levels of Phosphate Esters in Spirodela. *Plant Physiology* 1968, 43, (8), 1297-1308.
97. Bielecki, R. L., The problem of halting enzyme action when extracting plant tissues. *Analytical Biochemistry* 1964, 9, (4), 431-442.
98. Bligh, E. G.; Dyer, W. J., A rapid method of total lipid extraction and purification. *Canadian Journal of Biochemistry and Physiology* 1959, 37, (8), 911-917.
99. Floch, J., A simple method for the isolation and purification of total lipids from animal tissues. *The Journal of Biological Chemistry* 1957, 226, 497-509.
100. Miyata, K.; Hattori, A., A simple fractionation method for determination of phosphorus components in phytoplankton: Application to natural populations of phytoplankton in summer surface waters of Tokyo Bay. *Journal of Oceanography*



- 1986, 42, (4), 255-265.
101. Wang, X.; Jin, Y.; Wang, Z.; Mahar, R. B.; Nie, Y., A research on sintering characteristics and mechanisms of dried sewage sludge. *Journal of Hazardous Materials* 2008, 160, (2), 489-494.
102. Li, C.-Z., Importance of volatile–char interactions during the pyrolysis and gasification of low-rank fuels – A review. *Fuel* 2013, 112, 609-623.
103. Keown, D. M.; Hayashi, J.-i.; Li, C.-Z., Effects of volatile–char interactions on the volatilisation of alkali and alkaline earth metallic species during the pyrolysis of biomass. *Fuel* 2008, 87, (7), 1187-1194.
104. Rahim, M. U.; Gao, X.; Garcia-Perez, M.; Li, Y.; Wu, H., Release of Chlorine during Mallee Bark Pyrolysis. *Energy & Fuels* 2013, 27, (1), 310-317.
105. Lu, L.; Kong, C.; Sahajwalla, V.; Harris, D., Char structural ordering during pyrolysis and combustion and its influence on char reactivity. *Fuel* 2002, 81, (9), 1215-1225.
106. Pijolat, M.; Favergeon, L., Chapter 5 - Kinetics and Mechanisms of Solid-Gas Reactions. In *Handbook of Thermal Analysis and Calorimetry*, Vyazovkin, S.; Koga, N.; Schick, C., Eds. Elsevier Science B.V.: 2018; Vol. 6, pp 173-212.
107. Xu, Z.; Sun, X.; Khaleel, M. A., A generalized kinetic model for heterogeneous gas-solid reactions. *The Journal of Chemical Physics* 2012, 137, (7), 074702.
108. Smith, I. W., The combustion rates of coal chars: A review. *Symposium (International) on Combustion* 1982, 19, (1), 1045-1065.
109. Keown, D. M.; Hayashi, J.-I.; Li, C.-Z., Drastic changes in biomass char structure and reactivity upon contact with steam. *Fuel* 2008, 87, (7), 1127-1132.
110. Shim, H.-S.; Hurt, R. H., Thermal Annealing of Chars from Diverse Organic Precursors under Combustion-like Conditions. *Energy & Fuels* 2000, 14, (2), 340-348.
111. Radovic, L. R.; Walker, P. L.; Jenkins, R. G., Importance of catalyst dispersion in the gasification of lignite chars. *Journal of Catalysis* 1983, 82, (2), 382-394.
112. Senneca, O.; Salatino, P.; Masi, S., The influence of char surface oxidation on thermal annealing and loss of combustion reactivity. *Proceedings of the Combustion Institute* 2005, 30, (2), 2223-2230.
113. Cetin, E.; Moghtaderi, B.; Gupta, R.; Wall, T. F., Influence of pyrolysis conditions on the structure and gasification reactivity of biomass chars. *Fuel* 2004, 83, (16), 2139-2150.
114. Yip, K.; Xu, M.; Li, C.-Z.; Jiang, S. P.; Wu, H., Biochar as a Fuel: 3. Mechanistic Understanding on Biochar Thermal Annealing at Mild Temperatures and Its Effect on Biochar Reactivity. *Energy & Fuels* 2011, 25, (1), 406-414.
115. Nzihou, A.; Stanmore, B.; Sharrock, P., A review of catalysts for the gasification of biomass char, with some reference to coal. *Energy* 2013, 58, 305-317.
116. Mi, J.; Wang, N.; Wang, M.; Huo, P.; Liu, D., Investigation on the catalytic effects of AAEM during steam gasification and the resultant char reactivity in oxygen using Shengli lignite at different forms. *International Journal of Coal Science & Technology* 2015, 2, (3), 223-231.

117. Samaras, P.; Diamadopoulos, E.; Sakellaropoulos, G. P., The effect of mineral matter and pyrolysis conditions on the gasification of Greek lignite by carbon dioxide. *Fuel* 1996, 75, (9), 1108-1114.
118. Quyn, D. M.; Wu, H.; Hayashi, J.-i.; Li, C.-Z., Volatilisation and catalytic effects of alkali and alkaline earth metallic species during the pyrolysis and gasification of Victorian brown coal. Part IV. Catalytic effects of NaCl and ion-exchangeable Na in coal on char reactivity. *Fuel* 2003, 82, (5), 587-593.
119. Krerkkaiwan, S.; Fushimi, C.; Yamamoto, H.; Tsutsumi, A.; Kuchonthara, P., Influences of heating rate during coal char preparation and AAEMs on volatile–char interaction with different sources of biomass volatile. *Fuel Processing Technology* 2014, 119, 10-18.
120. Nowakowski, D. J.; Woodbridge, C. R.; Jones, J. M., Phosphorus catalysis in the pyrolysis behaviour of biomass. *Journal of Analytical and Applied Pyrolysis* 2008, 83, (2), 197-204.
121. Yao, W.; Li, J.; Feng, Y.; Wang, W.; Zhang, X.; Chen, Q.; Komarneni, S.; Wang, Y., Thermally stable phosphorus and nickel modified ZSM-5 zeolites for catalytic co-pyrolysis of biomass and plastics. *RSC Advances* 2015, 5, (39), 30485-30494.
122. Stevens, R.; van Es, D. S.; Bezemer, R.; Kranenbarg, A., The structure–activity relationship of fire retardant phosphorus compounds in wood. *Polymer Degradation and Stability* 2006, 91, (4), 832-841.
123. Dobele, G.; Rossinskaja, G.; Telysheva, G.; Meier, D.; Faix, O., Cellulose dehydration and depolymerization reactions during pyrolysis in the presence of phosphoric acid. *Journal of Analytical and Applied Pyrolysis* 1999, 49, (1), 307-317.
124. Puziy, A. M.; Poddubnaya, O. I.; Socha, R. P.; Gurgul, J.; Wisniewski, M., XPS and NMR studies of phosphoric acid activated carbons. *Carbon* 2008, 46, (15), 2113-2123.
125. Rosas, J. M.; Ruiz-Rosas, R.; Rodríguez-Mirasol, J.; Cordero, T., Kinetic study of the oxidation resistance of phosphorus-containing activated carbons. *Carbon* 2012, 50, (4), 1523-1537.
126. Valero-Romero, M. J.; García-Mateos, F. J.; Rodríguez-Mirasol, J.; Cordero, T., Role of surface phosphorus complexes on the oxidation of porous carbons. *Fuel Processing Technology* 2017, 157, 116-126.
127. Qian, T.-T.; Jiang, H., Migration of Phosphorus in Sewage Sludge during Different Thermal Treatment Processes. *ACS Sustainable Chemistry & Engineering* 2014, 2, (6), 1411-1419.
128. Huang, R.; Tang, Y., Evolution of phosphorus complexation and mineralogy during (hydro)thermal treatments of activated and anaerobically digested sludge: Insights from sequential extraction and P K-edge XANES. *Water Research* 2016, 100, 439-447.
129. Beck, J.; Müller, R.; Brandenstein, J.; Matscheko, B.; Matschke, J.; Unterberger, S.; Hein, K. R. G., The behaviour of phosphorus in flue gases from coal and secondary fuel co-combustion. *Fuel* 2005, 84, (14), 1911-1919.

130. Makoto, W.; Shoji, S.; Hajime, S., The Mechanism of the Hydrolysis of Condensed Phosphates. II. The Mechanism of the Degradation of Long-chain Polyphosphates. *Bulletin of the Chemical Society of Japan* 1975, 48, (3), 896-898.
131. Huang, R.; Tang, Y., Speciation Dynamics of Phosphorus during (Hydro)Thermal Treatments of Sewage Sludge. *Environmental Science & Technology* 2015, 49, (24), 14466-14474.
132. Uchimiya, M.; Hiradate, S.; Antal, M. J., Dissolved Phosphorus Speciation of Flash Carbonization, Slow Pyrolysis, and Fast Pyrolysis Biochars. *ACS Sustainable Chemistry & Engineering* 2015, 3, (7), 1642-1649.
133. Bruun, S.; Harmer, S. L.; Bekiaris, G.; Christel, W.; Zuin, L.; Hu, Y.; Jensen, L. S.; Lombi, E., The effect of different pyrolysis temperatures on the speciation and availability in soil of P in biochar produced from the solid fraction of manure. *Chemosphere* 2017, 169, 377-386.
134. Xu, G.; Zhang, Y.; Shao, H.; Sun, J., Pyrolysis temperature affects phosphorus transformation in biochar: Chemical fractionation and  $^{31}\text{P}$  NMR analysis. *Science of The Total Environment* 2016, 569-570, 65-72.
135. Liu, W.-J.; Zeng, F.-X.; Jiang, H.; Yu, H.-Q., Total recovery of nitrogen and phosphorus from three wetland plants by fast pyrolysis technology. *Bioresource Technology* 2011, 102, (3), 3471-3479.
136. Hossain, M. K.; Strezov, V.; Chan, K. Y.; Ziolkowski, A.; Nelson, P. F., Influence of pyrolysis temperature on production and nutrient properties of wastewater sludge biochar. *Journal of Environmental Management* 2011, 92, (1), 223-228.
137. Bourgel, C.; Véron, E.; Poirier, J.; Defoort, F.; Seiler, J.-M.; Peregrina, C., Behavior of Phosphorus and Other Inorganics during the Gasification of Sewage Sludge. *Energy & Fuels* 2011, 25, (12), 5707-5717.
138. Linak, W. P.; Wendt, J. O. L., Toxic metal emissions from incineration: Mechanisms and control. *Progress in Energy and Combustion Science* 1993, 19, (2), 145-185.
139. Quann, R. J.; Sarofim, A. F., Vaporization of refractory oxides during pulverized coal combustion. *Symposium (International) on Combustion* 1982, 19, (1), 1429-1440.
140. Zhang, L.; Ninomiya, Y., Emission of suspended  $\text{PM}_{10}$  from laboratory-scale coal combustion and its correlation with coal mineral properties. *Fuel* 2006, 85, (2), 194-203.
141. Shah, K. V.; Cieplik, M. K.; Bertrand, C. I.; van de Kamp, W. L.; Vuthaluru, H. B., Correlating the effects of ash elements and their association in the fuel matrix with the ash release during pulverized fuel combustion. *Fuel Processing Technology* 2010, 91, (5), 531-545.
142. Wang, Y.-g.; Chen, X.-j.; Yang, S.-s.; He, X.; Chen, Z.-d.; Zhang, S., Effect of steam concentration on char reactivity and structure in the presence/absence of oxygen using Shengli brown coal. *Fuel Processing Technology* 2015, 135, 174-179.
143. Christensen, K. A.; Stenholm, M.; Livbjerg, H., The formation of submicron

- aerosol particles, HCl and SO<sub>2</sub> in straw-fired boilers. *Journal of Aerosol Science* 1998, 29, (4), 421-444.
144. Wendt, J. O. L., Fundamental coal combustion mechanisms and pollutant formation in furnaces. *Progress in Energy and Combustion Science* 1980, 6, (2), 201-222.
145. Helble, J. J.; Sarofim, A. F., Influence of char fragmentation on ash particle size distributions. *Combustion and Flame* 1989, 76, (2), 183-196.
146. Baxter, L. L.; Mitchell, R. E.; Fletcher, T. H., Release of inorganic material during coal devolatilization. *Combustion and Flame* 1997, 108, (4), 494-502.
147. Smith, R. D.; Campbell, J. A.; Nielson, K. K., Characterization and formation of submicron particles in coal-fired plants. *Atmospheric Environment (1967)* 1979, 13, (5), 607-617.
148. Holve, D. J., In Situ Measurements of Flyash Formation from Pulverized Coal. *Combustion Science and Technology* 1986, 44, (5-6), 269-288.
149. Xiong, Y.; Kamal Akhtar, M.; Pratsinis, S. E., Formation of agglomerate particles by coagulation and sintering—Part II. The evolution of the morphology of aerosol-made titania, silica and silica-doped titania powders. *Journal of Aerosol Science* 1993, 24, (3), 301-313.
150. Yan, L.; Gupta, R. P.; Wall, T. F., The implication of mineral coalescence behaviour on ash formation and ash deposition during pulverised coal combustion. *Fuel* 2001, 80, (9), 1333-1340.
151. Xu, M.; Yu, D.; Yao, H.; Liu, X.; Qiao, Y., Coal combustion-generated aerosols: Formation and properties. *Proceedings of the Combustion Institute* 2011, 33, (1), 1681-1697.
152. Baxter, L. L., Char fragmentation and fly ash formation during pulverized-coal combustion. *Combustion and Flame* 1992, 90, (2), 174-184.
153. Senneca, O.; Urciuolo, M.; Chirone, R., A semidetailed model of primary fragmentation of coal. *Fuel* 2013, 104, (Supplement C), 253-261.
154. Kang, S. G.; Sarofim, A. F.; Beér, J. M., Effect of Char structure on residual ash formation during pulverized coal combustion. *Symposium (International) on Combustion* 1992, 24, (1), 1153-1159.
155. McLennan, A. R.; Bryant, G. W.; Stanmore, B. R.; Wall, T. F., Ash Formation Mechanisms during pf Combustion in Reducing Conditions. *Energy & Fuels* 2000, 14, (1), 150-159.
156. Yoshiie, R.; Tsuzuki, T.; Ueki, Y.; Nunome, Y.; Naruse, I.; Sato, N.; Ito, T.; Matsuzawa, Y.; Suda, T., Effects of coal types on ash fragmentation and coalescence behaviors in pulverized coal combustion. *Proceedings of the Combustion Institute* 2013, 34, (2), 2895-2902.
157. Anderson, P. J.; Morgan, P. L., Effects of water vapour on sintering of MgO. *Transactions of the Faraday Society* 1964, 60, (0), 930-937.
158. Wang, X.; Michael Daukoru, S.; Torkamani, S.; Wang, W.-N.; Biswas, P., Role of exhaust gas recycle on submicrometer particle formation during oxy-coal combustion.

- Proceedings of the Combustion Institute 2013, 34, (2), 3479-3487.
159. Duan, L.; Jiang, Z.; Chen, X.; Zhao, C., Investigation on water vapor effect on direct sulfation during wet-recycle oxy-coal combustion. *Applied Energy* 2013, 108, 121-127.
160. Kazanc, F.; Levendis, Y. A.; Maffei, T., Chemical Composition of Submicrometer Particulate Matter (PM1) Emitted from Combustion of Coals of Various Ranks in O<sub>2</sub>/N<sub>2</sub> and O<sub>2</sub>/CO<sub>2</sub> Environments. *Energy & Fuels* 2013, 27, (8), 4984-4998.
161. Kazanc, F.; Levendis, Y. A., Physical Properties of Particulate Matter Emitted from Combustion of Coals of Various Ranks in O<sub>2</sub>/N<sub>2</sub> and O<sub>2</sub>/CO<sub>2</sub> Environments. *Energy & Fuels* 2012, 26, (12), 7127-7139.
162. Sheng, C.; Lu, Y.; Gao, X.; Yao, H., Fine Ash Formation during Pulverized Coal Combustion A Comparison of O<sub>2</sub>/CO<sub>2</sub> Combustion versus Air Combustion. *Energy & Fuels* 2007, 21, (2), 435-440.
163. Ruscio, A.; Kazanc, F.; Levendis, Y. A., Characterization of Particulate Matter Emitted from Combustion of Various Biomasses in O<sub>2</sub>/N<sub>2</sub> and O<sub>2</sub>/CO<sub>2</sub> Environments. *Energy & Fuels* 2014, 28, (1), 685-696.
164. Zhang, L.; Jiao, F.; Binner, E.; Bhattacharya, S.; Ninomiya, Y.; Li, C.-Z., Experimental investigation of the combustion of bituminous coal in air and O<sub>2</sub>/CO<sub>2</sub> mixtures: 2. Variation of the transformation behaviour of mineral matter with bulk gas composition. *Fuel* 2011, 90, (4), 1361-1369.
165. Wen, C.; Yu, D.; Wang, J.; Wu, J.; Yao, H.; Xu, M., Effect of the Devolatilization Process on PM<sub>10</sub> Formation during Oxy-fuel Combustion of a Typical Bituminous Coal. *Energy & Fuels* 2014, 28, (9), 5682-5689.
166. Zhan, Z.; Fry, A.; Zhang, Y.; Wendt, J. O. L., Ash aerosol formation from oxy-coal combustion and its relation to ash deposit chemistry. *Proceedings of the Combustion Institute* 2015, 35, (2), 2373-2380.
167. Anthony, E. J.; Granatstein, D. L., Sulfation phenomena in fluidized bed combustion systems. *Progress in Energy and Combustion Science* 2001, 27, (2), 215-236.
168. Xu, Y.; Liu, X.; Zhou, Z.; Sheng, L.; Wang, C.; Xu, M., The role of steam in silica vaporization and ultrafine particulate matter formation during wet oxy-coal combustion. *Applied Energy* 2014, 133, (Supplement C), 144-151.
169. Wang, C.; Liu, X.; Li, D.; Wu, W.; Xu, Y.; Si, J.; Zhao, B.; Xu, M., Effect of H<sub>2</sub>O and SO<sub>2</sub> on the distribution characteristics of trace elements in particulate matter at high temperature under oxy-fuel combustion. *International Journal of Greenhouse Gas Control* 2014, 23, 51-60.
170. Jiao, F.; Chen, J.; Zhang, L.; Wei, Y.; Ninomiya, Y.; Bhattacharya, S.; Yao, H., Ash partitioning during the oxy-fuel combustion of lignite and its dependence on the recirculation of flue gas impurities (H<sub>2</sub>O, HCl and SO<sub>2</sub>). *Fuel* 2011, 90, (6), 2207-2216.
171. Jiao, F.; Zhang, L.; Yamada, N.; Sato, A.; Ninomiya, Y., Effect of HCl, SO<sub>2</sub> and H<sub>2</sub>O on the condensation of heavy metal vapors in flue gas cooling section. *Fuel*

- Processing Technology 2013, 105, 181-187.
172. Li, Q.; Meng, A.; Jia, J.; Zhang, Y., Investigation of heavy metal partitioning influenced by flue gas moisture and chlorine content during waste incineration. *Journal of Environmental Sciences* 2010, 22, (5), 760-768.
173. Zhang, M.; Gao, X.; Wu, H., A Method for the Quantification of Alkali and Alkaline Earth Metallic Species in Bioslurry Fuels. *Energy & Fuels* 2013, 27, (11), 6823-6830.
174. E.E.J.M. Temminghoff, V. J. G. H., *Plant analysis procedures* (2nd ed.), Kluwer Academic Publishers, Netherlands 2004.
175. Rahim, M. U.; Gao, X.; Wu, H., Determination of chlorine in solid fuels using an improved Eschka method. *Fuel* 2014, 129, 314-317.
176. Zhang, J.; You, C., Water Holding Capacity and Absorption Properties of Wood Chars. *Energy & Fuels* 2013, 27, (5), 2643-2648.
177. Wu, H.; Bryant, G.; Benfell, K.; Wall, T., An Experimental Study on the Effect of System Pressure on Char Structure of an Australian Bituminous Coal. *Energy & Fuels* 2000, 14, (2), 282-290.
178. Capablo, J.; Jensen, P. A.; Pedersen, K. H.; Hjuler, K.; Nikolaisen, L.; Backman, R.; Frandsen, F., Ash Properties of Alternative Biomass. *Energy & Fuels* 2009, 23, (4), 1965-1976.
179. Hou, M.; Liu, J.; Guo, S.; Yang, J.; Wang, C.; Xia, Y., Enhanced electrochemical performance of Li-rich layered cathode materials by surface modification with P2O5. *Electrochemistry Communications* 2014, 49, 83-87.
180. Armstrong, F. A. J.; Williams, P. M.; Strickland, J. D. H., Photo-oxidation of Organic Matter in Sea Water by Ultra-violet Radiation, Analytical and Other Applications. *Nature* 1966, 211, 481.
181. Martin, E. M.; Morton, R. K., The chemical composition of microsomes and mitochondria from silver beet. *The Biochemical journal* 1956, 64, (2), 221-235.
182. Takahashi, M.; Kato, S.; Iwasaki, S.; Miura, K., Technology for recovering phosphorus salt and zeolite from incinerated ash of sewage treatment sludge. *Journal of Advanced Science* 2001, 13, (3), 163-166.
183. Tada, C.; Nishimura, O.; Itayama, T.; Inamori, Y.; Matsumura, M.; Sudo, R., The Influence of Materials Released from Lake Sediment on The Growth of Three Kinds of Algae. *Japanese Journal of Water Treatment Biology* 2001, 37, (4), 161-172.
184. Tissari, J.; Sippula, O.; Kouki, J.; Vuorio, K.; Jokiniemi, J., Fine Particle and Gas Emissions from the Combustion of Agricultural Fuels Fired in a 20 kW Burner. *Energy & Fuels* 2008, 22, (3), 2033-2042.
185. Senneca, O.; Salatino, P.; Menghini, D., The influence of thermal annealing on oxygen uptake and combustion rates of a bituminous coal char. *Proceedings of the Combustion Institute* 2007, 31, (2), 1889-1895.
186. Liaw, S. B.; Wu, H., Leaching Characteristics of Organic and Inorganic Matter from Biomass by Water: Differences between Batch and Semi-continuous Operations. *Industrial & Engineering Chemistry Research* 2013, 52, (11), 4280-4289.

187. Veiga, N.; Torres, J.; Domínguez, S.; Mederos, A.; Irvine, R. F.; Díaz, A.; Kremer, C., The behaviour of myo-inositol hexakisphosphate in the presence of magnesium(II) and calcium(II): protein-free soluble InsP<sub>6</sub> is limited to 49  $\mu$ M under cytosolic/nuclear conditions. *Journal of inorganic biochemistry* 2006, 100, (11), 1800-1810.
188. Li, R.; Yin, J.; Wang, W.; Li, Y.; Zhang, Z., Transformation of phosphorus during drying and roasting of sewage sludge. *Waste Management* 2014, 34, (7), 1211-1216.
189. Jagtoyen, M.; Derbyshire, F., Activated carbons from yellow poplar and white oak by H<sub>3</sub>PO<sub>4</sub> activation. *Carbon* 1998, 36, (7), 1085-1097.
190. Laurendeau, N. M., Heterogeneous kinetics of coal char gasification and combustion. *Progress in Energy and Combustion Science* 1978, 4, (4), 221-270.
191. Banks, S. W.; Nowakowski, D. J.; Bridgwater, A. V., Impact of Potassium and Phosphorus in Biomass on the Properties of Fast Pyrolysis Bio-oil. *Energy Fuels* 2016, 30, (10), 8009-8018.
192. Wu, X.; Radovic, L. R., Inhibition of catalytic oxidation of carbon/carbon composites by phosphorus. *Carbon* 2006, 44, (1), 141-151.
193. Li, X.; Hayashi, J.-i.; Li, C.-Z., FT-Raman spectroscopic study of the evolution of char structure during the pyrolysis of a Victorian brown coal. *Fuel* 2006, 85, (12), 1700-1707.
194. Scott, S. A.; Davidson, J. F.; Dennis, J. S.; Fennell, P. S.; Hayhurst, A. N., The rate of gasification by CO<sub>2</sub> of chars from waste. *Proceedings of the Combustion Institute* 2005, 30, (2), 2151-2159.
195. Ballester, J.; Jiménez, S., Kinetic parameters for the oxidation of pulverised coal as measured from drop tube tests. *Combustion and Flame* 2005, 142, (3), 210-222.
196. Kelemen, S. R.; Freund, H., O<sub>2</sub> oxidation studies of the edge surface of graphite. *Carbon* 1985, 23, (6), 619-625.
197. Xu, Y.-J.; Li, J.-Q., The interaction of molecular oxygen with active sites of graphite: a theoretical study. *Chemical physics letters* 2004, 400, (4), 406-412.
198. Buhre, B. J. P.; Elliott, L. K.; Sheng, C. D.; Gupta, R. P.; Wall, T. F., Oxy-fuel combustion technology for coal-fired power generation. *Progress in Energy and Combustion Science* 2005, 31, (4), 283-307.
199. Riaza, J.; Álvarez, L.; Gil, M. V.; Pevida, C.; Pis, J. J.; Rubiera, F., Effect of oxy-fuel combustion with steam addition on coal ignition and burnout in an entrained flow reactor. *Energy* 2011, 36, (8), 5314-5319.
200. Gao, X.; Chen, Y.; Sheng, C.; Wu, H., Interaction between sodium vapor and reactor wall during biomass combustion and its influence on measurement of particulate matter emission. *Fuel* 2016, 165, (Supplement C), 260-263.
201. Kulmala, M.; Laaksonen, A., Binary nucleation of water–sulfuric acid system: Comparison of classical theories with different H<sub>2</sub>SO<sub>4</sub> saturation vapor pressures. *The Journal of Chemical Physics* 1990, 93, (1), 696-701.
202. Borgwardt, R. H., Calcium oxide sintering in atmospheres containing water and carbon dioxide. *Industrial & Engineering Chemistry Research* 1989, 28, (4), 493-500.

203. Baxter, L. L.; Miles, T. R.; Miles, T. R.; Jenkins, B. M.; Milne, T.; Dayton, D.; Bryers, R. W.; Oden, L. L., The behavior of inorganic material in biomass-fired power boilers: field and laboratory experiences. *Fuel Processing Technology* 1998, 54, (1), 47-78.
204. Hecht, E. S.; Shaddix, C. R.; Geier, M.; Molina, A.; Haynes, B. S., Effect of CO<sub>2</sub> and steam gasification reactions on the oxy-combustion of pulverized coal char. *Combustion and Flame* 2012, 159, (11), 3437-3447.
205. Rodríguez-Reinoso, F.; Molina-Sabio, M.; González, M. T., The use of steam and CO<sub>2</sub> as activating agents in the preparation of activated carbons. *Carbon* 1995, 33, (1), 15-23.
206. Tomków, K.; Siemienińska, T.; Czechowski, F.; Jankowska, A., Formation of porous structures in activated brown-coal chars using O<sub>2</sub>, CO<sub>2</sub> and H<sub>2</sub>O as activating agents. *Fuel* 1977, 56, (2), 121-124.
207. Lu, H.; Chen, H.; Li, W.; Li, B., Transformation of arsenic in Yima coal during fluidized-bed pyrolysis. *Fuel* 2004, 83, (6), 645-650.
208. Frandsen, F.; Dam-Johansen, K.; Rasmussen, P., Trace elements from combustion and gasification of coal—An equilibrium approach. *Progress in Energy and Combustion Science* 1994, 20, (2), 115-138.
209. Liu, G.-S.; Niksa, S., Coal conversion submodels for design applications at elevated pressures. Part II. Char gasification. *Progress in Energy and Combustion Science* 2004, 30, (6), 679-717.
210. Seames, W. S.; Fernandez, A.; Wendt, J. O. L., A Study of Fine Particulate Emissions from Combustion of Treated Pulverized Municipal Sewage Sludge. *Environmental Science & Technology* 2002, 36, (12), 2772-2776.
211. van Eyk, P. J.; Ashman, P. J.; Nathan, G. J., Mechanism and kinetics of sodium release from brown coal char particles during combustion. *Combustion and Flame* 2011, 158, (12), 2512-2523.
212. Hupa, M.; Karlstrom, O.; Vainio, E., Biomass combustion technology development - It is all about chemical details. *Proceedings of the Combustion Institute* 2017, 36, (1), 113-134.
213. Nunn, T. R.; Howard, J. B.; Longwell, J. P.; Peters, W. A., Product compositions and kinetics in the rapid pyrolysis of sweet gum hardwood. *Industrial & Engineering Chemistry Process Design and Development* 1985, 24, (3), 836-844.
214. Rice, F. O., The thermal decomposition of organic compounds from the standpoint of free radicals. I. Saturated hydrocarbons. *Journal of the American Chemical Society* 1931, 53, (5), 1959-1972.
215. Boström, D.; Skoglund, N.; Grimm, A.; Boman, C.; Öhman, M.; Broström, M.; Backman, R., Ash Transformation Chemistry during Combustion of Biomass. *Energy & Fuels* 2012, 26, (1), 85-93.
216. Cheng, J.; Zhou, J.; Liu, J.; Zhou, Z.; Huang, Z.; Cao, X.; Zhao, X.; Cen, K., Sulfur removal at high temperature during coal combustion in furnaces: a review. *Progress in Energy and Combustion Science* 2003, 29, (5), 381-405.



217. Wang, J.; Tomita, A., A Chemistry on the Volatility of Some Trace Elements during Coal Combustion and Pyrolysis. *Energy & Fuels* 2003, 17, (4), 954-960.
218. Ebbinghaus, B. B., Thermodynamics of gas phase chromium species: The chromium oxides, the chromium oxyhydroxides, and volatility calculations in waste incineration processes. *Combustion and Flame* 1993, 93, (1), 119-137.
219. Wang, N.; Chen, D.; Arena, U.; He, P., Hot char-catalytic reforming of volatiles from MSW pyrolysis. *Applied Energy* 2017, 191, 111-124.
220. Liu, P.; Le, J.; Zhang, D.; Wang, S.; Pan, T., Free radical reaction mechanism on improving tar yield and quality derived from lignite after hydrothermal treatment. *Fuel* 2017, 207, 244-252.
221. Watanabe, H.; Arai, F.; Okazaki, K., Role of CO<sub>2</sub> in the CH<sub>4</sub> oxidation and H<sub>2</sub> formation during fuel-rich combustion in O<sub>2</sub>/CO<sub>2</sub> environments. *Combustion and Flame* 2013, 160, (11), 2375-2385.
222. Yip, K.; Wu, H.; Zhang, D.-k., Effect of Inherent Moisture in Collie Coal during Pyrolysis Due to in-Situ Steam Gasification. *Energy & Fuels* 2007, 21, (5), 2883-2891.
223. Pepiot-Desjardins, P.; Pitsch, H.; Malhotra, R.; Kirby, S. R.; Boehman, A. L., Structural group analysis for soot reduction tendency of oxygenated fuels. *Combustion and Flame* 2008, 154, (1), 191-205.
224. Park, W.; Park, S.; Reitz, R. D.; Kurtz, E., The effect of oxygenated fuel properties on diesel spray combustion and soot formation. *Combustion and Flame* 2017, 180, 276-283.
225. Okuno, T.; Sonoyama, N.; Hayashi, J.-i.; Li, C.-Z.; Sathe, C.; Chiba, T., Primary Release of Alkali and Alkaline Earth Metallic Species during the Pyrolysis of Pulverized Biomass. *Energy & Fuels* 2005, 19, (5), 2164-2171.
226. Yu, J.; Lucas, J. A.; Wall, T. F., Formation of the structure of chars during devolatilization of pulverized coal and its thermoproperties: A review. *Progress in Energy and Combustion Science* 2007, 33, (2), 135-170.
227. Sheng, C.; Li, Y.; Liu, X.; Yao, H.; Xu, M., Ash particle formation during O<sub>2</sub>/CO<sub>2</sub> combustion of pulverized coals. *Fuel Processing Technology* 2007, 88, (11), 1021-1028.
228. Jiménez, S.; Pérez, M.; Ballester, J., Vaporization of Trace Elements and Their Emission with Submicrometer Aerosols in Biomass Combustion. *Energy & Fuels* 2008, 22, (4), 2270-2277.

*Every reasonable effort has been made to acknowledge the owners of copyright material. I would be pleased to hear from any copyright owner who has been omitted or incorrectly acknowledged.*

## APPENDIX I: COPYRIGHT PERMISSION STATEMENTS

A. Chapter 4, reprinted with permission from (Xujun Chen, Sui Boon Liaw, and Hongwei Wu. *A New Method for Quantifying Phosphorus of Various Occurrence Forms in Solid Fuels*, *Energy & Fuels* 2019, 33, 3311-3321). Copyright (2019) American Chemical Society



The screenshot shows the Copyright Clearance Center RightsLink interface. At the top left is the Copyright Clearance Center logo. To its right is the RightsLink logo. Further right are navigation buttons for Home, Create Account, Help, and an email icon. Below the logos is the ACS Publications logo with the tagline "Most Trusted. Most Cited. Most Read." To the right of the ACS logo, the following publication details are listed:

**Title:** A New Method for Quantifying Phosphorus of Various Occurrence Forms in Solid Fuels  
**Author:** Xujun Chen, Sui Boon Liaw, Hongwei Wu  
**Publication:** Energy & Fuels  
**Publisher:** American Chemical Society  
**Date:** Mar 1, 2019  
 Copyright © 2019, American Chemical Society

On the right side of the interface, there is a LOGIN button and a text box that reads: "If you're a copyright.com user, you can login to RightsLink using your copyright.com credentials. Already a RightsLink user or want to learn more?"

## PERMISSION/LICENSE IS GRANTED FOR YOUR ORDER AT NO CHARGE

This type of permission/license, instead of the standard Terms & Conditions, is sent to you because no fee is being charged for your order. Please note the following:

- Permission is granted for your request in both print and electronic formats, and translations.
- If figures and/or tables were requested, they may be adapted or used in part.
- Please print this page for your records and send a copy of it to your publisher/graduate school.
- Appropriate credit for the requested material should be given as follows: "Reprinted (adapted) with permission from (COMPLETE REFERENCE CITATION). Copyright (YEAR) American Chemical Society." Insert appropriate information in place of the capitalized words.
- One-time permission is granted only for the use specified in your request. No additional uses are granted (such as derivative works or other editions). For any other uses, please submit a new request.

BACK

CLOSE WINDOW

Copyright © 2019 Copyright Clearance Center, Inc. All Rights Reserved. [Privacy statement](#). [Terms and Conditions](#).  
 Comments? We would like to hear from you. E-mail us at [customercare@copyright.com](mailto:customercare@copyright.com)

B. *Chapter 5*, Reprinted with permission from (Xujun Chen and Hongwei Wu. Transformation and release of phosphorus during rice bran pyrolysis: Effect of reactor configurations under various conditions, *Fuel* 2019, 255, 115755). Copyright (2019). Published by Elsevier Inc

---

Home Create Account Help 



**Title:** Transformation and release of phosphorus during rice bran pyrolysis: Effect of reactor configurations under various conditions

**Author:** Xujun Chen, Hongwei Wu

**Publication:** Fuel

**Publisher:** Elsevier

**Date:** 1 November 2019

© 2019 Elsevier Ltd. All rights reserved.

**LOGIN**

If you're a **copyright.com user**, you can login to RightsLink using your copyright.com credentials.

Already a **RightsLink user** or want to [learn more?](#)

Please note that, as the author of this Elsevier article, you retain the right to include it in a thesis or dissertation, provided it is not published commercially. Permission is not required, but please ensure that you reference the journal as the original source. For more information on this and on your other retained rights, please visit: <https://www.elsevier.com/about/our-business/policies/copyright#Author-rights>

BACKCLOSE WINDOW

Copyright © 2019 [Copyright Clearance Center, Inc.](#) All Rights Reserved. [Privacy statement](#). [Terms and Conditions](#).  
Comments? We would like to hear from you. E-mail us at [customercare@copyright.com](mailto:customercare@copyright.com)

C, Chapter 7, reprinted with permission from (Xujun Chen and Hongwei Wu. *Volatile-char interactions: Roles of in situ volatiles with distinctly-different chemistry in determining char structure and reactivity*, *Proceedings of the Combustion Institute* 2019, 37, 2749-2755). Copyright (2018) The Combustion Institute. Published by Elsevier Inc.



RightsLink®

Home

Create Account

Help



**Title:** Volatile-char interactions: Roles of in situ volatiles with distinctly-different chemistry in determining char structure and reactivity

**Author:** Xujun Chen, Hongwei Wu

**Publication:** Proceedings of the Combustion Institute

**Publisher:** Elsevier

**Date:** 2019

© 2018 The Combustion Institute. Published by Elsevier Inc. All rights reserved.

**LOGIN**

If you're a [copyright.com](#) user, you can login to RightsLink using your [copyright.com](#) credentials.

Already a [RightsLink](#) user or want to [learn more?](#)

Please note that, as the author of this Elsevier article, you retain the right to include it in a thesis or dissertation, provided it is not published commercially. Permission is not required, but please ensure that you reference the journal as the original source. For more information on this and on your other retained rights, please visit: <https://www.elsevier.com/about/our-business/policies/copyright#Author-rights>

**BACK**

**CLOSE WINDOW**

Copyright © 2019 [Copyright Clearance Center, Inc.](#) All Rights Reserved. [Privacy statement](#). [Terms and Conditions](#). Comments? We would like to hear from you. E-mail us at [customer@copyright.com](mailto:customer@copyright.com)

**D.** Chapter 8, reprinted with permission from (Xujun Chen, Sui Boon Liaw and Hongwei Wu. *Effect of water vapour on particulate matter emission during oxyfuel combustion of char and in situ volatiles generated from rapid pyrolysis of chromated-copper-arsenate-treated wood*, *Proceedings of the Combustion Institute* 2019, 37, 4319–4327). Copyright (2018) The Combustion Institute. Published by Elsevier Inc.



RightsLink®

Home

Create Account

Help



**Title:** Effect of water vapour on particulate matter emission during oxyfuel combustion of char and in situ volatiles generated from rapid pyrolysis of chromated-copper-arsenate-treated wood

**Author:** Xujun Chen, Sui Boon Liaw, Hongwei Wu

**Publication:** Proceedings of the Combustion Institute

**Publisher:** Elsevier

**Date:** 2019

© 2018 The Combustion Institute. Published by Elsevier Inc. All rights reserved.

**LOGIN**

If you're a [copyright.com user](#), you can login to RightsLink using your copyright.com credentials. Already a [RightsLink user](#) or want to [learn more?](#)

Please note that, as the author of this Elsevier article, you retain the right to include it in a thesis or dissertation, provided it is not published commercially. Permission is not required, but please ensure that you reference the journal as the original source. For more information on this and on your other retained rights, please visit: <https://www.elsevier.com/about/our-business/policies/copyright#Author-rights>

**BACK**

**CLOSE WINDOW**

Copyright © 2019 [Copyright Clearance Center, Inc.](#) All Rights Reserved. [Privacy statement](#). [Terms and Conditions](#). Comments? We would like to hear from you. E-mail us at [customercare@copyright.com](mailto:customercare@copyright.com)

E. Chapter 9, reprinted with permission from (Xujun Chen, Sui Boon Liaw and Hongwei Wu. Important role of volatile–char interactions in enhancing PM<sub>1</sub> emission during the combustion of volatiles from biosolid, *Combustion and Flame* 2017, 182, 90-101). Copyright (2017) The Combustion Institute. Published by Elsevier Inc.



RightsLink®

Home

Create Account

Help



**Title:** Important role of volatile–char interactions in enhancing PM<sub>1</sub> emission during the combustion of volatiles from biosolid

**Author:** Xujun Chen, Sui Boon Liaw, Hongwei Wu

**Publication:** Combustion and Flame

**Publisher:** Elsevier

**Date:** August 2017

© 2017 The Combustion Institute. Published by Elsevier Inc. All rights reserved.

**LOGIN**

If you're a **copyright.com** user, you can login to RightsLink using your copyright.com credentials. Already a **RightsLink** user or want to [learn more?](#)

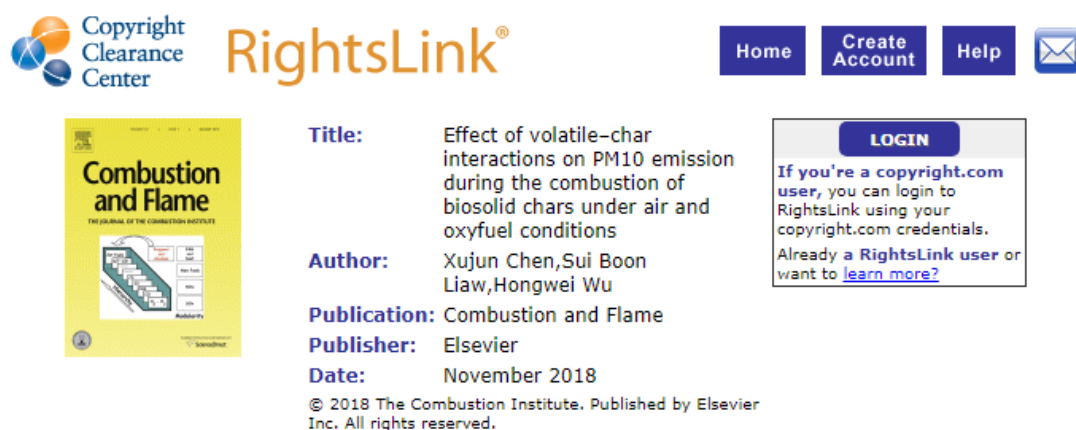
Please note that, as the author of this Elsevier article, you retain the right to include it in a thesis or dissertation, provided it is not published commercially. Permission is not required, but please ensure that you reference the journal as the original source. For more information on this and on your other retained rights, please visit: <https://www.elsevier.com/about/our-business/policies/copyright#Author-rights>

**BACK**

**CLOSE WINDOW**

Copyright © 2019 Copyright Clearance Center, Inc. All Rights Reserved. [Privacy statement](#). [Terms and Conditions](#). Comments? We would like to hear from you. E-mail us at [customercare@copyright.com](mailto:customercare@copyright.com)

F. Chapter 10, reprinted with permission from (Xujun Chen, Sui Boon Liaw and Hongwei Wu. *Effect of volatile-char interactions on PM<sub>10</sub> emission during the combustion of biosolid chars under air and oxyfuel conditions*, *Combustion and Flame* 2018, 197, 290-303). Copyright (2018) The Combustion Institute. Published by Elsevier Inc.



The screenshot shows the RightsLink interface. At the top left is the Copyright Clearance Center logo. To its right is the RightsLink logo. Further right are navigation buttons for Home, Create Account, Help, and an email icon. Below the logo is a thumbnail of the journal cover for 'Combustion and Flame'. To the right of the thumbnail are the following details:

- Title:** Effect of volatile-char interactions on PM<sub>10</sub> emission during the combustion of biosolid chars under air and oxyfuel conditions
- Author:** Xujun Chen, Sui Boon Liaw, Hongwei Wu
- Publication:** Combustion and Flame
- Publisher:** Elsevier
- Date:** November 2018

Below these details is the copyright notice: © 2018 The Combustion Institute. Published by Elsevier Inc. All rights reserved. To the right of the details is a LOGIN button and a text box that reads: 'If you're a copyright.com user, you can login to RightsLink using your copyright.com credentials. Already a RightsLink user or want to learn more?'.

Please note that, as the author of this Elsevier article, you retain the right to include it in a thesis or dissertation, provided it is not published commercially. Permission is not required, but please ensure that you reference the journal as the original source. For more information on this and on your other retained rights, please visit: <https://www.elsevier.com/about/our-business/policies/copyright#Author-rights>

BACK

CLOSE WINDOW

Copyright © 2019 Copyright Clearance Center, Inc. All Rights Reserved. [Privacy statement](#). [Terms and Conditions](#). Comments? We would like to hear from you. E-mail us at [customercare@copyright.com](mailto:customercare@copyright.com)

## APPENDIX II: ATTRIBUTION TABLES

[1] **Xujun Chen**, Hongwei Wu. Transformation and release of phosphorus during rice bran pyrolysis: Effect of reactor configuration under various conditions, *Fuel* **2019**, 255, 115755.

<b>Authors</b>	<b>Conception and design</b>	<b>Experiments conduction &amp; data acquisition</b>	<b>Data processing &amp; analysis</b>	<b>Interpretation &amp; discussion</b>	<b>Manuscript writing, revision and finalisation</b>	<b>Final Approval</b>
Hongwei Wu	×		×	×	×	×
<p>I acknowledge that these represent my contribution to the above research output and agree that this paper could be incorporated as part of Xujun Chen's thesis.</p> <p>Sign:</p>						



[2] **Xujun Chen**, Sui Boon Liaw, Hongwei Wu. A new method for quantifying phosphorus of various occurrence forms in solid fuels, *Energy & Fuels* **2019**, 33, 3311–3321.

<b>Authors</b>	<b>Conception and design</b>	<b>Experiments conduction &amp; data acquisition</b>	<b>Data processing &amp; analysis</b>	<b>Interpretation &amp; discussion</b>	<b>Manuscript writing, revision and finalisation</b>	<b>Final Approval</b>
Sui Boon Liaw					×	
<p>I acknowledge that these represent my contribution to the above research output and agree that this paper could be incorporated as part of Xujun Chen’s thesis.</p> <p>Sign:</p>						
Hongwei Wu	×		×	×	×	×
<p>I acknowledge that these represent my contribution to the above research output and agree that this paper could be incorporated as part of Xujun Chen’s thesis.</p> <p>Sign:</p>						

[3] **Xujun Chen**, Hongwei Wu. Volatile–char interactions: Roles of *in situ* volatiles with distinctly-different chemistry in determining char structure and reactivity, *Proceedings of the Combustion Institute* **2019**, 37, 2749-2755.

<b>Authors</b>	<b>Conception and design</b>	<b>Experiments conduction &amp; data acquisition</b>	<b>Data processing &amp; analysis</b>	<b>Interpretation &amp; discussion</b>	<b>Manuscript writing, revision and finalisation</b>	<b>Final Approval</b>
Hongwei Wu	x		x	x	x	x
<p>I acknowledge that these represent my contribution to the above research output and agree that this paper could be incorporated as part of Xujun Chen’s thesis.</p> <p>Sign:</p>						

[4] **Xujun Chen**, Sui Boon Liaw, Hongwei Wu. Effect of water vapour on particulate matter emission during oxyfuel combustion of char and in situ volatiles generated from rapid pyrolysis of chromated-copper-arsenate-treated wood, *Proceedings of the Combustion Institute* **2019**, 37, 4319-4327.

<b>Authors</b>	<b>Conception and design</b>	<b>Experiments conduction &amp; data acquisition</b>	<b>Data processing &amp; analysis</b>	<b>Interpretation &amp; discussion</b>	<b>Manuscript writing, revision and finalisation</b>	<b>Final Approval</b>
Sui Boon Liaw	x			x	x	
<p>I acknowledge that these represent my contribution to the above research output and agree that this paper could be incorporated as part of Xujun Chen's thesis.</p> <p>Sign:</p>						
Hongwei Wu	x		x	x	x	x
<p>I acknowledge that these represent my contribution to the above research output and agree that this paper could be incorporated as part of Xujun Chen's thesis.</p> <p>Sign:</p>						

[5] **Xujun Chen**, Sui Boon Liaw, Hongwei Wu. Effect of volatile–char interactions on PM<sub>10</sub> emission during the combustion of biosolid chars under air and oxyfuel conditions, *Combustion and Flame* **2018**, 197, 290–303.

<b>Authors</b>	<b>Conception and design</b>	<b>Experiments conduction &amp; data acquisition</b>	<b>Data processing &amp; analysis</b>	<b>Interpretation &amp; discussion</b>	<b>Manuscript writing, revision and finalisation</b>	<b>Final Approval</b>
Sui Boon Liaw	x			x	x	
<p>I acknowledge that these represent my contribution to the above research output and agree that this paper could be incorporated as part of Xujun Chen’s thesis.</p> <p>Sign:</p>						
Hongwei Wu	x		x	x	x	x
<p>I acknowledge that these represent my contribution to the above research output and agree that this paper could be incorporated as part of Xujun Chen’s thesis.</p> <p>Sign:</p>						

[6] **Xujun Chen**, Sui Boon Liaw, Hongwei Wu. Important role of volatile–char interactions in enhancing PM1 emission during the combustion of volatiles from biosolid, *Combustion and Flame* 2017, 182, 90–101.

<b>Authors</b>	<b>Conception and design</b>	<b>Experiments conduction &amp; data acquisition</b>	<b>Data processing &amp; analysis</b>	<b>Interpretation &amp; discussion</b>	<b>Manuscript writing, revision and finalisation</b>	<b>Final Approval</b>
Sui Boon Liaw	x			x	x	
<p>I acknowledge that these represent my contribution to the above research output and agree that this paper could be incorporated as part of Xujun Chen’s thesis.</p> <p>Sign:</p>						
Hongwei Wu	x		x	x	x	x
<p>I acknowledge that these represent my contribution to the above research output and agree that this paper could be incorporated as part of Xujun Chen’s thesis.</p> <p>Sign:</p>						